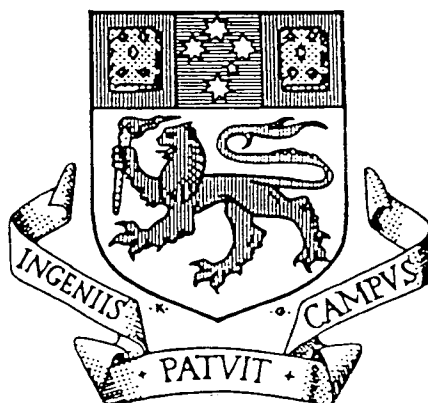


Proterozoic Geology and Mineralisation of the Greenmount Cu - Au - Co Deposit, Cloncurry District



Robert L Kremarov
B.Sc (Hons.)

A Research Thesis submitted in partial fulfilment of the requirements for the degree,
Master of Economic Geology



Centre for Ore Deposit
and Exploration Studies

A National KeyCentre at the University of Tasmania

CODES Key Centre

University of Tasmania

July 1995.

This thesis contains no material that has previously formed part of another higher degree or graduate diploma in any tertiary institution, and to the best of the author's knowledge and belief, no material that has been written or published by another person, except where due reference is provided.

Robert L Krcmarov
July 1993

Abstract

The Greenmount deposit is hosted by mid-Proterozoic graphitic and carbonaceous slates of the Marimo Slate near the contact with the calcareous and evaporitic metasediments of the Staveley Formation in the southern Marimo Basin, some 40 km south of Cloncurry. A diorite intrudes the sequence and is altered and veined but not mineralised.

Late brittle faults fragmented the geology and earlier tight D2 folds. The area around Greenmount is particularly disjointed and structurally complex. Alteration and mineralisation was localised in a "flat" ramp within a reverse fault/shear regime, and veining and mineralisation was in a dominantly brittle to brittle-ductile regime.

The Marimo Slate, the Staveley Formation and the diorite underwent alkali-rich metasomatism dominated by microcline with subordinate albite, sericite (retrogressed microcline) and lesser hematite, rutile, tourmaline, quartz, dolomite, \pm sulphides \pm magnetite.

Episodic veining comprises a stockwork of millimetre to metre wide veins, which in the Marimo Slate is dominated by microcline with lesser quartz, albite, phlogopite, apatite, ferroan dolomite and sulphides, and in the Staveley Formation is dominated by microcline, dolomite, calcite with lesser albite, muscovite, pyrite, biotite, magnetite and chalcopryite. Vein density generally decreases in the Staveley Formation away from the contact with the Marimo Slate. Mineralisation occurred syn-to post-veining and is characterised by elevated Au, Cu, Co, As, Mo, W \pm Pb \pm Zn \pm Bi \pm Cr \pm U \pm Rb \pm Ba. The most important economic metals are Au, Co and Cu. Sulphide mineralogies are dominated by pyrite and chalcopryite with lesser cobaltite and minor marcasite. Almost all of the mineralisation is hosted by the Marimo Slate.

Mineralisation and vein related sulphur isotope values generally cluster between 0 to +16‰ (mean 8.4‰), while diorite hosted sulphur is relatively lighter (mean -3.8‰) and diagenetic black slate hosted sulphur has a Proterozoic sea water signature (mean 19.1‰). The hydrothermal system was sulphur deficient. Fluid inclusions contain H₂O \pm CO₂ (dominant) \pm CH₄ (minor) \pm complex daughter salts. Combined with the wide range of minimum homogenisation temperatures, lack of phase separation evidence and two salinity populations, it would appear that fluid mixing of two different fluids occurred. One would have been a hotter (~ 320 - 500°C) hypersaline fluid and the other was a cooler (220 - 360°C) lower salinity fluid. The overall trend appears to be one of decreasing temperature and salinity, with increasing carbonate deposition later in the paragenesis.

Although the Cloncurry district black shale hosted deposits share some characteristics with the other slate belt and black shale hosted deposits, they do generally differ as a group. The reason for the differences are that the ore fluids in the district are oxidised and highly saline as a group, which supplies alkalis for the extensive alkali alteration and veining. Another fundamental difference is that gold transport is via a chloride rather than bisulphide complex and the high chloride content also permits $\text{Cu}\pm\text{Co}$ transport. Pb - Zn - Ag deposition is restricted by the amount of sulphur available in wallrocks. Veining and mineralisation is generally post-folding in a dominantly brittle regime.

These deposits thus form a distinct subclass which may be described as oxidised, alkali-rich slate belt $\text{Au}\pm\text{Cu-Co}$ deposits. Other deposits such as Muruntau, Bidjovagge and Blackbird may be included in this subclass.

Table of Contents

	Page No.
Chapter 1 Introduction	1
Ch 1.1 Location of Study Area	1
Ch 1.2 History of Discoveries of Mineralisation	1
Ch 1.3 Exploration History of the Southern Marimo Basin	2
Ch 1.4 Aims and Structure of this Thesis	4
 Chapter 2 Regional Geology	 6
Ch 2.1 Regional Overview	6
2.1.1 Introduction	6
2.1.2 Tectonic Framework	6
2.1.3 Stratigraphic Framework	7
2.1.4 Igneous Activity	15
2.1.5 Deformation Events and Structural Style	15
 Chapter 3 Geology and Structure of the South Eastern Marimo Basin	 20
Ch 3.1 Introduction	20
Ch 3.2 Lithostratigraphy	20
3.2.1 Corella Formation	20
3.2.2 Staveley Formation	20
3.2.3 Marimo Slate	23
3.2.4 Roxmere Quartzite	23
3.2.5 Intrusives	27
Ch 3.3 Regional Metasomatism	27
Ch 3.4 Structure	27
3.4.1 Folding	28
3.4.2 Faulting	29
Ch 3.5 Structural History	29
 Chapter 4 Geology of the Greenmount Area	 32
Ch 4.1 Introduction	32
Ch 4.2 Surface Geology	32
4.2.1 Lithostratigraphy	32
4.2.2 Pervasive Alteration	35
4.2.3 Structure	39
4.2.3.1 The Staveley Breccia Ridge	39
4.2.3.2 Structural Interpretation	40

Table of Contents

	Page No.
4.2.3.3 Structure and Morphology of the Main Orebody	41
4.2.3.4 Factors Controlling Mineralisation	41
Ch 4.3 Geology and Mineralisation of the Primary Zone	53
4.3.1 Staveley Formation	53
4.3.1.1 Lithologies	53
4.3.1.2 Metasomatism	56
4.3.1.3 Veining	56
4.3.1.4 Mineralisation and Sulphide Mineralogies	56
4.3.2 Marimo Slate	57
4.3.2.1 Lithologies	57
4.3.2.2 Metasomatism	57
4.3.2.3 Veining	66
4.3.2.4 Mineralisation and Sulphide Mineralogies	67
Ch 4.4 Diorite	78
Ch 4.5 Discussion and Paragenesis	83
Chapter 5 Geochemistry	85
Ch 5.1 Mineral Geochemistry	85
5.1.1 Microcline	85
5.1.2 Albite	85
5.1.3 Mica	86
5.1.4 Carbonate	88
5.1.5 Apatite	88
5.1.6 Magnetite	89
5.1.7 Pyrite	90
5.1.8 Chalcopyrite	93
Ch 5.2 Lithogeochemistry	94
5.2.1 Least Altered Staveley Formation	99
5.2.2 Metasomatised and Veined Staveley Formation	99
5.2.3 Marimo Slate	102
5.2.4 Pervasive Altered and Veined Marimo Slate	103
5.2.5 Diorite	103
5.2.6 Main Stage Mineralisation	103
Ch 5.3 The Geochemistry of Felsic Intrusives of the Marimo Basin	111

Table of Contents

	Page No.
Chapter 6 Stable Isotopes	116
Ch 6.1 Sulphur Isotopes	116
6.1.1 Procedures	116
6.1.2 Isotopic Variation	116
Ch 6.2 Carbon and Oxygen Isotopes	125
6.2.1 Method	126
6.2.2 Other Carbon and Oxygen Isotope studies	126
6.2.3 Results	130
 Chapter 7 Fluid Inclusion Study	 133
Ch 7.0 Introduction	133
Ch 7.1 Method of Study	133
Ch 7.2 Classification of Inclusion Types	134
Ch 7.3 Inclusion Types	134
7.3.1 Type I liquid - vapour inclusions	134
7.3.2 Type II liquid - CO ₂ vapour inclusions	134
7.3.3 Type IIIA liquid - vapour - solid inclusions	139
7.3.4 Type IIIB liquid - vapour - multisolid inclusions	139
7.3.5 Type IIIC liquid - CO ₂ vapour - multisolid inclusions	146
7.3.6 Type IV secondary liquid vapour inclusions	146
7.3.7 Type V solid inclusions	146
Ch 7.4 Thermometry	146
<u>Pressure Corrections</u>	146
<u>Effects of CO₂ vapour in inclusions</u>	147
<u>Behaviour of high salinity inclusions on heating</u>	147
<u>Solute character of fluid inclusions</u>	148
<u>The effects of CH₄ vapour in inclusions</u>	149
<u>Homogenisation temperatures</u>	150
<u>Discussion</u>	154

Table of Contents

	Page No.
Chapter 8 Discussion and Summary	157
Ch 8.0 Introduction	157
Ch 8.1 Ballarat-style slate belt gold deposits	157
Ch 8.2 Global examples of carbonaceous sediment hosted mineralisation	158
<u>The Ashanti Gold Belt - Ghana</u>	158
<u>The Muruntau Deposit - Uzbekistan</u>	159
<u>Synsedimentary to Diagenetic mineral deposits and</u>	
<u>Metalliferous black shales</u>	164
<u>Stratiform Cu - Co - Au deposits of the Idaho Cobalt belt</u>	166
<u>The Bidjovagge copper - gold deposit</u>	167
<u>Cloncurry District analogues</u>	169
Ch 8.3 Toward a new ore subclass-oxidised, alkali-rich slate belt	
Au±Cu-Co deposits	171
References	172

List of Figures

	Page No.
Chapter 1	
Figure 1.1 Stream sediment geochemistry of the Greenmount area.	3
Chapter 2	
Figure 2.1 Tectonic Zones.	6
Figure 2.2 Stratigraphic framework.	9
Figure 2.3 Stratigraphic column for the Malbon-Marimo area.	11
Figure 2.4 Location map of the Mount Isa Inlier and study area as well as a simplified summary geological map of the southern and central portions of the Eastern Fold Belt showing locations of major mineral deposits.	12
Figure 2.5 Compositional variation in the eastern half of the Williams and Naraku Batholiths.	17
Figure 2.6 Distribution of granite in the eastern Mount Isa Inlier.	17
Chapter 3	
Figure 3.1 Interpreted geology of the Eastern Marimo Basin.	24
Figure 3.1b Interpreted structures of the Eastern Marimo Basin.	25
Figure 3.2 Detailed stratigraphic column of evaporitic dolomites from the Staveley Formation at Just Found.	26
Figure 3.3 Structural model for major fault/shear zones.	30
Chapter 4	
Figure 4.1 Outcrop geology of the Greenmount area with fundamental structural elements, interpreted Marimo-Staveley contact and location of some drill holes relevant to this study.	33
Figure 4.2 Geological features corresponding to Plate 4.1.	34
Figure 4.3 Simplified geological interpretation of cross section 9300N	42
Figure 4.4 Simplified geological interpretation of cross section 9500N	43
Figure 4.5 Simplified geological interpretation of cross section 9600N	44
Figure 4.6 Simplified geological interpretation of cross section 9700N	45
Figure 4.7 Simplified geological interpretation of cross section 9800N	46
Figure 4.8 Simplified geological interpretation of cross section 9900N	47
Figure 4.9 Structural data plots for holes GTRC10 and GTRC11.	48
Figures 4.10 a-b Fault refraction and fold models for the Greenmount orebody.	49
Figure 4.10 c Schematic diagram showing zones of dilation in a reverse fault.	50
Figures 4.11 a-c Parageneses of the Marimo Slate, Staveley Formation and diorite.	84

List of Figures (continued)

	Page No.
Chapter 5	
Figure 5.1 Graph of pyrite trace element content based on pyrite morphology.	91
Figure 5.2 Graph of pyrite trace element content based on microprobe analyses of various pyrite occurrences.	93
Figure 5.3 Multi-element X-Y scatter plots on logarithmic scale, for various lithologies, alteration and vein types from samples for this study.	95
Figure 5.4 X-Y scatter plots on logarithmic scale for major elements versus Cu and Au for various lithologies.	97
Figure 5.5 Major element X-Y scatter plots for various lithologies.	98
Figure 5.6 Percentage change of various elements during metasomatism and veining for the Staveley Formation.	100
Figure 5.7 Percentage change of various trace and minor elements during pervasive alteration and veining for the Marimo Slate.	101
Figure 5.8 Chondrite normalised REE plots for the least altered diorite.	104
Figure 5.9 Plot of Au and Cu for all core holes where Au > 0.1 ppm or Cu > 500 ppm.	111
Chapter 6	
Figure 6.1 Histogram of all Greenmount sulphur isotope values.	118
Figure 6.2 Histogram of sulphur isotope values from veins at Greenmount.	118
Figure 6.3 Natural sulphur isotope reservoirs.	121
Figure 6.4 The $\delta^{34}\text{S}$ values for sulphur-bearing minerals in hydrothermal deposits.	121
Figure 6.5 A comparison of the sulphur isotopic ranges of deposits.	123
Figure 6.6 Plan of average sulphur isotope values at Greenmount.	124
Figure 6.7 Carbon and oxygen isotope plot for various carbonate occurrences at Greenmount.	127
Figure 6.8 a Carbon-oxygen isotope fields of all Starra sample groups.	129
Figure 6.8 b Regional carbonate, compared to Area 257 matrix carbonate.	129
Figure 6.8 c Veins in the Starra hangingwall metasediments.	129
Figure 6.8 d Veins in hornfels and dolerite.	129
Figure 6.9 Natural oxygen isotope reservoirs.	131
Figure 6.10 Natural $\delta^{13}\text{C}$ reservoirs.	131
Chapter 7	
Figure 7.1 Temperature ranges of minimum homogenisation temperatures based on inclusion type, mineral and host rock.	151
Figures 7.2 A,B,C. Histograms of minimum homogenisation temperatures (vapour bubble disappearance) for various minerals, regardless of host rock.	153
Figure 7.3 Th (min.) versus salinity plot for Type I, II and IV inclusions.	154
Chapter 8	
Figure 8.1 Geology of the Muruntau district.	151
Figures 8.2 Plan and cross section of the regional geology of the Muruntau district.	153

List of Plates

Chapter 3

Page No.

- Plate 3.1 (A)** View to the south on the Mt McCabe Track. **21**
- Plate 3.2 (B)** Staveley Formation "Trash Bed" of silicified nodular pseudomorphs of (?) Gypsum.
- Plate 3.3 (C)** Disseminated bedding parallel quartz pseudomorphing evaporitic sulfate minerals in feldspar - sericite (\pm dolomite), decalcified dolomite rock, from the Staveley Formation near the Just Found Prospect.
- Plate 3.4 (D)** Dissaggregated semi-massive, diagenetically altered dominantly silica - microcline) evaporitic bed from the Staveley Formation.
- Plate 3.5 (E)** Diagenetic displacive growth of anhydrite nodules into soft sediment with draping and slumping of overlying ex-calcilutite.
- Plate 3.6 (F)** Upper Corella Formation laminated dolomitic carbonate and siltstone.
- Plate 3.7 (G)** Highly strained Corella Formation.
- Plate 3.8 (H)** Close up of Corella Formation in Plate 3.7.

Chapter 4

Page No.

- Plate 4.1** Panorama of the Greenmount ore zone. **34**
- Plate 4.2 (A)** View from west of Greenmount, looking to the southeast. **37**
- Plate 4.3 (B)** Hematitic banded iron formation showing sedimentary structures.
- Plate 4.4 (C)** BIF outcrop forming ridges just west of Greenmount. Hosted by the Staveley Formation.
- Plate 4.5 (D)** Outcrop of Marimo Slate near Petes Prospect.
- Plate 4.6 (E)** Outcrop of black shale (Marimo Slate) which has undergone brittle style fracturing and veining by microcline-quartz-phlogopite. No preferred orientation of veins.
- Plate 4.7 (F)** Large cubic pyrite crystals with striated faces which form in some of the bleached alteration zones.
- Plate 4.8 (G)** Pyrite crystals with well developed pyritohedral forms from the pervasively altered shales at Painted Peaks Prospect.
- Plate 4.9 (H)** Pervasive albite-microcline alteration of Marimo Slate at Petes Prospect with late planar crosscutting quartz hematite veins.
- Plate 4.10 (I)** Similar to Plate 2.8 but with abundant disseminated pyrite (now weathered to iron oxides).
- Plate 4.11 (J)** Progressively feldspathised pelites from the Petes Prospect area.

List of Plates (continued)

Page No.

Chapter 4

51

Plate 4.12 (A) Intensely Alunite, kaolinite and microcline altered siltstone with large disseminated pyrite crystals and pseudomorphs from the Painted Peaks prospect.

Plate 4.13 (B) Colloform banded crustiform quartz and chalcedony veins in silicified siltstone from Mason's prospect.

Plate 4.14 (C) Tightly folded Corella Formation from Petes prospect.

Plate 4.15 (D) View looking south along the main Greenmount ore zone.

Plate 4.16 (E) View of the Greenmount area looking to the south east.

54

Plate 4.17 (A) Typical Staveley Formation bedded calcarenite-calcilutite.

Plate 4.18 (B) Partially weathered and vughy bedded calcarenite from the Staveley Formation.

Plate 4.19 (C) Near contact of Marimo Slate and Staveley Formation. The dark bands in the Staveley Formation dominantly comprise micaceous slate with quartz, microcline \pm dolomite, calcite and other gangue minerals. The relatively coarser and pale layers comprise a sutured mosaic of quartz, microcline and plagioclase (pseudomorphed and altered by sericite) as well as lesser dolomite, calcite and other gangue minerals.

Plate 4.20 (D) Partly weathered and vuggy-bedded Staveley Formation.

Plate 4.21 (E) Close-up of pervasive and incipient orange coloured hematite dusted microcline alteration of Staveley Formation lithologies with calcite matrix and thin cross cutting calcite veins.

Plate 4.22 (F) Cavities formed by dissolution of calcite in partly weathered Staveley Formation lithologies.

Plate 4.23 (G) Close up of right side of Plate 4.17.

Plate 4.24 (H) Pyrite-calcite matrix to brecciated and intensely hematite dusted microcline altered Staveley Formation.

58

Plate 4.25 (A) Intensely altered and contact hornfelsed Staveley Formation adjacent to diorite now comprising an albite, calcite, microcline, quartz and magnetite assemblage.

Plate 4.26 (B) As for Plate 4.25 but under crossed polars.

Plate 4.27 (C) From same section as Plate 4.25 but alteration assemblage comprises calcite and pyrite.

Plate 4.28 (D) Photomicrograph of calcite, microcline, albite, quartz and pyrite matrix to brecciated Staveley Formation.

List of Plates (continued)

Page No.

Chapter 4

60

Plate 4.29 (A) Photomicrograph showing small magnetite cubes (opaque) concentrated in particular beds of the Staveley Formation adjacent to a coarse calcite vein.

Plate 4.30 (B) Ragged, chalcopyrite occurring preferentially within or near late coarse calcite patches, veins or matrix.

Plate 4.31 (C) Coarser grained pyrite and chalcopyrite occurring in or near coarser calcite patches in the Staveley Formation.

Plate 4.32 (D) A relatively large poikiloblastic grain of magnetite (pale grey) intergrown with calcite, quartz, feldspar, pyrite (white) and chalcopyrite (yellow) indicating synchronous crystallisation of all phases.

62

Plate 4.33 (A) Typical fissile thinly laminated carbonaceous and graphitic shale and slate from the Marimo Slate.

Plate 4.35 (B) Central column of core shows a coarsely crystalline phlogopite (dark laths), quartz, microcline vein.

Plate 4.34 (C) Left column of core showing early pervasive feldspar alteration of shale sometimes follows bedding (and may predate folding) and clearly predates some microcline veining. Right column of core shows late thin sulphidic veinlets with sericitic selvages, superimposed on earlier pervasively altered shale.

Plate 4.36 (D) Weak pervasive feldspar alteration (superimposed by a vein) diminishing in intensity away from the main ore zone.

64

Plate 4.37 (A) Intensely tourmalinised and feldspathised slate with some rutile aggregates.

Plate 4.38 (B) Pervasive feldspar alteration front with disseminated pyrite.

Plate 4.39 (C) Feldspathised slate adjacent to feldspathic vein.

Plate 4.40 (D) Sericitic carbonaceous slate with feldspathic lenses.

68

Plate 4.41 (A) Central column of core shows a microcline, quartz and phlogopite (dark laths near bottom) vein hosted by unaltered black shale.

Plate 4.42 (B) Several generations of quartz-microcline veins cutting each other adjacent to intensely feldspathic altered shale with microcline veins which has been brecciated.

Plate 4.43 (C) Pervasively sericitised shale with disseminated chalcocite blebs, veined by a microcline-chalcocite vein.

Plate 4.44 (D) Pervasive feldspar altered shale with irregular pyrite stringer veins.

Plate 4.45 (E) Part of a wide hematite dusted coarse microcline vein, which has been fractured and veined by a pyrite vein.

Plate 4.46 (F) Brecciated massive pyrite-microcline vein.

Plate 4.47 (G) Pervasively feldspathised shale which has been veined by microcline then fractured.

Plate 4.48 (H) A microcline vein with a feldspathic selvage, has been fractured perpendicular to vein walls and filled by late chalcopyrite.

List of Plates (continued)

Page No.

Chapter 4

70

Plate 4.49 (A) Higher grade ore zone assaying about 1.25 g/t Au and 2.57% Cu is hosted by argyllised black shale (yellow) which was veined by feldspars, mica and pyrite then strongly brecciated and filled by gangue minerals including pyrite and chalcopyrite. Most of the chalcopyrite was replaced by chalcocite.

Plate 4.50 (B) Close up view of Plate 4.49.

Plate 4.51 (C) An irregular, coarse microcline-quartz vein which is hosted by unaltered black shale, has been fractured and filled by chalcopyrite and pyrite.

72

Plate 4.52 (A) Photomicrograph of microcline, phlogopite, quartz and pyrite vein in feldspathised slate.

Plate 4.53 (B) Photomicrograph of patchy albitisation of slate near a feldspathic vein.

Plate 4.54 (C) Photomicrograph of albite, quartz, phlogopite, apatite and rutile vein in altered slate.

Plate 4.55 (D) Photomicrograph of microcline, quartz, phlogopite, chlorite, pyrite and chalcopyrite vein from the same sample and thin section as Plates 4.53 and 4.54.

Plate 4.56 (E) Photomicrograph of quartz, microcline, albite, phlogopite, rutile, apatite, pyrite and calcite vein in feldspathised slate with disseminated pyrite.

Plate 4.57 (F) Photomicrograph of late planar sericite vein cutting a quartz-chalcopyrite vein which cuts an early microcline dominated vein.

74

Plate 4.58 (A) Photomicrograph of a portion of a microcline, quartz, apatite and sulphide vein showing euhedral pyrite in massive chalcopyrite and sphalerite being replaced by covellite.

Plate 4.59 (B) Photomicrograph of ragged elongate aggregates of pyrite in places retain relicts of marcasite and lie in massive chalcopyrite from a microcline, quartz, phlogopite, rutile and sulphide vein in relatively unaltered graphitic shale.

Plate 4.60 (C) Photomicrograph of a portion of a microcline, quartz, albite, apatite, phlogopite and sulphide vein in graphitic slate, showing large pyrite crystals may contain ragged inclusions of chalcopyrite and pyrrhotite.

Plate 4.61 (D) Photomicrograph of a portion of a microcline, quartz, phlogopite and sulphide vein hosted by foliated and crenulated graphitic slate, showing that small grains of pyrite and chalcopyrite favour microcline rather than quartz.

76

Plate 4.62 (A) Photomicrograph of a portion of a microcline, quartz, phlogopite and sulphide vein showing a thin trail of chalcopyrite (top half of photograph) filling a cleavage trace in feldspar.

Plate 4.63 (B) Photomicrograph of a planar vein containing ragged chalcopyrite grains with small pyrite crystals and aggregates sparsely disseminated in pervasively feldspathised wallrock.

Plate 4.64 (C) Photomicrograph of a late clay filled fracture in feldspathised wallrock which is flanked by very fine grained replacement pyrite in the vein selvage.

Plate 4.65 (D) Portion of an abundant massive pyrite vein which is strongly fractured.

List of Plates (continued)

Page No.

Chapter 4

79

Plate 4.66 (A) Fine grained diorite with thin calcite veins.

Plate 4.67 (B) Microdiorite with thin calcite veins and a thicker hematite dusted microcline, calcite and biotite vein.

Plate 4.68 (C) Calcite vein in microdiorite with a hematite dusted microcline selvage.

Plate 4.69 (D) Calcite veins of brittle style in altered diorite.

Plate 4.70 (E) An irregular calcite vein with large aggregates of granular pyrite from the altered margins of the microdiorite.

Plate 4.71 (F) Quartz, calcite and pyrite vein in heavily chloritised and carbonated microdiorite.

81

Plate 4.72 (A) Photomicrograph of chloritised (green) and carbonated microdiorite with disseminated magnetite.

Plate 4.73 (B) Photomicrograph of a microcline, calcite, quartz and pyrite vein in chloritised microdiorite.

Plate 4.74 (C) Photomicrograph of a sericitised plagioclase rich part of a plagioclase, calcite, microcline, biotite and rutile vein in microdiorite.

Plate 4.75 (D) Photomicrograph of carbonated and biotite altered microdiorite with disseminated (and aggregates of) magnetite.

Chapter 7)

Page No.

135

Plate 7.1 (A) Primary Type II fluid inclusions in carbonate.

Plate 7.2 (B) Coexisting Type III and Type III B fluid inclusions in quartz.

Plate 7.3 (C) Coexisting Type II and Type III A inclusions in carbonate.

Plate 7.4 (D) Type III C liquid - CO₂ vapour - multisolid inclusion in quartz. This particular inclusion includes a hematite solid.

Plate 7.5 (E) Halite - hydrocarbon ? inclusion in centre of field of view with smaller Type II inclusion above it.

137

Plate 7.6 (A) Large primary Type I liquid - vapour inclusions.

Plate 7.7 (B) Secondary Type IV liquid - vapour inclusions in carbonate.

Plate 7.8 (C) Pseudosecondary Type I inclusions in carbonate.

Plate 7.9 (D) Type III (c) liquid - CO₂ vapour - unidentified solid - halite (halite almost invisible in this photograph) in quartz.

Plate 7.10 (E) Coexisting Type II and Type III A inclusions in quartz.

List of Tables

TABLE No.	Page No.
1.1 Mount Isa Inlier Discovery History of some significant deposits.	5
2.1 Descriptions of stratigraphic units, Mount Isa Inlier.	8
2.2 Granites of the Williams Batholith.	16
2.3 A summary of the timing of geological events in the Mount Isa Inlier.	18
4.1 Pervasive Alteration Sample Descriptions of Hole and Depth.	36
4.2 XRD Analysis of Pervasively Altered Samples From Pete's and Painted Peaks Prospects.	36
5.1 Average of microcline microprobe analyses for various occurrences of microcline.	86
5.2 Average of albite microprobe analyses for various occurrences of albite.	87
5.3 Average microprobe analyses of various occurrences of mica.	87
5.4 Average microprobe analyses of carbonates hosted by the Staveley Formation.	88
5.5 Average microprobe analyses of apatite in veins hosted by the Marimo Slate.	89
5.6 Average microprobe analyses of magnetite hosted by diorite.	90
5.7 Average microprobe analyses of pyrite based on the pyrite morphology.	91
5.8 Average microprobe analyses of various occurrences of pyrite.	92
5.9 Average microprobe analyses of chalcopyrite hosted by veins and wallrock in the Marimo Slate.	94
5.10 Elements Gain - Loss budget of the Staveley Formation through the various paragenetic events.	102
5.11 Trace element analyses for lithologies, alteration, veins and mineralisation hosted by the Marimo Slate.	105
5.12 Trace element analyses for lithologies, alteration and veins hosted by the Staveley Formation and diorite intrusive.	106
5.13 Whole rock analyses of various rock types.	107
5.14 Average geochemical analyses of various rock types, alteration styles and mineralisation.	108
5.15 Downhole minor and trace element geochemistry for hole GDH-01.	109
5.16 Downhole minor and trace element geochemistry for hole GDH-03.	110
5.17 Geochemical whole rock analyses of intrusives near Greenmount.	113
5.18 Geochemical whole rock analyses of felsic intrusives of the Marimo Basin Environs.	114
6.1 Sulphur isotope analyses for samples from Greenmount.	117
6.2 A summary of the statistical variation of $\delta^{34}\text{S}\%$ for all samples as a function of rock-type and occurrence.	119
6.3 Mean $\delta^{34}\text{S}\%$ for all sulphides as a function of rock type and distance from the Pkm - Pks lithostructural contact.	125
6.4 $\delta^{34}\text{S}\%$ values for Marimo Slate hosted pyrites as a function of pyrite morphology.	125

List of Tables (continued)

Page No.

TABLE No.

6.5	Ranges of C-O isotopic data from relatively unmetamorphosed Proterozoic northern Australian and Canadian hypersaline dolomite sequences.	126
7.1	Summary of the main characteristics of different populations of fluid inclusions in various minerals from Greenmount.	139
7.2	Optical properties of the identified daughter phases in Type IIIA,B and C multiphase solid inclusions.	140
7.3		
7.4	First melting temperatures for various aqueous multiphase solid systems.	148
7.5	Average of minimum homogenisation temperatures based on fluid inclusion type, host mineral and host rock.	152
7.6	Minimum homogenisation temperature based on host mineral and inclusion generation.	152
8.1	Isotopic - Geochemical and physicochemical parameters of Muruntau mineralisation. (Data from Zairi and Kurbanov, 1992) stages of paragenesis.	162

List of Appendices

Appendix No.	Title
1	Index of samples
2	Drill hole logs
3	Thin section descriptions
4	Microprobe analyses
5	Laser Raman Spectra

Acknowledgments

I am sincerely grateful for the enthusiastic supervision, encouragement and advice given by Dr Garry Davidson.

Homestake Gold of Australia Limited provided most of the financial support as well as use of company data and support facilities for the thesis production. Special thanks go to Dick Tastula (Managing Director), Norm Lehrman (Exploration Manager), Ross Glossop, Gary Maddocks and particularly Jim Stewart (Principal Geologist) for his encouragement and many useful discussions. Numerous Homestake geologists contributed substantially to the early work on this project and they are all thanked. I am particularly grateful to Margaret Henderson for her word processing skills and Shirley Stumpers and Theresa Duits for drafting of maps. Their patience and skill is appreciated. Karen Krcmarov is thanked for assisting in editing and compiling this thesis.

Dr Khin Zaw is thanked for providing advice on fluid inclusions, and Professor Ross Larges' general advice is appreciated. Singori Blackwell provided assistance with fluid inclusion instrument operation. Mike Power from the Central Science Laboratories at the University of Tasmania patiently assisted with sulphur isotope analyses and Nathan Duhig performed the carbon and oxygen isotope analyses. Thin sections were prepared by Mike Dineen, as well as Phil Robinson and Naomi Deards of the Geology Department. Geochemical analyses were largely carried out by Australian Laboratory Services (Townsville) and Bequerel Laboratories (Lucas Heights). Andrew McNeill is kindly thanked for his assistance with the Microprobe.

The academic staff, post graduate and undergraduate fraternity provided a stimulating intellectual and social environment at the CODES Key Centre.

Finally, I sincerely thank my parents for their perpetual encouragement of my education, particularly my late father Stevan Krcmarov, who taught me the value of education and the treasure of knowledge.

I am eternally grateful to my wife Karen, and children Dylan and Jasmin, for their kind, selfless support and encouragement over the years and for enduring my long absences, lost weekends and late nights.

Chapter 1 Introduction

Ch 1.1 Location of Study Area

The Greenmount Deposit is located on the Kuridala 1:100,000 Geological Special sheet and the Duchess 1:250,000 sheet (SF54-6) at approximately latitude 21° 02' and longitude 140° 32'. The universal grid reference is 54KVB521741.

The Greenmount Area is situated 35km directly south of the township of Cloncurry which is 1,760km by road from Brisbane and 125km east of Mt Isa. Numerous station tracks access the area. Best access is from a track commencing 5km south of Slaty Creek on the sealed Cloncurry - Duchess Road or by station tracks commencing Cloncurry, via Roxmere Station then to Copper Canyon and following the Cloncurry River to the Martin Creek junction.

Ch 1.2 History of Discoveries of Mineralisation

The Cloncurry Area has had a rich and colourful history which has best been described by Blainey (1970). The first explorers to approach the region were John Stokes in 1841, then Ludwig Leichhardt in 1845, who perished on a journey from the east coast to Arnhem Land. The ill-fated Burke and Wills expedition of 1860 - 1861 passed by the area where the present township of Cloncurry is located and made general notes on the lithologies. In 1861, expeditions were lead by Landsborough and McKinlay, in search of Burke and Wills. It was on McKinlay's expedition that he first discovered a specimen of copper in quartz (McKinlay, 1863). Pastoralist Ernest Henry discovered iron ore at Mount Leviathan in 1866, and the first copper deposit at Cloncurry in 1866 which he called "Great Australian".

Henry and his partner Roger Scheaffe, were the first non-indigenous settlers in the region in 1867. In the same year, Henry found numerous other copper showings, including the Crusader and Dobbyn mines. Alluvial gold was discovered at Top Camp and in the Selwyn Ranges by Holmes. In the years that followed numerous gold and copper showings were discovered. Kalkadoon aborigines led Henry to copper at Argylla, and other prospectors to numerous copper showings in 1880. Two years later, Henry found copper at Mt Oxide. In 1884, copper was discovered by McPhail and Johnson at Kuridala. Then in 1886 alluvial gold was discovered immediately south of the area which is now the Greenmount Deposit. In a near by area, more alluvial gold was discovered at Last Call. Copper mineralisation was discovered at Mt Elliot by John Elliot in 1899. The Cloncurry district was declared a Goldfield in 1889 and a Mineral Field in 1899. Improved transport, communications and infrastructure, together with profitable mining saw a prosperous period for the region, and the towns population peaked at 7,795 from 1910 to 1920 (Homestake, 1989). The Mt Isa lead-zinc deposit was

discovered by John Campbell Miles, when he noticed gossanous mineralisation (which turned out to be cerussite) while his horse was drinking from a waterhole. Four years later copper was discovered by accident while drilling the lead-zinc deposit. In the same year, copper was discovered at Gunpowder. Until 1980, relatively few significant discoveries were made but notable exceptions are the Hilton, Mary Kathleen, Duchess and Lady Loretta mines. Since 1980, numerous significant discoveries have been made including Starra, Osborne, Century, Cannington and Ernest Henry (Table 1.1).

Ch 1.3 Exploration History of the Southern Marimo Basin

An open file search at the Queensland Mines Department revealed that until 1986 most exploration was dominated by the search for copper mineralisation. Some of the companies exploring the area include National Lead Company., MIM, Kennecott and Western Nuclear (1954), Carpentaria Exploration Company (1963, 1971-1976), Frio Mining (1970), BHP (1973), Amoco (1977-1978), Valdora Minerals (1985-1988) and Homestake Australia Limited (1988-present).

Until 1989, most work in the immediate Greenmount vicinity had been conducted by National Lead Company, and CEC. Valdora Minerals was the first company to target the greater area, primarily for gold and PGE's, considered it prospective for Kupferscheifer style mineralisation. In 1988 Homestake entered into a Joint Venture with Valdora and commenced a large detailed and systematic stream sediment sampling programme, primarily using the BLEG method, over most of the Marimo Basin. The bulk leach extractable gold (BLEG method) involves the collection of 5Kg of -6mm sediment from the active or semi-trap sites of a stream, and extraction of gold by leaching the sample for 24 hours with a sodium cyanide solution. Gold is then extracted onto di-isobutane ketone (DIBK) and analysed by atomic absorption spectroscopy (AAS). This is essentially a partial extraction technique. A large anomaly extending from the Greenmount to Vulcan area was delineated (Figure 1.1). Stewart (1991) documents much of the early geochemistry. The Greenmount orebody was intersected in one hole in 1991 (Stewart, 1991 & 1994) and defined by RAB and RC percussion drilling in 1992. Since then numerous holes including core drilling have defined a global inferred resource of approximately 3.6 million tonnes at about 1.5% Cu, 0.77 g/t Au and 420 ppm Co.

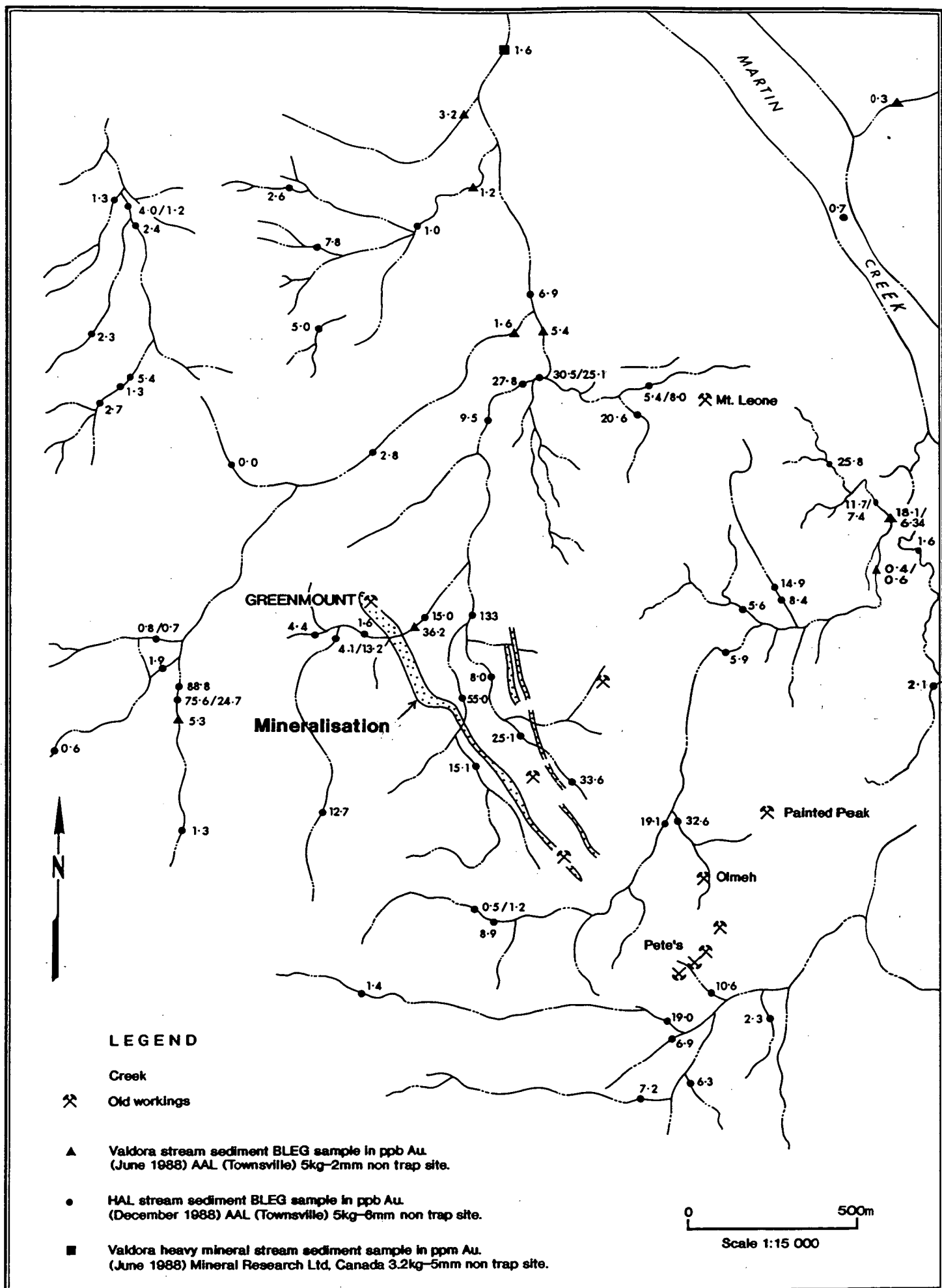


Figure 1.1 Stream sediment geochemistry of the Greenmount area.
(Modified from Stewart, 1991)

Ch 1.4 Aims and Structure of this Thesis

The primary aim is to document the style of alteration and mineralisation at the Greenmount deposit.

More specifically, the study has the following aims:-

- (1) Describe the mineralogical and textural features of the primary ore zone of the Greenmount deposit, and to develop a paragenetic sequence which will provide a framework for subsequent analytical work.
- (2) Describe the geology and structure of the southern Marimo Basin, which has been refined by the author and other Homestake geologists, as well as by structural consultants.
- (3) Determine the detailed geochemistry of the various stages of the paragenesis including alteration, vein sets and mineralisation.
- (4) Determine the geochemistry and characteristics of several intrusives in the area to ascertain their mineralising potential and possible relationships to mineralisation at Greenmount.
- (5) Determine characteristics of mineralising fluids to place some constraints on ore forming processes and the origin of fluids and metals.

The aim of this study is not to document the complex structural history of the deposit area, nor is it to document the supergene ore zone, or the fine spatial distribution of mineralisation within the ore zone. These are beyond the scope of this study. To achieve these aims, a programme of research has been undertaken which includes compilations of regional and prospect scale mapping, sampling of local intrusive rocks, logging and sampling of diamond drill core, and detailed petrologic examination of the samples using petrographic, mineral chemistry, fluid inclusion and stable isotope techniques.

The investigation is broadly divided into three parts: stratigraphic and lithostructural characterisation, geochemical characterisation, and isotopic and fluid characterisation.

Chapter two provides a regional overview and tectonostratigraphic framework. Chapter three details the revised structural and lithostratigraphic setting of the area. Chapter four describes the local geology, alteration, textural and mineralogical features of the deposit and develops a paragenetic sequence. Chapter five briefly examines the geochemistry of local intrusives and details the geochemistry and mineral species of the deposit. Chapter six and seven look at the physicochemical conditions of mineralising fluids and the isotopic characterisation of the deposit, respectively.

**TABLE 1.1 : MOUNT ISA INLIER
DISCOVERY HISTORY OF SOME SIGNIFICANT DEPOSITS**

DEPOSIT	TONNES (millions)	GRADE					DISCOVERY YEAR	DISCOVERY METHOD
		Au g/t	Cu (%)	Pb (%)	Zn (%)	Ag (g/t)		
Mt Leviathan (Fe)	N/S	-	-	-	-	-	1866	Searching for pastoral country
Great Australia●	1.2	-	1.2	-	-	-	1867	Searching for pastoral country
Bower Bird	alluvial	-	-	-	-	-	1867	Prospecting
Top Camp	alluvial	-	-	-	-	-	1867	Prospecting
Gilded Rose	0.3	5.5	-	-	-	-	1873	Prospecting
Dugald River ●	43	-	-	2.1	13.1	42	1870's	Prospecting
Mount Oxide	28	-	0.5	-	-	-	1882	Prospecting
Last Call	alluvial	-	-	-	-	-	1886	Prospecting
Kuridala	2.1	0.3	1.37	-	-	-	1890's	Prospecting
Mt Dore	26.0	-	1.10	-	-	5.0	1890's	Prospecting
Mt Elliot	2.68	1.44	3.15	-	-	-	1899	Prospecting
Mt Isa Pb-Zn ■	150	-	-	7	6	100	1923	Prospecting
Mt Isa Cu ■	1255	-	1.5	-	-	-	1927	By accident while
	255	-	3.3	-	-	-	mineable	drilling Pb-Zn deposit
Gunpowder ■	-30	-	1.5	-	-	-	1927	Prospecting
Hilton-Hilton N ■	102	-	-	6.3	10.6	118	1947	Prospecting
Ska1 (U)	2.7	0.13%	-	-	-	-	1954	Prospecting
Mary Kathleen (U)	9.5	0.13%	-	-	-	-	1954	Prospecting
Constance Range (Fe)	365	0.50%	-	-	-	-	1956	Geological mapping
Duchess (P ₂ O ₅)	1900	17.3%	-	-	-	-	1966	Geological mapping
Lady Loretta	8.3	-	-	8.5	18.4	125	1969	Soil geochemistry
Pegmont	11.0	-	-	8.35	3.67	11	1971	Aeromagnetic anomaly
Maramungee	1.4	-	-	-	4.4	-	1974	Aeromagnetic anomaly
Selwyn ■	5.3	5.0	2.0	-	-	-	1980	Re-evaluation/Rock geochemistry
Osborne●	11.3	1.3	3.0	-	-	-	1985	Aeromagnetic anomaly/Re-evaluation
Eloise●	3.2	1.5	5.8	-	-	19	1988	Ground TEM
Tick Hill ■	0.47	2.7	-	-	-	-	1989	Stream BLEG geochemistry
Century ●	118.0	-	-	1.5	10.2	35	1990	Regional soil geochemistry
Cannington ●	45	-	-	11.9	4.8	5.20	1990	Aeromagnetic anomaly
Ernest Henry ●	97.0	0.8	1.6	-	-	-	1991	Aeromagnetic anomaly/TEM
Greenmount	~3.6	0.8	1.5	-	-	-	1991	Geochemistry

■ Operating mines

● Advanced feasibility studies

NB. Figures in italics refer to the elements in parentheses adjacent to the deposit name.

References

Milner (1993); Bresciannini (1992); Beardsmore (1993); Davidson et al (1989); Kary and Harley (1990); Stewart (1991,1993); McLean and Benjamin (1993); Crooks (1993); Williams and Blake (1994); Connor et al. (1990); Newberry (1991); Williams and Heineman (1993); Jobsons's (1994); Homestake (1993); Skrzeczyneki (1993); Roache (1994); Derrick (1994).

CHAPTER 2 *Regional Geology*

Ch 2.1 Regional Overview

Ch: 2.1.1 Introduction

The first major effort to deduce the geological history for the Mt Isa Inlier was jointly undertaken by the Geological Survey of Queensland (GSQ) and the Bureau of Mineral Resources (BMR - now AGSO), and was reported in Carter et al. (1961). The most notable revisionary work has been by Derrick et al. (1976 a-e; 1977 a, b; 1978, 1980), Bultitude et al. (1977), Donchak et al. (1983), Blake (1987), Blake and Page (1988), Ryburn et al. (1988), Davidson (1988), Beardsmore et al. (1988), Beardsmore (1992) and Blake and Stewart (1992).

Ch 2.1.2 Tectonic Framework

The Mt Isa Inlier is broadly divided into three major north-south trending tectonic units separated by strike slip faults and fault zones. (Blake, 1987); The Western Fold Belt, the Kalkadoon-Leichhardt Belt and the Eastern Fold Belt (Figure 2.1).

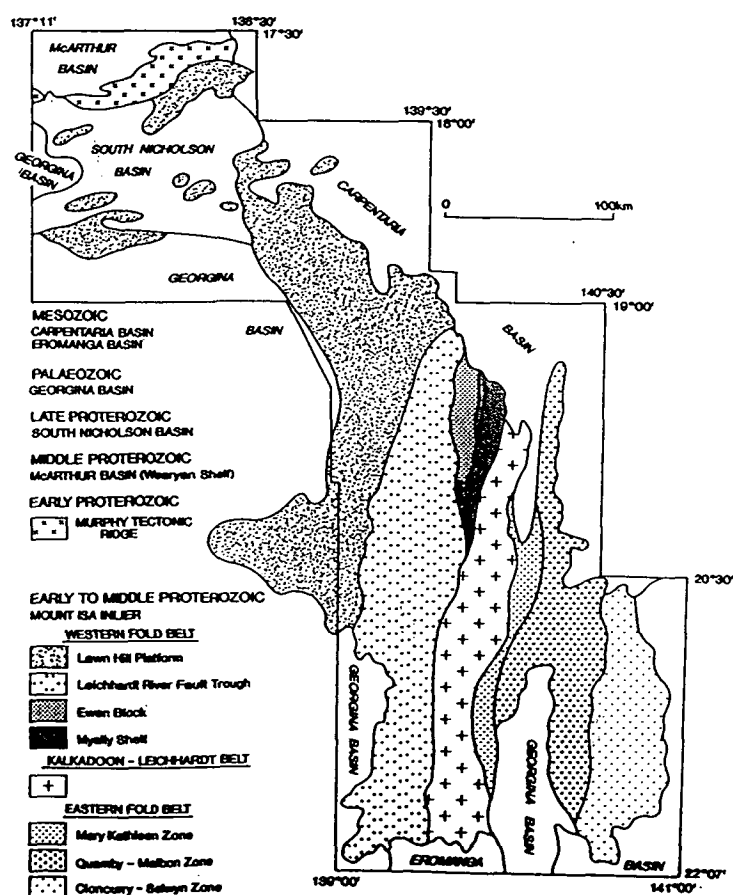


Figure 2.1 Tectonic Zones (Blake, 1987)

Blake (1987) has further subdivided the Eastern Fold Belt into the Mary Kathleen, Quamby-Malbon and Cloncurry-Selwyn zones. Within this tectonic framework four major Proterozoic sequences have been defined (Blake, 1987). The oldest rocks exposed, the basement, represent sedimentary, volcanic and intrusive rocks which were highly deformed and metamorphosed during the 1900 - 1870 Ma Barramundi Orogeny, and overlain by three younger sequences of Proterozoic volcanosedimentary rocks. Cover sequence 1 (1875 - 1850 Ma) consists mainly of subaerial felsic volcanics, cover sequence 2 (mostly 1790 - 1760 Ma) and cover sequence 3 (mostly 1680 - 1670 Ma) comprise felsic and mafic volcanics and predominantly shallow water sediments (Figure 2.2; Blake, 1987).

Ch 2.1.3 Stratigraphic Framework

Cover sequence 1 is confined to the Kalkadoon - Leichhardt Belt. It consists mainly of the Leichhardt Volcanics and the coeval granites of the Kalkadoon and Ewen Batholiths. These range in age from about 1870 to 1850 Ma (Page 1988). Wyborn (1988) suggests that they are part of an Australia-wide 1880 - 1840 Ma felsic magmatic event.

Cover sequence 2 ranges in age from about 1790 Ma, the age of the Bottletree Formation at the base of the Leichhardt River Fault Trough succession, to perhaps 1760 or 1720 Ma (Page, 1988; Blake and Stewart, 1992). Cover sequence 2 occurs in all three major tectonic units. In the eastern part of the Kalkadoon-Leichhardt Belt, the Ballara Quartzite and overlying Corella Formation, correlatives of the Quilalar Formation, crop out on both sides of a north-south trending highly deformed zone known as the Wonga Belt. East of this belt, in the Mary Kathleen Zone of Blake (1987) they lie unconformably on basement Kuribayia Migmatite (Blake, 1992), and include significant amounts of basaltic volcanics. The cover sequence 2 units on both sides of the Wonga Belt are intruded by, and hence older than, 1760 - 1730 Ma granites of the Wonga Batholith (Pearson et al., 1992, Blake and Stewart, 1992).

Cover sequence 2 dominates the Eastern Fold Belt. The oldest rocks occur in the western part of this belt and have been mapped as Argylla Formation (Tewinga Group), which comprises a package of acid volcanics and sediments, averaging 2000 thick and dated as 1780 Ma (Page, 1978). The Tewinga Group is overlain by the Malbon group which commences with a 900 to 2,300m thick sequence of amygdaloidal iron and titanium-rich tholeiitic basalt and clastics, termed the Marraba Basalt (Derrick, 1980). The Marraba Basalt is overlain by the Mitakoodi Quartzite which is mainly comprised of thickly laminated sandstone, but contains some intercalated pillowed basalt flows and siltstone-shale bands. (Table 2.1).

TABLE 2.1

DESCRIPTIONS OF STRATIGRAPHIC UNITS, MOUNT ISA INLIER

(modified from Blake and Stewart, 1992).

Unit	Main rock types at lowest metamorphic grade (maximum thickness in metres)
Quamby Conglomerate <u>COVER SEQUENCE 3</u>	Conglomerate, lithic sandstone (300+)
Tommy Creek beds McNAMARA GROUP	Calcareous and pelitic metasediments, bimodal volcanics (1000+)
MOUNT ISA GROUP	Dolomite, siltstone; quartz sandstone and conglomerate at base (8500)
Surprise Creek Formation	Siltstone, shale - commonly dolomitic or pyritic; quartz sandstone and conglomerate at base (4500+)
Carters Bore Rhyolite	Sandstone, siltstone, shale (2000+)
Fiery Creek Volcanics	Porphyritic rhyolite, conglomerate (200+)
Bigie Formation	Rhyolite, basalt, sandstone, conglomerate (250)
<u>SOLDIERS CAP GROUP</u>	Lithic and feldspathic sandstone, conglomerate (600)
<u>? COVER SEQUENCE 3</u>	Greywacke, siltstone, sandstone, metabasalt (5000+)
Lady Clayre Dolomite	Dolomite, dolomitic siltstone (3000)
Coocerina Formation	Calcareous black shale, scapolitic siltstone (400)
Knapdale Quartzite	Sandstone (2000+)
<u>COVER SEQUENCE 2 -west of Pilgrim Fault</u>	
MOUNT ALBERT GROUP	
White Blow Formation	Pelitic and calcareous metasediments (1000)
Deighton Quartzite	Feldspathic, lithic and quartz sandstone (2700)
Corella Formation	Banded calc-silicate rocks, metapelite, metasiltstone, marble, felsic and mafic volcanics (1000+)
Ballara Quartzite	Quartz and feldspathic sandstone (1250)
Quilalar Formation	Quartz and feldspathic sandstone in lower part; calcareous and micaceous siltstone, greywacke, sandstone and dolomite in upper part (1500+)
Argylla Formation	Felsic volcanics (2000)
Magna Lynn Metabasalt	Metabasalt, sandstone (1500)
HASLINGDEN GROUP	
Myally Subgroup	Feldspathic and quartz sandstone (3700+)
Eastern Creek Volcanics	Metabasalt, sandstone (7200)
Mount Guide Quartzite	Greywacke, conglomerate in lower part; quartz sandstone in upper part (6000+)
Bottletree Formation	Greywacke, conglomerate, bimodal volcanics (3000)
<u>COVER SEQUENCE 2 -east of Pilgrim Fault</u>	
MARY KATHLEEN GROUP	
Roxmere Quartzite	Feldspathic sandstone (2000+)
Corella beds	Banded and brecciated calc-silicate rocks (1000+)
Doherty Formation	Banded and brecciated calc-silicate rocks (1000+)
Marimo Slate	Carbonaceous slate and siltstone (2000)
Staveley Formation	Evaporitic and partly calcareous sandstone, siltstone, shale, mudstone and basalt (2000+)
Answer Slate	Partly carbonaceous slate and siltstone (1000+)
Kuridala Formation	Greywacke, siltstone, carbonaceous slate (1000+)
Overhang Jaspilite	Siltstone, chert, marble, jaspilite (1000)
MALBON GROUP	
Mitakoodi Quartzite	Quartz and feldspathic sandstone (3000)
Marraba Volcanics	Mafic volcanics, siltstone, sandstone (3500)
Argylla Formation	Felsic volcanics, sandstone (2000+)
<u>COVER SEQUENCE 1</u>	
Leichhardt Volcanics	Felsic volcanics (1000+)
Orient beds	Sandstone, siltstone, conglomerate, carbonates (1000+)
Candover Metamorphics	Siltstone, sandstone, bimodal volcanics (1000+)
<u>BASEMENT</u>	
Yaringa Metamorphics	Schist, gneiss, migmatite
Kurbayia Migmatite	Migmatite, gneiss, schist
Plum Mountain Gneiss	Quartzofeldspathic gneiss
Double Crossing Metamorphics	Gneiss, schist, migmatite

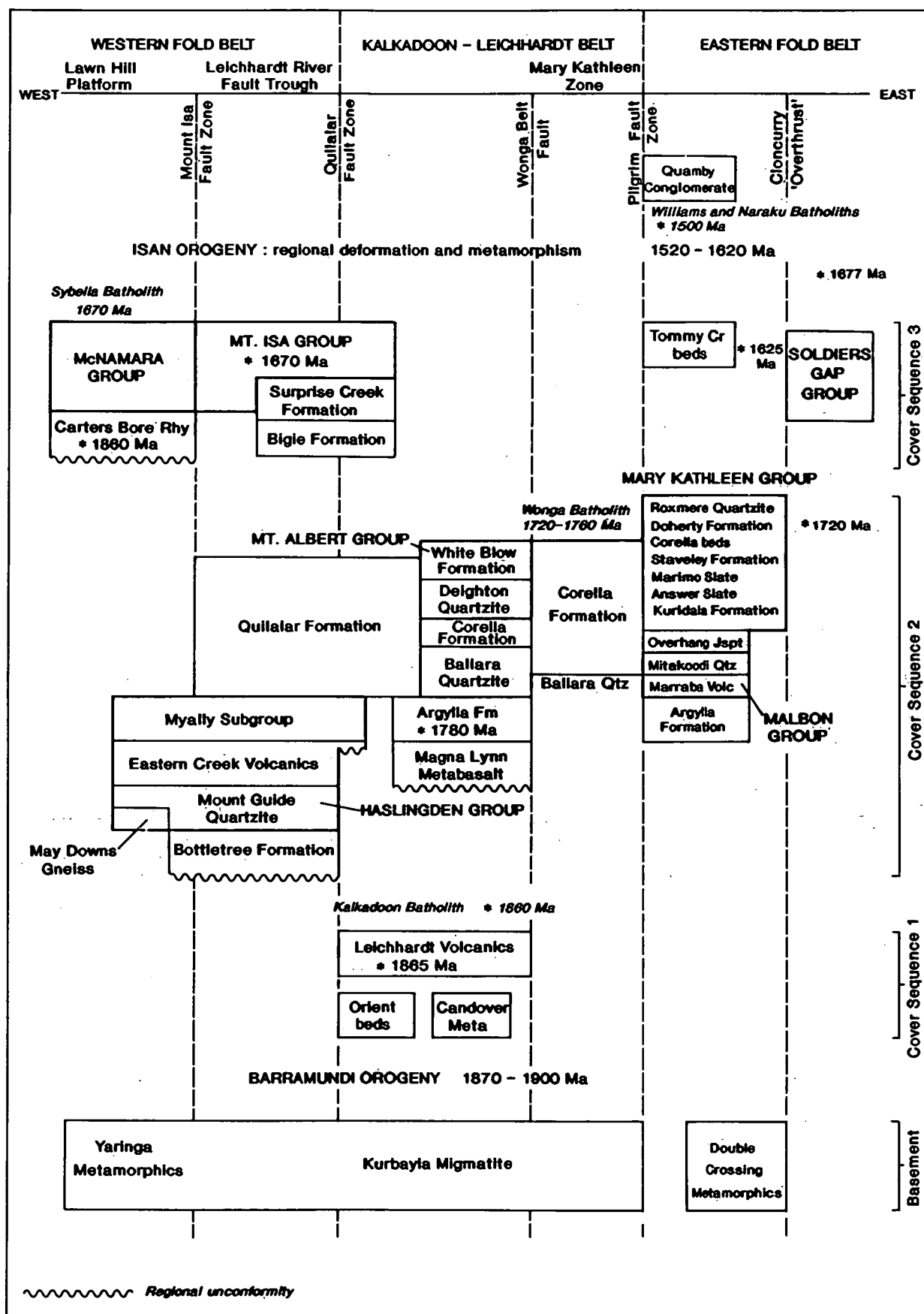


Figure 2.2 Stratigraphic framework. (Modified from Blake and Stewart 1992)

Stewart (1991,1994) tentatively suggests that this basalt quartzite package forms a significant time stratigraphic marker between the rift basins and, by implication, may correlate with the Eastern Creek volcanics (Western Fold Belt) and the Toole Creek Volcanics - Mt Norna Quartzite (Soldiers Cap Group, Eastern Fold Belt), however this is not supported by recent age dating of the Soldiers Cap Group at <1677 Ma by Page (1993).

Conformably overlying the Malbon Group is the Mary Kathleen Group which consists predominantly of metasediments, including evaporites, carbonates, calcsilicate rocks and black slate. The Mary Kathleen Group commences with the 300 to 900 metre thick Overhang Jaspilite which consists of thinly bedded limestone, shale, siltstone, marl and jaspilite beds, for which Derrick (1980) suggests a shallow, evaporitic, intertidal to platform environment. This unit is well known for its baryte and manganese accumulations. In the Kuridala area, this is conformably overlain by the Answer Slate which may be up to 1,000m thick (Donchak et al., 1983), but relationships and correlations with overlying units are not clear.

In the Marimo Basin area, Derrick (1980) suggests that the Marimo Slate and the Corella Formation are partly equivalent and both overlie the Overhang Jaspilite (Figure 2.3; Plate 3.1). Loosveld (1988) suggests that the contact of the Marimo Slate with the underlying Overhang Jaspilite is concordant, but highly strained and may even be conformable.

The Corella Formation is the most extensively expressed formation in the Eastern Fold Belt and is estimated to be from 2000 to 4000m thick (Figure 2.4). It comprises banded and brecciated limestones and calcsilicates, sometimes scapolitic, often karstified, as well as pelitic and psammitic units. Blake (1982) has broadly subdivided the Corella Formation into three zones. The Corella Formation in the Marimo Basin Area is described as Blake's "central and eastern zones".

The intensely metasomatised Doherty Formation was previously mapped by Carter et al. (1961) as Corella Formation. Donchak and others (1983) suggest that the Doherty Formation, which consists predominantly of altered calc-silicate rocks (Blake, 1982) and contains a quartz porphyry that has been dated at 1725 ± 3 Ma (Page, 1993), is distinguishable from the Corella Formation containing the designated type section of Carter et al. (1961), and is in contact with units which are not obvious correlatives of those adjacent to the type section of the Corella Formation (Blake, 1982). Williams and Blake (1993) suggest that the Doherty Formation may in part be an altered equivalent of the meta-evaporite and carbonate-rich Corella Formation. This view is supported on the Cloncurry 1:100,000 sheet by Ryburn et al., (1988).

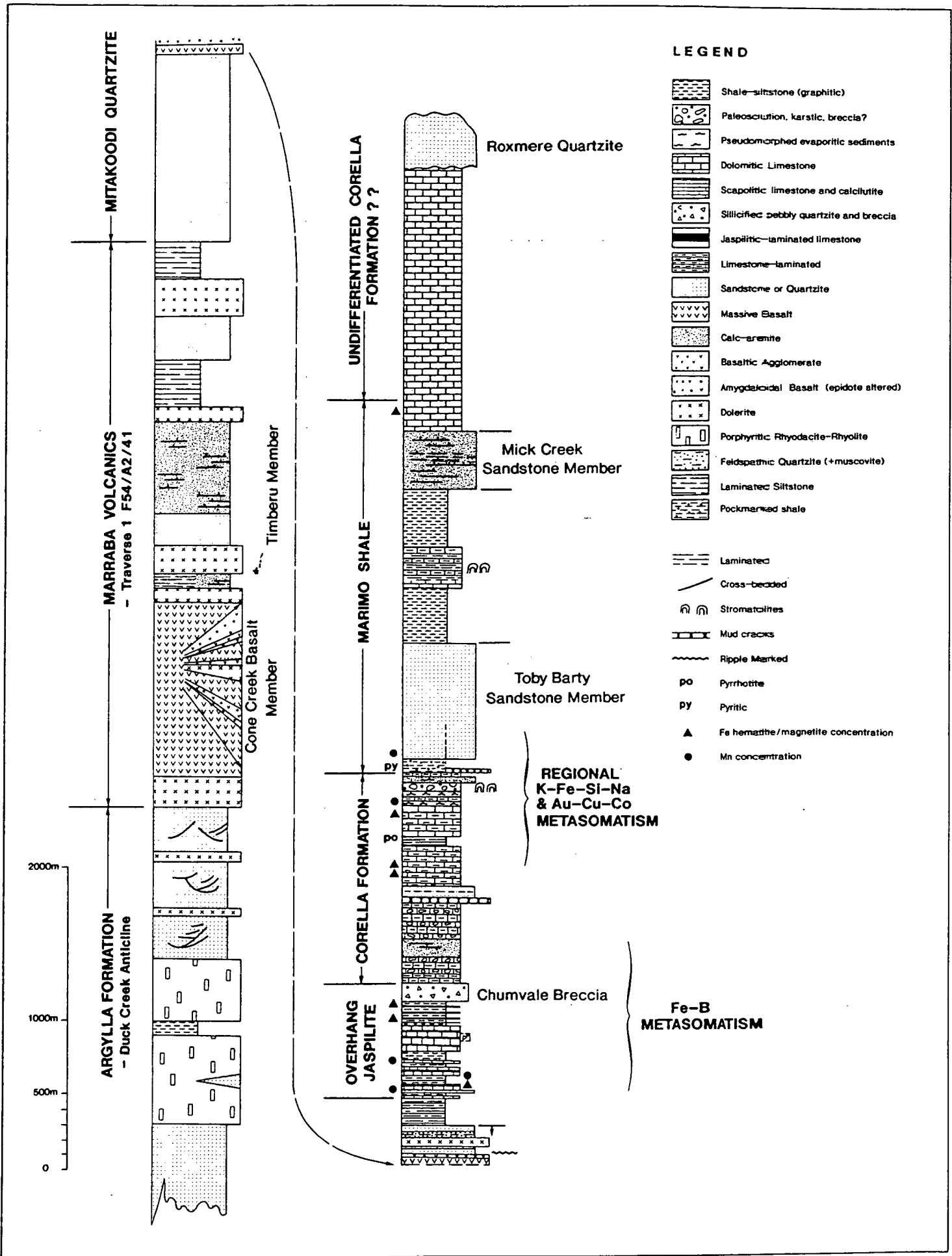


Figure 2.3 Stratigraphic Column for the Malbon - Marimo Area (From Derrick et al., 1971, 1977 ; Stewart., 1994)

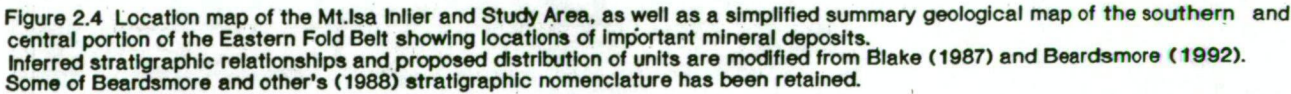


Figure 2.4 Location map of the Misisa Inlier and Study Area, as well as a simplified summary geological map of the southern and central portion of the Eastern Fold Belt showing locations of important mineral deposits. Inferred stratigraphic relationships and proposed distribution of units are modified from Blake (1987) and Beardsmore (1992). Some of Beardsmore and other's (1988) stratigraphic nomenclature has been retained.

Conformably overlying the Corella Formation is the Staveley Formation, which Ryburn et al. (1988) suggest may lie between the Marimo Slate and Corella beds, as it shares characteristics with both. It is at least 2,000 metres thick, and comprises an evaporitic metasedimentary package with subordinate altered basalts (Davidson et al., 1989; Stewart, 1991, 1994; Blake, 1987). This unit will be discussed in more detail in chapters 3 and 4.

Conformably overlying and transitional to the Staveley Formation is the Marimo Slate which comprises variably carbonaceous slate and siltstone with subordinate sandstone, chert, cherty siltstone, breccia and marble (Blake, 1987). This unit will also be discussed in more detail in chapters 3 and 4.

The Roxmere Quartzite, comprising dominantly feldspathic sandstone, has previously been assigned to the Mount Albert Group of cover sequence 3 by Derrick et al. (1977), however Loosveld (1989, 1992) and Ryburn (1988) suggest that it may belong to the Mary Kathleen Group.

Cover sequence 3 is largely confined to the Western Fold Belt and western part of the Kalkadoon-Leichhardt Belt, where it overlies cover sequence 2 disconformably and locally with angular unconformity (Blake and Stewart, 1992). The oldest unit may be the Carters Bore Rhyolite, dated at 1680 Ma by Page (1993). This rift-type unit is overlain by sag-phase sediments of the Surprise Creek Formation, Mt Isa Group and McNamara Group. An age of 1653 ± 7 Ma has been confirmed for the Mt Isa Group from thin felsic tuff in the Urquhart Shale by Page (1993). The latter two Groups correlate with the McArthur Group of the McArthur Basin.

The isotopic dating indicates a time gap of about 70 Ma between deposition of cover sequences 2 and 3 in the Western Fold Belt; each is probably associated with different basin forming events.

Some possible cover sequence 3 units are exposed within fault bounded blocks in the Eastern Fold Belt. These are the Knapdale Quartzite, Coocerina Formation, Lady Clayre Dolomite, and probably that part mapped as Corella Formation that containing the Dugald River Shale Member, all of which crop out in the vicinity of the Dugald River prospect and the Tommy Creek Beds between Cloncurry and Mary Kathleen (Blake and Stewart, 1992). The Tommy Creek Beds, previously mapped as part of the Corella Formation (Derrick, 1980), include felsic volcanics dated at 1626 Ma (Hill et al., 1992) and hence are appreciably younger than the Mt Isa Group.

Blake and others (1983), Laing and Beardsmore (1986), and Beardsmore and others (1988) correlated the Soldiers Cap Group with the lithologically similar Kuridala Formation. The Soldiers Cap group comprises the Llewellyn Creek Formation (dominantly turbidites and greywackes) conformably overlain by the quartzofeldspathic sediment dominated Mt Norna Quartzite, and the Toole Creek Volcanics, which predominantly consist of tholeiitic basalts, banded iron formations and volcanoclastics. Beardsmore and others (1988) also defined two additional units, which comprise the Fullarton River Group. They proposed to abolish the Kuridala Formation and to upgrade the status of the Soldiers Cap Group to include the Kuridala Formation and the Fullarton River group as comprising the Maronan Supergroup, which was correlated with Blake's (1987) cover sequence 1, the Leichhardt Volcanics (1875 to 1865 Ma; Page, 1978, 1983).

Their arguments have, however, been questioned by Loosveld (1988) who argues for an age of approximately 1780 - 1759 Ma, and correlated the Soldiers Cap Group with Blake's (1987) cover sequence 2, and therefore between 1810 and 1880 Ma. Derrick (1976), Blake and others (1984) and Laing and Beardsmore (1986) drew lithostratigraphic comparisons between parts of the Eastern Fold Belt and parts of the Willyama Supergroup near Broken Hill, now dated at 1690 ± 5 Ma (Page and Laing, 1992). The Gandry Dam Gneiss (Fullarton River Group) of Beardsmore et al. (1988) has recently been dated at 1677 ± 9 Ma (Page, 1993). This is a maximum depositional age for this part of the sequence and indicates that they are much younger than hitherto considered, synchronous with Blake's (1987) cover sequence 3. The contact of the central Soldiers Cap group with the Marimo - Staveley Block is either tectonic (the Cloncurry Overthrust) or obscured under calc-silicate breccias (Loosveld, 1992).

Deposition of cover sequence 3 was terminated by the Isan Orogeny, a period of high temperature and low pressure metamorphism (1620 Ma - 1520 Ma). This orogeny post-dates the Sybella Batholith (1670 Ma: Page, 1978), and was closely followed, at around 1500 Ma (Page, 1988), by intrusion of granite plutons (Naraku and Williams Batholiths) in the Eastern Fold Belt (Blake and Stewart, 1992).

Sometime later in the Proterozoic, coarse clastics of the Quamby Conglomerate were deposited in the Eastern Fold Belt, and crop out in two narrow fault bounded areas, close to the Pilgrim Fault Zone. It is folded but not metamorphosed.

Ch 2.1.4 Igneous Activity

Igneous activity in the Mt Isa Inlier commenced sometime prior to the 1870 Ma Barramundi Orogeny and probably ended at around 1116 ± 12 Ma (Page, 1983) with the emplacement of the Lakeview Dolerite. Throughout this period, the magmatism was predominantly bimodal. Wyborn et al. (1987, 1988) discuss the petrology, geochemistry and geochronological signatures of Australian Proterozoic igneous rocks. Of particular interest to this study are the Williams and Naraku Batholiths which are the dominant intrusive suites of the Eastern Fold Belt (Table 2.2). These 1560 - 1480 Ma granites are mineralogically and chemically distinct from any other felsic intrusives in the Mt Isa Inlier, and show the best evidence for crystal fractionation producing a series of coeval but compositionally distinct plutons (Wyborn, 1992). Widespread metasomatic alteration and brecciation of the country rocks and granite is associated with the more SiO_2 - enriched phases. Wyborn (1992) suggests that these highly fractionated I-type granites are petrogenetically similar to the granites of the Stuart Shelf region (Hiltaba Granite; Wyborn et al., 1987) including the host rocks at the Olympic Dam Cu-Au-U deposit. Figure 2.5 shows the compositional variation in the Williams Batholith and Figure 2.6 shows the distribution of granites in the eastern Mount Isa Inlier.

Ch 2.1.5 Deformation Events and Structural Style

The Mt Isa Inlier has a complex Proterozoic history of deformation, dominated at different periods by extension, shortening and transcurrent faulting. For example, kinematic indicators on the Cloncurry Overthrust show all three movement styles (P. Williams, pers. com., 1993).

The first major deformation event was the Barramundi Orogeny which was dated at around 1870 Ma (Page, 1988). This east-west compressional event, tightly folded and partially melted some units prior to the onset of Leichhardt volcanism of cover sequence 1 (Table 2.2). The Barramundi event has not been identified in the Eastern Fold Belt.

The Barramundi compressional deformation was followed by extension from 1870 - 1760 Ma, leading to basin formation and deposition of cover sequences 1 and 2, with probably two phases of rifting and thermal subsidence.

Further extension occurred between 1760 and 1700 Ma. This was pre-Isan Orogeny and probably coeval and emplacement of the spatially associated granites of the Wonga Batholith. Extensional structures post-dating cover sequence 2 have been documented by Holcombe and others (1992). Pearson and others (1992), Oliver and others (1992) and Passchier (1986).

Name of Unit (reference to definition)	Lithology	Relationships
Foliated granites Blackeye Granite (Blake & others, 1981a)	Foliated leucocratic granodiorite and minor pegmatite	Intrudes Doherty Formation
Cowie Granite (Blake & others, 1981a)	Generally foliated biotite-bearing leucocratic granite, granodiorite, and tonalite: pegmatite	Intrudes Soldiers Cap Group and Doherty Formation: intruded by Squirrel Hills Granite
Maramungee Granite (Blake & others, 1981a)	Generally foliated biotite-bearing leucocratic granite, granodiorite, and tonalite: pegmatite	Intrudes Soldiers Cap Group; cut by dolerite dyke
Non-foliated granites Wimberu Granite (Carter & others, 1961)	Commonly porphyritic granite and granodiorite containing biotite and/or hornblende = clinopyroxene: subordinate finer-grained non-porphyritic biotite granite: minor aplite and pegmatite	Intrudes Argylla Formation. Marraba Volcanics, Mitakoodi Quartzite. Overhang Jaspilite. Answer Slate. Doherty Formation, Staveley Formation and metadolerite.
Gin Creek Granite (Blake & others, 1981a)	Partly porphyritic biotite granite: subordinate slightly foliated line to coarse leucogranite containing muscovite and tourmaline, and intensely foliated biotite granite with abundant inclusions mostly of gneiss and schist derived from the Double Crossing metamorphics; minor biotite microgranite, aplite, and greisen	Intrudes Double Crossing Metamorphics, Answer Slate, Staveley Formation, Kuridala Formation and metadolerite
Mount Angelay Granite (Blake & others, 1981a)	Partly porphyritic granite containing biotite and/or hornblende and/or clinopyroxene; minor leucogranite, porphyritic microgranite, contaminated grey granite, aplite, and pegmatite; xenoliths common near margins of granite	Intrudes Soldiers Cap Group and Doherty Formation; cut by dolerite dykes
Mount Cobalt Granite (Blake & others, 1981a)	Biotite granite and minor aplite	Intrudes Kuridala Formation and metadolerite
Mount Dore Granite (Blake & others, 1981a)	Biotite and hornblende-biotite granite, porphyritic in places: Minor microgranite, aplite, pegmatite and greisen	Intrudes Kuridala Formation and metadolerite
Saxby Granite (Blake & others, 1981a)	Biotite and hornblende-bearing granite: minor leucogranite, xenolithic diorite, monzonite, granodiorite, aplite and pegmatite	Intrudes Soldiers Cap Group, Doherty Formation, and metadolerite: cut by dolerite dykes
Squirrel Hills Granite (Blake & others, 1981a)	Commonly porphyritic granite containing hornblende and/or biotite and locally clinopyroxene; minor aplite, porphyritic microgranite, monzonite, and granoliorite; rare pegmatite	Intrudes Soldiers Cap Group and Kuridala, Doherty, and Staveley Formations, Cowie Granite, and metadolerite; cut by dolerite dykes
Yellow Waterhole Granite (Blake & others, 1981a)	Partly porphyritic biotite and hornblende-biotite granite: minor aplite	Intrudes Kuridala Foundation
Undivided granite	Foliated leucocratic tonalite and pegmatite; biotite granite: minor hornblende-biotite tonalite	Intrudes Soldiers Cap Group, Kuridala Formation, and Doherty Formation

TABLE 2.2

Granites of the Williams Batholith. From Blake et al. (1984).

Figure 2.5
 Compositional variation in the eastern half of the Williams and Naraku Batholiths.
 Lines indicate the level of erosion on the relevant 1:100 000 Sheet area. (from Wyborn, 1992)

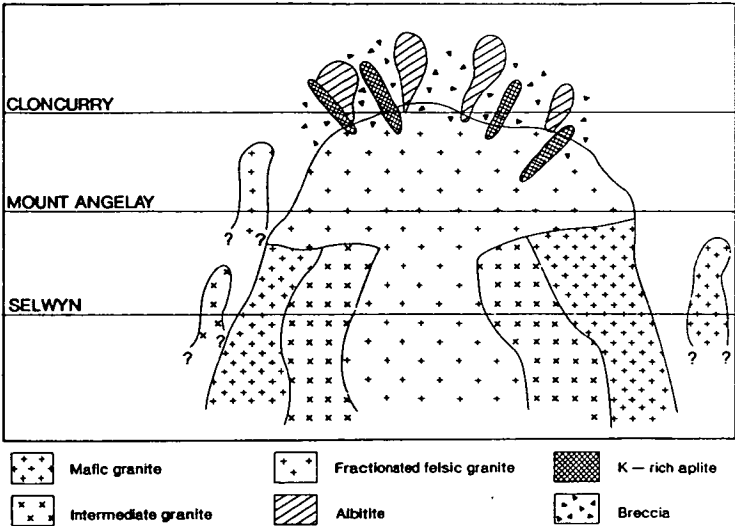
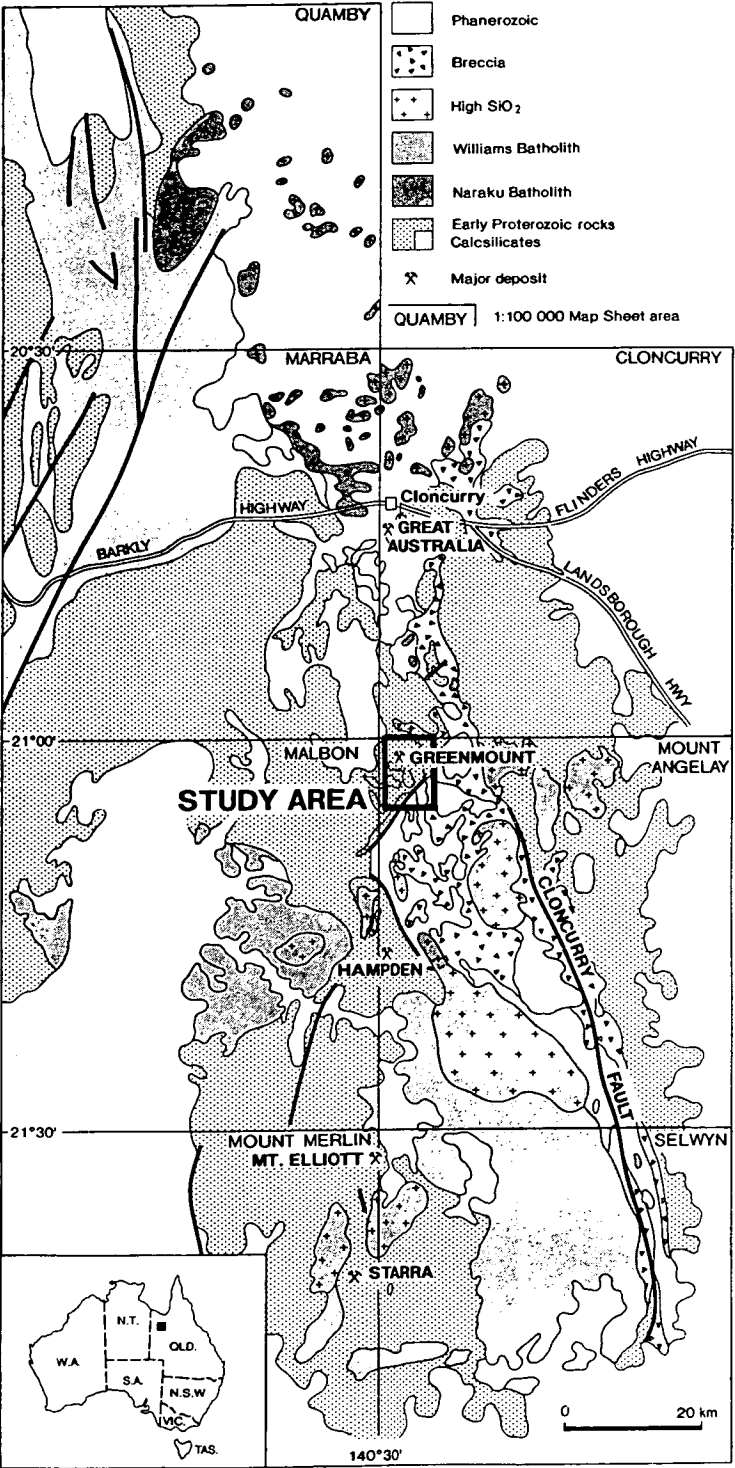


Figure 2.6
 Distribution of granite in the eastern Mount Isa Inlier.
 (NB. Breccias have only been distinguished in regional mapping in the Cloncurry, Mount Angelay, and Selwyn 1:100 000 Sheets: they may be more extensive on the remaining map sheets.)
 Modified from Blake (1987: Geology of the Mount Isa & Environs, Queensland & Northern Territory 1:500 000 scale map. Bureau of Mineral Resources, Canberra.)



<u>EVENT</u>	<u>AGE</u>
Major deformations: Isan Orogeny	
D3: (Page and Bell, 1986)	1510 ± 13 Ma
D2: (Page and Bell, 1986)	1544 ± 12 Ma
D1: (Page and Bell, 1986)	1610 ± 13 Ma
Major deformations: Barramundi Orogeny	1885 ± 10 Ma
Major igneous intrusion episodes (Wyborn et al. 1988)	1560 - 1480 Ma 1700 - 1670 Ma 1760 - 1740 Ma 1820 - 1800 Ma 1870 - 1840 Ma
First appearance of red-beds, carbonates and evaporites throughout the Mount Isa Inlier	1780 - 1740 Ma
Main sedimentation, commencing with widespread basic volcanism, including:	
Cover Sequence 3	1680 - 1670 Ma
Cover Sequence 2	1808 - 1720 Ma
	1808 - 1670 Ma
(Page 1978, 1983a, 1983b)	
Felsic volcanism of Cover Sequence 1 (Page 1983)	1865 - 1852 Ma
Oldest crust below the Mount Isa region (as indicated by inherited zircons within the Eastern Creek Volcanics)	2100 - 1800 Ma 2700 - 2500 Ma

TABLE 2.3 *A summary of the timing of geological events in the Mount Isa Inlier.
(adapted from Davidson, 1989)*

Between 1700 and 1660 Ma, a further period of extension was associated with cover sequence 3 and possible related to emplacement of the Weberra Granite and the Sybella Batholith. Cover sequence 3 was probably deposited in extensional basins and comprises basal rift-type deposits succeeded by typical thermal subsidence sediments.

The next major deformation event was the Isan Orogeny, between 1620 and 1520 Ma. The first phase was termed D1 by Bell (1983) and comprised dominantly north-south compression which resulted in thrusting and folding. This has been dated at around 1620 Ma by Page and Bell (1986).

A later phase of east-west compression, D2, resulted in the formation of the major north trending upright folds characteristic of much of the Mt Isa Inlier. Peak regional metamorphism occurred during D2, which has been dated at around 1520 Ma (Page and Bell, 1986).

Shortly after the Isan Orogeny, crustal extension emplaced the large granite plutons of the Williams and Naraku Batholiths, during D3 at around 1500 Ma.

Subsequent transcurrent faulting cut and hence post date Isan folds. The major faults may have displacements of many kilometres, but many do not mark abrupt changes in metamorphic grade, and so appear to have predominantly horizontal displacements (Blake and Stewart, 1992). Many have probably been reactivated several times, including during the Phanerozoic.

CHAPTER 3 Geology and Structure of the South Eastern Marimo Basin

Ch 3.1 Introduction

Much of the following compilation is based on work conducted by numerous Homestake Geologists, Stewart (1991, 1994), structural consultants ERA-Maptec (1994) and the author. This section significantly revises and changes the corresponding portion of the published Cloncurry 1:100,000 map (Ryburn et. al., 1988).

Ch 3.2 Lithostratigraphy

The stratigraphy has been described in detail by Stewart (1991). A non-structurally juxtaposed interface between the Staveley Formation and the overlying Marimo Slate, from the Just Found area was described in detail and evaporitic textures were documented for the Staveley Formation (Plates 3.2 to 3.5). Stewart (1991,1994) views the Staveley Formation as transitional to the Corella Formation and the Marimo Slate and that the Marimo Basin may have been a shale depocentre on the Mary Kathleen Shelf. Under the Schreiber (1988) classification, a peritidal coastal sabkha or intertidal-supratidal setting seems likely. Several other conformable and transitional contacts between the Corella, Staveley and Marimo Slate rock types have been described by ERA - Maptec (1994). Other stratigraphic packages in the area include the Roxmere Quartzite, numerous small mafic intrusives as well as small felsic intrusives which are probably apophyses of the Williams Batholith (Figure 3.1). The metamorphic grade, defined by the presence of biotite-sericite, is lower to middle greenschist facies.

Ch 3.2.1 Corella Formation

The Corella Formation in the area is dominantly a grey-white laminated, often scapolitic limestone-calcsilicate granofels (Plate 3.6 to 3.8). It is generally a relatively hard and impermeable unit which often forms ridges and hills.

Ch 3.2.2 Staveley Formation

Ryburn et al. (1988) describe the Staveley Formation primarily as a fine to medium grained, massive to well bedded sandstone unit with subordinate proportions of siltstone and calcareous, albitic and dolomitic rocks with some sedimentary banded iron formations. They note ripple marks, halite casts, desiccation cracks and extensive brecciation.

Plate 3.1 (A) View to the south on the Mt McCabe Track. The hills represent the Overhang Jaspilite (black pinnacle is a supergene manganese deposit). The Corella Formation and the Marimo Slate are to the left and underfoot.

Plate 3.2 (B) Staveley Formation “Trash Bed” of silicified nodular pseudomorphs of (?) Gypsum. Note the apparent displacive growth in soft sediment on the far left. Sample from the Just Found Prospect.

Plate 3.3 (C) Disseminated bedding parallel quartz pseudomorphing evaporitic sulfate minerals in feldspar - sericite (\pm dolomite), decalcified dolomite rock, from the Staveley Formation near the Just Found Prospect.

Plate 3.4 (D) Dissaggregated semi-massive, diagenetically altered dominantly silica - microcline) evaporitic bed from the Staveley Formation. Silicified pseudomorphs are after salts and sulfates, including halite, gypsum and anhydrite.

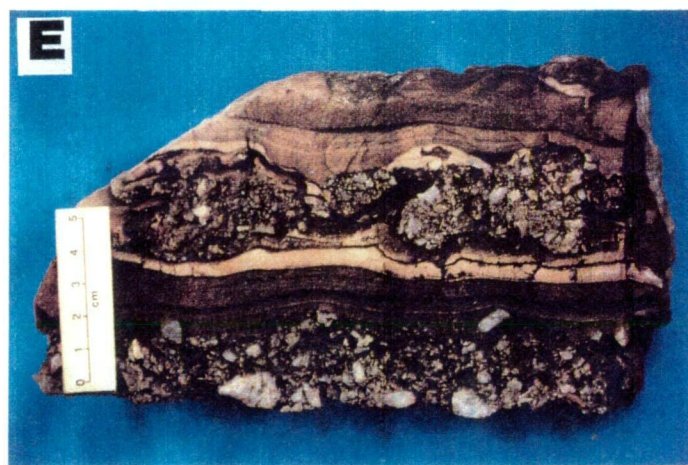
Plate 3.5 (E) Diagenetic displacive growth of anhydrite (now pseudomorphed by quartz) nodules into soft sediment with draping and slumping of overlying ex-calcilutite. The central silicified intraformational breccia displays relict enterolithic layering which became increasingly disaggregated and brecciated. Many of the cherty (anhydrite nodule) pseudomorphs contain fresh chalcopyrite and pyrite inclusions, commonly assaying around 2000 ppm Cu.

Plate 3.6 (F) Upper Corella Formation laminated dolomitic carbonate and siltstone, approximately 2km south of the Greenmount deposit.

Plate 3.7 (G) Highly strained Corella Formation exhibiting spaced cleavage and weak S-C fabric. View is approximately 400m west of the Greenmount deposit, looking north. The dark pinnacle is one of many possibly detrital haematitic banded iron formations hosted by the Staveley Formation. The NE trending Greenmount fault occurs somewhere between the carbonates in the foreground and the BIF in the background.

Plate 3.8 (H) Close up of Corella Formation in Plate 3.7.

• *Plates 3.1 to 3.5 Courtesy of J.I. Stewart*



A conformable sequence of the Staveley Formation (80 - 100m wide) as measured near the Just Found prospect, comprises from the base, increasingly evaporitic dolomite, interbedded nodular evaporite dolomite, interbedded calcarenite and dolomite, laminated to massive limestone, laminated dolomite, interbedded laminated mud-chip dolomite and massive recrystallised dolomite, nodular evaporitic dolomite, laminated dolomite and evaporite beds, slumped evaporitic dolomite, pockmarked ankeritic feldspathic dolomite, passing up into the Marimo Slate (Figure 3.2).

A range of textures observed by Stewart (1991) in these chertified evaporitic sediments includes enterolithic layers, disaggregated nodules, cauliflower textured and embayed nodules (after diagenetic alteration of sulphates), shingle beds, desiccation cracks, soft sediment slumping and abundant hypersaline fluid inclusions (Plates 3.2 to 3.5).

Ankerite-dolomite, hematite and chalcopyrite inclusions in “chert” nodules may provide evidence that these shallow marine evaporitic sulphates underwent Ca-Mg-Fe carbonate metasomatism and copper enrichment during diagenetic disintegration of the sulphate forms but prior to general silicification (Stewart, 1994).

Evaporitic features are often absent or not recognised in many other parts of the Staveley Formation. Recent mapping has revealed that the Staveley Formation is more extensive than previously recognised (Figure 3.1).

Ch 3.2.3 Marimo Slate

The Marimo Slate is dominated by massive to laminated, grey to dark grey with subordinate variably carbonaceous siltstone calcaneus slate, phyllite, metasiltstone and fine metasandstone (Plate 4.1). It is the dominant unit in the area.

Ch 3.2.4 Roxmere Quartzite

The Roxmere Quartzite is always fault bounded and consists mainly of grey, medium to thin bedded, cross bedded and ripple-marked impure quartzite and quartzo-feldspathic sandstone.

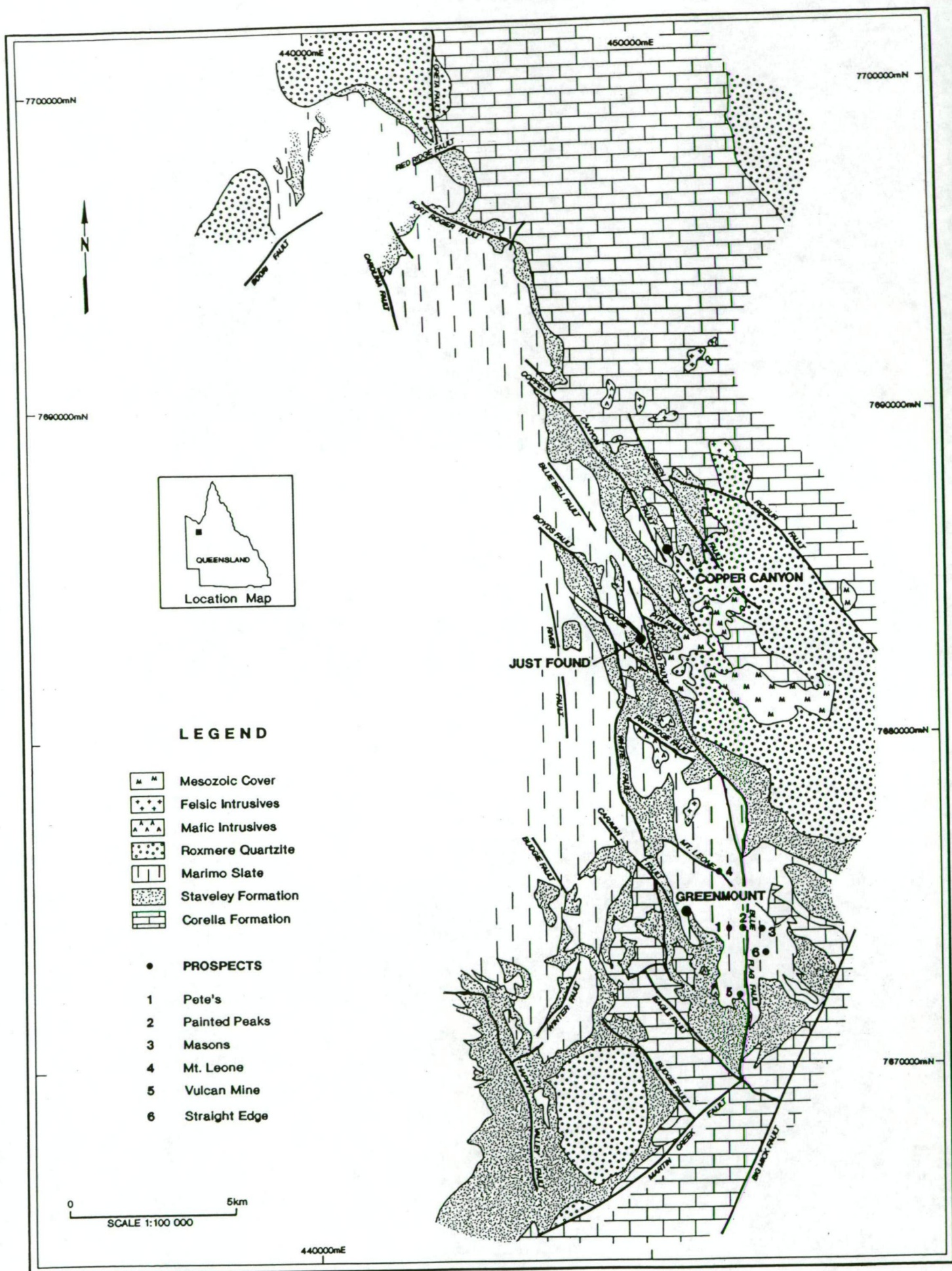


Figure 3.1 Interpreted geology of the Eastern Marimo Basin. Compiled from Homestake mapping, Ryburn et. al. (1988) and ERA-Maptec (1994).



Figure 3.1b Interpreted structures of the Eastern Marimo Basin. (Modified from ERA-Maptec 1994)

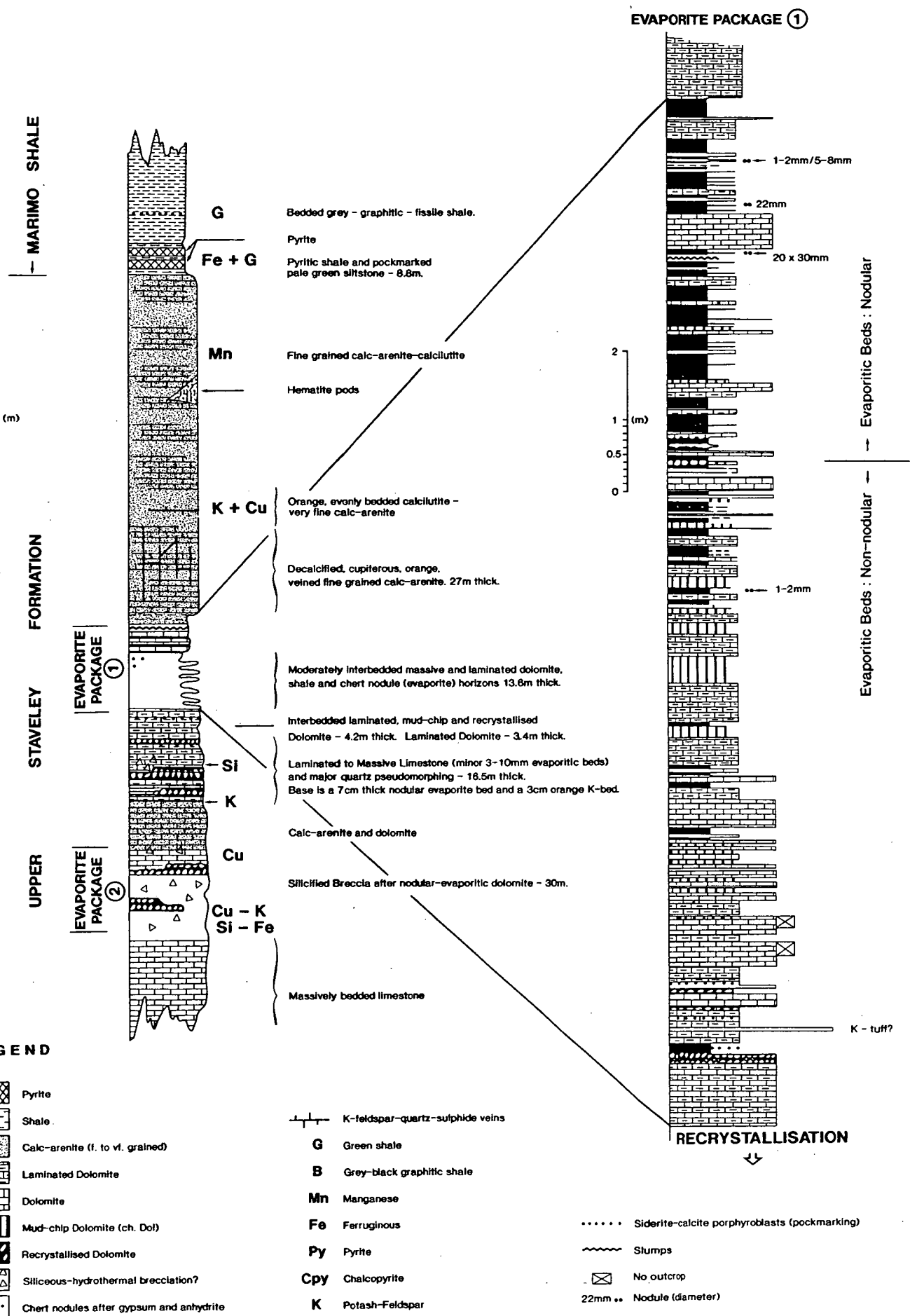


Figure 3.2 Detailed Stratigraphic Column of Evaporitic Dolomites from the Staveley Formation at Just Found. (Stewart, 1991)

Ch 3.2.5 *Intrusives*

Numerous mafic intrusives consisting chiefly of gabbros and dolerites occur throughout the area. No attempt has been made to classify them into the scheme of Ellis and Wyborn (1984), but morphology and textures suggest that most are probably post-metamorphic E3 dykes.

Several felsic plutons occur throughout the area. All are post-metamorphic, unfoliated granites which are petrogenetically related to the Williams Batholith. Several of these have been sampled and geochemically analysed (Chapter 5). Whole rock and trace element analyses reveal that all are highly differentiated sodic I-type granites, with Na₂O contents, commonly in excess of 5 wt%. Some are classified as albitites (Wyborn, Pers. com., 1994).

Ch 3.3 *Regional Metasomatism*

Stewart (1991,1994), interprets numerous regional metasomatic events which are often observed near the Marimo Slate - Staveley Formation boundary. Some of the dominant regional metasomatic events are diagenetic chalcopyrite - pyrite mineralisation commonly around 2,000 ppm Cu at the Just Found prospect), ankerite alteration, early silicification of sulphates, microcline metasomatism of paleosolution karst breccias and incipient regional B - Ti metasomatism manifest as tourmaline and rutile alteration which possibly precedes and may be related to later Na, K and Fe metasomatic events, dolomite-albite alteration, post-metamorphic pervasive Na and K feldspar metasomatism and albite-dolomite-chalcopyrite-scapolite alteration.

3.4 *Structure*

The overall level of deformation in the study area is fairly mild with a low metamorphic grade, perhaps up to lower greenschist facies. Deformation is heterogeneous with more deformed areas associated with fault zones and fold closures. Most of the fault zones exhibit brittle-ductile textures and pressure solution is probably the dominant mechanism within them. Pervasive, slaty fabrics have only developed in fine grained lithologies near fold cores whilst arenites are rarely cleaved. The geology of the area is strongly dissected by late brittle faults which dismember earlier fold geometries resulting in blocks of coherent geology juxtaposed with blocks in which the structural grain may be at a slightly or significantly different orientation (Figure 3.1b). Bedding surfaces are often difficult to identify in the Marimo Slate (Plates 4.4 and 4.5).

Ch 3.4.1 Folding

The major folds within the study area were created during D2 deformation in roughly E-W compression resulting in N-S trending fold traces. Fold wavelengths vary from kilometric scale to outcrop scale. These orientations have been modified by later deformation within ductile and brittle shear zones which developed from late D2 times onward. E-W trending fold axes are also present but are infrequent in comparison to N-S folds. The present geometry of fold orientations is highly variable as many of the folds are generated and controlled by local shear geometrics.

North-south trending folds were formed during D2, by analogy with Beardsmore (1992), and are generally tight, to isoclinal and upright with axial planes dipping steeply east or west. ERA - Maptec (1994) suggest that the Marimo Basin owes its overall sigmoidal geometry to N-S folds and synchronous or later faulting on NE and NW trending structures. The core of the "basin" formed by a regionally broad syncline with a wavelength of several kilometres.

Homestake geologists have defined a second regionally extensive D2 fold - the Greenmount Anticline. This was based on the geometry of the Marimo Slate around a core of Staveley Formation in the south of the study area (450000mE, 7674000mN). The north trending fold has a wavelength of several kilometres. Mapping in the area by ERA - Maptec indicates that a complex fold core does exist within the arenites and calc-silicates of what is now thought to be Roxmere Quartzite lithologies. However, the blocks of Marimo Slate which would comprise the eastern limb of the fold do not strike NW as would be suggested by the fold shape but have a N-S grain. It is difficult to prove whether this was originally the eastern limb of the anticline.

Whatever the original geometry, it is clear that the present boundaries to this block of Marimo Slate are structurally controlled and that it should be thought of in terms of a shear zone setting rather than a fold (ERA - Maptec, 1994).

East-west folds are much less frequent than northerly folds and are not the result of a regional N-S compression event but are controlled by local sets of circumstances.

The folds are not always associated with a well defined axial schistosity, and hence an intersection lineation between bedding and cleavage is often not visible. The axial planar foliation is only pervasive very close to the fold hinges. Pressure solution seams are present with coarser lithologies whilst slaty cleavage is only found in fine grained rocks. There is no

sign of a regional second cleavage, the primary cleavage is often reoriented in fault zones and where two fabrics are present the overprinting fabric is related to shearing (Plate 4.4).

Ch 3.4.2 Faulting

Kinematic indicators on fault zones are rarely observed. The following types of fault zones are recognised:-

- (i) Silicified ridges, often haematite stained.
- (ii) Quartz-haematite breccia ridges.
- (iii) Mylonite zones
- (iv) Arenaceous breccia zones
- (v) Shear zones in Marimo Slate
- (vi) Bleached feldspar-sericite-clay-pyrite alteration zones (mostly found south of Greenmount).

NW to NNW trending structures generally have a sinistral shear component and developed fairly late in the tectonic history. Some are part of a regional conjugate system of shears created in approximate E-W compression.

NE to NNE trending structures generally have dextral shear components but may also show dip-slip movement.

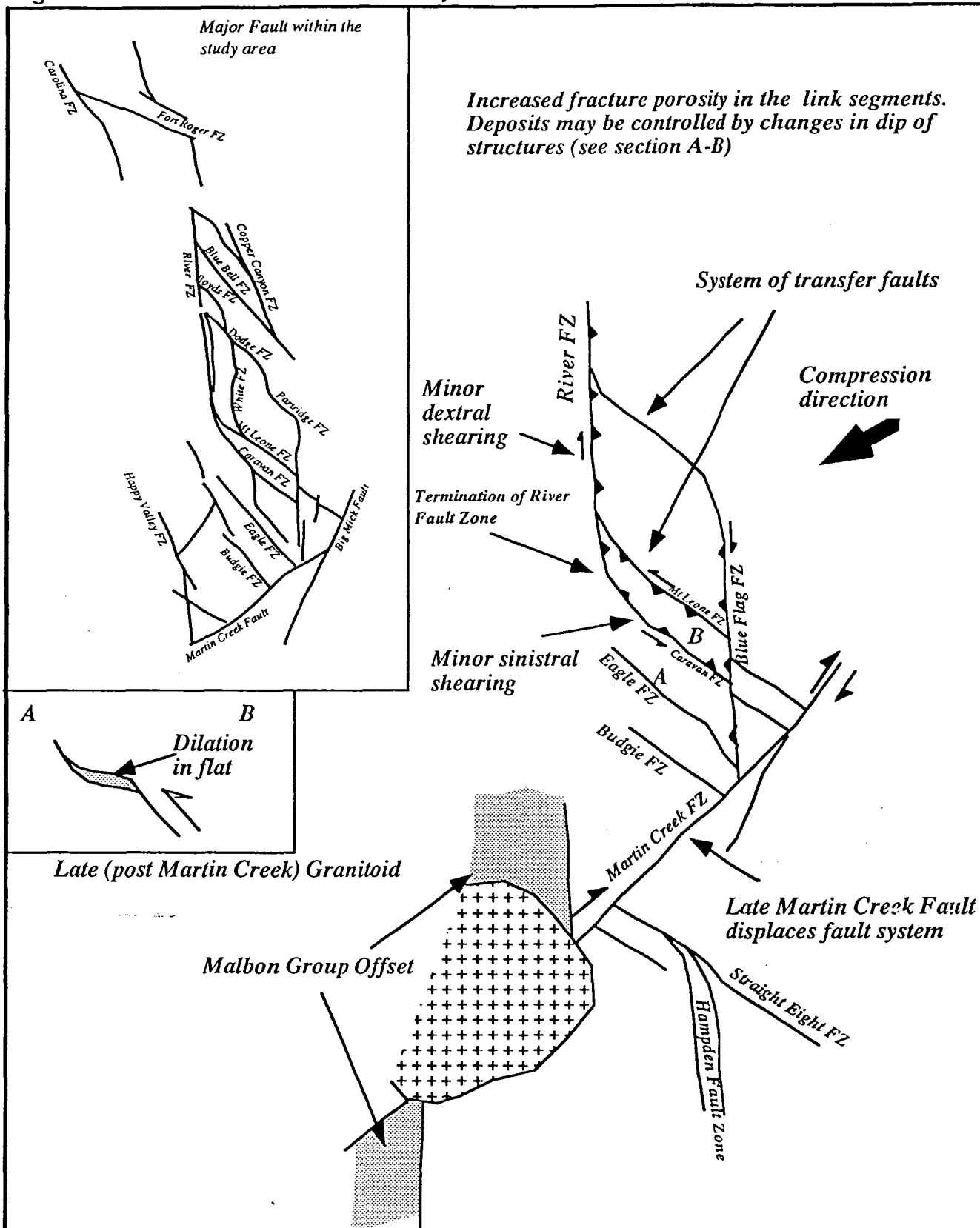
NNE to N to NNW trending structures are grossly compressional with only minor strike-slip components.

Ch 3.5 Structural History

The structural history of the eastern Marimo Basin can be summarised as follows (Figure 3.3):-

1. Coeval sedimentation of Marimo Slate, Staveley, Corella and Doherty Formations. This is inferred from the occurrence of Staveley and Corella Formation on both sides of the Marimo Slate and the similar appearance of the Doherty and Corella Formation in the field and on TM imagery.
2. N-S folding - large scale closures such as the Leviathan and Fort Roger folds form in a N-S orientation, with an axial planar cleavage poorly developed on the limbs. Fold axes are doubly plunging.

Figure 3.3 Structural model for major fault / shear zones (From ERA-Maptec, 1994)



A structural model for the major fault / shear zones in the study area. The straight Eight Fault Zone is thought to be equivalent to the Mt Leone and caravan Fault Zones. The Martin Creek Fault is a late structure which off-sets the earlier anastomosing fault system but is itself overprinted by granitoid intrusion. The earlier system involved transfer of shear from the River Fault Zone onto the Hampden fault Zone via the NW trending array of structures. This may link the shearing found at the Selwyn Mine with that on the River Fault Zone.

3. Ductile shear during ENE-WSW compression. This event is responsible for the formation of NW sinistral shears, NNW to NNE dip-slip shears with some dextral component, and N-S asymmetrical folds. Most mylonitic fabrics date from this episode. The anastomosing architecture of the faulting is probably established at this stage.
4. Ductile-brittle shear during EW compression producing NW sinistral faults and NE dextral faults.

CHAPTER 4 *Geology of the Greenmount Area*

Ch 4.1 Introduction

The area has previously been mapped by numerous Homestake geologists (including the author) and also by ERA - Maptec (1994b), who conducted a structural appraisal of the area. This study details some of the surface alteration features of the area and particularly focusses on the alteration and mineralisation features observed in drill core. This is the first study to constrain the paragenesis. Six diamond drillholes (and numerous percussion holes) were logged in detail, and 44 thin and 13 polished thin sections were made to assist in descriptions.

Ch 4.2 Surface Geology

A map of the surface geology, structure and alteration for the Greenmount area is shown in Figure 4.1.

Ch 4.2.1 Lithostratigraphy

The lithostratigraphy is similar to that described in Chapter 3.2. The Corella Formation dominantly comprises laminated dolomitic carbonate and pelite as well as subordinate chloritic siltstones (Plate 3.6) which has been metamorphosed to lower-mid greenschist facies defined by the mineral assemblage chlorite-biotite-dolomite-scapolite. The presence of high strain zones is easily identified by the “mackerel texture” or spaced cleavage imparted on this relatively unaltered and impermeable unit (Plate 3.7 and 3.8).

The Staveley Formation is dominantly represented by a variably chloritic metasiltstone-metasandstone package which is often incipiently potassified and hematite dusted giving the rock an orangey appearance (Plate 4.2) locally termed “red-rock alteration” by some workers (e.g. Williams, 1994). The Staveley Formation also contains numerous hematitic banded iron formations (BIF's) which exhibit numerous sedimentary features including cross-bedding (Plates 4.3 and 4.4). Joyce (1993) states that the petrography suggests that the origin of the iron is detrital hematite. Joyce also notes a minor mafic to intermediate volcanoclastic component to the BIF's. Stewart (1991) described iron and potassium metasomatised “pillows” with iron rich selvages from the Staveley Formation just west of Greenmount, but was unable to ascertain whether they were true mafic pillow lavas or structural boudins. The author has observed structural evidence (eg. “domino model” or “bookshelf sliding”

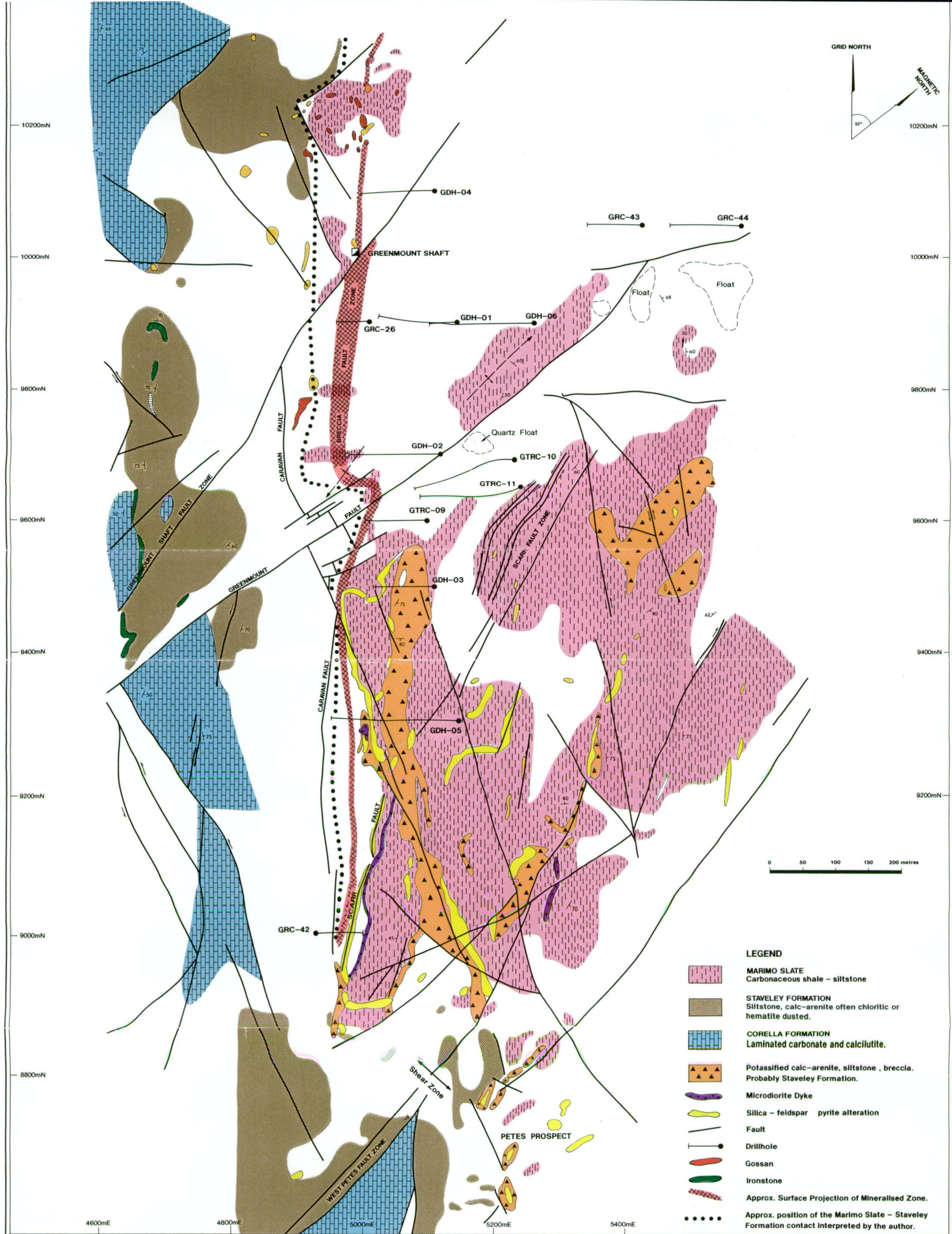
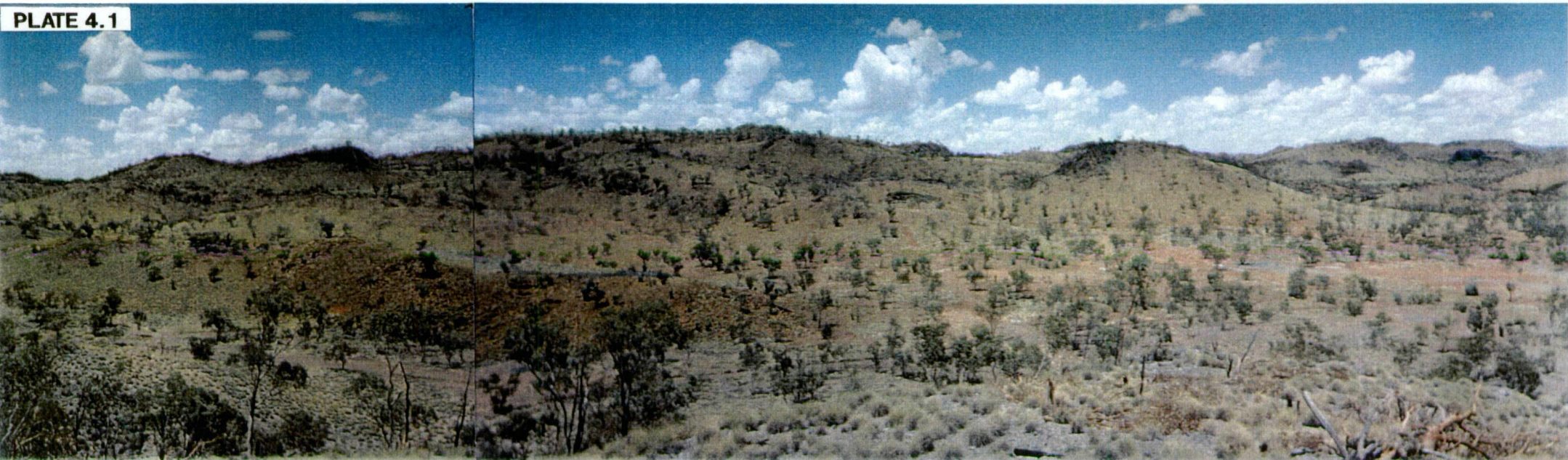
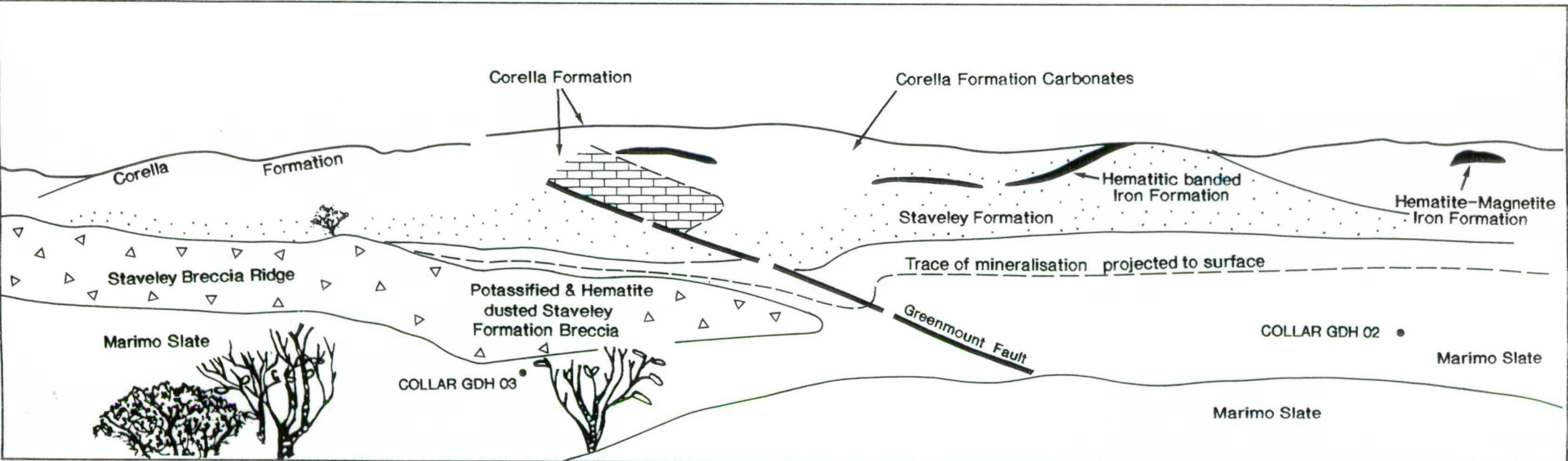


Figure 4.1 OUTCROP GEOLOGY OF THE GREENMOUNT AREA WITH FUNDAMENTAL STRUCTURAL ELEMENTS, INTERPETED MARIMO - STAVELEY CONTACT AND LOCATION OF SOME DRILLHOLES RELEVANT TO THIS STUDY.

(Compilation from mapping by ERA - Maptec (1994b), Homestake geologists (1988 - 1994) and author.

FIGURE 4.2 Geological features corresponding to Plate 4.1



structures) which indicates that the features are structural boudins and block rotation suggests a sinistral sense of shear.

In addition, a unit informally termed the “Staveley Breccia” occurs mainly within the Marimo Slate package. It also forms a distinct ridge (the “Staveley Breccia Ridge”) which occurs sub-parallel to the main ore zone (Plate 4.1 and Figure 4.2). Clasts range from pebble up to boulder size and are compositionally and lithologically similar to the Staveley Formation with a calcite matrix. It is still not entirely clear whether it is a facies change of the Marimo Slate or whether it is true Staveley Formation which has been brecciated due to structural arching. This will be discussed in more detail in chapter 4.2.3.1.

The Marimo Slate is distinctly grey coloured except where pervasively altered to feldspar-silica-pyrite-clay. It dominantly comprises carbonaceous shale which contains variable pyrite and mica content. It is usually fissile with a strong cleavage which obliterates bedding (Plate 4.5). The Marimo Slate hosts the main ore zone in a brittle vein array which can only be observed at a few very small outcrops (Plate 4.6). The contact with the Staveley Formation is not seen in outcrop in the Greenmount area.

The Jasmin Granite is a weathered fine grained albitised granite which crops out (<3 hectares) approximately 800m south of the southern extremity of the mineralised zone (i.e. grid 8200N). An altered microdiorite dyke crops out subparallel to the main mineralised zone. It varies in width from 1m to 4m at the surface to >30m at depth and is in excess of 600m long and 200m deep. Its apparent linearity and isolated occurrence may suggest that in a structural context it is a relatively late feature. Other small intrusives (including a tonalite dyke just east of the Vulcan Mine) occur sparsely through the area. None of the intrusives are foliated or metamorphosed.

Ch 4.2.2 Pervasive Alteration

In addition to the pervasive potassification and hematite dusting of Staveley-type lithologies, the Marimo Slate contains a series of white “bleached” alteration zones (\pm coarse pyrite, Plates 4.7 and 4.8) which vary in size up to about 120m wide or 1,150m long. These alteration zones are often seen to cut across cleavage and foliation but are themselves cut by quartz \pm microcline veins (Plates 4.9, 4.10 and 4.11).

A suite of five samples were collected from both mineralised and barren intersections of reverse circulation percussion holes which were drilled into some of the larger “bleached zones” at the Petes and Painted Peaks prospects (Plate 4.12). These were sent to petrologist

Dr Doug Mason for X-ray diffraction analysis for this study. The samples were pulverised and then analysed by XRD at Amdel Mineral Services Laboratory. The XRD traces were interpreted with the assistance of a computer-based mineral search-match programme. The results are summarised in Tables 4.1 and 4.2 below:-

**Table 4.1 - Pervasive Alteration
Sample Descriptions of Hole and Depth**

Sample	Locations	Hole & Depth	Comment
14902	Painted Peaks Prospect	PPRC-2, 78-80m	Barren
14904	Petes Prospect	PRC-04, 50-51m	Barren
14905	Petes Prospect	PRC-07, 54-56m	1.96 g/t Au, 169 ppm Cu, 1469 ppm Co, 357ppm Co
14906	Painted Peaks Prospect	PPRC-1, 70-71m	0.79 g/t Au, 1.55% Cu, 578 ppm Co
14907	Petes Prospect	PRC-04, 63-64m	0,.68 g/t Au, 191 ppm Cu, 578 ppm Co

**Table 4.2 - XRD Analysis of Pervasively Altered Samples
From Pete's and Painted Peaks Prospects (from Mason, 1994)**

Mineral	14902	14904	14905	14906	14907
Albite	D	D	D	Tr-A	D
K-feldspar (microcline)	-	Tr-A	-	D	Tr
Quartz	Tr	A-SD	A	Tr-A	SD
Mica	-	-	Tr	-	Tr
Chlorite	-	Tr	-	-	-
Pyrite	-	Tr-A	-	Tr	-
Dolomite	-	A	-	-	-
Smectite	-	-	-	-	Tr

D = Dominant. Used for the component apparently most abundant, regardless of its probable percentage level.

CD = Co-dominant. Used for two (or more) predominating components, both or all of which are judged to be present in roughly equal amounts.

SD = Sub-dominant. The next most abundant component(s) providing its percentage level is judged above about 20%.

A = Accessory. Components judged to be present between the levels of roughly 5 and 20%.

Tr = Trace. Components judged to be below about 5%.

Plate 4.2 (A) View from west of Greenmount, looking to the southeast. The ore zone is located in the valley between the camp and the dark BIF outcrop in the middle distance. It extends to the right of the field of view, in the wedge of grey-black shales, between the linear orange unit (Staveley Breccia Ridge) and the larger orange unit in the foreground on the right. The orange colour is due to haematite dusted potassic alteration.

Plate 4.3 (B) Hematitic banded iron formation showing sedimentary structures. Sample located just west of Greenmount.

Plate 4.4 (C) BIF outcrop forming ridges just west of Greenmount. Hosted by the Staveley Formation.

Plate 4.5 (D) Outcrop of Marimo Slate near Petes Prospect. Note the strong development of cleavage and the crosscutting relationship of the weak “bleaching”.

Plate 4.6 (E) Outcrop of black shale (Marimo Slate) which has undergone brittle style fracturing and veining by microcline-quartz-phlogopite. No preferred orientation of veins. Outcrop located near main ore zone just west of GTRC-9.

Plate 4.7 (F) Large cubic pyrite crystals with striated faces which form in some of the bleached alteration zones.

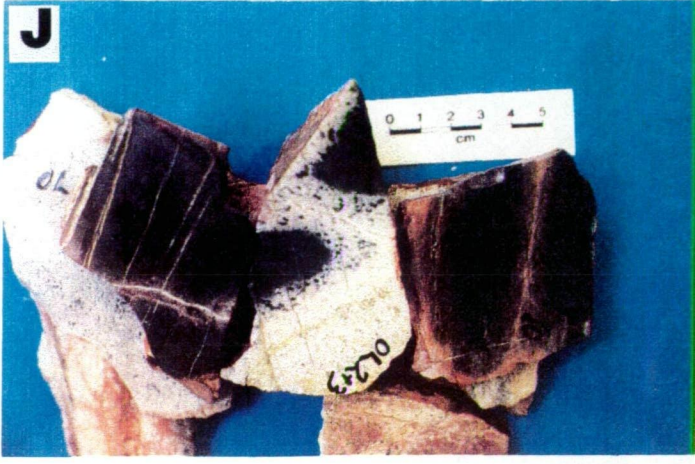
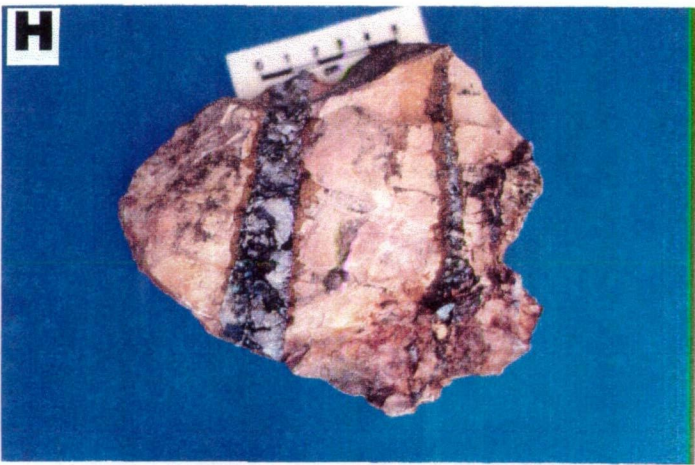
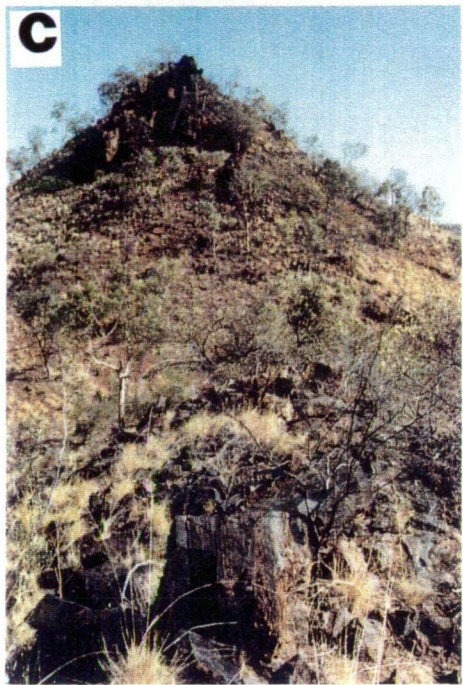
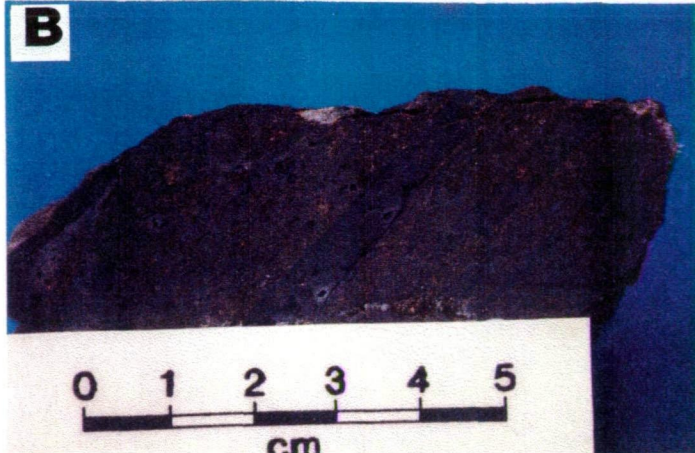
Plate 4.8 (G) Pyrite crystals with well developed pyritohedral forms from the pervasively altered shales at Painted Peaks Prospect.

Plate 4.9 (H) Pervasive albite-microcline alteration of Marimo Slate at Petes Prospect with late planar crosscutting quartz hematite veins.

Plate 4.10 (I) Similar to Plate 2.8 but with abundant disseminated pyrite (now weathered to iron oxides).

Plate 4.11 (J) Progressively feldspathised pelites from the Petes Prospect area.

* *Plates 4.3, 4.9, 4.10 and 4.11 courtesy of J.I. Stewart.*



From this work it can be seen that the alteration is dominated by albite or microcline, with lesser phlogopite, quartz, pyrite, chlorite, dolomite and smectite. Thin sections also revealed the presence of tourmaline, apatite and rutile (Mason, 1994). It can be seen that fertile mineralised systems are indistinguishable from barren systems on the basis of mineralogy. This could imply that the pervasive alteration was an earlier alteration event and that veins and mineralisation was superimposed on whichever bleached zone was near the mineralising structures (this is considered unlikely).

Another style of alteration worth noting is the “epithermal” quartz alteration which occurs at the Masons prospect (Plate 4.13) and has been described in the region by Williams and Blake (1994).

Ch 4.2.3 Structure

Late brittle faults fragmented the geology and earlier tight folds (Plate 4.14) creating a series of fault-bounded blocks, ranging up to several kilometres across. The geology is complex as there are several phases of shearing present which post-date regional folding and cleavage formation. This has juxtaposed several fault bounded blocks, where the structural grain can change dramatically. Some of the blocks and their boundaries control locally developed structures (ERA - Maptec, 1994b). The area around Greenmount appears particularly disjointed. It lies in a regional structural domain dominated by NW trending major structures which are thought to have developed as termination or transfer structures to the River Fault Zone (Figure 3.3). ERA - Maptec (1994b) suggest that the area of Marimo Slate between the Caravan Fault Zone and the Mount Leone Fault zone to the north is not the eastern limb of the Greenmount Anticline as suggested by Stewart (1991), but is probably a shear bounded lozenge.

4.2.3.1 The Staveley Breccia Ridge

The enigmatic Staveley Breccia Ridge comprises potassified and hematite dusted arenaceous and pelitic clasts cemented by calcite, which forms a distinctly orange coloured ridge which parallels the main ore zone for at least 600m (Figures 4.1 and 4.2, Plates 4.1 and 4.16). The strong alteration, relatively high porosity and proximity to mineralisation warrants some discussion in this study. The complex geometry of the ridge is modified by NW trending sinistral structures and the NW end of the ridge appears to end abruptly in the vicinity of the Greenmount Fault (Figure 4.1). The outcrop pattern of the breccia bifurcates in a number of places and the thickness of the breccia zone varies rapidly. The Marimo Slate commonly strikes at high angles to the ridge trends, but as the ridge is approached, the slate swings into it

and parallels the contact. The slate has a sheared appearance at several outcrops close to the contacts and almost always has a subvertical dip. Stewart (1994) has interpreted this unit as an anticlinal fold closure with mineralisation folded around the hinge, however examination of bedding - cleavage relationships within the slate indicate that the folding is present but not in the correct geometry for the breccia ridge to be a fold core. The closest cleavage data on both the western and eastern side of the ridge consistently indicate that a syncline, not an anticline, lies to the west and hence the breccia ridge occupies a fold limb and not a fold core position.

ERA - Maptec (1994b) prefer a fault/shear model which can explain some inconsistencies that a fold model cannot. They suggest that strike-slip fault zones which have a component of compression or extension across them, can have similar geometries to those of the Staveley Breccia Ridge, and slivers of rock can be exhumed in the core of a braided fault system. At Greenmount, the controlling faults would have been compressional structures. The author has observed up to several metres of sheared or faulted offset between the Marimo Slate - Staveley Breccia contact. Cross-section interpretations by the author (Figures 4.3 to 4.5) are also consistent with a fault shear model.

4.2.3.2 *Structural Interpretation*

ERA - Maptec (1994b) have interpreted four main structural trends.

1. NNW to N trending fault zones which have apparent dextral displacement and are thought to be the youngest of the four structural trends. They include the Greenmount Fault, the West Pete's fault zone and the Greenmount Shaft Fault (Figure 4.1).

Although mineralisation is found along some of these structures, they seem to post-date mineralisation and dissect mineralised structures. In general, they appear to be partitioning structures across which the structural level and prospectivity change.

2. ESE trending structures have a consistent sinistral component of shearing and are only cross-cut by NNW-N trending dextral structures but post-date the other fault trends and mineralisation.
3. Some NNW trending structures have good indications of sinistral shearing from the geometry of minor folding. They are bedding parallel and appear to be one of the main controls on mineralisation. The Scarr Fault Zone is included in this group.
4. NW trending structures are all associated with the regionally extensive Caravan Fault Zone and dip moderately to steeply east. The Caravan Fault Zone (Figures 4.1 and

3.3) is thought to have a sinistral component of shearing locally forming the contact between the Marimo Slate and the Staveley Formation. Drill hole data interpreted by the author, indicates that the contact dips around 50 - 70° to the east, subparallel to the Greenmount orebody. It also includes the Breccia Fault Zone which is interpreted as splaying from the main Caravan Fault Zone and steepening upward to control the ridge of Staveley Breccia. The main Greenmount orebody is interpreted as lying within the continuation of the Breccia Fault Zone to the west of the Greenmount Fault. The NNW trending sinistral faults could have developed at the same time as the Caravan Fault system.

4.2.3.3 *Structure and Morphology of the Main Orebody*

The structure and morphology of the main orebody and alteration has been interpreted by the author and is presented as a series of cross-sections in Figures 4.3 to 4.9. The mineralised zone is best developed between 9550 mN and 10000 mN. This zone contains no natural exposure and is covered by a blanket of recent fluvial sediments up to 6 m thick (Plate 4.15). Drill hole cross sections (Figures 4.3 to 4.9) indicate that the orebody dips at around 45° to the east and is subparallel to the Marimo Slate - Staveley Formation contact. The contact is locally formed by the Caravan Fault Zone although conformable contacts could be intercepted between fault strands. The orebody trends NW and is cut to the SE and NW by the Greenmount and Greenmount Shaft Faults respectively. These may be revealing a higher structural level of the orebody (ERA - Maptec, 1994b). Mineralisation does continue past these cross faults, but is less significant and hence the main part of the orebody may have been eroded away in these positions.

4.2.3.4 *Factors Controlling Mineralisation*

The contact of the Marimo Slate with other lithologies is a regionally important control on mineralisation. The evaporitic Staveley Formation may have concentrated shearing. On a local scale there is no evidence for local strike-slip control such as fault jogs (Sibson 1987) on mineralisation. Sparse outcrop shows that many veins and mineralised structures are subparallel to the Greenmount Fault, however the trend of the entire orebody may be controlled by structures oblique to the mineralisation. Figure 4.10a shows that a swarm of structures subparallel to the Greenmount and Greenmount Shaft Faults could create an orebody at a high angle to their strike (ERA - Maptec, 1994b). As they pass through the Marimo - Staveley contact they refract and widen and create local dilation zones which appear to be part of a NW structural zone. Alternatively, these structures may be associated with the sinistral NNW set of structures, which are known to be mineralised, and not the dextral

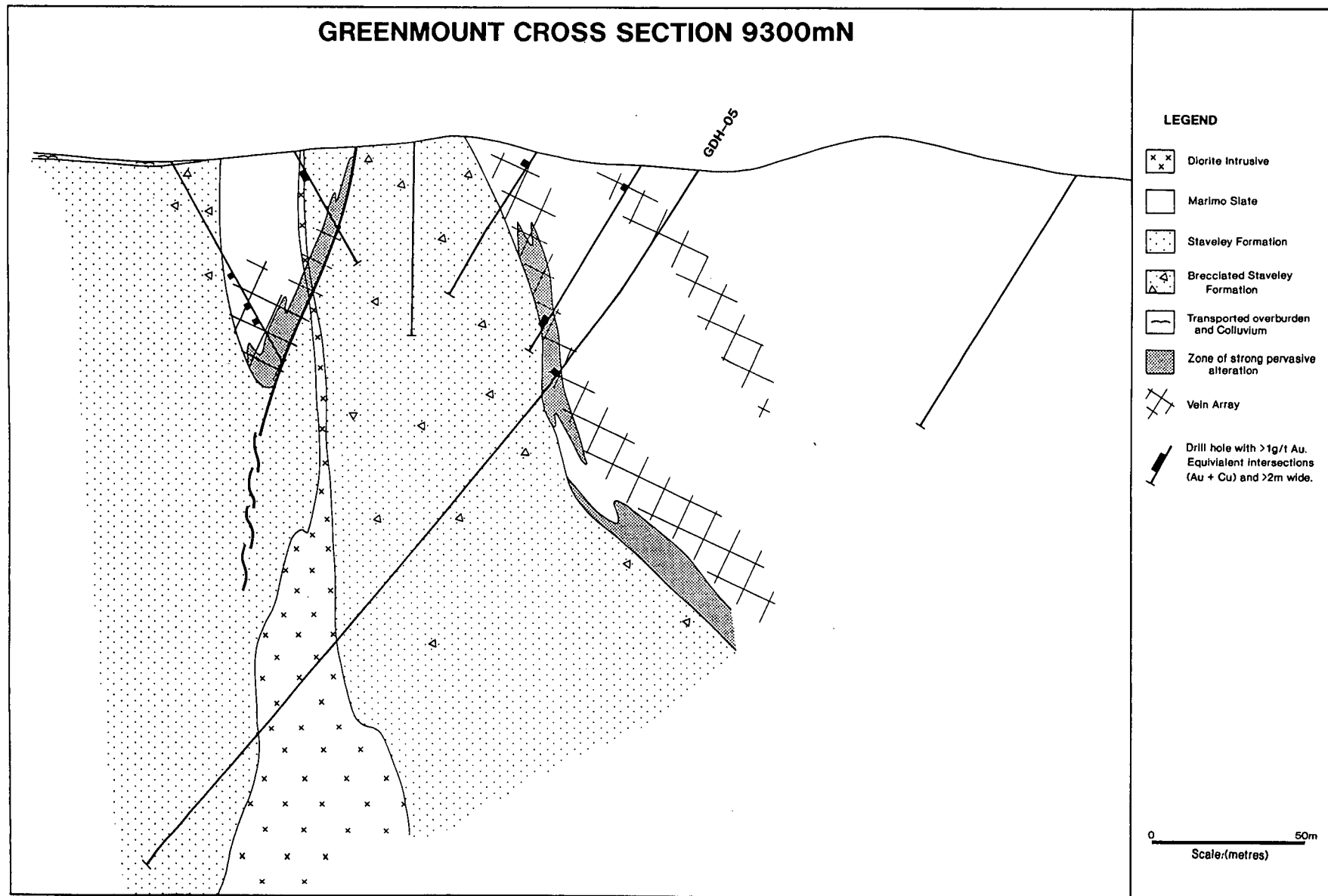


Figure 4.3 Simplified Geological Interpretation of Cross Section 9300mN

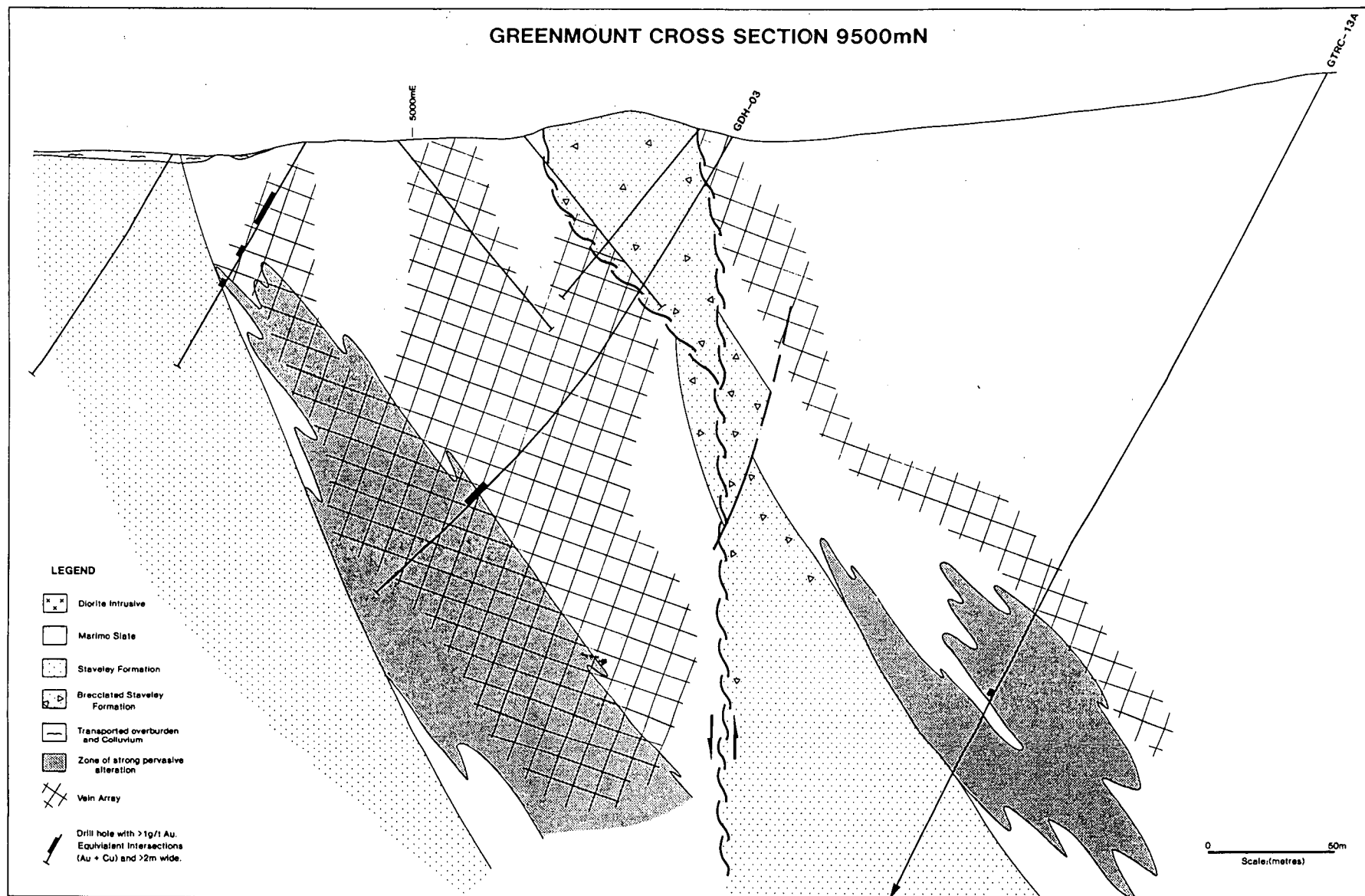


Figure 4.4 Simplified geological interpretation of cross section 9500mN

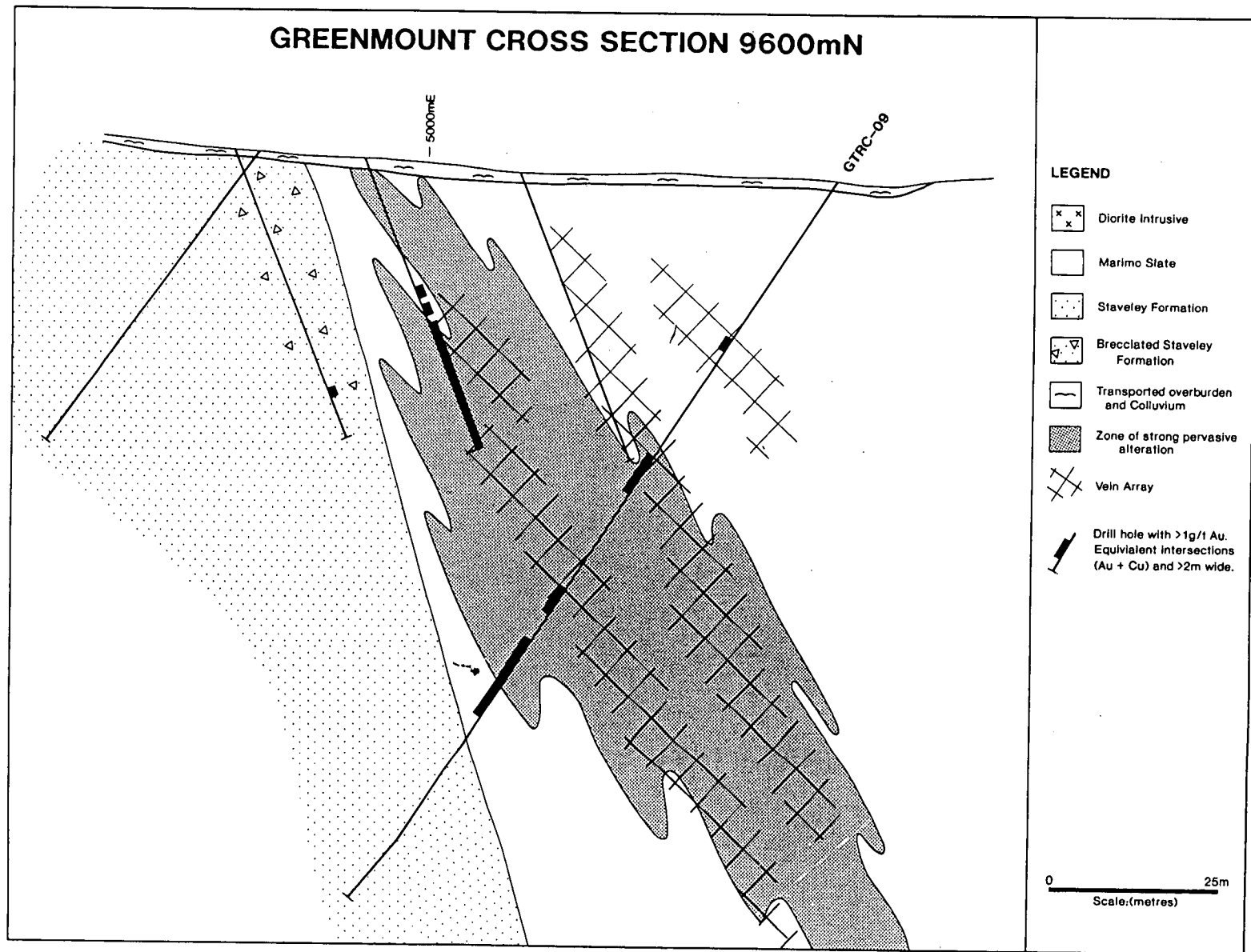


Figure 4.5 Simplified geological interpretation of cross section 9600mN

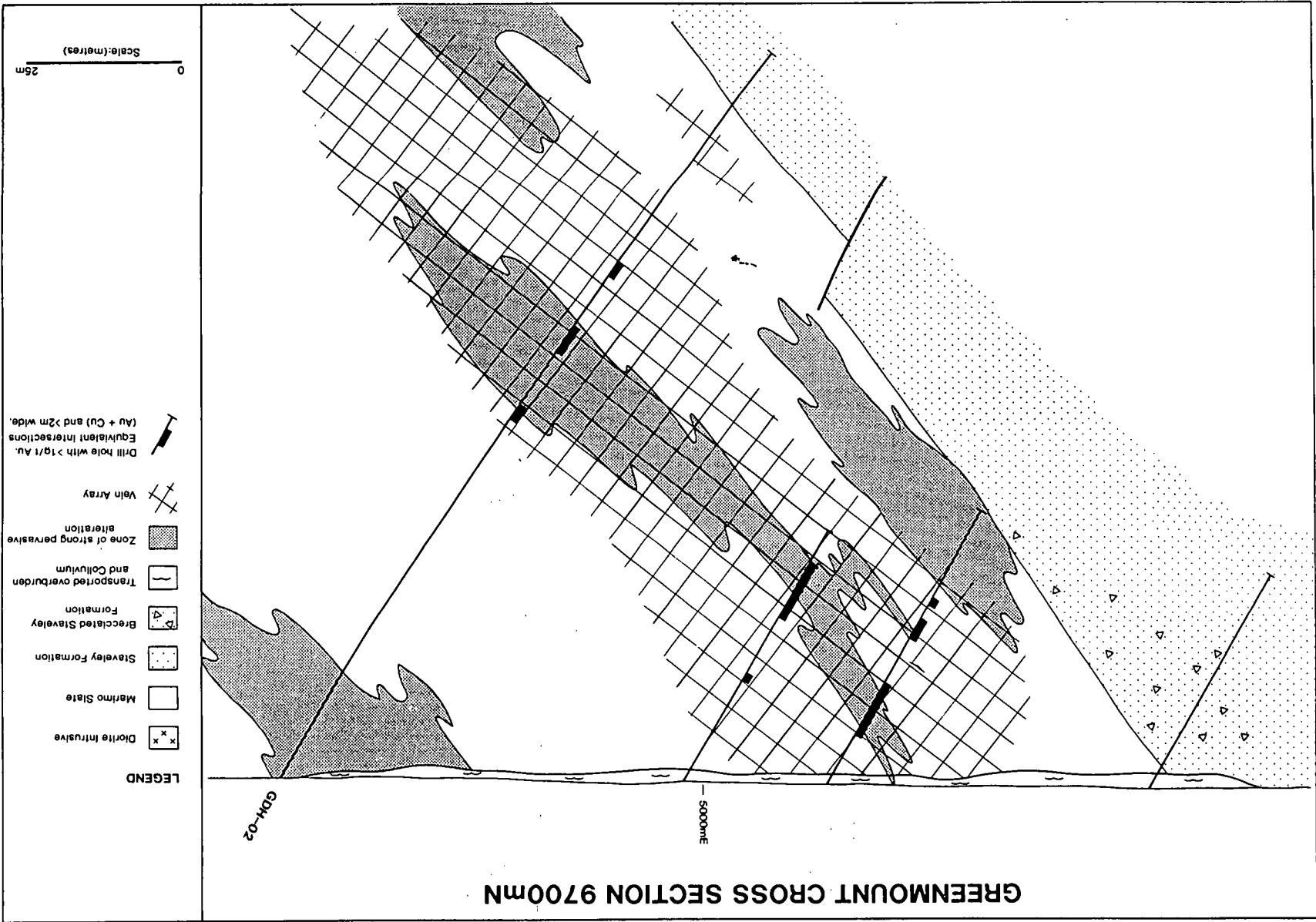


Figure 4.6 Simplified geological interpretation of cross section 9700mN

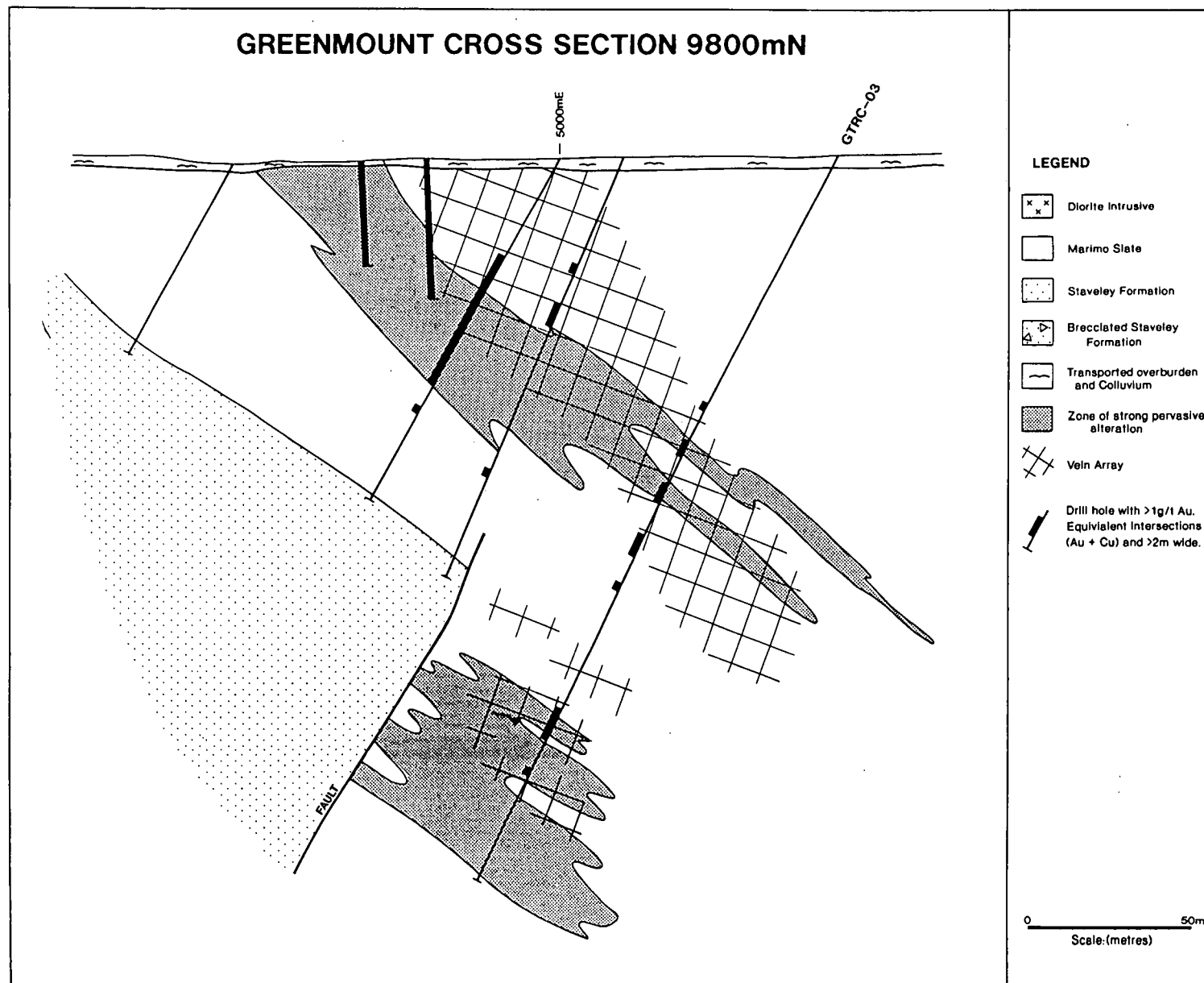


Figure 4.7 Simplified geological interpretation of cross section 9800mN

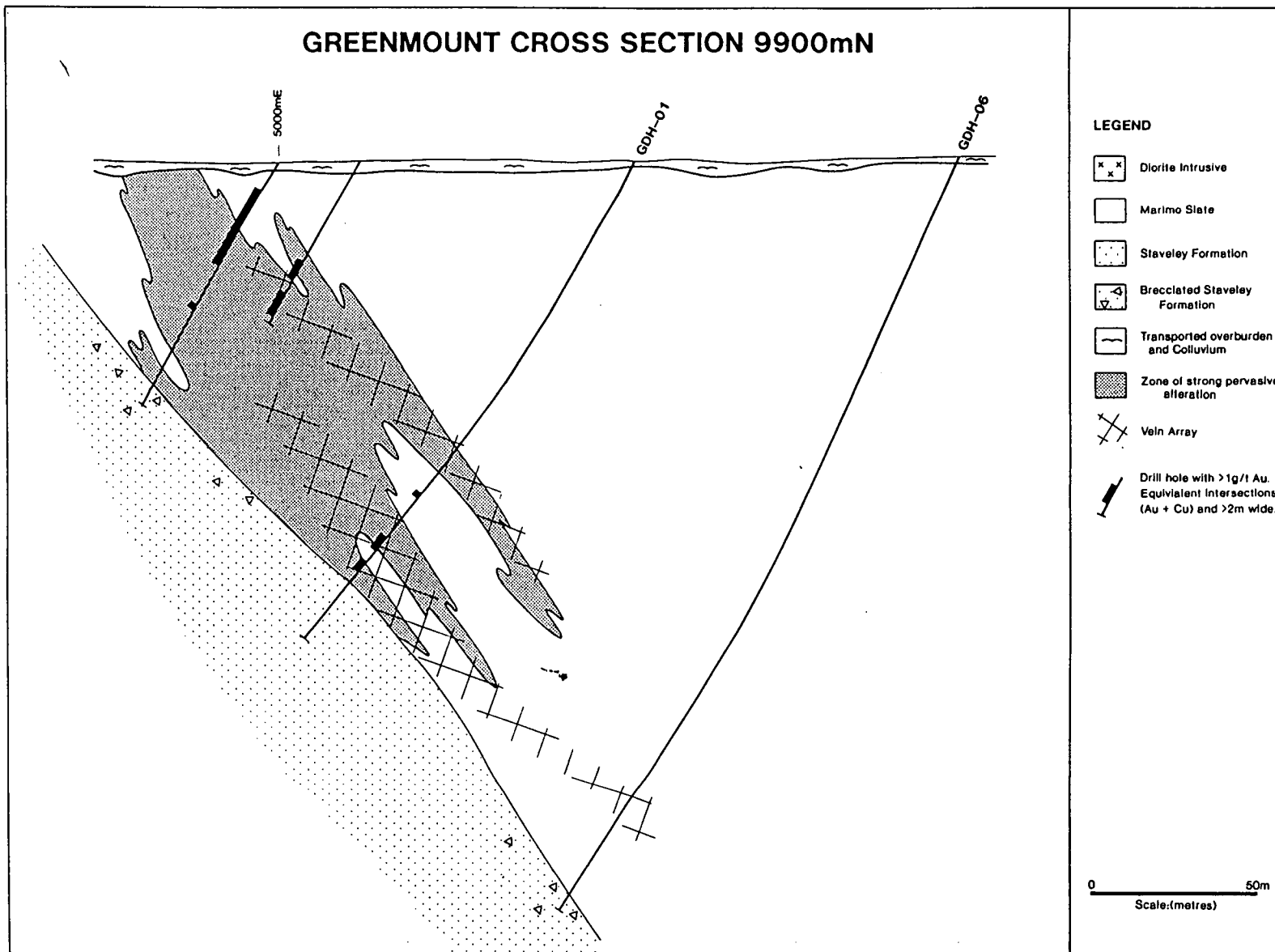
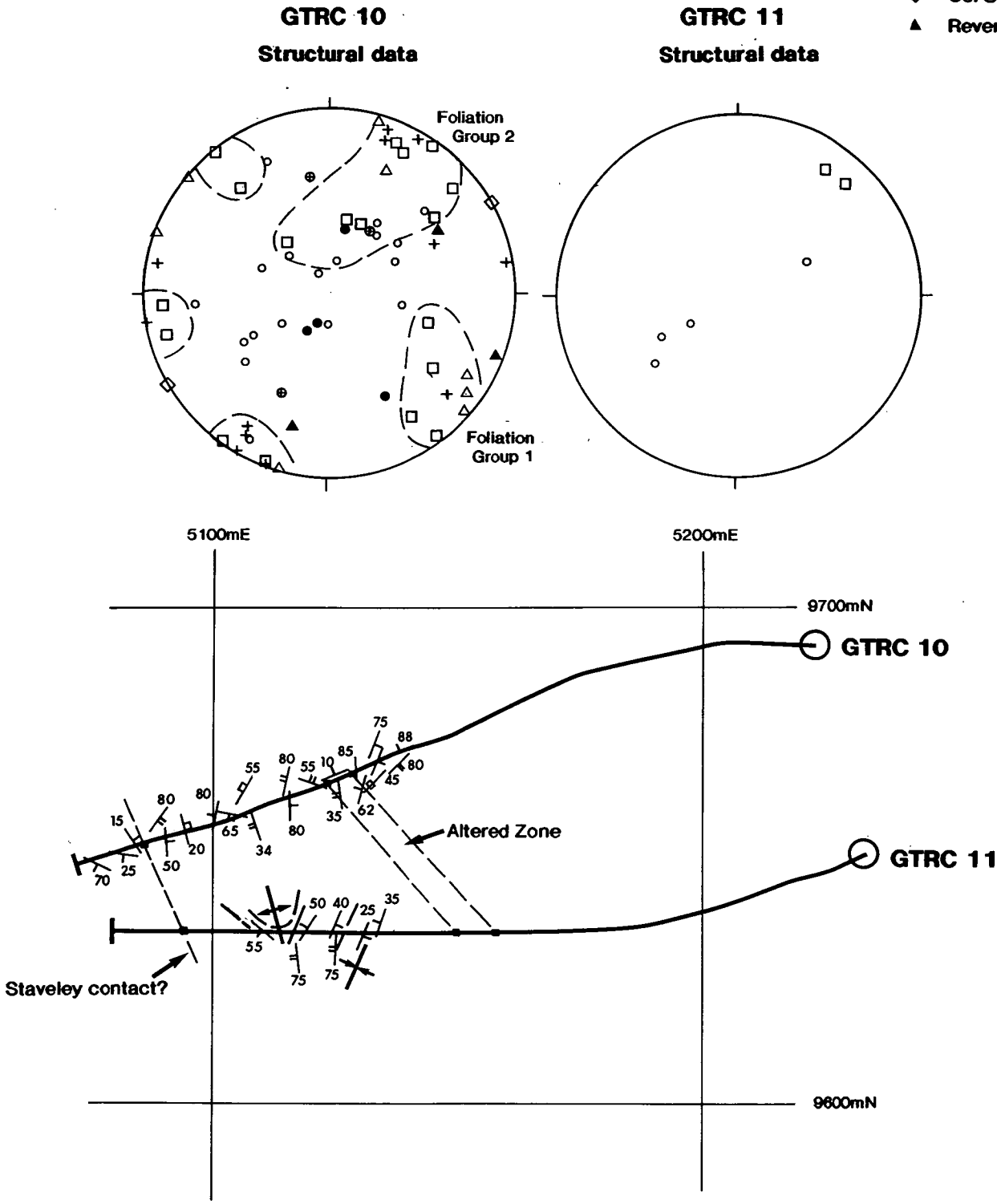


Figure 4.8 Simplified geological interpretation of cross section 9900mN

Figure 4.9 Structural data plots for holes GTRC 10 & GTRC 11.
(modified from ERA Maptec, (1994b))

- Bedding
- Foliation
- + Veins
- △ Fold axes
- Faults
- ◇ Ss/SI
- ▲ Reverse Faults



Structural data measured in orientated core in holes GTRC 10 and GTRC 11. The data indicate that there is folding and shearing in the holes. Bedding and foliation have a variety of orientations.

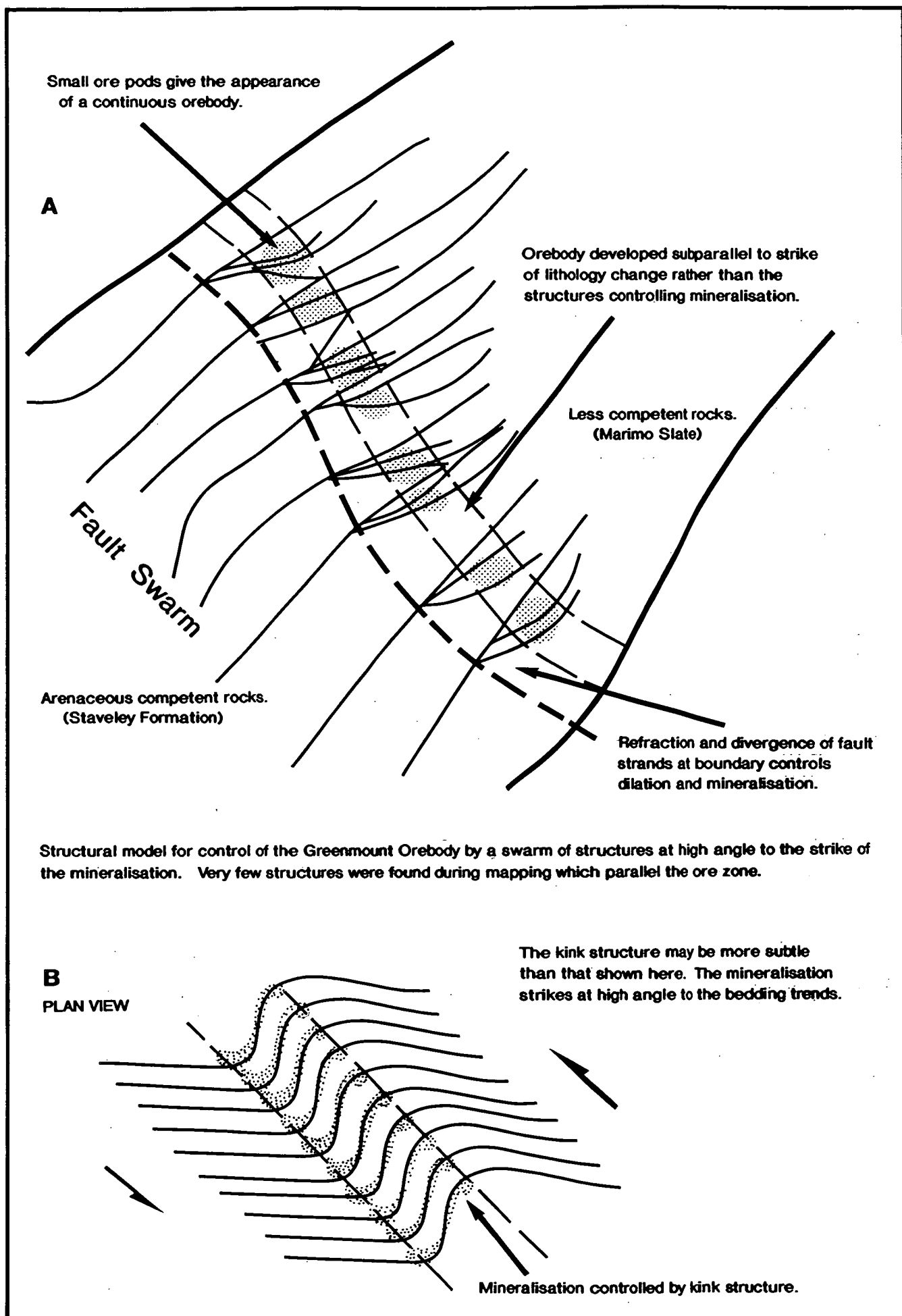


Figure 4.10a Fault refraction and fold models for the Greenmount Orebody
(Modified from ERA-Maptec, 1994)

Greenmount Fault system. Figure 4.10b shows that the orebody may also be controlled by a kink structure which bedding rotates in and out of.

However, the author contends that there are no apparent structures or common vein orientations in support of either of these models (Figure 4.9) and proposes that alteration and mineralisation may have been localised in a “flat” ramp within a reverse fault regime (Figure 4.10c). This interpretation is consistent with the authors observation that the most intensely altered and mineralised part of the system occurs where the Marimo Slate - Staveley Formation contact is less steeply dipping and is also consistent with the interpretation of the Staveley Breccia being an exhumed sliver of Staveley Formation within a braided (reverse) fault/shear system (Figure 4.3).

Davidson (pers. com., 1995) suggests that two alternative possibilities may be:

1. Vein zones formed as early attempts to fault in the general Caravan Fault position, synchronous with alteration and mineralisation, the activity of which “hardened” the rock and so caused the main fault to develop further east.
2. There was an early alteration which caused the veins/alteration to partition to less altered parts of the rock, away from the Caravan Fault.

The author contends that the latter possibility may be likely as the Marimo Slate is relatively soft and fissile to the east of the Breccia Fault Zone and the main orebody, but becomes progressively hardened towards the Caravan Fault, and thus there may have been a subtle early pervasive silicification event adjacent to the Caravan Fault.

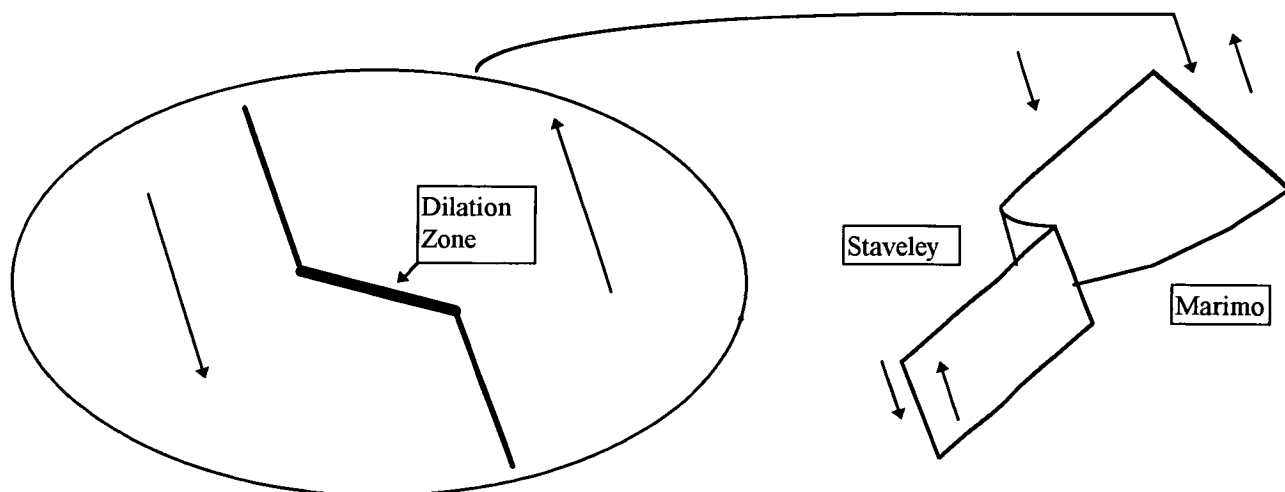


Figure 4.10c Schematic diagram showing zones of dilation in a reverse fault.

Plate 4.12 (A) Intensely Alunite, kaolinite and microcline altered siltstone with large disseminated pyrite crystals and pseudomorphs from the Painted Peaks prospect.

Plate 4.13 (B) Colloform banded crustiform quartz and chalcedony veins in silicified siltstone from Mason's prospect.

Plate 4.14 (C) Tightly folded Corella Formation from Petes prospect.

Plate 4.15 (D) View looking south along the main Greenmount ore zone. Photographed from about the 9700 N line the orebody is approximately 20 m wide at this point, but covered by colluvium.

Plate 4.16 (E) View of the Greenmount area looking to the south east. The spinifex covered orange unit in the foreground is potassified and hematite dusted Staveley Formation. The dark grey unit is the Marimo Slate and the GERC-15 drill pad is located to the centre-left. The linear dark orange unit forming the small ridge in the middle distance is the Staveley Breccia Ridge. The large hill to the extreme right is Mason's prospect and the hills in the far distance are capped by Mesozoic sediments.

- *Plates 4.12 (A) and 4.13 (B) courtesy of J I Stewart (1991).*



4.3 *Geology and Mineralisation of the Primary Zone*

All drill holes on the Greenmount Deposit were examined for this study. Seven core holes and six RC percussion holes were logged. Five of these core holes were logged in detail and a total of 57 thin or polished thin sections were collected to aid in establishing an alteration and mineralisation paragenesis. Drill hole observations are attached in Appendix 3 and summary petrographic descriptions are attached as Appendix 2. Many petrographic sections were described by consultants, Dr Stan Joyce (1993) and Dr Douglas Mason (1994), but all were examined and described by the author for this study. The following sections separately describe features observed in the Marimo Slate and Staveley Formation - type rocks including the Staveley Breccia, and intrusive rocks.

4.3.1 *Staveley Formation*

4.3.1.1 *Lithologies*

The Staveley Formation comprises a package of relatively porous and usually at least partially weathered metasediments (Plate 4.18 and 4.22). The protolith appears to have been a calcilutite-calcarenite. No evaporitic textures were recognised, but if initially present, would have been destroyed by subsequent shearing and metasomatism.

Plates 4.17 to 4.24 show typical Staveley Formation lithologies. The finer dark bands comprise micaceous slate (biotite, muscovite, sericite) with quartz, dominantly potassic feldspars, \pm dolomite and calcite and fine granular specks of rutile, tourmaline and specular hematite (Plates 4.17, 4.19 and 4.23). The coarser silty to sandy layers are porous, more weathered and show a sutured mosaic of quartz-microcline and plagioclase pseudomorphed by sericite as well as lesser dolomite and calcite with possible traces of chalcocite. It should be noted that some of the quartz contains abundant hypersaline fluid inclusions with up to 3 daughter salts and a vapour bubble, possibly suggesting derivation by diagenesis of an evaporitic package of sediments (Hurst, 1989; Light and Posey, 1989).

Plate 4.17 (A) Typical Staveley Formation bedded calcarenite-calclutite in hole GDH-02 at around 207 m depth. Note the orangey-brown colouration on the right which is due to microcline alteration which is often hematite dusted.

Plate 4.18 (B) Partially weathered and vuggy bedded calcarenite from the Staveley Formation at around 184 m depth from hole GDH-01.

Plate 4.19 (C) Near contact of Marimo Slate (column on extreme left) and Staveley Formation. The dark bands in the Staveley Formation dominantly comprise micaceous slate with quartz, microcline \pm dolomite, calcite and other gangue minerals. The relatively coarser and pale layers comprise a sutured mosaic of quartz, microcline and plagioclase (pseudomorphed and altered by sericite) as well as lesser dolomite, calcite and other gangue minerals. From hole GDH-02 at around 199.7 m depth.

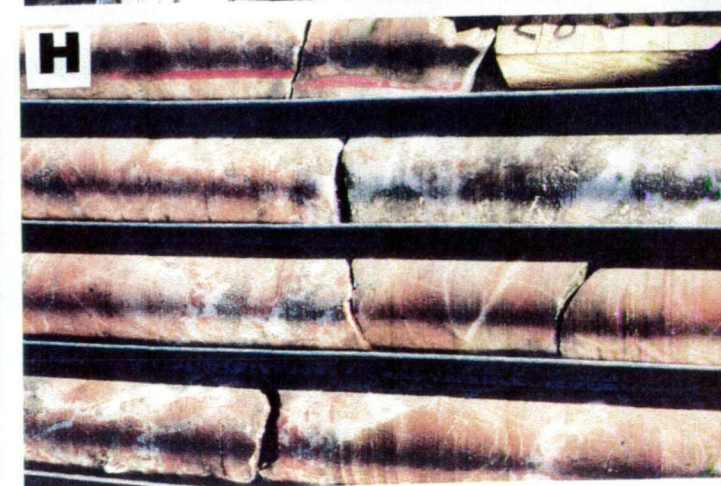
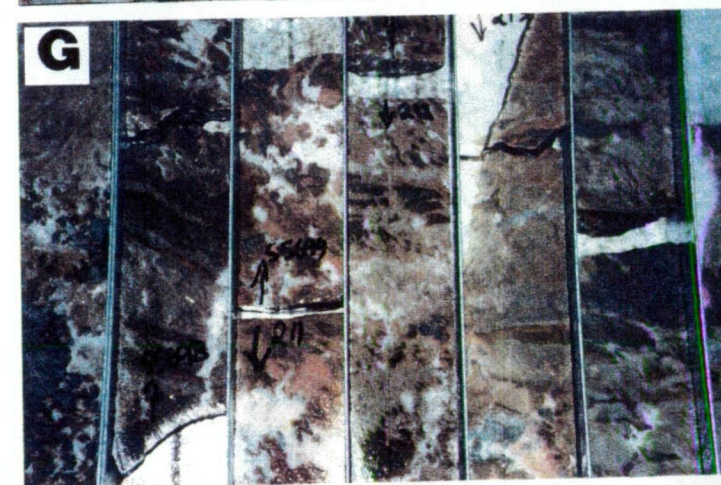
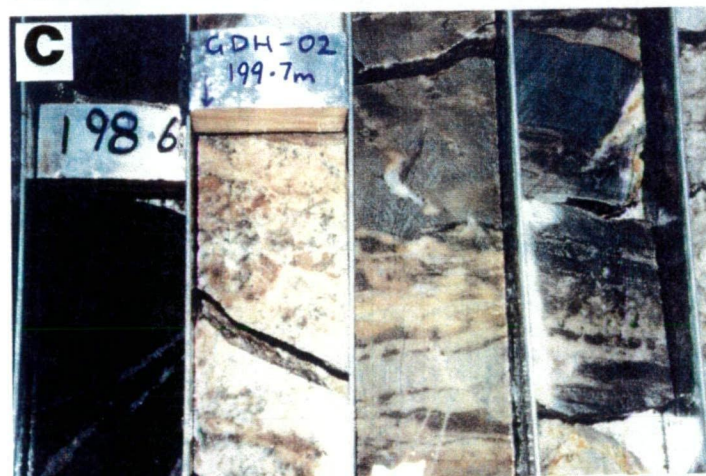
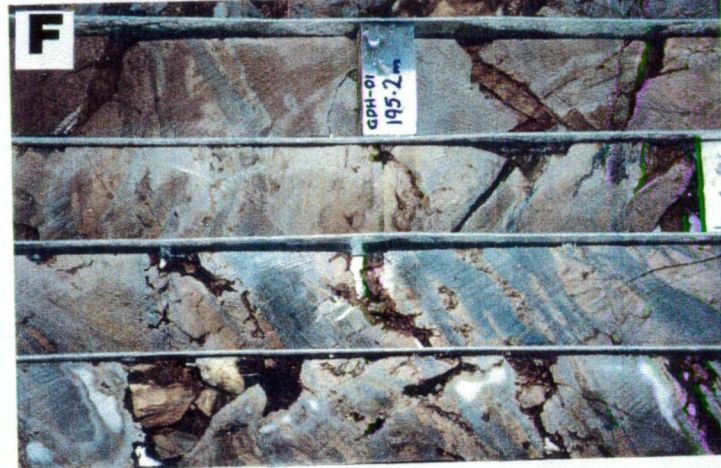
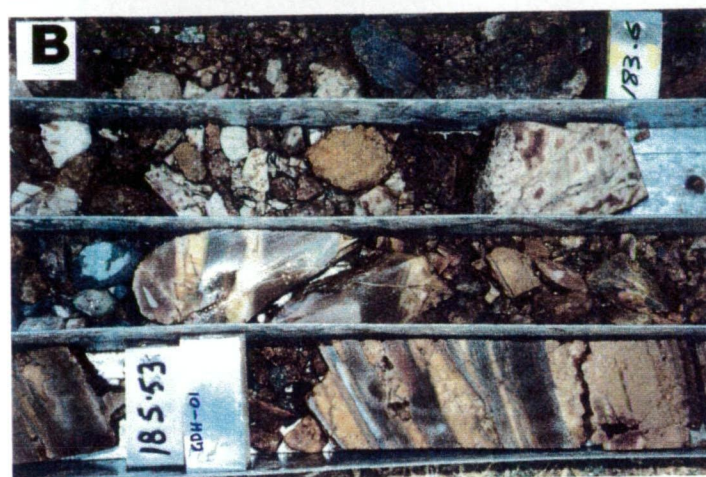
Plate 4.20 (D) Partly weathered and vuggy-bedded Staveley Formation from hole GDH-04 at about 187 m depth.

Plate 4.21 (E) Close-up of pervasive and incipient orange coloured hematite dusted microcline alteration of Staveley Formation lithologies with calcite matrix and thin cross cutting calcite veins.

Plate 4.22 (F) Cavities formed by dissolution of calcite in partly weathered Staveley Formation lithologies from hole GDH-01 at around 195 m depth.

Plate 4.23 (G) Close up of right side of Plate 4.17.

Plate 4.24 (H) Pyrite-calcite matrix to brecciated and intensely hematite dusted microcline altered Staveley Formation from hole GTRC-10 at around 261 m depth.



4.3.1.2 *Metasomatism*

Staveley Formation lithologies commonly display a weak to strong preferred orientation of tourmaline crystals which occurs only in the host rock (not observed in veins) and is interpreted to be pre- to syn-metamorphic in origin. Similarly, the less common rutile aggregates are assigned to the same event. Perhaps one of the most striking and characteristic features of the Staveley Formation is the ubiquitous pervasive potassic alteration dominated by microcline with lesser biotite. The microcline is usually dusted with fine hematite which gives it a pink-orange appearance (Plates 4.20, 4.21, 4.23 and 4.24). Some of the Staveley Formation has been albitised, but this is less common. The feldspathisation may have occurred any time from diagenesis through to post peak metamorphism. A later timing is preferred due to the fine grained nature of alteration. Some of the feldspars have undergone patchy retrogression to sericite. In hole GDH-05 some of the Staveley Formation has been finely magnetised in proximity to a magnetic diorite intrusive (Plates 4.25 to 4.27 and Plate 4.29).

4.3.1.3 *Veining*

Vein density generally decreases away from the Marimo - Staveley contact. Some veins are planar, others are irregular or even brecciated and cut by later veins (Plates 4.19 and 4.21). Vein textures are dominantly tensional, and open space filling texture is common (Plate 4.24). Vein emplacement was in a brittle to brittle-ductile dynamic regime.

Early veins are dominated by microcline and calcite with lesser albite-quartz-muscovite-pyrite and rare biotite and dolomite. These progressively give way to dominantly quartz and calcite with subordinate pyrite and muscovite, minor microcline and rare albite, biotite, dolomite, magnetite and chalcopyrite (Plate 4.28). Plate 4.32 shows a relatively large poikiloblastic grain of magnetite intergrown with non-opaque gangue, pyrite and chalcopyrite. This suggests synchronous crystallisation of all phases. It should be noted that halite bearing fluid inclusions can be found in quartz. Evidence of clear cross-cutting relationships are rare and these veins are probably a part of an evolving system, however clearly late calcite, pyrite and dolomite transgress all earlier veins (Plate 4.21). Several late occurrences of fluorite are noted, generally in vughs which pseudomorph calcite.

4.3.1.4 *Mineralisation and Sulphide Mineralogies*

The Staveley Formation is relatively unmineralised and elevated grades are largely restricted to wider late pyrite veins almost always within several tens of metres of the Marimo Slate contact. The main sulphide noted is pyrite with chalcopyrite largely restricted to calcite bearing veins,

matrix or patches often near the diorite intrusive or Marimo-Staveley contact (Plates 4.30 and 4.31).

In thin section, the pyrite in the wallrock is generally euhedral and hexagonal. In almost all veins, the pyrite crystals show common 120° interface and intercrystal angles typical of annealed pyrite. Although occurring at most stages of the paragenesis, the greatest proportion of pyrite appears to be associated with late calcite.

4.3.2 Marimo Slate

4.3.2.1 Lithologies

The Marimo Slate is dominated by a thinly laminated to massive carbonaceous and often graphitic siltstone-shale package (Plate 4.33). Primary sedimentary features have generally been overprinted by a strong axial planar cleavage, however rare graded bedding indicates that the Marimo Slate is younging away from the Staveley Formation and hence younger than it. The Marimo Slate is generally more fissile away from the ore zone.

4.3.2.2 Metasomatism

Many petrographic sections contain up to several percent uniformly disseminated tourmaline and aggregates of rutile which tend to be aligned with the D_2 foliation and hence, may be of metamorphic or metamorphically remobilised diagenetic origin (Plate 4.37).

The black shale has often been pervasively feldspathised or sericitised. The left column of core in Plate 4.34 shows that early pervasive feldspathisation sometimes follows bedding (and may be pre-folding) and clearly predates some microcline veining. The right column of core shows late thin sulphidic veinlets with a sericitised selvage superimposed on earlier pervasively feldspathised shale. This fine-grained pervasive alteration gives the distinct appearance of bleaching, and elimination of organic matter can be observed as an alteration front (Plate 4.38). The feldspathisation is microcline dominated with generally lesser albite (Plate 4.39). Some retrogression of feldspars to sericite is evident (Plate 4.40). Disseminated pyrite, chalcopyrite and chalcocite sometimes accompanies the bleaching but chalcopyrite and chalcocite are only observed in sericite or microcline alteration (Plates 4.33 and 4.38). This style of pervasive alteration generally cuts across foliation and often obliterates it, and sometimes is brecciated or argillised.

Plate 4.25 (A) Photomicrograph of intensely altered and contact hornfelsed Staveley Formation adjacent to diorite now comprising an albite, calcite, microcline, quartz and magnetite assemblage. Section is from sample 85059 from GDH-05 at 208.7 m depth. Frame width is 1.1 mm.

Plate 4.26 (B) As for Plate 4.25 but under crossed polars.

Plate 4.27 (C) Photomicrograph from same section as Plate 4.25 but alteration assemblage comprises calcite and pyrite (crossed polars; frame width 4.3 mm). Ca = calcite, Py = pyrite, Mic = microcline, Ab = albite, Qtz = quartz, Mt = magnetite.

Plate 4.28 (D) Photomicrograph of calcite, microcline, albite, quartz and pyrite matrix to brecciated Staveley Formation from sample 85057 from hole GDH-05 at 134.15 m depth (crossed polars; frame width 1.1 mm).

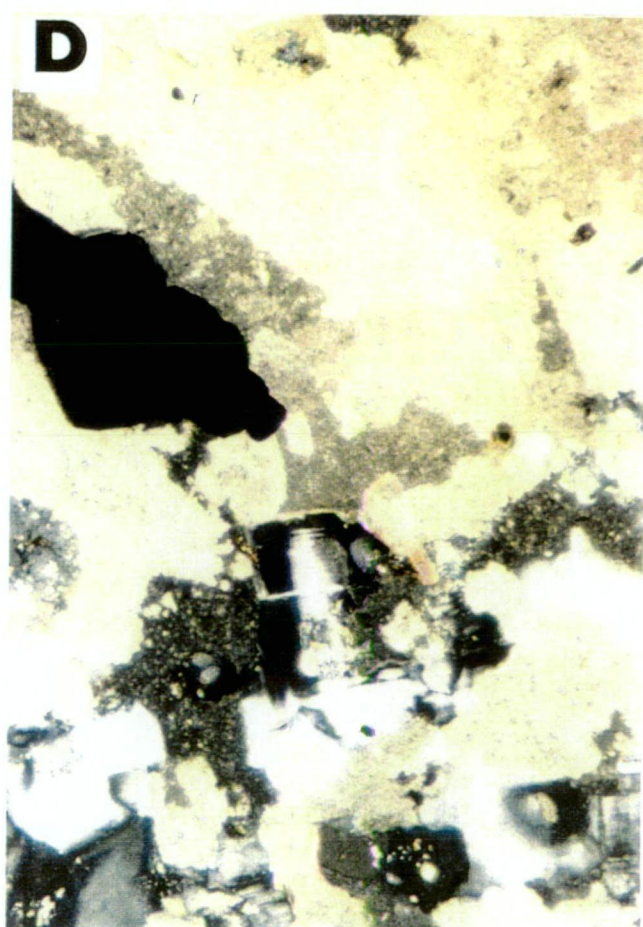
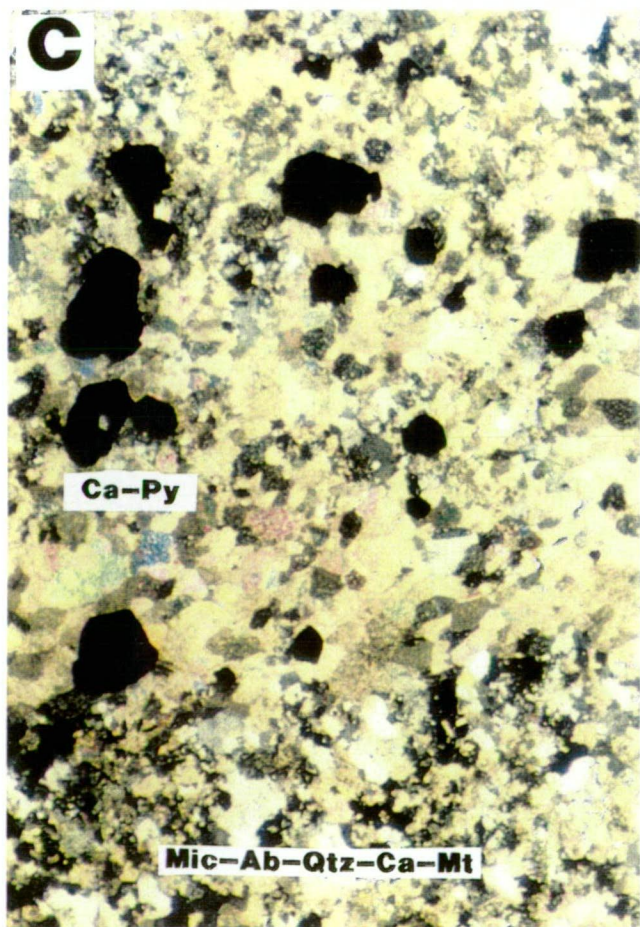
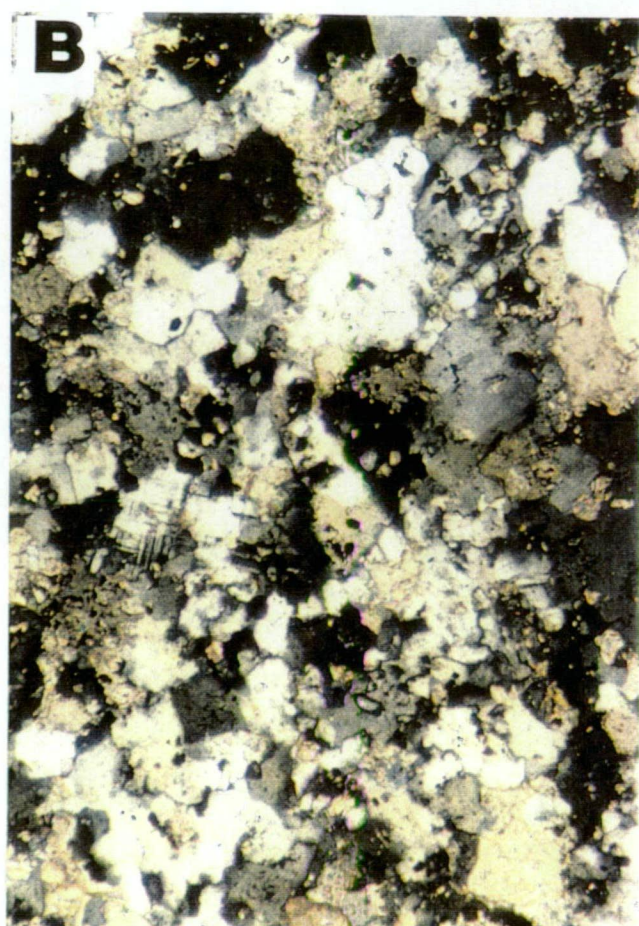
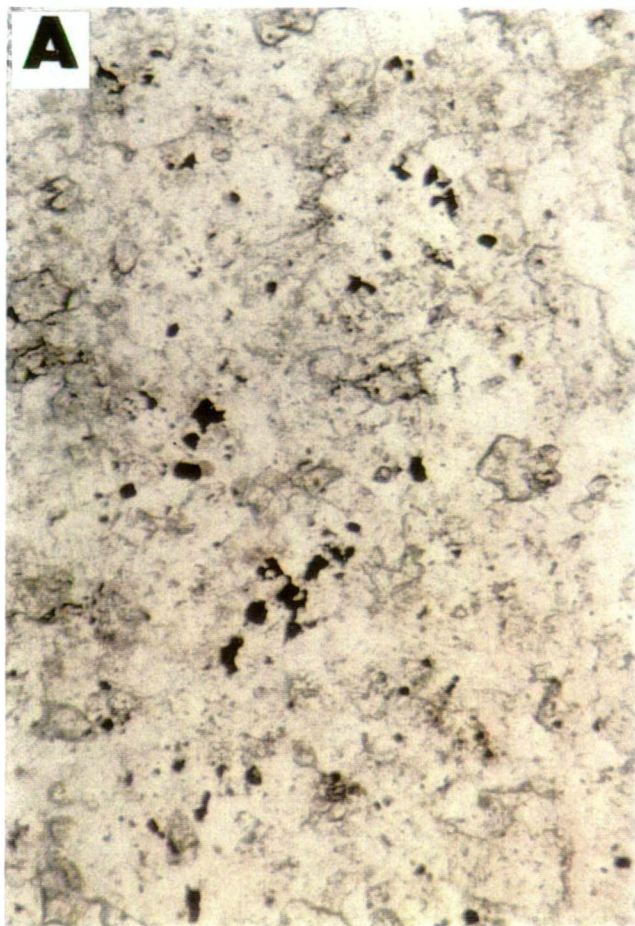


Plate 4.29 (A) Photomicrograph showing small magnetite cubes (opaque) concentrated in particular beds of the Staveley Formation adjacent to a coarse calcite vein. Small ragged biotite flakes may occur in calcite patches. (Sample 85055 from hole GDH-05 at 102.2 m depth; frame width 1.4 mm; transmitted plane polarised light).

Plate 4.30 (B) Photomicrograph showing ragged, chalcopyrite occurs preferentially within or near late coarse calcite patches, veins or matrix. Note the magnetite crystal protruding into the calcite matrix (Sample 85055; frame width 1.4 mm; reflected plane polarised light).

Plate 4.31 (C) Photomicrograph showing coarser grained pyrite and chalcopyrite tend to occur in or near coarser calcite patches in the Staveley Formation (Sample 85058 from hole GDH-05 at 140.0 m depth; frame width 1.4 mm; reflected plane polarised light).

Plate 4.32 (D) Photomicrograph showing a relatively large poikiloblastic grain of magnetite (pale grey) is intergrown with calcite, quartz, feldspar, pyrite (white) and chalcopyrite (yellow) indicating synchronous crystallisation of all phases (Sample 85058; frame width 1.4 mm; reflected plane polarised light).

*** Note**

Ca = calcite

Biot = biotite

Mt = magnetite

Cpy = chalcopyrite

Py = pyrite

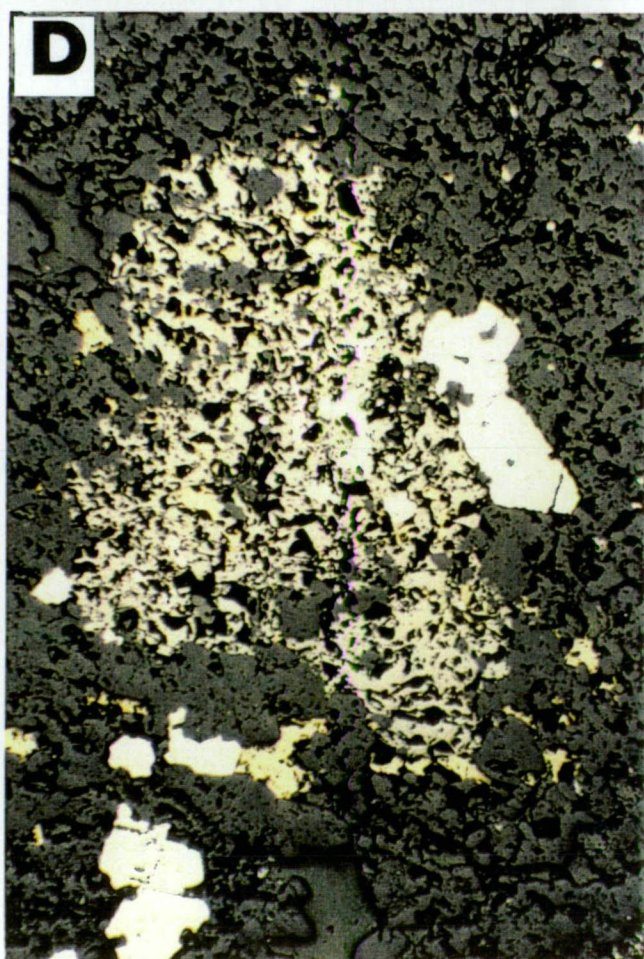
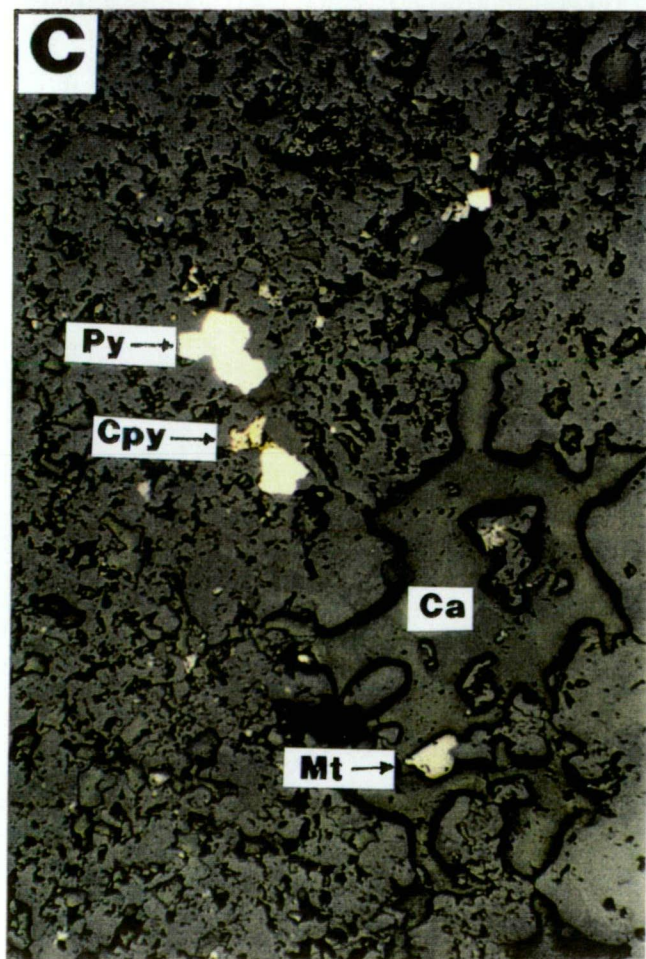
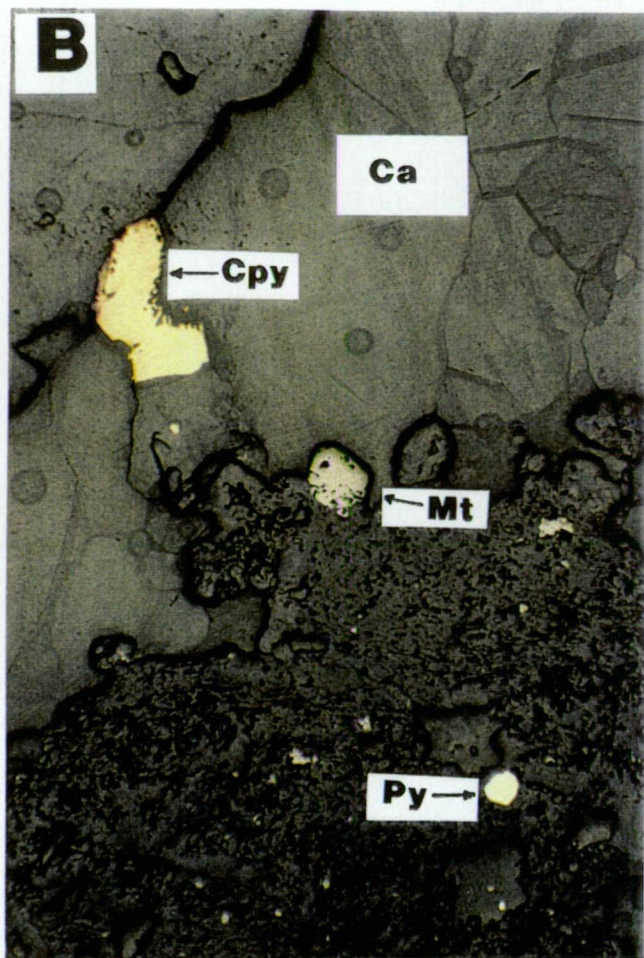
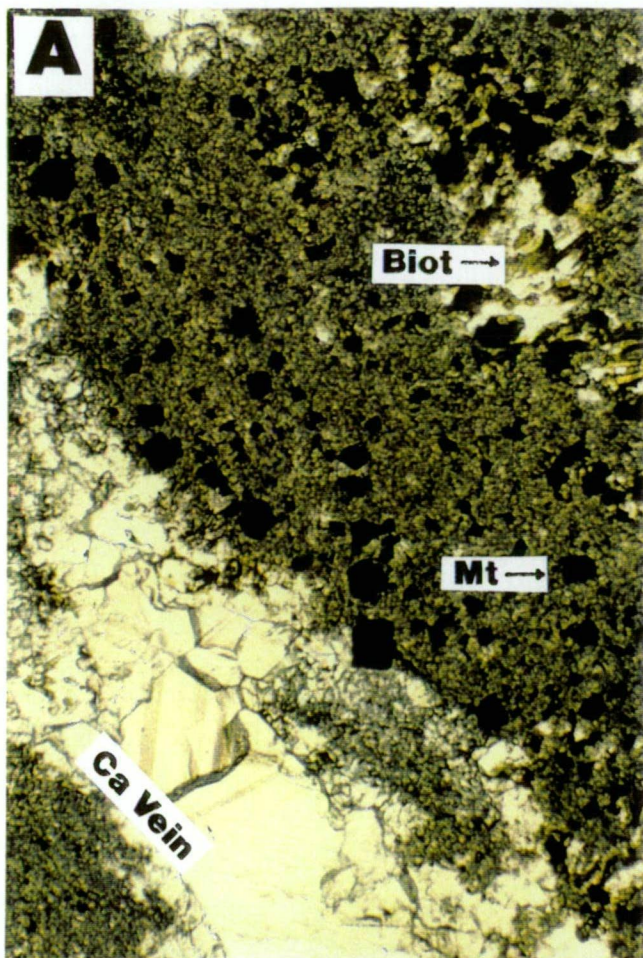


Plate 4.33 (A) Typical fissile thinly laminated carbonaceous and graphitic shale and slate from the Marimo Slate in hole GDH-01 at around 122 m depth. The spots are very fine grained aggregates of (diagenetic/metamorphic ?) pyrite.

Plate 4.34 (C) Left column of core shows early pervasive feldspar alteration of shale sometimes follows bedding (and may predate folding) and clearly predates some microcline veining. Right column of core shows late thin sulphidic veinlets with sericitic selvages, superimposed on earlier pervasively altered shale.

Plate 4.35 (B) Central column of core shows a coarsely crystalline phlogopite (dark laths), quartz, microcline vein.

Plate 4.36 (D) Weak pervasive feldspar alteration (superimposed by a vein) is diminishing in intensity away from the main ore zone in hole GTRC-11 at around 256 m depth.

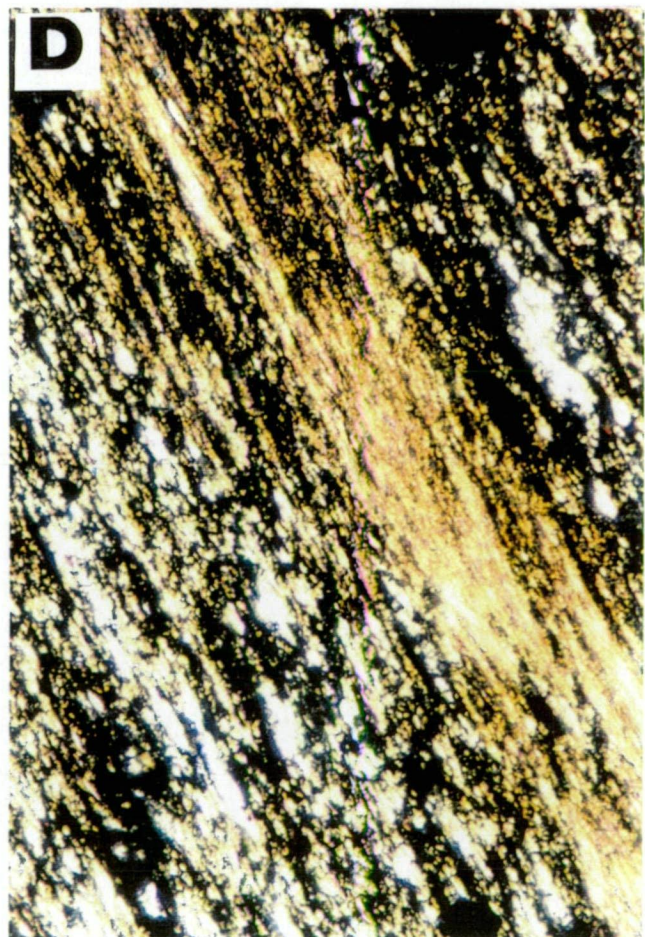
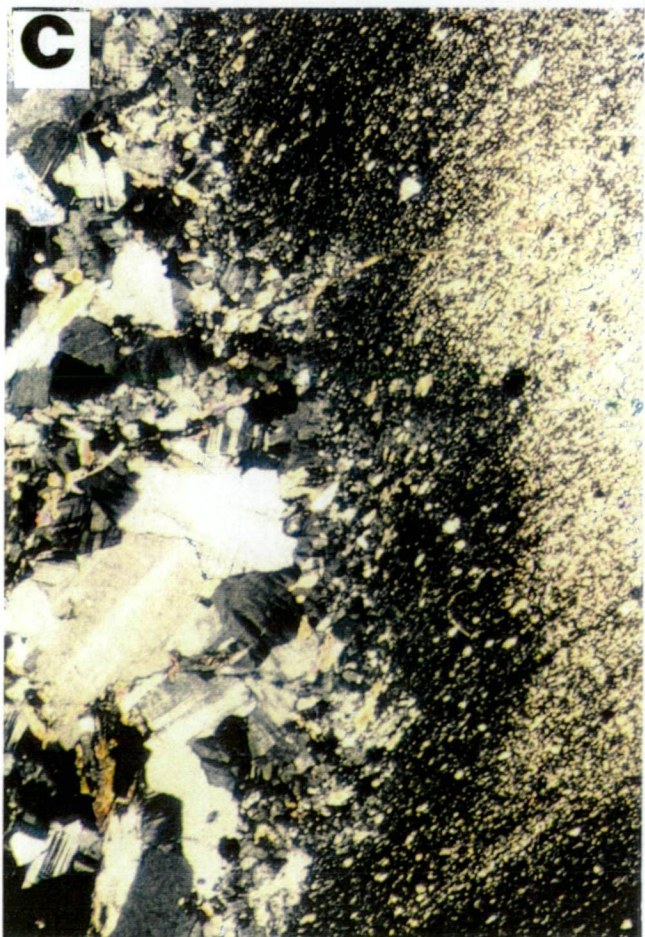
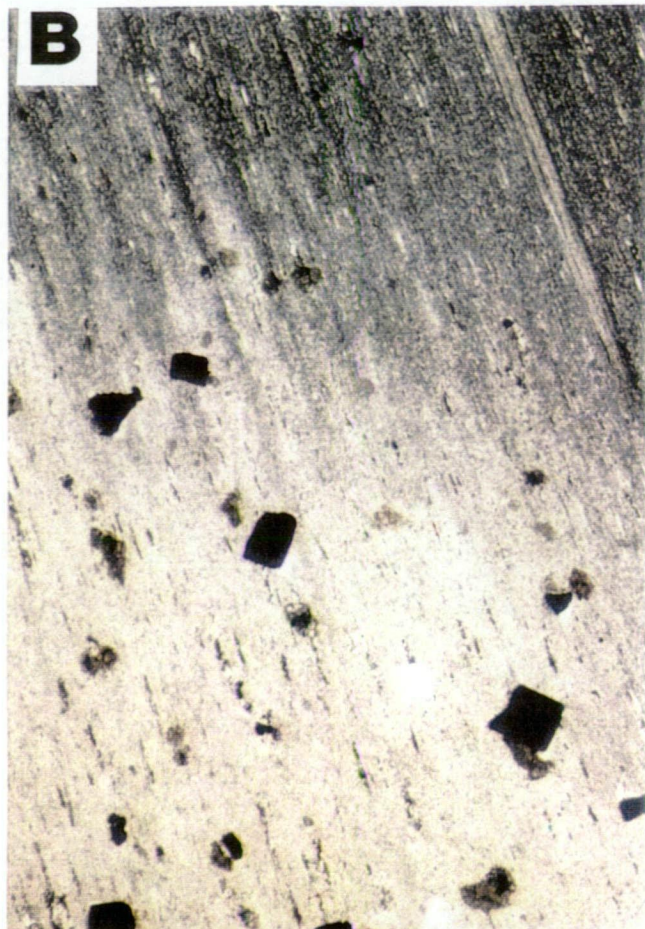
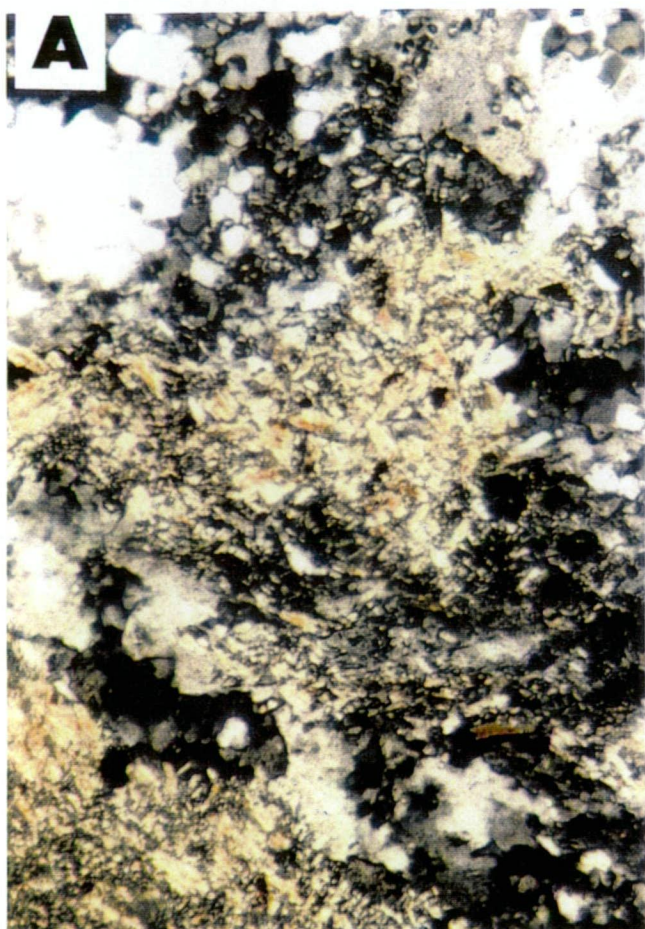


Plate 4.37 (A) Photomicrograph showing intensely tourmalinised (orange laths) and feldspathised slate with some rutile aggregates (Sample 85035 from hole GDH-03 at 146.0 m depth; frame width 1.1 mm; crossed polars).

Plate 4.38 (B) Photomicrograph showing pervasive feldspar alteration front with disseminated pyrite (Sample 85011 from hole GDH-01 at 156.5 m depth; frame width 4.3 mm; plane transmitted light).

Plate 4.39 (C) Photomicrograph showing feldspathised slate adjacent to feldspathic vein (Sample 85011; frame width 4.3 mm; crossed polars).

Plate 4.40 (C) Photomicrograph showing sericitic carbonaceous slate with feldspathic lenses (Sample 85009 from hole GDH-01 at 119.8 m depth; frame width 1.1 mm; crossed polars).



Subsequent veining may or may not be superimposed. In drill core the bleached zones may be up to 20 - 30 metres wide and when superimposed by later veining and mineralisation, they generally host the strongest mineralisation and define the main ore zone. They appear to feather out at depth and along strike (Plate 4.36). The bleaching is probably an immediate precursor to brittle failure and veining. The alteration zones can be correlated between the holes but do not appear to be parallel to bedding dips and hence, must be created by cross-cutting structures.

4.3.2.3 *Veining*

Veins in the Marimo Slate are dominated by microcline with lesser quartz, albite, phlogopite, apatite and sulphides with minor amounts of other minerals. Veins do not appear to be of metamorphic origin as suggested by Mason (1994). Episodic fracturing in a brittle to brittle-ductile regime initiated several stages of veining. Earlier veins have often been brecciated or cut by later veins (Plates 4.42, 4.45 and 4.48). They may be irregular in shape (Plate 4.41), folded (Plates 4.42 and 4.35), fractured (Plates 4.45, 4.47 and 4.48) or sometimes ghost-like (Plate 4.41). Late veins are planar and cut across all other fabrics (Plate 4.48). The most mineralised veins are usually superimposed on the earlier pervasive alteration but also occur in relatively unaltered black shale (Plate 4.41).

The earliest veins are dominated by coarsely crystalline microcline, to 10 mm (Plate 4.45) with trace amounts of pyrite and occasionally albite with trace amounts of quartz, phlogopite, rutile, pyrite and apatite.

The main stage of veining always includes microcline, usually as a major component, with variable amounts of quartz, phlogopite, albite, apatite and minor amounts of pyrite, chalcopyrite, covellite, chalcocite, cobaltite, rutile, marcasite and rare amounts of calcite and chlorite. These veins are generally discordant and planar, but occasionally may be strained, folded, fractured or ghost-like. They are typically 1-10 cm wide. Plates 4.52 to 4.57 show photomicrographs of typical vein assemblages. Plate 4.57 shows an early microcline dominated vein which was cut by a quartz-chalcopyrite vein which in turn was cut by a late planar sericite vein.

Some open space filling textures are observed. Chalcopyrite often fills interstices between crystals and appears to be spatially associated with quartz and microcline (Plate 4.51). Some of the veins have been dismembered by pressure solution seams resulting in a chaotic

appearance. This indicates an active shear system with progressive solution and redeposition of minerals.

These veins are cut by thinner (0.1 mm to 10 mm) generally planar but frequently irregular sericite dominated veins with variable amounts of chalcopyrite, chalcocite, quartz and chlorite (Plate 4.57). Preferred vein orientations are not apparent (Figure 4.4). Veins away from the main altered and mineralised zone generally comprise quartz-pyrite with subordinate feldspars, eg. in holes GDH-06 and GDH-04.

4.3.2.4 *Mineralisation and Sulphide Mineralogies*

The sulphide species present in veins and host rock include pyrite, chalcopyrite, chalcocite, covellite, with lesser marcasite, cobaltite and rare sphalerite and pyrrhotite (Plates 4.48 to 4.52 and 4.58 to 4.65). In the altered host rock, chalcopyrite occurs as sparsely disseminated grains and, in one instance as micron sized inclusions in rutile. In the veins, chalcopyrite forms as ragged grains or aggregates which often enclose euhedral and subhedral pyrite (Plates 4.58 and 4.59). Rare anhedral sphalerite to 300 microns is also seen as inclusions in chalcopyrite (Plate 4.60). These may form by exsolution, coprecipitation or replacement (Bortnikov et al., 1991). Much of the chalcopyrite occurs in interstices between microcline as well as inclusions peppered through microcline (Plates 4.61 and 4.62), phlogopite and quartz, where it may be replaced by the secondary copper minerals. Some thin discontinuous veinlets of chalcopyrite can be seen to cut across quartz and feldspar crystals (Plate 4.62). Some ragged grains and veinlets extend from the vein into the wallrock. Most of the chalcopyrite is within or adjacent to veins. Occasionally it can be seen to replace feldspar rims. Although minor chalcopyrite accompanied most stages of the paragenesis, most chalcopyrite was introduced during the main stage and particularly the later stages of veining. Erythrite was identified by microprobe disseminated in the wallrock as well as in veins.

Euhedral pyrite cubes occur disseminated in feldspathised host rock (Plate 4.63). Ragged disseminated pyrite occurs in argillic altered host rock which has been brecciated. The pyrite in host rock often contains minute gangue inclusions. The pyrite in veins occurs as anhedral to euhedral cubic and hexagonal (annealed) crystals and aggregates (Plates 4.58 and 4.59). The aggregates often display intense fracturing similar to Mt Dore (Beradsmore, 1992; Plate 4.65). Pyrite is often enclosed within chalcopyrite and microcline as well as occurring at grain boundaries. Host rock and vein pyrite may be replaced by covellite and chalcocite. Very fine grained pyrite can be seen replacing chalcopyrite near its margins and near microfractures. This is also associated with traces of fine replacement style pyrrhotite (Plate 4.60). Marcasite is observed within elongate pyrite.

Plate 4.41 (A) Central column of core shows a microcline, quartz and phlogopite (dark laths near bottom) vein hosted by unaltered black shale. Note the irregular ghost like veins in other columns.

Plate 4.42 (B) Several generations of quartz-microcline veins cutting each other adjacent to intensely feldspathic altered shale with microcline veins which has been brecciated (left column of core).

Plate 4.43 (C) Pervasively sericitised shale with disseminated chalcocite blebs, veined by a microcline-chalcocite vein (centre).

Plate 4.44 (D) Pervasive feldspar altered shale with irregular pyrite stringer veins.

Plate 4.45 (E) Part of a wide hematite dusted coarse microcline vein, which has been fractured and veined by a pyrite vein (fourth column from left).

Plate 4.46 (F) Brecciated massive pyrite-microcline vein.

Plate 4.47 (G) Pervasively feldspathised shale which has been veined by microcline then fractured.

Plate 4.48 (H) The central column shows a microcline vein with a feldspathic selvage, has been fractured perpendicular to vein walls and filled by late chalcopyrite. The left column shows a late planar quartz vein.

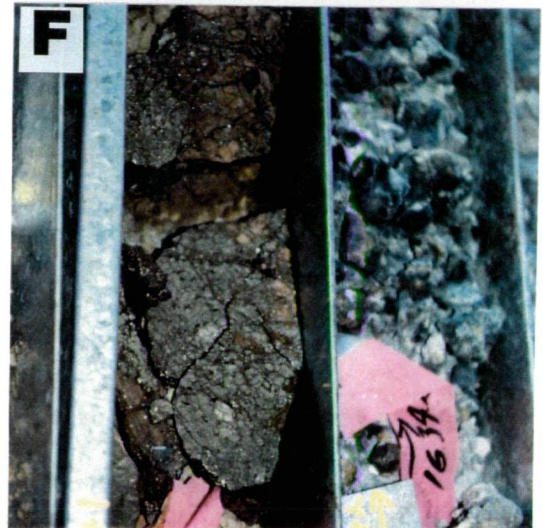
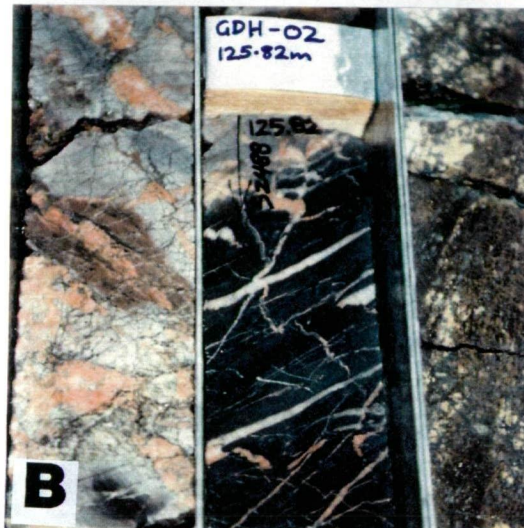
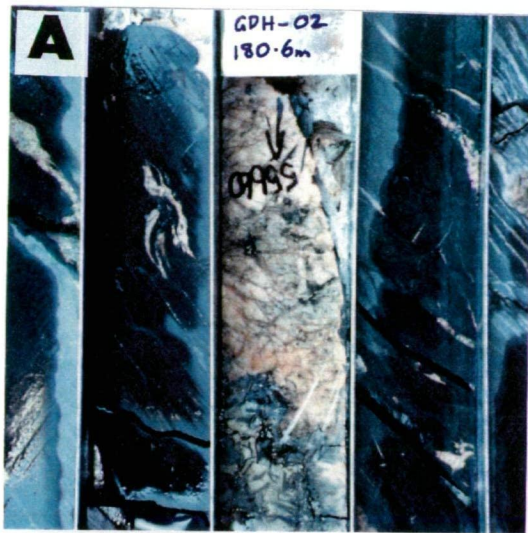


Plate 4.49 (A) Higher grade ore zone assaying about 1.25 g/t Au and 2.57% Cu is hosted by argyllised black shale (yellow) which was veined by feldspars, mica and pyrite then strongly brecciated and filled by gangue minerals including pyrite and chalcopyrite. Most of the chalcopyrite has been replaced by chalcocite. .

Plate 4.50 (B) Close up view of Plate 4.49.

Plate 4.51 (C) An irregular, coarse microcline-quartz vein which is hosted by unaltered black shale, has been fractured and filled by chalcopyrite and pyrite.

.

.

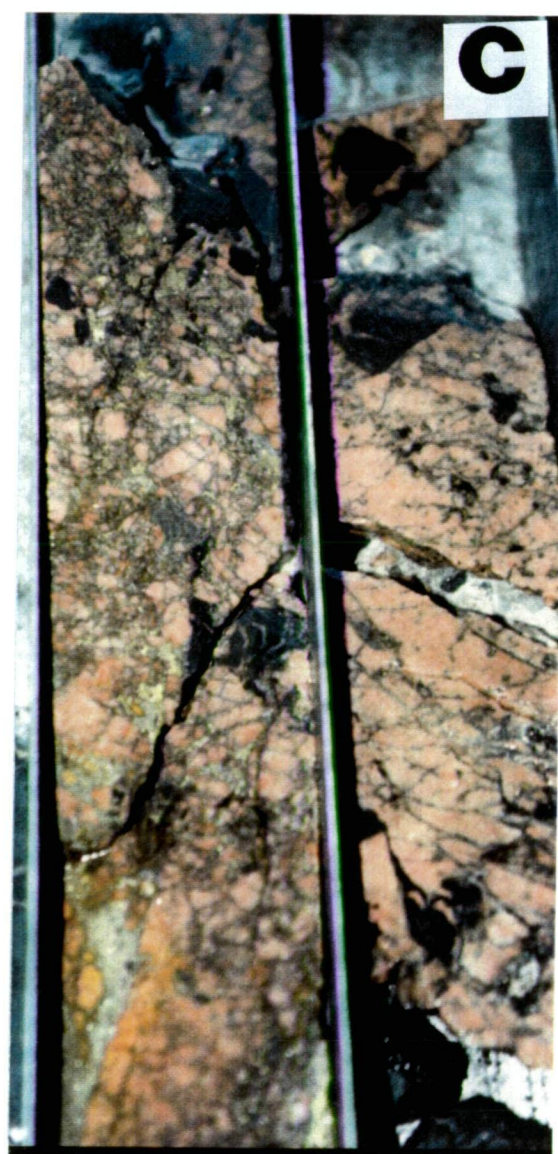
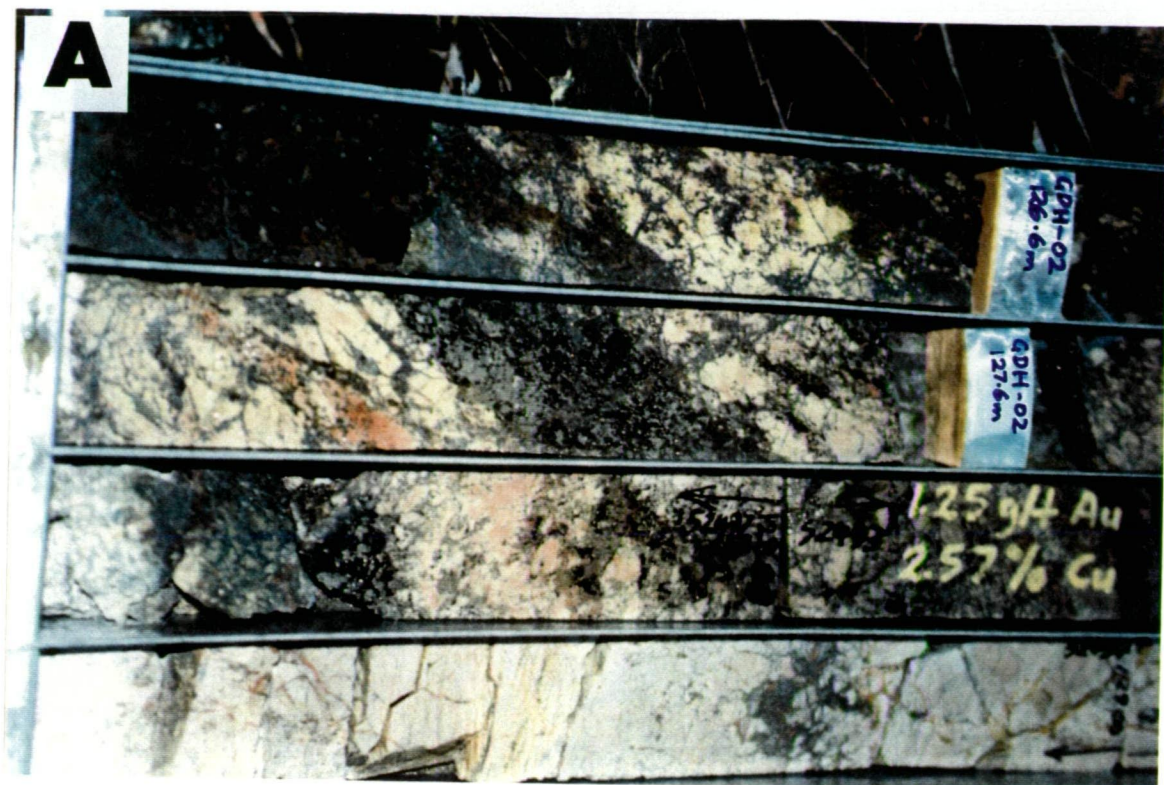


Plate 4.52 (A) Photomicrograph of a microcline, phlogopite, quartz and pyrite vein in feldspathised slate (Sample 85011 from hole GDH-01 at 156.5 m depth; frame width 3.6 mm; crossed polars).

Plate 4.53 (B) Photomicrograph of patchy albitisation of slate near a feldspathic vein (Sample 85007 from hole GDH-01 at 128.45 m depth; frame width 3.6 mm; crossed polars).

Plate 4.54 (C) Photomicrograph of an albite, quartz, phlogopite, apatite and rutile vein in altered slate (Sample 85007; frame width 3.6 mm; crossed polars).

Plate 4.55 (D) Photomicrograph of a microcline, quartz, phlogopite, chlorite, pyrite and chalcopyrite vein from the same sample and thin section as Plates 4.53 and 4.54 (frame width 3.6 mm; crossed polars).

Plate 4.56 (E) Photomicrograph of a quartz, microcline, albite, phlogopite, rutile, apatite, pyrite and calcite vein in feldspathised slate with disseminated pyrite (Sample 85004 from hole GDH-01 at 124.5 m depth; frame width 3.6 mm; crossed polars).

Plate 4.57 (F) Photomicrograph of a late planar sericite vein cutting a quartz-chalcopyrite vein which cuts an early microcline dominated vein (Sample 85022 from hole GDH-02 at 142.0 m depth; frame width 3.6 mm; crossed polars).

*** Note**

Phg = phlogopite

Chl = chlorite

Mic = microcline

Cpy = chalcopyrite

Py = pyrite

Ap = apatite

Qtz = quartz

Ab = albite

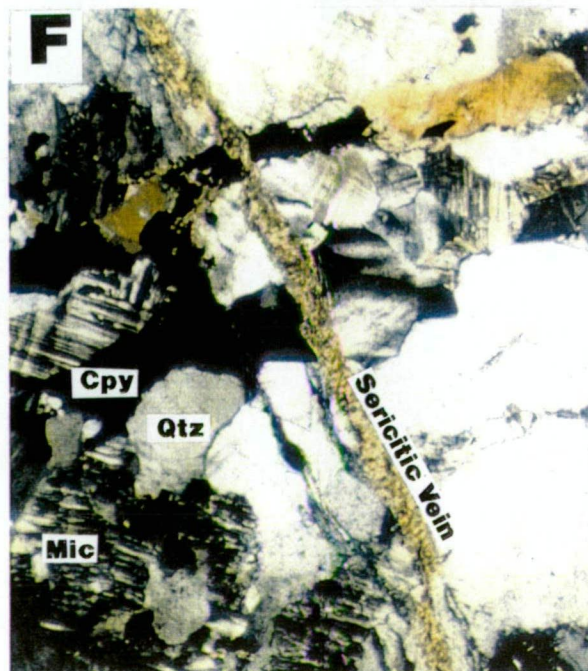
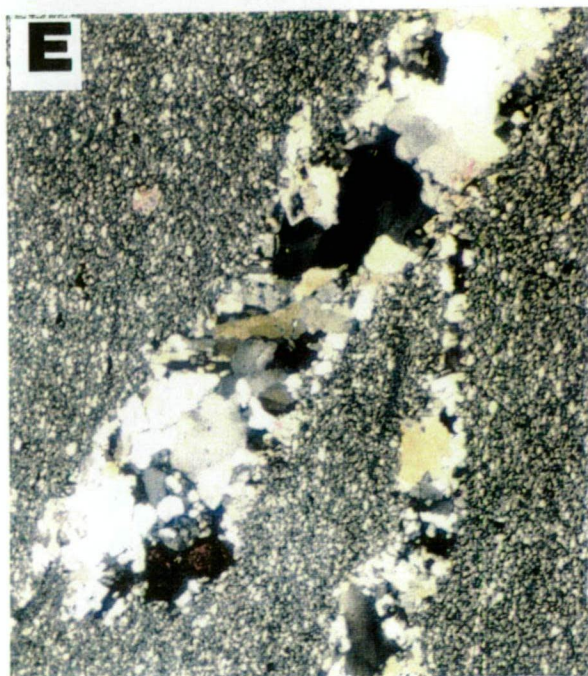
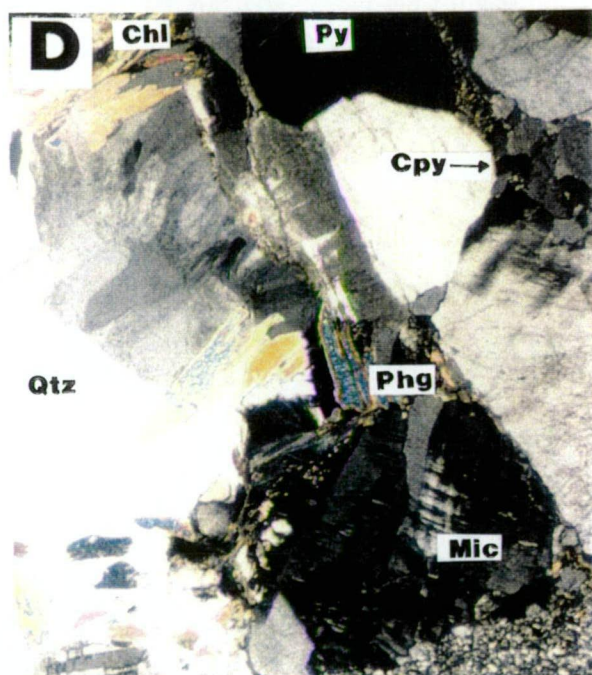
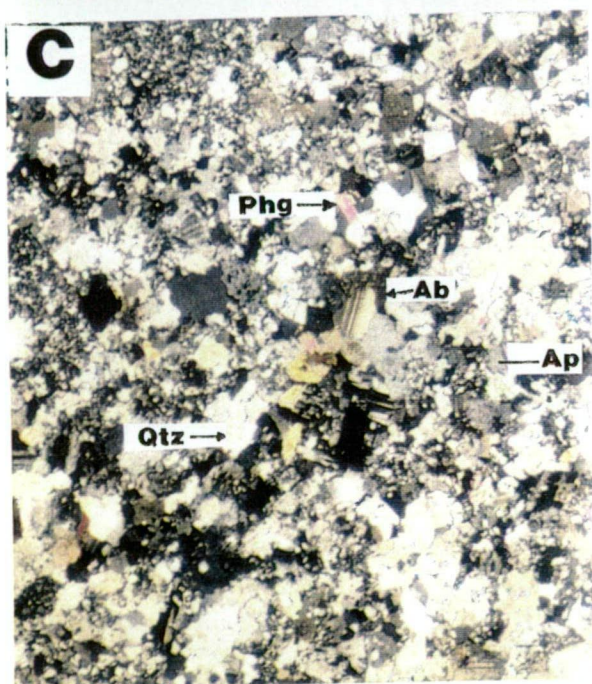
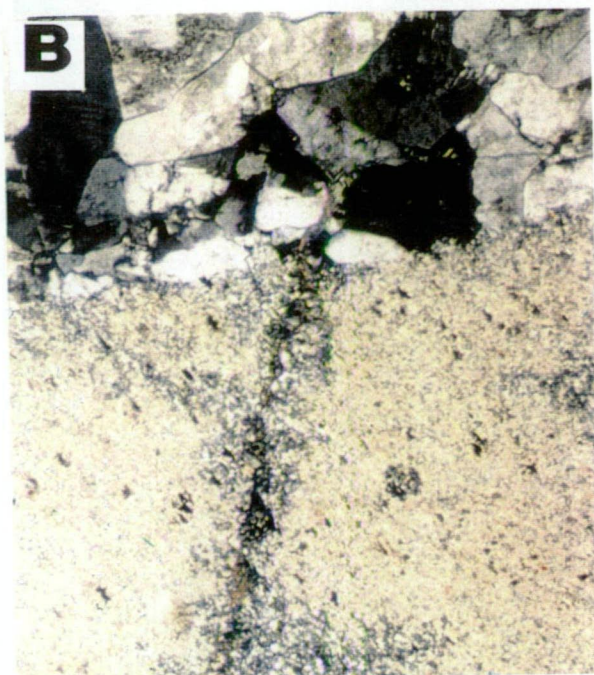
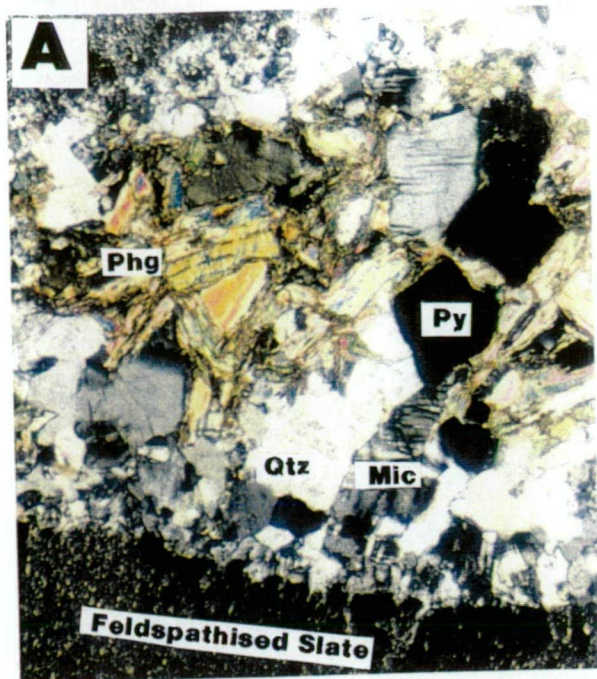


Plate 4.58 (A) Photomicrograph showing a portion of a microcline, quartz, apatite and sulphide vein showing euhedral pyrite in massive-chalcopyrite and sphalerite (grey) being replaced by covellite (blue). Note the 120° angles between pyrite euhedra may suggest that annealing may have occurred. Some chalcopyrite is also being replaced by covellite (Sample 85006 from hole GDH-01 at 128.4 m depth; frame width 0.8 mm; reflected plane polarised light).

Plate 4.59 (B) Photomicrograph showing ragged elongate aggregates of pyrite (creamish white) in places retain relicts of marcasite (best observed at high magnification) and lie in massive chalcopyrite from a microcline, quartz, phlogopite, rutile and sulphide vein in relatively unaltered graphitic shale (Sample 85023 from hole GDH-02 at 149.8 m depth; frame width 0.8 mm; reflected plane polarised light).

Plate 4.60 (C) Photomicrograph showing a portion of a microcline, quartz, albite, apatite, phlogopite and sulphide vein in graphitic slate, showing large pyrite crystals may contain ragged inclusions of chalcopyrite (yellow) and pyrrhotite (grey-brown) - (Sample 85019 from hole GDH-02 at 135.0 m depth; frame width 0.33 mm; reflected plane polarised light).

Plate 4.61 (D) Photomicrograph showing a portion of a microcline, quartz, phlogopite and sulphide vein hosted by foliated and crenulated graphitic slate, showing that small grains of pyrite (white) and chalcopyrite (yellow) favour microcline (centre; darker grey) rather than quartz (left and right; paler grey) - (Sample 85025 from hole GDH-02 at 177.7 m depth; frame width 1.6 mm; reflected plane polarised light).

* Note Sph = sphalerite

 Cov = covellite

 Mic = microcline

 Cpy = chalcopyrite

 Py = pyrite

 Pho = pyrrhotite

 Qtz = quartz

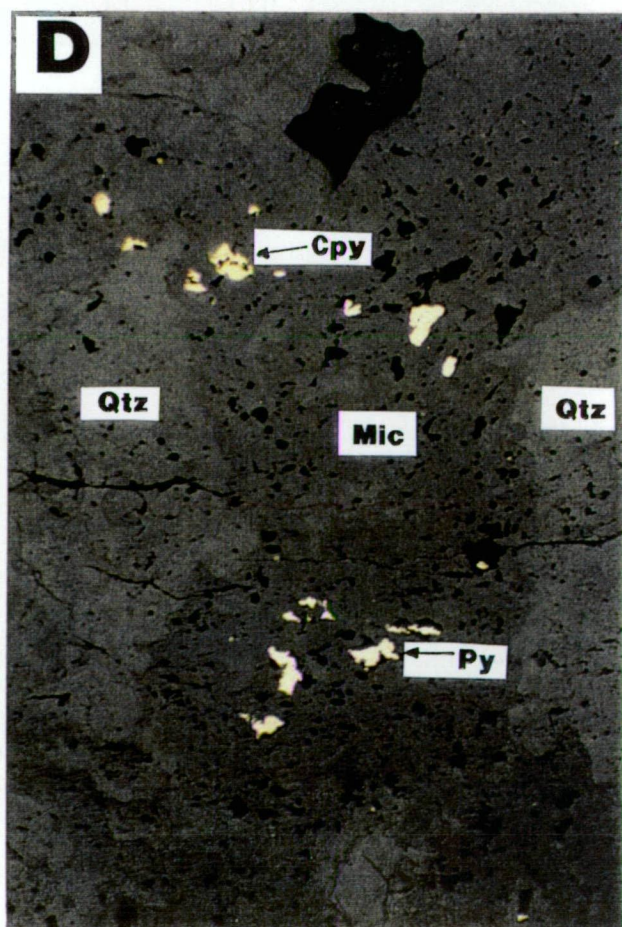
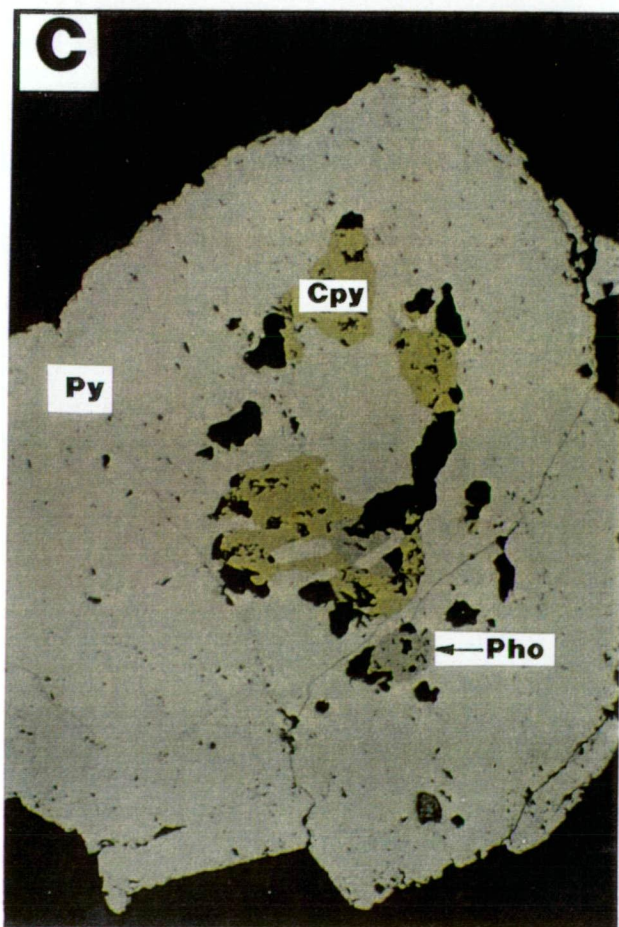
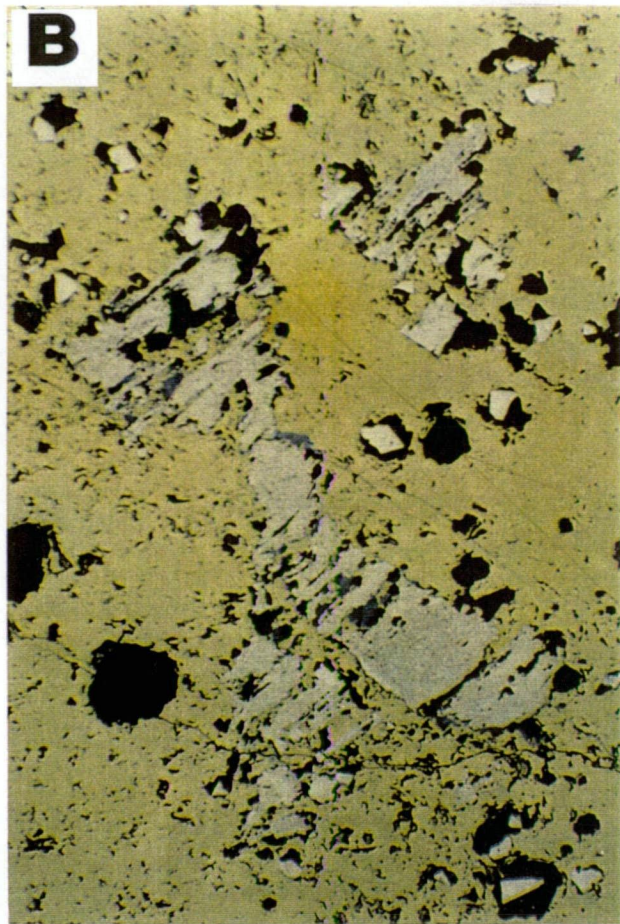
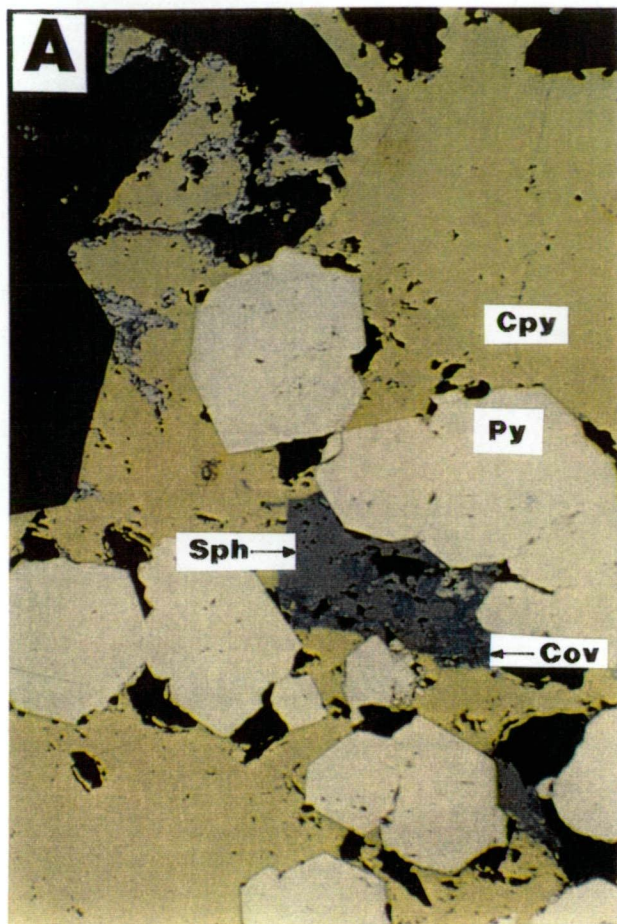


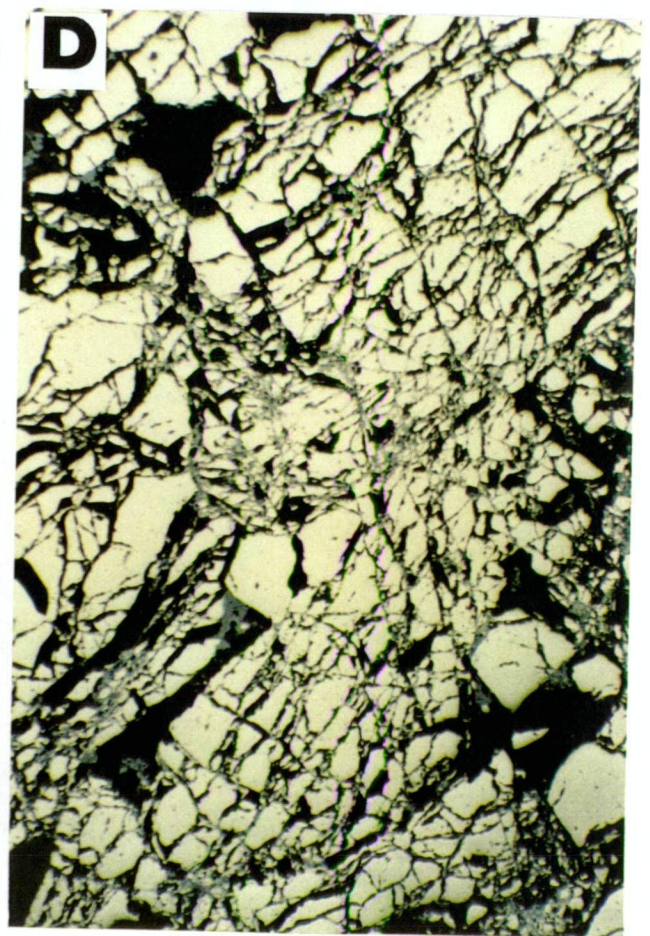
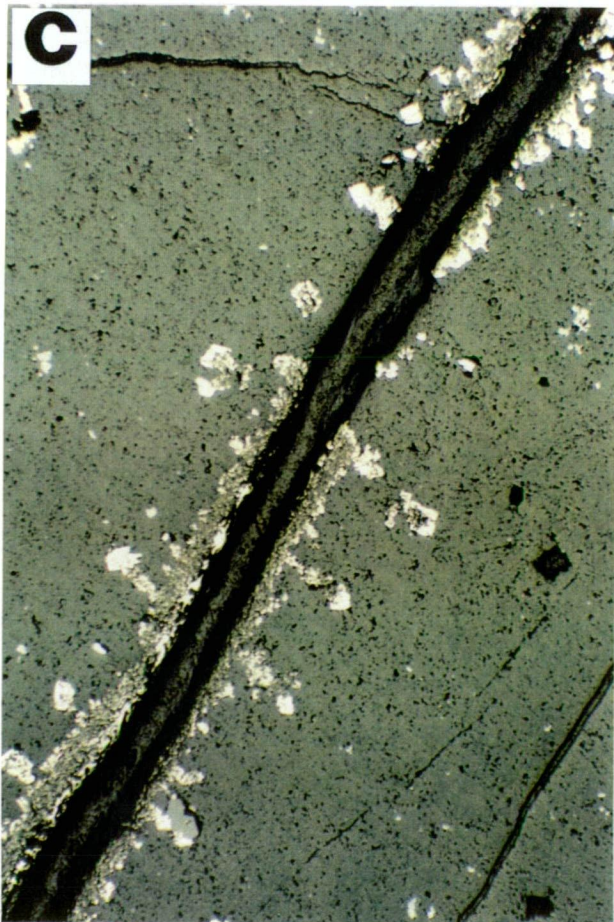
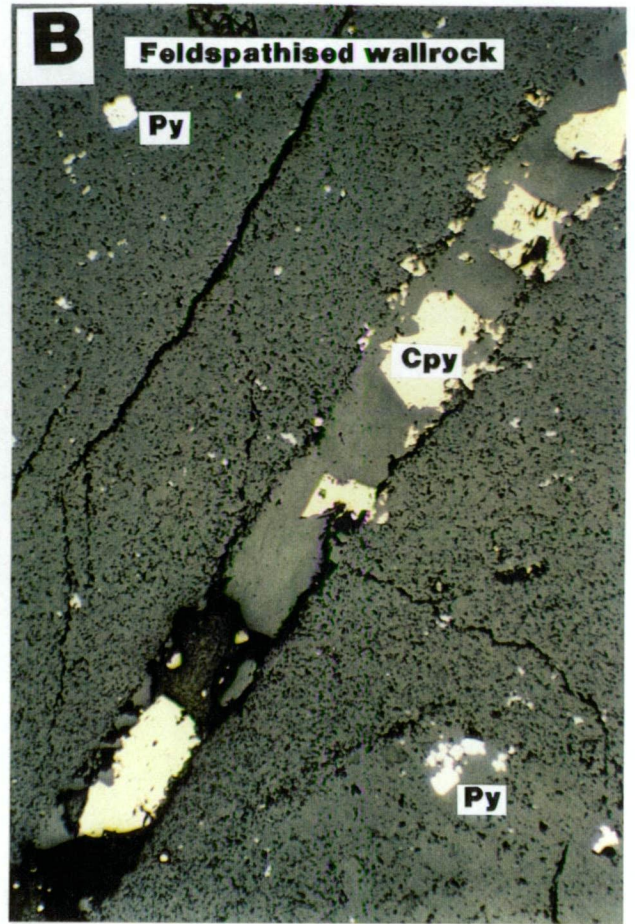
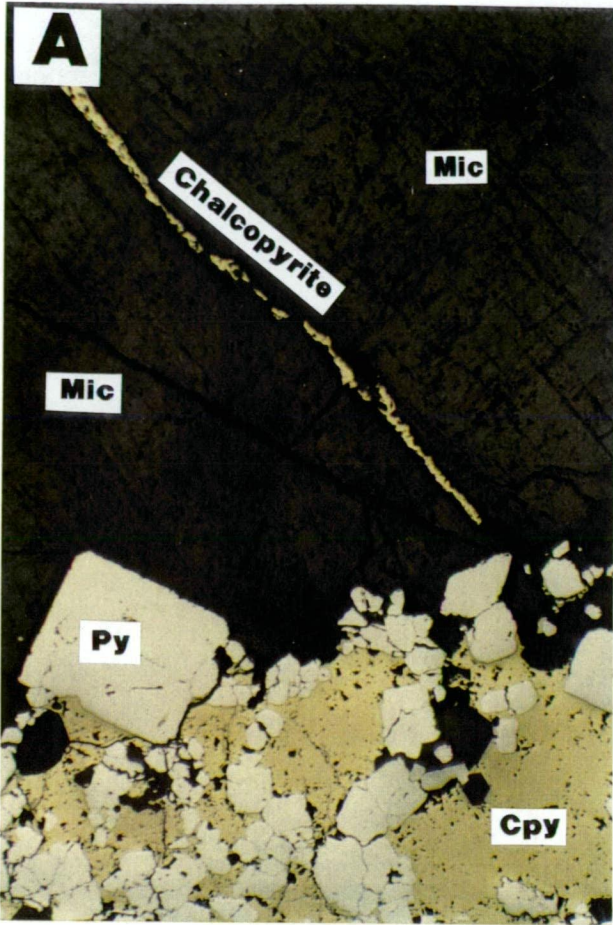
Plate 4.62 (A) Photomicrograph of a portion of a microcline, quartz, phlogopite and sulphide vein showing a thin trail of chalcopyrite (top half of photograph) filling a cleavage trace in feldspar (Sample 85021 from hole GDH-02; frame width 1.6 mm; reflected plane polarised light).

Plate 4.63 (B) Photomicrograph of a planar vein containing ragged chalcopyrite grains (pale yellow). Small pyrite crystals and aggregates (white) are sparsely disseminated in pervasively feldspathised wallrock (upper left and lower right) - (Sample 85020 from hole GDH-02 at 139.5 m depth; frame width 1.6 mm; reflected plane polarised light).

Plate 4.64 (C) Photomicrograph of a late clay filled fracture in feldspathised wallrock which is flanked by very fine grained replacement pyrite in the vein selvage. This illustrates that the sulphide components were mobile during very late fracturing (Sample 85033 from hole GDH-03 at 140.9 m depth; frame width 1.6 mm; reflected plane polarised light).

Plate 4.65 (D) Photomicrograph of a portion of an abundant massive pyrite vein (creamish-white) which is strongly fractured. Minute chalcopyrite inclusions within the pyrite can be seen at high magnification (Sample 85034 from hole GDH-03 at 141.7 m depth; frame width 1.6 mm; reflected plane polarised light).

*** Note** Mic = microcline
 Cpy = chalcopyrite
 Py = pyrite



aggregates (Plate 4.59), and may have been more common prior to inversion to pyrite (Mason, 1994).

Ch. 4.4 Diorite

The diorite crops out on surface as a several metre wide dyke, but was intersected in two core holes (GDH-03 and GDH-05), where it was up to 40 m wide and intensely magnetic. It intrudes the Staveley Formation and appears to have a contact aureole which is gradational and comprises several alteration assemblages comprising some of the following minerals:

hematite dusted albite, quartz, magnetite, calcite, hematite dusted microcline, rutile and pyrite (Plates 4.66 to 4.75).

The diorite is fine grained and originally contained hornblende or pyroxene which has been pseudomorphed by biotite and chlorite. The diorite now comprises plagioclase, biotite, calcite, sphene, magnetite and rutile with some disseminated pyrite and traces of chalcopyrite. Joyce (1993) suggested that inferred ilmenite has been replaced by magnetite and sphene. The diorite is frequently chloritised and carbonated with patchy pervasive epidote and sericite alteration (Plates 4.66, 4.72 and 4.73). Veins are dominated by calcite and pyrite (Plates 4.70, 4.71 and 4.73) which post date the hematite dusting, but some veins comprising albite and microcline (which have been partly retrogressed to sericite) with later calcite, biotite and minor rutile have been observed.

Plate 4.66 (A) Fine grained diorite with thin calcite veins. Top row of core has been pervasively sericitised. From hole GDH-05 at about 248 m depth.

Plate 4.67 (B) Microdiorite with thin calcite veins and a thicker hematite dusted microcline, calcite and biotite vein in the centre of the photograph, from hole GDH-05 at about 221 m depth.

Plate 4.68 (C) Left column of core showing a calcite vein in microdiorite with a hematite dusted microcline selvage. Vein is at 225 m depth from hole GDH-05.

Plate 4.69 (D) Calcite veins of brittle style in altered diorite, from hole GDH-05 at 226 m depth.

Plate 4.70 (E) Right column shows an irregular calcite vein with large aggregates of granular pyrite from the altered margins of the microdiorite.

Plate 4.71 (F) Quartz, calcite and pyrite vein in heavily chloritised and carbonated microdiorite from hole GDH-03 at 161 m depth.

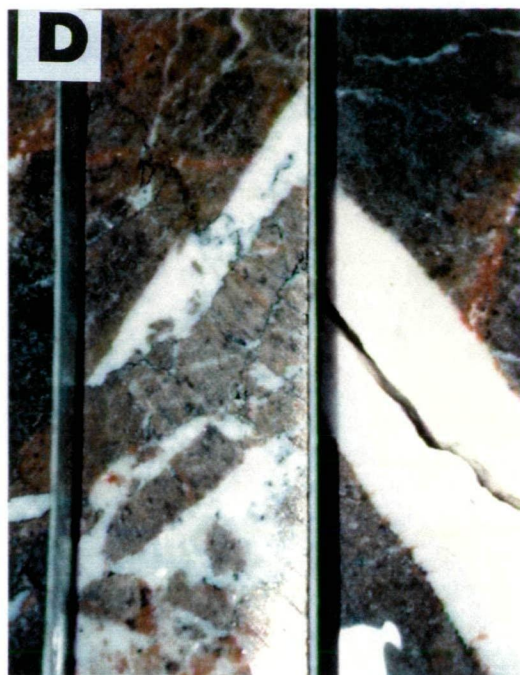
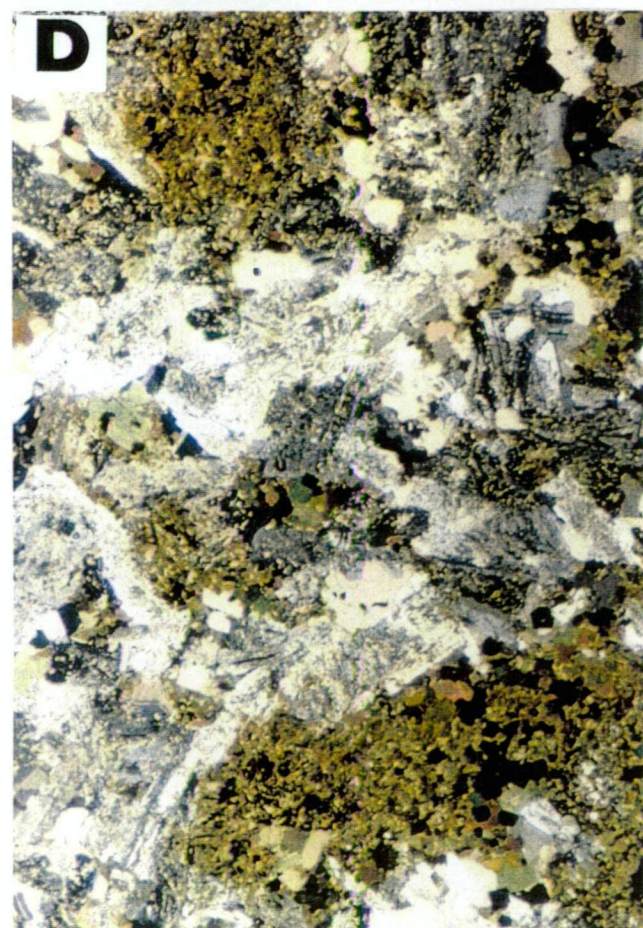
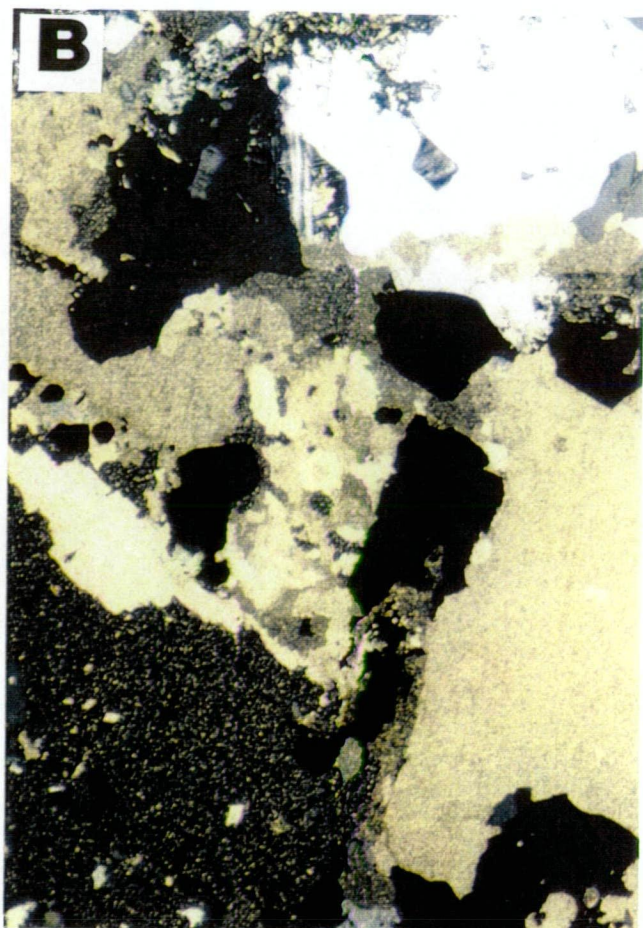
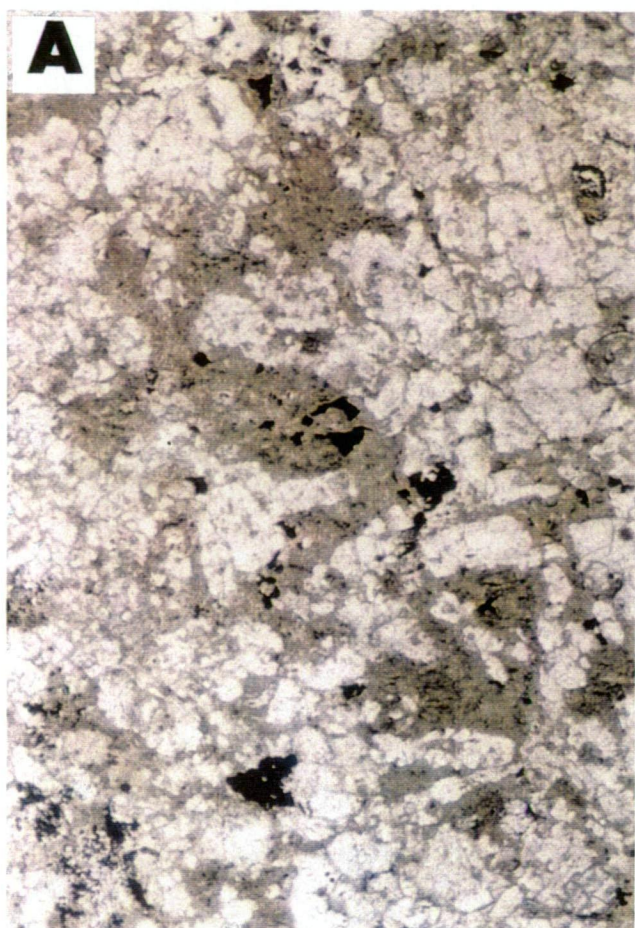


Plate 4.72 (A) Photomicrograph of chloritised (green) and carbonated microdiorite with disseminated magnetite (black) - (Sample 85037 from hole GDH-03 at 161.2 m depth; frame width 4.3 mm; plain light).

Plate 4.73 (B) Photomicrograph of a microcline, calcite, quartz and pyrite vein in chloritised microdiorite (Sample 85037; crossed polars; frame width 4.3 mm).

Plate 4.74 (C) Photomicrograph of a sericitised plagioclase-rich part of a plagioclase, calcite, microcline, biotite and rutile vein in microdiorite (Sample 85063 from hole GDH-05 at 247.5 m depth; frame width 4.3 mm; crossed polars).

Plate 4.75 (D) Photomicrograph of carbonated and biotite altered microdiorite with disseminated (and aggregates of) magnetite (black) - (Sample 85062 from hole GDH-05 at 218.8 m depth; frame width 4.3 mm; crossed polars).



4.5 *Discussion and Paragenesis*

Some of the following points should be noted prior to establishing the paragenesis.

- * Albite bearing veins usually occur in at least partially albitised host rock and microcline dominated veins usually occur in pervasively microcline-sericite altered host rock possibly suggesting at least some host rock - vein interaction.
- * Microcline in veins hosted by sericitised host rock is usually not altered to sericite itself. This would imply a near neutral pH fluid during and post dating the veining.
- * Apatite or rutile in veins, always co-exist with quartz, suggesting contemporaneity. Apatite never co-exists with calcite and is not present in Staveley Formation veins and lithologies. This possibly suggests a host rock (fO_2) control on precipitation of apatite and that carbonate and phosphate did not co-exist. Apatite always co-exists with quartz (and microcline) as at the Mt Dore Deposit (Beardsmore, 1992).
- * Very late chalcopyrite in stringers and veins usually co-exists with sericite, but most earlier chalcopyrite is feldspar stable.
- * When quartz co-exists with albite, microcline is always present and may be a reaction product, i.e. alkali exchange of feldspars.
- * Fluorite is only present as a late stage in the Staveley Formation. The main halogen bearing minerals in Marimo Slate hosted veins are apatite and phlogopite (see Chapter 5), which are in earlier veins in the paragenesis.

The paragenetic sequence for each host rock is shown in Figure 4.11.

Figure 4.11a

MARIMO SLATE

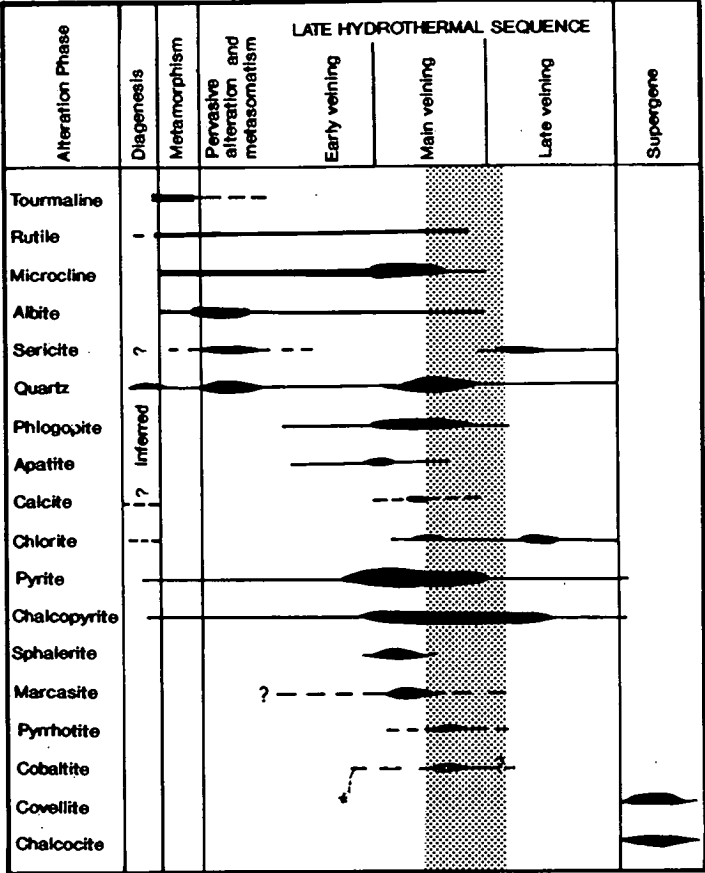


Figure 4.11b

STAVELEY FORMATION

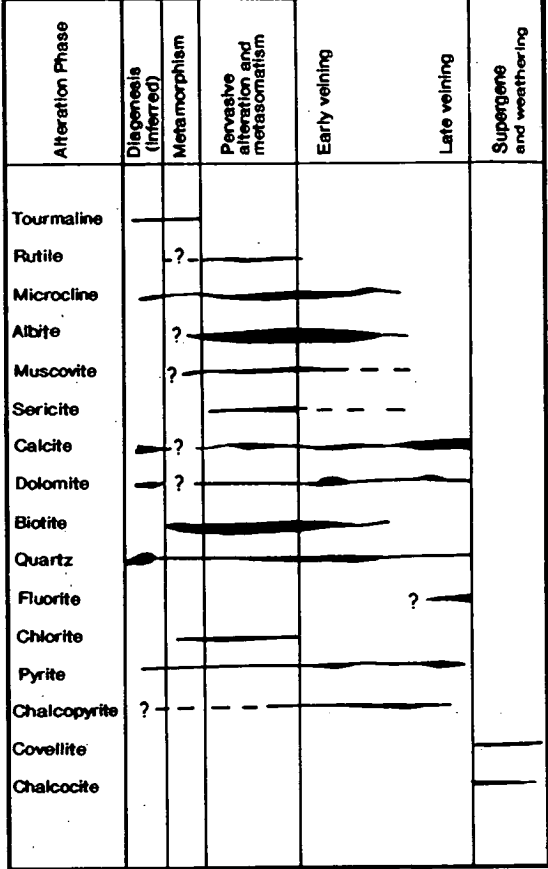
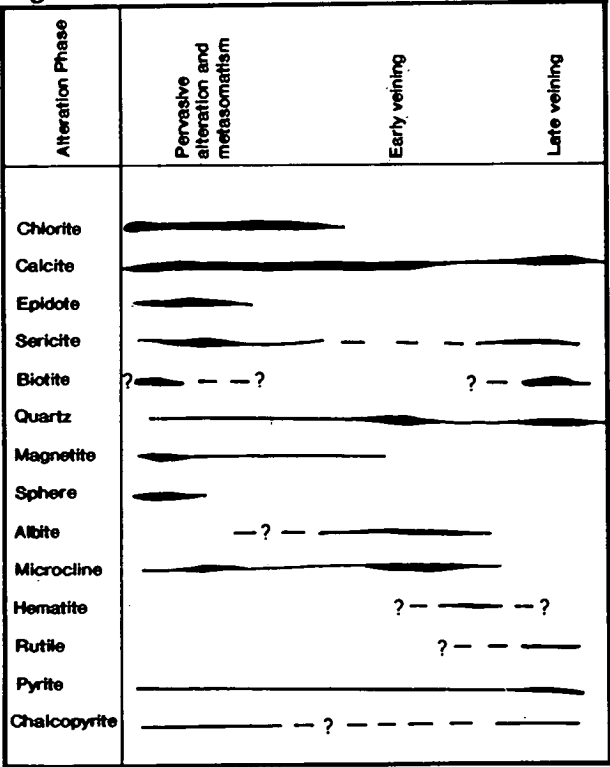


Figure 4.11c

DIORITE



MAIN MINERALISATION

CHAPTER 5 *Geochemistry*

Ch 5.1 Mineral Geochemistry

Silicate, carbonate, sulphide and oxide minerals from various stages of the paragenesis were analysed by microprobe, to determine if there was any composition change. In addition, the relative timing of alteration of the three major lithologies remains uncertain hence geochemical fingerprinting of common minerals eg. feldspars and mica, may provide a clue (although host rock composition may also control mineral geochemistry). Appendix 4 shows all 72 individual mineral analyses from nine sample sections.

5.1.1 Microcline

Structural formulae were calculated on the basis of 8 oxygens and the results indicate that there is remarkably little variation in vein hosted microcline chemistry regardless of host rock (Table 5.1). Similarly, Staveley Formation wallrock hosted microcline is compositionally similar but the main difference is a slightly lower barium and higher iron content. Some substitution for K by Na and Ba occurs but most samples closely approach the ideal potassium end-member composition. There is no detectable Ca in the microcline. Minor iron is probably due to the fine hematite dusting. Microcline compositions are similar to those hosted by carbonaceous slate or siltstone at Mt Dore reported by Beardsmore (1992), but have a slightly lower Ba and Ca content. No examples of anomalously barium-rich potassium feldspars were recorded at Greenmount, but such have been locally observed at Mt Dore by Scott (1988) who reports that barium rich feldspars (up to 12.4 mol% celsian) are orthoclase, whereas "normal" potassium feldspar is microcline. Beardsmore (1992) suggests that the localised occurrences probably reflect host, rather than fluid compositions.

5.1.2 Albite

Structural formulae were calculated on the basis of 8 oxygens and results indicate that there is almost no variation in vein hosted albite regardless of host rock. (Table 5.2). Diorite hosted albite contains slightly higher Ca and Cr content and this is probably a function of host rock composition. Most samples approach the ideal end-member composition of albite.

TABLE 5.1 Average of microcline microprobe analyses for various occurrences of microcline.

MARIMO SHALE HOSTED			STAVELEY FORMATION VEIN HOSTED			STAVELEY FORMATION WALLROCK HOSTED		
% Cations based on 8 O			% Cations based on 8 O			% Cations based on 8 O		
MAJOR ELEMENTS AVERAGE			AVERAGE			AVERAGE		
n = 7			n = 5			n = 3		
	%	Cations		%	Cations		%	Cations
SiO ₂	63.48	2.98		63.82	2.97		64.15	2.98
TiO ₂	0.01	0		0	0		0.01	0
Al ₂ O ₃	18.56	1.03		18.76	1.03		18.68	0.68
K ₂ O	16.11	0.96		15.69	0.93		15.66	0.93
Na ₂ O	0.36	0.03		0.66	0.06		0.77	0.07
BaO	0.1	0		0.27	0		0.04	0
SrO	0.18	0		0.17	0		0.18	0
FeO	0.06	0		0.01	0		0.15	0.01
MnO	0.02	0		0.03	0		0.01	0
CaO	0	0		0	0		0	0
MgO	0	0		0	0		0	0
Cr ₂ O ₃	0.02	0		0.02	0		0	0
TOTAL	98.9	5		99.43	4.99		99.65	4.67
Albite	3.25		Albite	5.94		Albite	8.44	
Orthoclase	96.56		Orthoclase	93.55		Orthoclase	91.28	
Anorthite	0.01		Anorthite	0.02		Anorthite	0.01	
Celsian	0.18		Celsian	0.49		Celsian	0.26	

5.1.3 Mica

Structural formulae were calculated on the basis of 24 OH, O, F and Cl. Results showed considerable chemical variation of petrographically identified phlogopite, depending on the (vein in) hostrock (Table 5.3). The Mg : Fe ratio of mica in diorite is slightly less than two and hence falls within the biotite field (Deer et al., 1966).

Compared to Staveley Formation hosted veins, the phlogopite in Marimo Slate hosted veins contains anomalously high fluorine (average 4.56% F) as well as significantly higher K, Mg and Si, and substantially lower Fe and Ti.

Diorite hosted biotite is compositionally similar to Staveley Formation hosted phlogopite, but the Mg and F content is significantly lower while the Ti and Cl content is higher. Mineralised veins in the Marimo Slate have substantially lower Fe and Ca content and higher Si, Mg and K content compared to brecciated, altered and mineralised carbonaceous slate from Mt Dore as reported by Beardsmore (1992). The fluorine content of phlogopite was not analysed by Beardsmore.

TABLE 5.2 Average of albite microprobe analyses for various occurrences of albite.

MARIMO SHALE HOSTED			STAVELEY FORMATION HOSTED			DIORITE HOSTED		
% Cations based on 8 O			% Cations based on 8 O			% Cations based on 8 O		
	AVERAGE			AVERAGE			AVERA	
	n = 2			n = 4			n = 8	
	%	Cations		%	Cations		%	Cations
SiO ₂	67.58	2.98		67.72	2.99		67.2	2.9
TiO ₂	0	0		0.01	0		0	
Al ₂ O ₃	19.92	1.03		19.85	1.03		20.59	1.0
K ₂ O	0.11	0.01		0.13	0.01		0.15	0.0
Na ₂ O	11.06	0.94		10.72	0.92		10.51	0.8
BaO	0.01	0		0	0		0.01	
SrO	0.26	0.04		0.28	0.01		0.23	0.0
FeO	0.04	0		0.02	0		0.07	
MnO	0	0		0.01	0		0	
CaO	0.23	0.01		0.22	0.01		1.01	0.0
MgO	0.01	0		0.01	0		0.01	
Cr ₂ O ₃	0.02	0		0.02	0		0.09	
TOTAL	99.24	5.01		98.99	4.97		99.87	4.9
Albite		98.25	Albite		98.17	Albite		94.0
Orthoclase		0.62	Orthoclase		0.75	Orthoclase		0.8
Anorthite		1.12	Anorthite		0.68	Anorthite		5.0
Celsian		0.02	Celsian		0	Celsian		0.0

TABLE 5.3 Average microprobe analyses of various occurrences of mica.

MARIMO SHALE HOSTED			STAVELEY FORMATION HOSTED			DIORITE HOSTED		
% Cations on 24 (O, OH, F, Cl) basis			% Cations on 24 (O, OH, F, Cl) basis			% Cations on 24 (O, OH, F, Cl) basis		
	n = 8			n = 5			n = 3	
	%	Cations		%	Cations		%	Cation
SiO ₂	44.39	6.32		37.22	4.82		37.07	5.
TiO ₂	0.23	0.03		0.86	0.1		1.39	0.
Al ₂ O ₃	12.76	2.13		13.99	2.52		13.61	2.
MgO	22.08	4.73		17.96	4.06		15.54	3.
CaO	0.01	0		0.05	0.01		0.01	
MnO	0.02	0		0.04	0		0.03	
FeO	3.64	0.44		15.05	1.94		15.13	1.
Na ₂ O	0.04	0.01		0.08	0.02		0.1	0.
K ₂ O	10.23	1.87		8.14	1.54		9.89	1.
H ₂ O	2.03	0		2.67	0		3.44	
F	4.56	0		2.61	0		0.55	
Cl	0.05	0		0.17	0		0.74	
TOTAL	100.04	15.53		98.84	15.01		97.5	15.
O = F	-1.92			-1.10			-0.23	
O = Cl	-0.01			-0.04			-0.17	
TOTAL	98.11			97.7			97.1	

5.1.4 Carbonate

Structural formulae were calculated on the basis of 6 oxygens. Petrographically, both calcite and dolomite occur in altered Staveley Formation lithologies, as veins, matrix and disseminations. Both appear to be in a similar paragenetic position but the reason for the development of one or the other is not clear. Carbonate from only one section was analysed. The sample contained an earlier microcline - quartz - calcite - muscovite - pyrite vein cut by a late calcite pyrite vein. The carbonate composition from both veins was similar (Appendix 4) and is ferroan dolomite in composition. The average of five analyses is presented in Table 5.4.

TABLE 5.4 Average microprobe analyses of carbonates hosted by the Staveley Formation.

CARBONATE MICROPROBE ANALYSES STAVELEY FORMATION HOSTED		
% Based on 6 O		
MAJOR ELEMENTS	AVERAGE n = 5	
	%	Cations
Ca(CO ₃)	52.34	0.98
Mg(CO ₃)	35.59	0.79
Fe(CO ₃)	12.55	0.2
Mn(CO ₃)	1.00	0.02
Al ₂ (CO ₃) ₃	0.01	0
Ti(CO ₃) ₂	0.02	0
Si(CO ₃) ₂	0.03	0
Zn(CO ₃)	0.03	0
Na ₂ (CO ₃)	0.02	0
K ₂ (CO ₃)	0.01	0
TOTAL	101.6	1.99

5.1.5 Apatite

At Greenmount, apatite is only found in veins hosted by the Marimo Slate, and thus a strong redox control on formation of apatite can be inferred. Apatite formed in veins which carried some minor disseminated mineralisation, prior to main mineralising event. Apatite can therefore potentially provide valuable information on the chemistry of the fluid immediately preceding mineralisation, and can also be a useful indicator of F and Cl abundances in the hydrothermal fluid from which it precipitated (Korzhinskiy, 1981; Sisson, 1987).

Structural formulae were calculated on a 26 (O, OH, F, Cl) basis. Only three apatite crystals from two mineralised samples were analysed (Appendix 4). No attempt was made to determine compositional zoning. All three analyses yielded apparently greater than stoichiometric amounts of Cl and F per unit cell (Table 5.5). The proportion of hydroxylapatite cannot be determined in these specimens since this component is assumed to make up the remainder of any unit cell after fluor - and chlorapatite components have been calculated. Compared to Mt Dore apatites from all various lithologies (Beardsmore, 1992), Greenmount apatites have a higher total halogen content and a higher F : Cl ratio. The average of all Mt Dore apatites is 3.67% F and 0.31% Cl.

TABLE 5.5 Average microprobe analyses of apatite in veins hosted by the Marimo Slate.

APATITE MICROPROBE ANALYSES MARIMO SHALE HOSTED		
% Cations on 26 - (O, OH, F, Cl) basis		
MAJOR ELEMENTS	AVERAGE n = 3	
	%	Cations
P ₂ O ₅	40.33	5.78
CaO	55.33	0
SiO ₂	0.01	0
MgO	0	10.04
FeO	0.02	0
SrO	0	0
BaO	0.01	0
H ₂ O	0	0
F	5.57	0
Cl	0.03	0
TOTAL	101.3	15.82
O = F	-2.35	
O = Cl	-0.01	
TOTAL	98.94	

5.1.6 Magnetite

Three analyses of magnetite on one section of diorite were completed. Structural formulae were calculated on the basis of 4 oxygens. A significant amount of vanadium has substituted for Fe³⁺ (Table 5.6) but the composition is close to the theoretical end member composition (Deer et al., 1966). The magnetite structure contains negligible amounts of titanium. The Ti was probably taken up in rutile which co-exists with magnetite.

TABLE 5.6 Average microprobe analyses of magnetite hosted by diorite.

**MAGNETITE MICROPROBE ANALYSES
DIORITE HOSTED**

Cations on 4 O Basis
MAJOR ELEMENTS AVERAGE n=3

	%	Cations
TiO ₂	0.02	0
Al ₂ O ₃	0.03	0
V ₂ O ₃	0.29	0.01
Cr ₂ O ₃	0.02	0
Fe ₂ O ₃	67.71	1.99
MgO	0.01	0
MnO	0.02	0
FeO	30.5	1
ZnO	0.02	0
TOTAL	98.62	3

5.1.7 Pyrite

Scott (1988) identified four types of pyrite on the basis of textures and Co + Ni contents at Mt Dore. Early pyrite (Type I), which he interprets to be syngenetic, has a high Ni and low Co and Cu content. All other types (II to IV) have variable Ni contents and elevated Cu or Co where associated with chalcopyrite. At Greenmount possible syngenetic pyrite (from sample 85009) contains low Co and low Ni.

This study examines the pyrite composition at Greenmount, based on texture as well as occurrence in host.

Euhedral hexagonal, anhedral and fractured pyrite are observed petrographically. The latter two only occur in veins or matrix hosted by Marimo Slate or Staveley Formation. Only euhedral hexagonal pyrite is observed disseminated in the wallrock. Some pyrite contains silicate inclusions. A description of the pyrites analysed is attached to Appendix 4. From Table 5.7 and Figure 5.1, it can be seen that the euhedral pyrite contains relatively more Co, Hg and Pb, while the anhedral or fractured pyrite contains relatively more Cu, Se, Cd, As, Ag, Ni and Bi.

A single anhedral pyrite with a very fine grained pyrite overgrowth showed that the later overgrowth contained less Co, Zn, Se and Ag and more As and Ni.

TABLE 5.7 Average microprobe analyses of pyrite based on the pyrite morphology.

PYRITE MICROPROBE ANALYSES

TRACE ELEMENT	Average of all euhedral pyrite	Average of all anhedral pyrite	Average of all fractured pyrite	Core of anhedral pyrite	Overgrowth core
	n=9	n=3	n=3	n=1	n=1
	Wt %	Wt %	Wt %	Wt %	Wt %
Fe	44.73	46.04	45.26	46.80	46.17
S	51.14	51.65	48.87	52.55	52.03
Co	1.22	0.35	0.35	0.73	0.32
Cu	0.01	0.03	0.04	n.d.	n.d.
Zn	0.02	0.01	0.00	0.02	0.00
Mn	0.00	0.00	0.00	n.d.	n.d.
Se	0.02	0.03	0.07	0.05	0.01
Cd	0.02	0.00	0.07	n.d.	n.d.
Hg	0.32	0.00	0.16	n.d.	n.d.
As	0.26	0.34	0.00	0.03	0.98
Ag	0.01	0.07	0.01	0.11	0.09
Sb	0.00	0.00	0.00	n.d.	n.d.
Ni	0.27	0.43	n.d.	0.02	0.84
Pb	0.13	0.03	n.d.	0.03	0.03
Bi	0.59	1.10	0.00	n.d.	n.d.
TOTAL	98.74	100.07	94.83	100.34	100.47

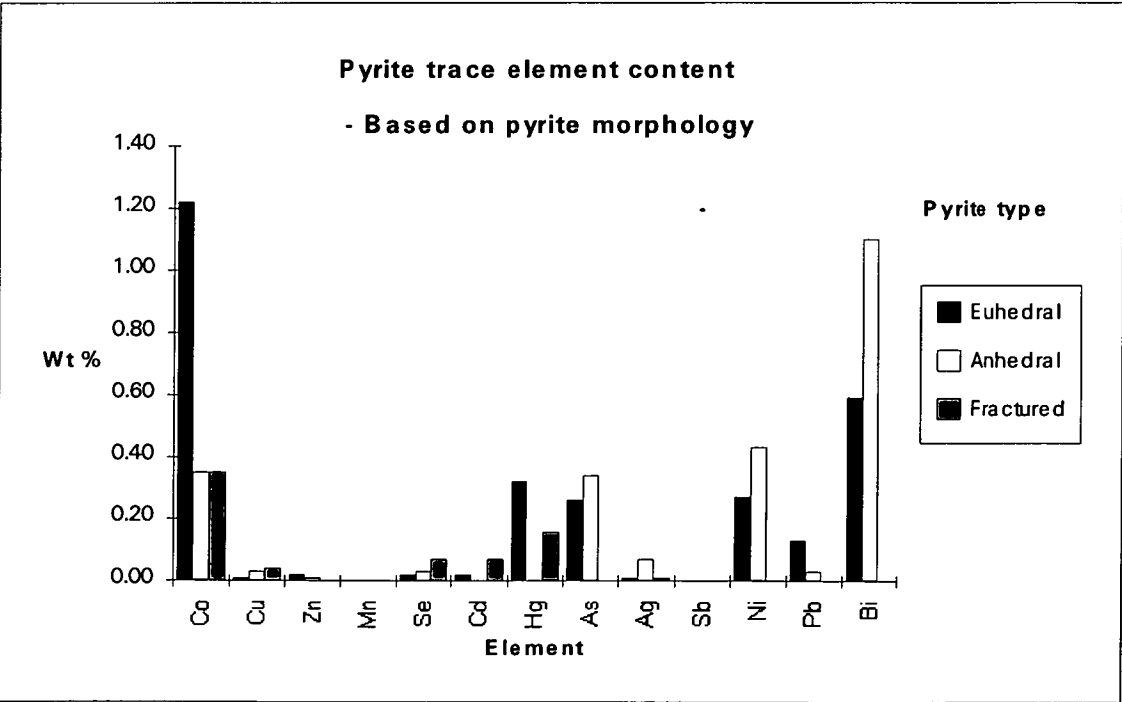


Figure 5.1 Graph of pyrite trace element content based on pyrite morphology.

Disseminated euhedral pyrite in the Staveley Formation wallrock contains the highest Co content (20 100 ppm). The Co content of pyrite in Marimo Slate hosted veins is higher than for pyrite disseminated (and possibly syngenetic) in the Marimo Slate (Table 5.8 and Figure 5.2). Disseminated and vein hosted pyrite within the Marimo Slate is more elevated in Ni and As than in the Staveley Formation and is highest of all when in Marimo Slate hosted veins. The bismuth content appears to be relatively higher for pyrite in Staveley Formation wallrock and veins or matrix, but it should be noted that no bismuth analyses are available for disseminated pyrite hosted by Marimo Slate wallrock.

TABLE 5.8 Average microprobe analyses of various occurrences of pyrite.

PYRITE MICROPROBE ANALYSES MARIMO SHALE VEIN / MATRIX HOSTED		
TRACE ELEMENT	AVERAGE n = 8	
	Wt %	Normalised atom. c
Fe	45.53	33.75
S	50.65	65.52
Co	0.56	0.4
Cu	0.04	0.02
Zn	0.01	0
Mn	0.00	0
Se	0.04	0.02
Cd	0.05	0.02
Hg	0.24	0.05
As	0.51	0.28
Ag	0.04	0.01
Sb	0.00	0
Ni	0.48	0.32
Pb	0.1	0.02
Bi	0.27	0.06
TOTAL	98.52	100.47

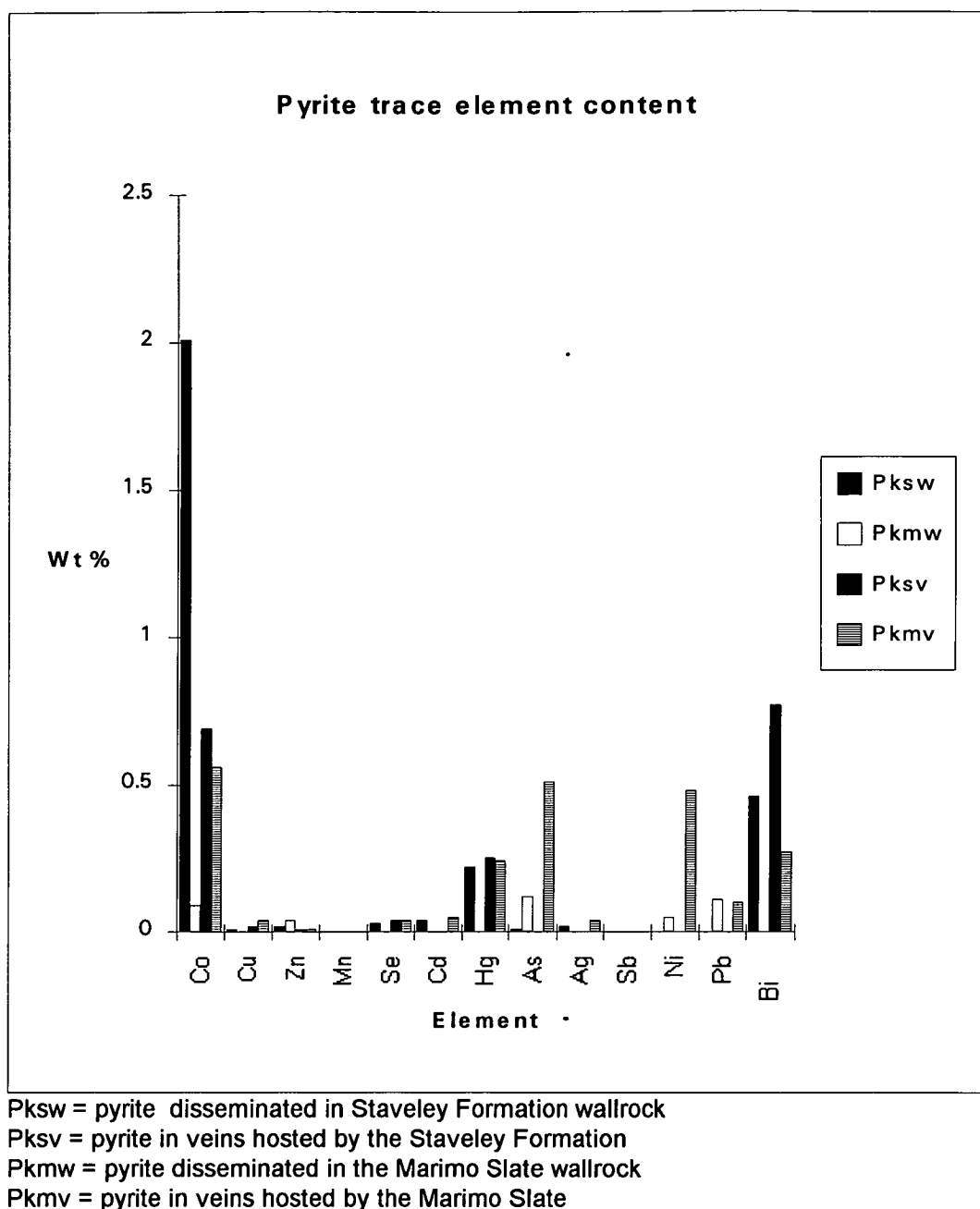


Figure 5.2 Graph of pyrite trace element content based on microprobe analyses of various pyrite occurrences.

5.1.8 Chalcopyrite

Nine analyses were determined on chalcopyrite from mineralised Marimo Slate hosted veins and two on chalcopyrite disseminated in very weakly altered Marimo Slate wallrock. The most notable compositional difference is that the former contains a maximum of 300 ppm Hg and the latter contains 4,000 ppm and 2,300 ppm Hg (Table 5.9). Mercury analyses are not available for wallrock hosted pyrite in the Marimo Slate, and so a relative comparison of the possibly syn-diagenetic sulphide species cannot be made.

TABLE 5.9 Average microprobe analyses of chalcopyrite hosted by veins and wallrock in the Marimo Slate.

MARIMO SHALE VEIN / MATRIX HOSTED			MARIMO SHALE WALL ROCK HOSTED		
TRACE ELEMENT	AVERAGE n = 9		AVERAGE n = 2		
	Wt %	Normalised atom. c	Wt %	Normalised atom. c	
Fe	25.64	23.53	29.45	24.44	
S	30.54	48.87	33.77	48.82	
Co	0	0	0.02	0.02	
Cu	33.85	27.56	36.53	26.65	
Zn	0.01	0	0.01	0	
Mn	0.01	0.01	0.01	0	
Se	0.01	0.01	0.03	0.02	
Cd	0.06	0.02	0	0	
Hg	0	0	0.32	0.07	
As	n.d.		n.d.		
Ag	n.d.		n.d.		
Sb	n.d.		n.d.		
Ni	n.d.		n.d.		
Pb	n.d.		n.d.		
Bi	n.d.		n.d.		
TOTAL	90.12	100	100.14	100.02	

Ch 5.2 Lithogeochemistry

Although almost all lithologies have been altered to some degree, examples of the least altered specimens were analysed for whole rock major and trace elements. In addition, pervasively altered lithologies, veins in the various lithologies and the mineralisation were also sampled by cutting suitable specimens of core with a saw. Care was taken to avoid sampling weathered or supergene altered samples. Details of the analytical methods are described in Table 5.11.

Figures 5.3 to 5.5 show two element variation diagrams for the least altered lithologies compared to each other as well as to altered and mineralised samples. The rationale for the binary plots was to try to determine how anomalous alteration and ore elements behave with respect to each other in the various lithologies at various stages of the paragenesis. The trace element analyses are tabulated in Tables 5.11 and 5.12 while the major elements are shown in Table 5.13. The average analyses of groups of samples are shown in Table 5.14. Very few major element analyses were collected and caution should be used when interpreting the data. Figure 5.5 shows that there is no systematic trend of the major elements plotted, except for a depletion of potassium with an increase in silica content.

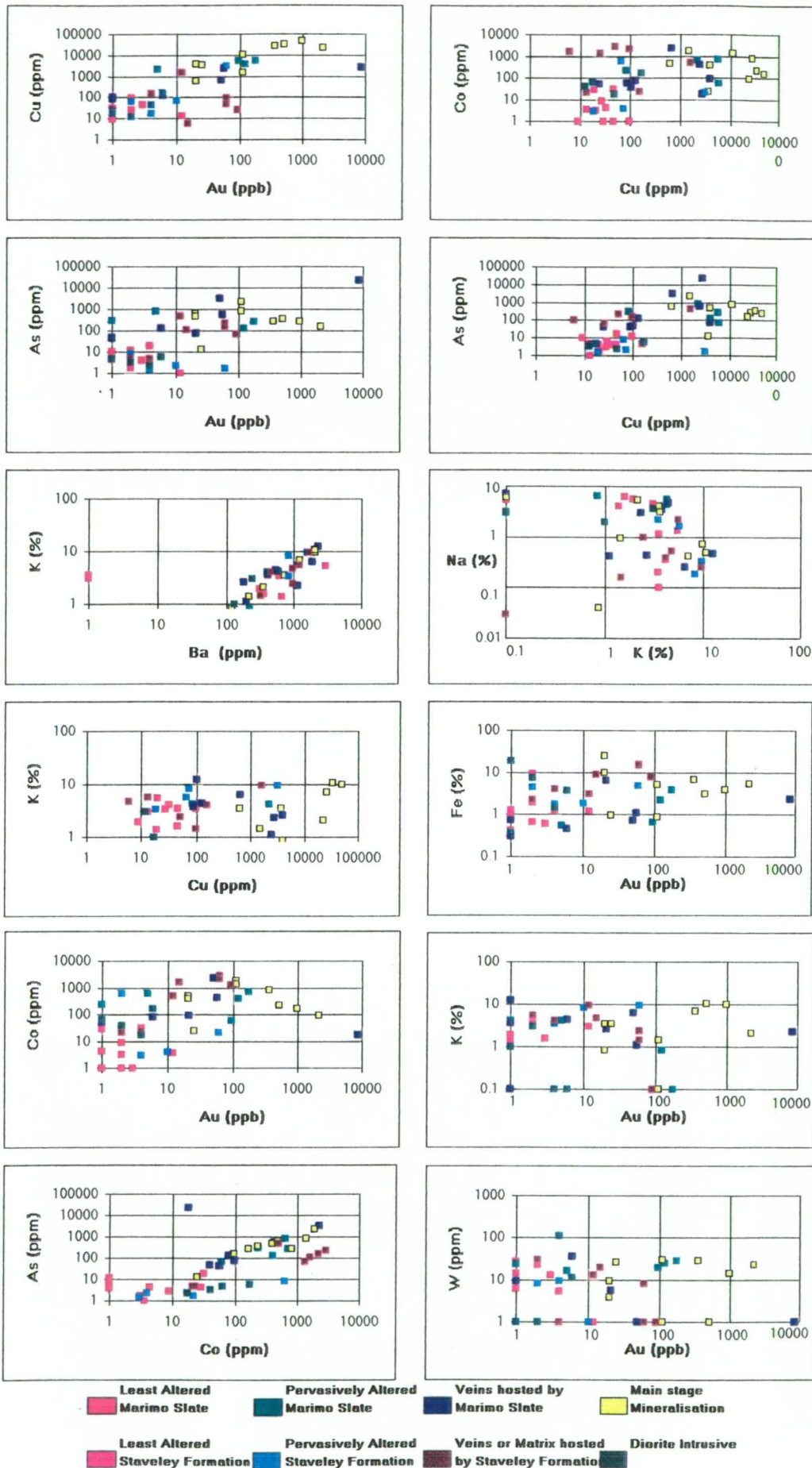


Figure 5.3 Multi-element X-Y Scatter Plots on Logarithmic Scale for various lithologies, alteration and vein types from samples for this study.

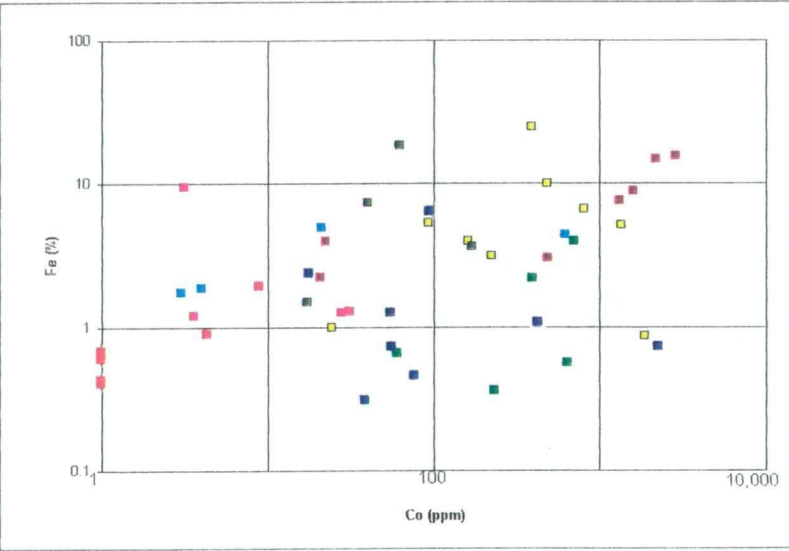
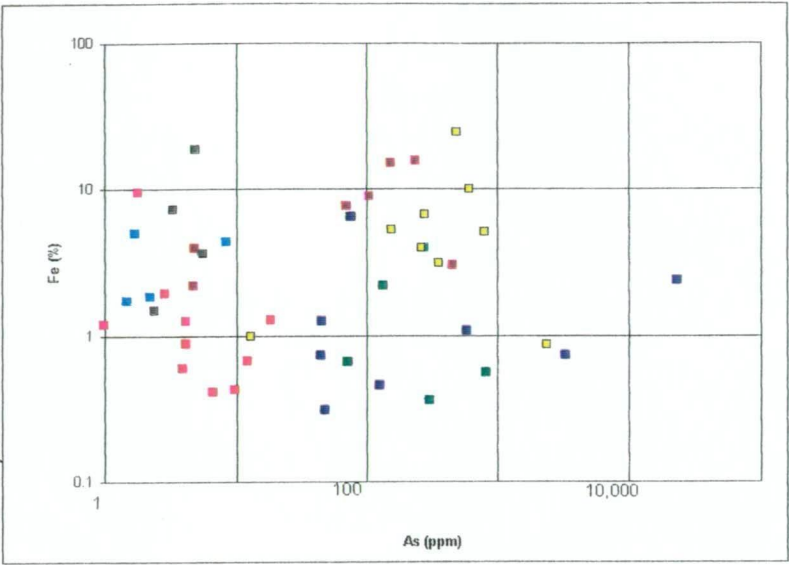
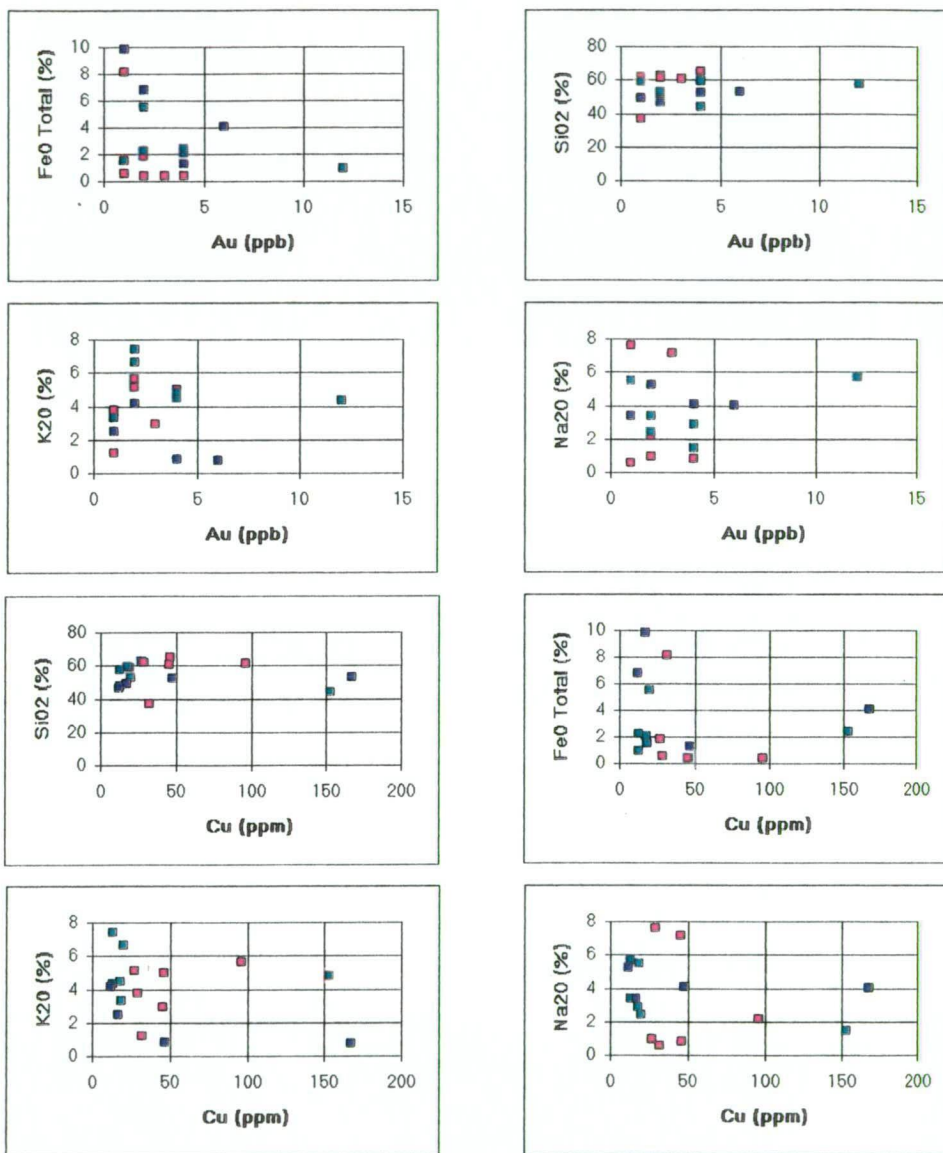


Figure 5.3 (continued)



■ Least Altered Marimo Slate
 ■ Least Altered Staveley Formation
 ■ Diorite Intrusive

Figure 5.4 X-Y Scatter Plots on Logarithmic Scale
 for major elements versus Cu and Au
 for various lithologies.

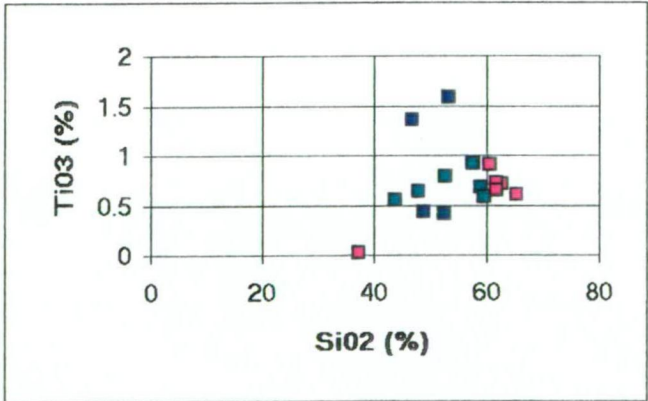
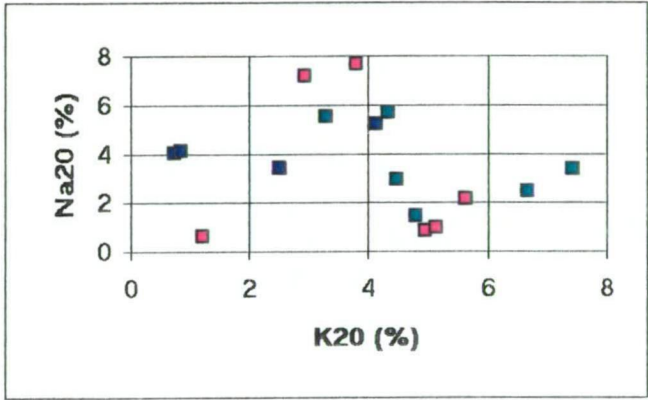
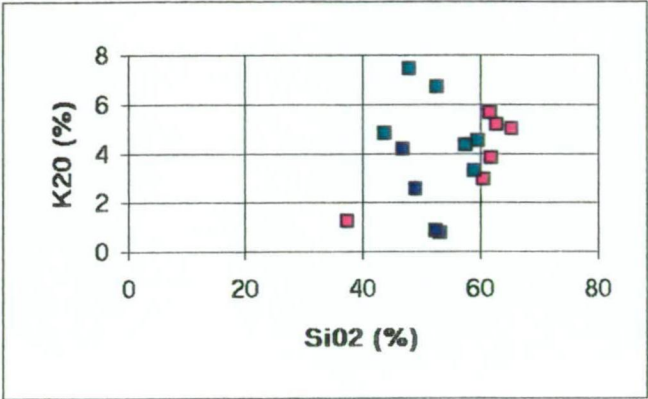


Figure 5.5 Major Element X-Y Scatter Plots for various lithologies.

5.2.1 Least Altered Staveley Formation

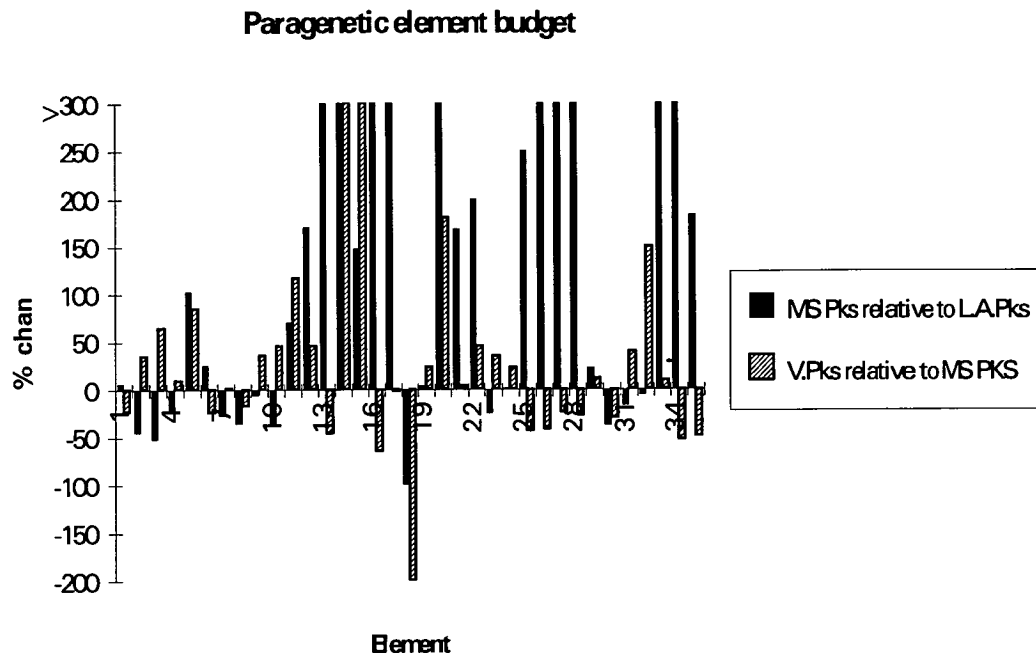
The Staveley Formation is always altered (Chapter 4), and hence the data presented represents diagenetically altered and metamorphosed rocks which have been least altered by hydrothermal activity.

The Staveley Formation is unusually alkalic (9.33% Na₂O + K₂O) for a metasandstone (Table 5.14). The high level of Na and K is not unusual though, for an evaporite derived sediment. The three trace element analyses of least altered Staveley Formation do not show anomalous Cu, Au, Co levels and hence at the locality sampled, would not appear to constitute a suitable "protore source" as documented at Just Found prospect by Stewart (1991).

5.2.2 Metasomatised and Veined Staveley Formation

The alteration of the Staveley Formation is discussed in Chapter 4. This section outlines the geochemistry of altered and veined Staveley Formation compared to the least altered equivalent. Only one sample of metasomatised pervasively altered Staveley Formation was analysed for major elements and four samples for trace and minor elements. The results indicate that metasomatism is accompanied by a significant gain in Si, Ca, Mg, Mn, Au, Cu, Co, Sb, Ba, Cs, Cr, Eu, Lu, Mo, Rb, Se, U, Yb, Zn and a significant loss in Al, Fe, Na, Ti, P, Br, Hf and Ta. It appears that the rare earth elements were relatively inert with only a slight heavy rare earth element enrichment.

Similarly the Staveley Formation wallrock host to veins shows a significant gain (relative to pervasively altered and metasomatised Staveley Formation) of Al, Fe, Ca, K, P, Mn, Au, Co, As, Cs, Ce, Eu, Hf, La, W, Yb and a significant loss of Si, Mg, Cu, Sb, Lu, Mo, Rb, Zn i.e. all the elements lost during veining were initially gained during pervasive alteration. Figure 5.6 shows the percentage change of various elements during metasomatism and veining.



Position of element along x-axis

SiO ₂	= 1	Na ₂ O	= 8	As	= 15	Eu	= 22	Sm	= 29
Al ₂ O ₃	= 2	K ₂ O	= 9	Sb	= 16	Hf	= 23	Ta	= 30
Fe ₂ O ₃	= 3	P ₂ O ₅	= 10	Ba	= 17	La	= 24	Th	= 31
FeO	= 4	MnO	= 11	Br	= 18	Lu	= 25	W	= 32
CaO	= 5	Au	= 12	Ce	= 19	Mo	= 26	U	= 33
MgO	= 6	Cu	= 13	Cs	= 20	Pb	= 27	Yb	= 34
TiO ₂	= 7	Co	= 14	Cr	= 21	Rb	= 28	Zn	= 35

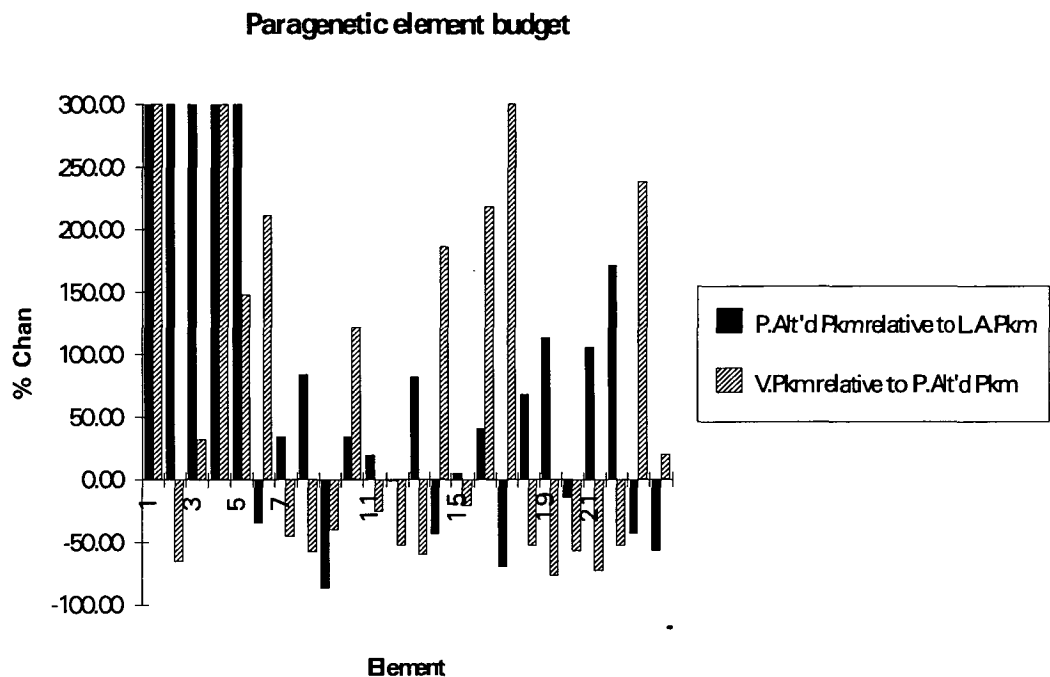
Pks = Staveley Formation

MS = Metasomatised

V. = Veined

L.A. = Least altered

Figure 5.6 - Percentage change of various elements during metasomatism and veining for the Staveley Formation.



Position of element along x-axis

Au	= 1	Sb	= 5	Cs	= 9	La	= 13	Rb	= 17	W	= 21
Cu	= 2	Ba	= 6	Cr	= 10	Lu	= 14	Sm	= 18	U	= 22
Co	= 3	Br	= 7	Eu	= 11	Mo	= 15	Ta	= 19	Yb	= 23
As	= 4	Ce	= 8	Hf	= 12	Pb	= 16	Th	= 20	Zn	= 24

Pkm = Marimo Slate

P. Alt'd = Pervasively altered

V. = Veined

L.A. = Least altered

Figure 5.7 Percentage change of various trace and minor elements during pervasive alteration and veining for the Marimo Slate.

TABLE 5.10 Elements Gain - Loss budget of the Staveley Formation through the various stages of paragenesis.

METASOMATISM		VEINING	
(relative to least altered sample)		(wallrock relative to metasomatism)	
ELEMENTS	<i>Ca Au Mn Cs Eu Yb</i>	<i>Ca Au Mn Cs Eu Yb</i>	
GAINED	Cu Co Sb Ba Si Mg Cr	Co As Ce Hf P K	
	Lu Mo Pb Rb Se U Zn	La W Al Fe	
ELEMENTS	Al Br Fe Hf Ta	Si Mg Cu Sb Lu	
LOST	Na Ti P	Mo Rb Zn	

Table 5.10 above shows that at both stages of the paragenesis Ca, Au, Mn, Cs, Eu and Yb were gained.

5.2.3 Marimo Slate

Compared to the North American Shale Composite (NASC - Gromet et al., 1984) the analyses of the least altered Marimo Shales (n = 7) indicate that the Marimo Shale is enriched in Na, Al, K, Ti, Cr, Br, Rb, Zr, Cs, La, Ce, Sm, Yb, W, Th and U, and depleted in Ca, Mn, Fe, Co, As, Sb, Ba, Eu and Hf.

Some workers have attempted to apply discrimination diagrams to determine clastic provenance eg. Roser and Korsch (1988); Cullers et al. (1988) and Bhatia and Crook (1986). Cullers et al. (1988) showed that the immobile elements La and Th are more abundant in felsic than in basic rocks where as Sc and Co are more common in basic rocks.

Compared to the average of the least altered Staveley Formation the average of the least altered Marimo Slate contains significantly more Si, Al, Cu, As, Sb, Ba, Ce, Cs, Cr, Eu, Hf, La, Lu, Mo, Pb, Rb, Sm, Th, W, U, Yb and Zn, and less Fe, Ca, Mg, Na, P, Mn, Co and Ta.

Derrick et al. (1971) analysed 20 samples of the Marimo Slate from the Marraba 1:100,000 Sheet in the western part of the Marimo Basin. They noted that most of the important metallic elements (eg. Cu, Pb, Zn, Co, Ni, etc) are present in below average concentrations (except in several samples). Compared to analyses from this study, the Marimo Slates from the western Marimo Basin are significantly higher in Si, Mg, P, Co, Ba and lower in Ti, Al, Na, K, Cr, Zn, Rb.

5.2.4 Pervasive Altered and Veined Marimo Slate

No major elements were analysed for pervasively altered and/or veined Marimo Slate. Five pervasively altered Marimo Slate samples and then veined samples were analysed for trace elements (Table 5.14). The results indicate that pervasive alteration is accompanied by a significant increase in Au, Cu, Co, As, Sb, Br, Ce, Cr, La, Pb, Sm, Ta, Sb, U. and decrease in Ba, Cs, Lu, Rb, Yb, Zn (Figure 5.7). Hence there appears to be a light rare earth element enrichment and a heavy rare earth element and large ion lithophile element depletion.

The results also indicate that veining is accompanied by a significant increase (relative to pervasively altered slate) of Au, Co, As, Sb, Ba, Cr, Lu, Pb, Rb, Yb, Zn and decrease in Br, Cu, Ce, Cs, Eu, Hf, La, Sm, Ta, Th, W, U. The veined slate appears to be high field strength element and LREE depleted and HREE enriched when compared to pervasively altered slate.

5.2.5 Diorite

The diorite is always altered to some degree and hence major element data have not been used to attempt a geochemical classification (eg. Cox et al., 1979; Streckeisen and Le Maitre, 1979).

The negative Eu anomaly for the average least altered diorite presented in Figure 5.8 indicates that potassium feldspar (and/or plagioclase) may have been removed from the melt. The relative depletion in the middle REE (i.e. 5 m) may indicate that hornblende was also removed from the melt.

Whole rock and major element analyses of the least altered diorite (Table 5.14) suggest that the Au and As values are very low and hence may not be a suitable source for mineralisation of these elements. Conversely, Cu, Co, Cr, Sb and U may be sufficiently abundant to constitute a source of these elements during mineralisation.

5.2.6 Main Stage Mineralisation

The mineralisation at Greenmount is characterised by elevated Au, Cu, Co, As, Mo, W \pm Pb \pm Zn \pm Bi \pm Cr \pm U \pm Rb \pm Ba (Tables 5.11, 5.14, 5.15 and 5.16). The most important and economic metals are Au, Co and Cu. A plot of Au versus Cu for all Homestake Gold of Australia Limited core holes where Au is greater than 0.1 ppb or Cu is greater than 500 ppm (below the base of oxidation) shows a gross positive correlation (Figure 5.9).

The variation diagrams presented in Figure 5.3 show that for main stage mineralisation, there is a good positive correlation of Au - Cu, As - Co (probably due to cobaltite controlling As and Co) and a weak Cu - K correlation, which is due to minute inclusions of microcline in

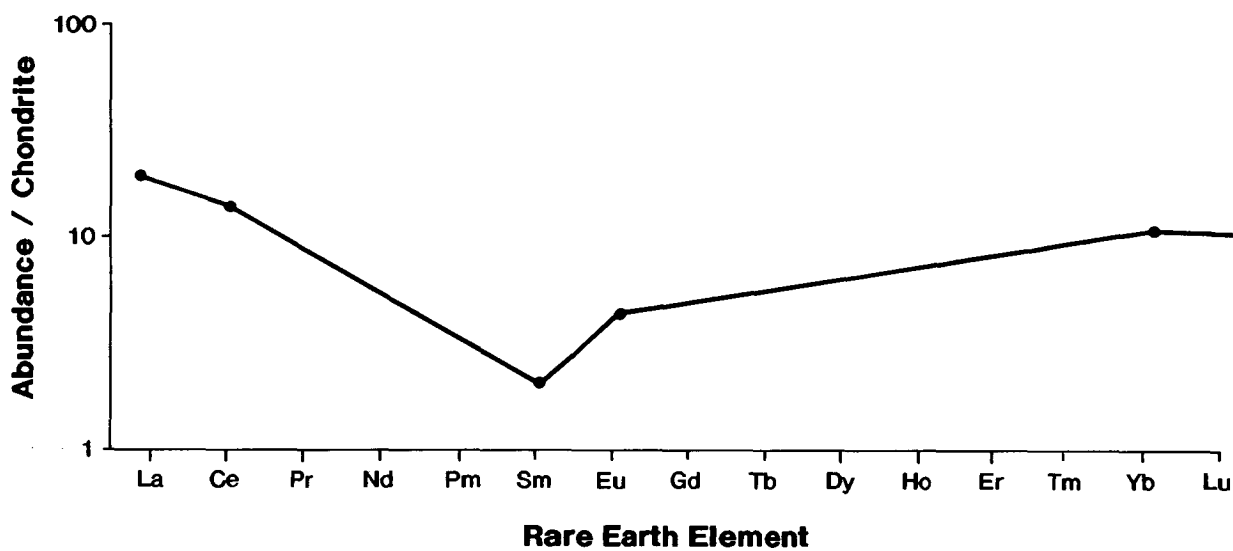


Figure 5.8.

Chondrite normalised (Boynton, 1994) values for the rare earth elements from the least altered diorite. Samples analysed by neutron activation analysis (Table 5.12). Detection limits (in ppm) are La 0.5, Ce 2.0, Sm 0.2, Eu 0.5, Yb 0.5 and Lu 0.2. Note that analysed Sm values are 3 to 4 times detection limit but Eu values are almost at the detection limit.

SAMPLE NO & DESCRIPTION		FIRE		ICP		ANALYSES BY NEUTRON ACTIVATION UNLESS DENOTED OTHERWISE																									ICP									
		ASSAY																																						
		AU (ppb)	AU (ppb)	Cu	Co	As	Sb	Ba	Bi	Br	Ce	Cs	Cr	Eu	Hf	Ir	Fe%	La	Lu	Mo	Mo	K%	Pb	Rb	Sm	Sc	Se	Ag	Na%	Ta	Th	W	U	Yb	Zn					
LEAST ALTERED MARIMO SLATE																																								
85009	Sparsely pyritic graphitic slate (PKM)	4	10.5	46	31.1	18.7	0.62	417	<5	<2	101	7.58	193	0.8	4.5	<20	1.3	47	0.4	7	<5	3.5	<5	186	6.9	14	<5	<5	0.1	<1	17.3	5.4	14	3	41					
85619Sh	Black shale (PKM) hosting microcline vein	<1	<5	9	<1	9.84	<0.2	312	<5	<2	523	<1	166	1.8	6.7	<20	0.4	250	0.6	9	<5	1.9	<5	34.8	35	11	<10	<5	5.7	3.7	36.1	28	5.2	4	<5					
85623	Graphitic slate (PKM)	2	<5	27	8.87	2.88	0.5	610	<5	<2	121	10.1	124	1.3	5.8	<20	2	55	0.7	6	<15	3.4	11	221	8.6	17	<5	<5	0.2	1.9	20.3	<2	11	4.6	19					
85611	Silicified shale with <1% disseminated diagenetic (?) pyri	3	<5	45	<1	3.99	0.68	360	<5	<2	159	<1	200	0.6	6.6	<20	0.6	74	0.5	11	6.2	1.6	<5	62.6	10	5.8	<5	<5	6.2	0	20	13	9.4	3.2	48					
85612 Sh	Black shale (Pkm) hosting qtz-py-mic vein	<1	26.3	29	<4	6.77	<0.5	432	<5	7.7	185	5.39	207	<1	6	<20	0.4	89	0.5	8	<20	<2	<5	160	13	8.6	<15	<20	5.5	<5	21.1	<8	7.5	3.4	21					
85624A	Black shale hosting 85624B (PKM)	<1	<5	32	4.34	4.25	0.88	521	<5	<2	157	12.3	181	1.3	6.5	<20	0.9	72	0.6	7	<10	4.1	5	229	11	18	<5	<5	0.4	2.7	22.1	6.2	7.1	3.8	64					
85626 Sh	Black shale hosting 85626 QPY (PKM)	2	<30	96	<6	12.5	<1	<700	<5	<5	114	11.3	150	<2	4.1	<70	0.7	58	0.6	8	<80	3.5	6	338	11	15	<30	<30	1.1	<5	21	23	<10	3.7	35					
PERVASIVELY ALTERED MARIMO SLATE																																								
85008 Ph	Phlogopite/feldspar altered sandy unit in PKM	<1	<10	83	235	306	4.62	586	<5	3.8	1280	2.51	182	2.3	5.6	<20	0.4	592	0.3	<5	<10	4.2	<5	153	82	15	<20	<10	4.5	<3	28.9	24	10	2.3	<5					
85607	Intensely albitised and possibly sericitised fine grained sediment with disse. sulfide and some sulfide stringer	95	215	5870	60.2	72.4	2.56	<100	<5	<2	103	<1	376	<0.5	5	<20	0.7	50	0.2	9	<20	<0.5	<5	<20	6.5	1.9	<5	<5	6.5	3.4	8.43	20	13	1.8	17					
85608 Abs	Pervasively albitised shale with late sulfide stringers (Pk	175	226	5620	709	278	1.23	<100	<5	<2	11.7	<1	126	<0.5	4.9	<20	4	5.7	0.3	12	<30	<0.5	7	40.2	1.9	4.9	<5	<5	6.2	3.2	16.1	29	22	1.9	21					
85608 Ab	Least sulfidic albitised shale (Pkm)	121	154	3970	402	136	0.97	220	<5	<2	7.11	<1	265	0.8	6.4	<20	2.2	3	0.3	10	<40	0.8	6	<20	1.6	6	<5	<5	6.5	3.6	23.1	25	32	2.1	25					
85618	Feldspathised pelite similar to 85032 Ab but with less sulfides (PKM)	5	<5	2200	641	826	<0.5	408	<5	3.5	381	1.64	223	1.7	6.2	<20	0.6	185	0.3	11	<40	4.1	9	68.2	25	2.1	<5	<11	5.7	2.6	21.1	16	29	2.5	8					
MARIMO SLATE HOSTED VEINS																																								
85007Ab	Early albite vein in PKM	<1	<50	24	55	45.5	<2	1000	<5	<5	90.1	<5	541	2.7	7	100	1.3	49	0.2	<5	<20	<6	<5	<200	9.2	2.7	<50	<50	7	<10	<4	<20	<20	1.9	<5					
85008 Ab	Vein of Ab (65) - qtz (30)-Mic (5) with tr. Ca-Phl-Rt	<1	<10	87	56	45	<0.4	408	<5	<2	1050	<2	571	2.3	4.8	<20	0.7	480	2.3	8	<20	3.7	6	150	65	11	<10	<10	3.6	<3	28.1	9.4	22	17	27					
85605	Vein material comprising Mic (75)-qtz (25) with 5% pale euhedral py adjacent to grains. Hosted by black shale	50	35.1	646	2260	3290	1.87	1860	<5	<5	6.34	2.09	753	<0.5	<0.5	<20	0.7	2.1	<0.2	8	5	6.4	<5	162	1.3	1.4	<5	<10	0.3	<1	2.35	<4	<4	0.6	17					
85609 MS	Coarse microcline vein with disseminated sulfides (Pkm)	8500	7770	2780	17.8	2.34%	39.4	1160	55	<50	54.1	<1	253	<0.5	1.1	<20	2.4	21	<0.2	15	59	2.3	6	100	3.9	37	<10	<10	3	<1	7.27	<6	31	0.7	8					
85609 QS	Qtz - mic vein with disseminated sulfides (Pkm)	56	629	2450	429	587	1.19	195	<5	<2	15.4	<1	348	<0.5	0.6	<20	1.1	7	<0.2	<5	<5	1.1	30	25.4	1	1.6	<5	<5	0.4	<1	1.45	<2	5.1	0.7	40					
85610	Mic (95) - qtz (5) vein with very little sulfide (Pkm)	<1	<5	102	38.5	48.2	<0.2	2280	<5	<2	<2	<1	172	<0.5	<0.5	<20	0.3	0.6	<0.2	<5	<10	12	26	293	<0.2	0.4	<5	<5	0.5	<1	<0.5	<2	7.8	<0.5	<5					
85612V	Qtz (80) - py (35) - mic (5) vein with 70%black shale dilution ie. 85612 Sh (Pkm)	20	26.2	610	485	613	0.69	717	<5	2.2	82.4	<1	618	0.8	3.1	<20	10	40	0.4	8	<10	3.5	<5	1476	6.3	6.2	<5	<5	3.2	<1	13.3	9.4	5.8	2.9	50					
85619M	Coarse pink unfractured microcline vein (PKM)	6	<5	127	77.5	127	<0.2	537	<5	<2	76.5	<1	155	<0.5	6.6	<20	0.5	36	0.7	9	<30	4.4	<5	99.1	5.8	8.8	<5	<5	4.7	3	9.67	36	21	4.7	<5					
85626 QPY	Qtz (80)-py (20) vein in black shale (PKM)	21	18.8	3910	95.5	76.6	0.97	180	<5	<2	66	3.36	762	<0.5	2.9	<20	6.5	32	0.6	8	<5	2.7	63	147	4.7	7.3	<5	<5	0.4	<1	10.2	5.7	4.2	2.1	15					
85606	Quartz - microcline-phlogopite vein	110	54	1470	1870	2350	2.47	218	<5	5.5	38.3	<1	1030	1	<0.5	<20	0.9	0.8	4.1	10	21	1.4	8	35.9	9.2	4.1	<5	<10	0.9	2.8	11.3	<4	5	41	14					
MAIN STAGE MINERALISATION IN MARIMO SLATE & VEINS IN MARIMO SLATE																																								
85018 AB	Feldspathised pelite with disseminated sulfides and some vein material	25	23.2	3690	24.3	12.8	0.81	721	<5	2.4	15.3	2.85	215	<0.5	5.7	<20	1	7.2	0.5	11	<40	3.5	5	108	2.1	11	<5	<10	4.2	2.9	17.5	27	23	2.6	20					
85018V	Vein-matrix to 85018Ab. Comprises mic (53)-ab(15)-Py (15) phl (15) - cpy (2). This was veined by late thin ser-qtz ve	360	357	2.62%	805	279	0.88	1230	<5	<2	6.06	<2	260	<0.5	3.8	<20	6.7	2.3	<0.2	15	8.8	7	<5	137	1.6	7.7	<5	<10	0.4	3	17.2	29	11	0.9	35					
85032 Ab	Intensely feldspathised (ab) and weakly brecciated pelite with late sulfidic veins (PKM)	2120	841	2.23%	93.4	155	1.38	356	<5	<2	11.3	<1	182	<0.5	4.9	<20	5.3	5.7	<0.2	27	27	2.1	9	36.6	1.1	0.8	<5	<5	5.4	2.7	1.86	23	12	1.1	24					
85032M	Brecciated microcline vein in above sample with late sulfidic veins (PKM)	962	600	4.93%	163	264	1.23	2040	<5	2	8.61	<1	5.5	<0.5	0.8	<20	4	3.6	<0.2	120	200	9.8	17	2300	1.5	0.4	11	<5	0.7	<1	78.4	14	167	0.7	89					
85608 V	Quartz - mic vein with late sulfides. Same amount of sulfides as 85608 Abs (Pkm)	110	124	1.07%	1350	799	<0.5	<200	<5	3	12.6	2.63	432	<0.5	6.7	<20	5.2	5.9	0.4	17	<40	<1	8	<40	2.5	9.2	<10	<10	6.2	<2	19.2	30	27	3	20					
85609T3	Brecciated microcline vein with late cpy-py stringers (Pkm) ie. 85612 Sh (Pkm)	512	655	3.31%	226	353	0.62	2070	<5	<2	915	<1	361	1.4	1.9	<20	3.1	455	<0.2	13	100	11	8	227	55	1.2	<10	<5	0.5	<2	29.3	<3	79	0.9	45					
85624B	20cm wide pyrite vein (partly oxidised) with minor qtz hosted by 85624A (PKM)	20	26.2	610	485	613	0.69	717	<5	2.2	82.4	<1	618	0.8	3.1	<20	10	40	0.4	8	<10	3.5	<5	1476	6.3	6.2	<5	<5	3.2	<1	13.3	9.4	5.8	2.9	50					
		20	21.6	3980	393	491	3.07	119	<5	<2	14.2	1.41	576	0.7	<0.5	<20	25	3.8	2.7	16	<5	0.9	20	69.7	2	2	<5	<5	0	<1	1.54	3.8	<2	20	38					

Note

- Samples from drill core.
- Entire sample pulverised to -180 micron. Quartz wash between samples.
- Gold Fire Assays by ALS Townsville using 50gm charge.
- NAA Analytical Results are Neutron Activation Analyses, by Bequerel Laboratories.
- Gold assays in ppb. Iron, potassium and sodium quoted as percentage values. All other values in ppm except where indicated.
- (PKS) indicates hosted by Staveley Formation. (PKM) indicates hosted by Marimo Slates. (DYKE) indicates hosted by diorite.

Abbreviations

SAMPLE NO & DESCRIPTION		FIRE ASSAY		ICP	ANALYSES BY NEUTRON ACTIVATION UNLESS DENOTED OTHERWISE																				ICP										
		AU (ppb)	AU (ppb)		Cu	Co	As	Sb	ICP			Ce	Cs	Cr	Eu	Hf	Ir	Fe%	La	Lu	ICP		K%	Pb		Rb	Sm	Sc	Se	Ag	Na%	Ta	Th	W	U
LEAST ALTERED STAVELEY FORMATION																																			
85616	Paler clast of laminated altered pelite comprising dominantly of feldspars and calcite (PKS)	<1	<5	19	28.4	4.24	0.52	662	<5	2.3	150	<1	170	0.9	5.2	<20	1.3	72	0.3	<5	<5	1.4	<5	85.7	9.1	6.1	<5	<5	4.2	<1	14	14	<2	2.1	<5
85617	Darker clast of laminated altered pelite comprising dominantly of sericite, brown biotite and feldspar (PKS)	12	17.8	13	3.6	<2	<0.4	<200	<5	<2	165	<2	143	0.5	5.7	<20	1.2	84	0.3	<5	<10	3.1	<5	9.4	12	27	<10	<10	4.6	4.9	21	<4	<4	2.1	7
85621	Dark green clast of laminated pelite only no calcite matrix (20%) in sample - compare with 85620 (PKS)	2	<5	20	3.15	1.79	<0.4	3000	<5	<2	101	11	212	1	4.6	<20	9.5	47	<0.2	<5	<10	5.4	<5	401	6.9	19	<5	<5	1.3	1.5	21	<2	5.8	1.5	<5
PERVASIVELY ALTERED STAVELEY FORMATION																																			
85013	Slightly weathered qtzofeldspathic slt weakly ser with tr cc. (PKS)	10	5.7	72	4	2.23	0.65	824	<5	<2	68.3	3	416	1.2	0.5	<20	1.9	26	2.4	6	<10	8.3	5	474	10	12	<5	<5	0.2	<1	3	<2	6.9	20	6
85013 PY	As for 85013 but containing disseminated PY (PKS)	60	58.5	3160	21.1	1.71	1.58	1570	<5	<2	204	<1	123	0.6	0.5	<20	5	106	0.2	<5	<5	9.6	8	298	13	2.6	<5	<5	0.3	<1	11	<2	<2	1.9	11
85014	Kaolinised and sulfidic siltstone (PKS)	2	<5	65	622	8.44	0.88	1150	<5	<2	148	<1	401	1.7	6.8	<20	4.4	72	0.2	<5	<5	5.6	<5	170	9.8	42	<5	<10	1.6	1.9	22	8.1	<2	2.2	9
85622	Clast only of pink - orange fine grained pelite (PKS)	4	<5	18	3.04	1.49	0.83	838	<5	<2	14.9	<1	181	0.5	4.1	<20	1.8	7.3	<0.2	42	51	3.4	<5	89.9	1.4	5.7	<5	<5	2.2	2.1	5.3	9.5	8.7	1	<5
STAVELEY FORMATION WITH VEINS OR MATRIX																																			
85052	Carbonated and albitised pelite with disseminated py (5) and late calcite -py veins (PKS)	61	52.6	50	2890	239	<0.4	977	<5	3.1	18.1	4.8	310	0.8	1.9	<20	16	6.7	0.3	6	<5	2.4	<5	100	3.1	42	<5	<10	1	1.7	7.2	<4	<4	2.4	<5
85056	Platy dismembered segments of altered laminated pelite cemented by earlier Ab-mic-bi-qtz-py and later progressive Ca-mt (PKS)	2	<5	13	20.8	4.83	0.34	1200	<5	<2	242	1.7	176	2.3	3.8	<20	2.2	117	0.4	<5	<5	5.6	<5	212	16	14	<5	<5	2.2	<1	16	31	4.6	3.1	<5
85604	Slightly weathered laminated weakly brecciated pelite with 5% disseminated py (PKS)	12	35.6	1580	494	458	0.47	1670	<5	<2	193	<1	524	0.9	5.4	<20	3.1	95	0.6	16	<10	9.5	10	232	14	14	13	<5	0.3	1.2	20	13	8.9	3.8	13
85620	Dark green clasts of laminated pelite(PKS) with calcite matrix (20%) containing 2% py and tr. cpy	4	5	153	22.7	4.88	0.58	457	<5	<2	86.4	2.5	152	1.2	3.5	<20	4	41	0.4	6	<5	4.1	<5	210	6.3	13	<5	<5	0.4	<1	14	<2	3.6	2.7	<5
STAVELEY FORMATION VEINS																																			
85054	Thick vein of he dusted microcline - Ca-py (PKS)	15	22.7	6	1610	105	<0.2	972	<5	<2	24	<1	193	1	2.7	<20	9	10	0.7	9	<10	4.7	<5	105	4.9	28	<5	<10	0.5	2.3	9.7	20	7.2	4.5	10
85054V	Later vein of coarse Ca with disseminated py (tr) cutting above vein	61	32.2	97	2200	155	<0.44	326	<5	<2	55	3.1	344	2.2	0.5	<20	15	21	1.5	5	<5	1.5	<5	39.1	11	51	<5	<10	0.2	<1	3.6	8.3	<2	11	<5
85615	Late Manganoan calcite vein with 10% py in aggregates and as vugh/vein fill. Tr Fluorite (PKS)	90	90.3	25	1330	70.2	<0.2	<100	<5	4.7	51.8	<1	161	2.6	0.5	<20	7.7	17	4.2	<5	<5	<0.5	91	<20	6.9	38	<5	<10	0	<1	18	<4	3.2	27	12
DIORITE INTRUSIVE																																			
85037	Chloritised and carbonated microdiorite with disseminated sulfides. Ca-qtz, py-mic veins. No magnetite (DYKE)	6	<5	167	172	5.6	0.98	<100	<5	3.2	9.75	<1	373	0.6	3	<20	3.7	3.9	0.4	50	54	<0.2	<5	31.4	1.5	28	<5	<5	3	<1	1.8	11	51	2.2	11
85059-R	Part of zoned alteration assemblage adjacent to microdiorite comprises Ca (25) - Ab (54)-qtz-tr.mt/ (DY	4	<5	47	17.2	2.35	0.51	<100	<5	<2	181	<1	161	5.1	9.2	<20	1.5	106	1.1	10	17	<0.5	5	30.4	15	13	<5	<5	3.2	3.6	20	114	<2	6.5	12
85059Gy	As for 85059R but comprising Ab (30)-qtz (24)-mt (22)-bi (20) minor Ca, tr.py (dyke)	<1	<5	17	62.4	4.87	<0.2	132	<5	<2	223	2.9	184	6.9	4.3	<20	19	147	0.4	<5	<5	1	<5	190	17	16	<5	<5	2	<1	13	<2	<2	3.6	<5
85062	Altered microdiorite with mt (4) (DYKE)	2	<5	12	40	3.29	0.68	238	<5	<2	13.2	9.6	130	0.5	1.9	<20	7.3	7.1	0.3	5	<5	3.1	<5	313	2	32	<5	<5	3.7	2	1.8	<2	<2	2.2	6
Note															Abbreviations																				
(i) Samples from drill core.															Ab	Albite	mt	Magnetite																	
(ii) Entire sample pulverised to -180 micron. Quartz wash between samples.															mic	Microcline	he	Hermatite																	
(iii) Gold Fire Assays by ALS Townsville using 50gm charge.															qtz	quartz	Rt	Rutile																	
(iv) NAA Analytical Results are Neutron Activation Analyses, by Bequerel Laboratories.															Ca	Calcite	tr	Trace																	
(v) Gold assays in ppb. Iron, potassium and sodium quoted as percentage values. All other values in ppm except where indicated.															bi	Biotite	py	Pyrite																	
(vi) (PKS) indicates hosted by Staveley Formation. (PKM) indicates hosted by Marimo Slates. (DYKE) indicates hosted by diorite.															Phl	Phlogopite	cpy	Chalcopyrite																	
															ser	Sericite	cc	Chalcocite																	
Table 5.12 Trace element analyses for lithologies alteration and veins hosted by the Staveley Formation and diorite intrusive.																																			

Table 5.12 Trace element analyses for lithologies alteration and veins hosted by the Staveley Formation and diorite intrusive.

TABLE 5.13

WHOLE ROCK ANALYSES OF VARIOUS ROCK TYPES

LEAST ALTERED SHALE

	85009	85623	85611-SH	85612-SH	85626-SH	Slate with Qtz-py vein 85624
SiO ₂	65.30	62.70	60.50	61.80	61.70	37.40
Al ₂ O ₃	15.40	17.30	17.40	17.80	17.20	4.89
Fe ₂ O ₃	2.20	3.16	1.31	1.19	1.15	33.60
FeO	0.42	1.83	0.42	0.56	0.42	8.18
CaO	0.25	0.05	0.24	0.24	0.21	0.10
MgO	0.97	1.49	0.68	0.85	1.28	1.37
TiO ₂	0.60	0.71	0.90	0.72	0.65	0.02
Na ₂ O	0.83	0.98	7.18	7.63	2.16	0.60
K ₂ O	4.98	5.15	2.93	3.80	5.64	1.22
P ₂ O ₅	0.03	0.13	0.04	0.05	0.11	0.14
MnO	<0.01	0.01	<.01	<.01	<.01	0.15
SrO	<.01	<.01	<.01	<.01	<.01	<.01
ZrO ₂	0.03	0.04	0.04	0.04	0.03	0.01
L.O.I.	9.71	7.66	8.06	5.53	9.09	16.50
TOTAL	100.72	101.21	99.70	100.21	99.64	104.18

LEAST ALTERED STAVELEY FORMATION

METASOMATISED
STAVELEY Fm.

VEINED STAVELEY FORMATION

	85616	85617	85621	85622	85620	85056
SiO ₃	59.00	57.60	52.90	59.70	43.90	48.10
Al ₂ O ₄	12.10	19.60	16.00	8.82	10.70	13.10
Fe ₂ O ₄	2.11	2.30	12.20	2.65	5.31	3.40
FeO	1.55	0.99	5.50	2.11	2.40	2.26
CaO	6.63	2.37	1.40	7.04	15.90	10.20
MgO	2.47	2.37	3.63	3.56	2.18	3.23
TiO ₃	0.68	0.91	0.78	0.58	0.55	0.63
Na ₂ O	5.53	5.70	2.44	2.91	1.46	3.38
K ₂ O	3.30	4.34	6.68	4.49	4.82	7.42
P ₂ O ₆	0.19	0.18	0.24	0.13	0.18	0.19
MnO	0.10	0.03	0.07	0.12	0.33	0.19
SrO	0.01	0.01	<.01	<.01	0.02	0.01
ZrO ₃	0.03	0.03	0.03	0.03	0.03	0.03
L.O.I.	7.51	3.76	3.74	10.20	15.00	10.70
TOTAL	101.21	100.19	105.61	102.34	102.78	102.84

DIORITE

	85037	85062	85059R	85059GY
SiO ₃	53.40	46.90	52.70	49.10
Al ₂ O ₄	12.30	13.30	7.75	7.68
Fe ₂ O ₄	5.83	10.90	2.26	27.70
FeO	4.09	6.77	1.27	9.87
CaO	5.41	4.17	16.80	3.13
MgO	5.71	7.25	0.92	3.53
TiO ₃	1.58	1.35	0.41	0.43
Na ₂ O	4.02	5.22	4.11	3.42
K ₂ O	0.75	4.15	0.85	2.52
P ₂ O ₆	0.12	0.12	0.02	0.21
MnO	0.11	0.05	0.11	0.03
SrO	<.01	0.01	0.01	<.01
ZrO ₃	0.02	0.02	0.04	0.03
L.O.I.	10.60	6.81	14.20	2.77
TOTAL	103.94	107.02	101.45	110.42

SAMPLE DESCRIPTIONS

85009	Sparsely pyritic graphitic slate	85616	Paler clast of laminated altered pelite comprising dominantly of feldspars and calcite
85623	Graphitic slate	85617	Darker clast of laminated altered pelite comprising dominantly of sericite, brown biotite and feldspar
85611	Silicified shale with < 1% disseminated diagenetic (?) pyrite	85621	Dark green clast of laminated pelite only no calcite matrix (20%) in sample - compare with 85620
85612 Sh	Black shale hosting qtz-py-mic vein		
85624A	Black shale including 85624B (qtz-py vein)		
85626 Sh	Black shale hosting 85626 QPY (qtz-py vein)		
		85622	Clast only of pink - orange fine grained pelite
85037	Chloritised and carbonated microdiorite with disseminated sulfides. Ca-qtz, py-mic veins. No magnetite.		
85062	Altered microdiorite with mt (4%)	85056	Platy dismembered segments of altered laminated pelite cemented by earlier Ab-mic-bi-qtz-py and later progressive Ca-mt
85059Gy	As for 85059R but comprising Ab (30)-qtz (24)-mt (22)-bi (20) minor Ca, tr.py	85620	Dark green clasts of laminated pelite with calcite matrix (20%) containing 2% py and tr. cpy
85059-R	Part of zoned alteration assemblage adjacent to microdiorite comprises Ca (25) - Ab (54)-qtz-tr.mt		

Table 5.14 Average geochemical analyses of various rock types alteration styles & mineralisation.

	average L.A.Pkm n=5	average L.A.Pks n=3	METASOMATISED STAVELEY Fm. n=1	average Veined Pks n=2	average L.A. DIORITE n=2	average altered DIORITE n=2
Major Element	%	%	%	%	%	%
SiO2	62.4	56.5	59.7	46	50.15	50.9
Al2O3	17.02	15.9	8.82	11.9	12.8	7.72
Fe2O3	1.8	5.54	2.65	4.36	8.37	14.98
FeO	0.73	2.68	2.11	2.33	5.43	5.57
CaO	0.2	3.47	7.04	13.05	4.79	9.97
MgO	1.05	2.82	3.56	2.71	6.48	2.23
TiO2	0.72	0.79	0.58	0.59	1.47	0.42
Na2O	3.76	4.56	2.91	2.42	4.62	3.77
K2O	4.5	4.77	4.49	6.12	2.45	1.69
P2O5	0.07	0.2	0.13	0.19	0.12	0.12
MnO	0	0.07	0.12	0.26	0.08	0.07
SrO	0	0.01	<.01	0.02	0.01	0.01
ZrO2	0.04	0.03	0.03	0.03	0.02	0.04
L.O.I.	8.01	5	10.2	12.85	8.71	8.49
TOTAL	100.3	102.34	102.34	102.81	105.5	105.94

Trace Element Analyses in (ppm) Unless indicated	n=7	n=3	n=4	n=4	n=2	n=2	Perov. Alt'd Pkm	Veined Pkm	Main Mineral- isation n=7
Au (ppb)	5.26	5.9	16	23.3	0	0	79	876	516
Cu	40.67	10.7	829	449	89.5	32	3549	1221	18735
Co	6.3	11	163	857	106	39.8	408	538	442
As	8.4	1.4	3.47	177	4.4	3.6	324	3058	371
Sb	0.38	0	0.99	0.35	0.83	0.26	1.88	4.66	1.09
Ba	379	221	1096	1076	119	66	243	756	907
Bi	0	0	0	0	0	0	0	5.5	0
Br	1.1	0.8	0	0.77	1.59	0	1.47	0.8	1.2
Ce	194	105	109	135	11.5	202	357	148	133
Cs	6.7	0	0.8	2.24	4.8	1.43	0.83	0.5	0.9
Cr	174	104	280	291	252	173	234	520	331
Eu	0.8	0.3	0.9	1.31	0.31	6.03	0.95	0.7	0.4
Hf	5.7	3.6	2.7	3.64	2.47	6.73	5.61	2.6	3.4
Ir	0	0	0	0	0	0	0	0	0
La	92	52	53	65	5.53	126.5	167	67	65
Lu	0.5	0.2	0.7	0.4	0.32	0.73	0.28	0.8	0.5
Mo	8	0	12	7	27.5	5	8.4	6.6	28
Pb	3.1	0	3.3	2.5	0	2.5	4.4	14	8.4
Rb	176	32	258	189	172	110	52.3	249	544
Sm	14	7	8.6	9.6	1.78	15.9	23.5	11	9
Se	13	11	16	21	30	14.55	5.95	8	4.9
Se	0	0	0	3.2	0	0	0	0	1.3
Ag	0	0	0	0	0	0	0	0	0
Ta	1.2	1.6	1	0.7	1	1.8	2.56	0.6	1.1
Th	23	12	10	14	1.8	16.25	19.5	8.4	22
W	11	4.7	4.4	11	5.55	57	22.7	6.1	17
U	7.8	0	3.9	4.3	25.2	0	21.2	10	41
Yb	3.7	1.4	6.4	3	2.2	5.03	2.1	7.1	4
Zn	33	2.3	6.5	3.3	8.5	6	14.2	17	40

Abbreviations

Pkm = Marimo Slate
Pks = Staveley Formation
L.A. = Least altered
Perov. = Pervasive

Analyses

Au by Fire Assay at A.L.S. Townsville (commercial Laboratory)
Cu, Pb, Zn, Mo, Bi by I.C.P. at A.L.S.
All other minor and trace elements By neutron activation analyses.

Table 5.15 Downhole minor and trace element geochemistry for hole GDH -01

Sample No.		From-To (m)	Interval (m)	Au	Cu	Pb	Zn	Ag	As	V	Co	P	Ba	F	U	Bi	Mo	W	Sn
37837	Weathered Pkm	10-12	2.0	<0.01	35	5	<5	<0.2	83	18	31.6	293	634	670	15.5	0.2	3.2	<1	<5
37843	"	20-22	2.0	<0.01	85	<5	<5	0.4	309	65	38.7	399	647	870	13.0	1.0	16.9	3	<5
37848	"	30-32	2.0	<0.01	45	6	<5	0.4	233	69	23.9	243	674	690	10.3	1.0	8.6	3	<5
37854	Bk Pkm	40-42	2.0	<0.01	25	9	8	0.5	148	98	4.9	141	637	530	14.1	2.1	10.7	3	<5
37859	"	50-52	2.0	<0.01	55	10	<5	0.3	99	96	6.4	130	642	400	9.6	0.9	8.0	2	<5
37865	"	60-62	2.0	<0.01	70	12	<5	0.4	128	106	25.5	174	648	460	15.0	2.0	11.6	4	<5
37871	"	70-72	2.0	<0.01	75	7	6	0.4	115	92	17.5	162	618	420	13.4	2.4	10.1	4	<5
37876	"	80-82	2.0	<0.01	80	7	<5	0.4	123	99	21.6	207	587	360	16.7	1.3	9.5	3	<5
37882	"	90-92	2.0	<0.01	155	9	15	0.3	127	101	21.0	270	592	350	14.3	1.5	9.9	3	<5
53477	pyritic black slate	101.5-105.45	3.95	<0.01	140	10	<5	0.3	127	115	20.6	281	526	630	16.8	2.8	11.5	3	<5
53485	"	118.0-119.0	1.0	<0.01	95	5	15	0.4	95	89	36.5	121	552	1360	17.8	3.9	9.3	4	<5
53505	"	135.0-136.0	1.0	0.17	5500	6	14	0.9	58	101	34.6	218	617	690	16.6	1.7	10.7	2	<5
53511	"	140.67-141.7	1.03	0.01	4250	5	13	0.9	19	98	37.2	326	696	730	15.9	1.3	6.3	3	<5
53516	"	148.75-151.0	2.25	<0.01	60	5	7	<0.2	249	47	93.7	479	780	1100	21.4	10.4	5.1	<1	<5
53531	Pervasive alt'n & veining	162.64-163.00	0.36	0.31	0.50%	<5	<5	1	554	14	566	399	609	270	23	4.5	13	21	<5
53532	"	163.00-164.00	1.0	0.24	1.16%	<5	<5	2	866	27	868	298	35	270	11	2.4	15	26	<5
53533	"	164.00-165.00	1.0	0.25	1.83%	<5	<5	2	312	14	250	228	26	300	11	2.4	13	17	<5
53534	"	165.00-166.00	1.0	0.27	0.75%	<5	<5	1	552	19	665	230	173	480	34	5.5	16	12	<5
53535	"	166.00-167.00	1.0	0.78	3.17%	16	10	5	326	47	328	798	1700	1460	53	18.6	55	10	9
53536	"	167.00-168.00	1.0	2.92	4.09%	<5	6	7	322	32	403	630	106	660	25	7.6	34	22	<5
53537	"	168.00-168.62	0.62	0.44	1.40%	<5	<5	2	851	19	798	329	30	300	25	3.0	16	15	<5
53538	Bk shale with veins	168.62-169.00	0.38	0.16	0.35%	<5	<5	1	344	62	302	508	663	520	32	0.9	13	10	<5
53539	"	169.00-170.00	1.0	0.05	0.33%	<5	<5	1	662	77	641	345	260	670	30	0.9	13	17	<5
53540	"	170.00-170.64	0.64	0.37	1.17%	7	9	3	7510	21	1.01%	469	530	290	31	3.8	30	<10	<5
53541	"	170.64-171.00	0.36	0.04	0.39%	<5	<5	1	1960	94	1930	279	357	800	17	1.5	16	25	<5
53542	"	171.00-172.00	1.0	0.02	0.04%	<5	<5	<1	838	41	668	508	369	420	9	0.6	12	19	<5
53543	"	172.00-173.00	1.0	<0.01	0.02%	<5	<5	<1	559	37	461	434	325	500	10	0.4	12	27	<5
53544	"	173.00-174.00	1.0	0.15	0.19%	<5	<5	<1	273	49	235	484	707	1040	8	0.7	13	15	<5
53545	"	174.00-175.03	1.03	<0.01	0.06%	<5	<5	<1	1820	71	1390	357	306	1410	17	0.7	13	10	<5
53546	Intense pervasive alt'n +/- sulphides	175.03-176.07	1.04	0.44	1.33%	<5	15	2	901	53	1050	309	697	1100	22	2.5	15	19	<5
53547	"	176.07-176.70	0.63	1.33	3.37%	32	31	5	448	17	575	492	745	1110	17	8.7	53	28	<5
53548	"	176.70-177.50	0.80	0.29	3.77%	12	44	4	243	125	348	439	1380	1690	24	7.8	45	19	<5
53549	"	177.50-178.50	1.0	4.44	12.00%	43	43	12	546	61	999	476	1060	980	33	6.9	60	<10	<5
53551	"	178.50-179.00	0.5	0.03	0.31%	7	22	<1	150	18	925	252	1110	470	<4	1.5	66	<10	<5
53552	"	179.00-181.00	2.0	0.12	0.43%	7	19	<1	202	14	502	186	1290	340	<4	1.7	14	24	<5
53553	It'd Pks with K-spar vein	181.00-182.20	1.2	0.29	1.18%	23	16	7	372	61	491	406	1260	610	35	3.4	1680	23	<5
53554	& sulphides	182.20-183.10	0.9	0.05	1.30%	9	11	2	429	90	1230	195	1020	1010	10	4.1	779	29	<5
53555	"	183.10-183.60	0.5	0.03	0.72%	8	9	3	324	106	691	271	1890	1040	5	4.7	44	14	<5
53562	Pks	188.8-189.8	1.10	<0.01	85	<5	17	0.4	30	107	110	633	1207	530	8.3	1.2	12.4	7	<5
53572	"	198.0-199.0	1.0	<0.01	80	<5	15	0.4	36	113	70.5	991	530	680	6.6	1.2	13.7	6	<5
53584	"	209.5-209.95	0.45	<0.01	35	<5	<5	0.3	12	85	6.2	860	799	530	17.4	0.8	3.3	5	<5

Interval 162.64 - 183.60 metres (20.96 metres) averages 0.57 g/t Au, 1.75% Cu and 0.10% Co.

Analytical results by ALS (Townsville and Brisbane)

Au by Method PM 209 (Fire Assay)

Cu by Method G001 and A101 (A.A.S.) for samples >5000 ppm

Pb Zn V P by IC587 (I.C.P.)

Ag As Bi Mo Co W U by MS532

Sn B by XRF1

* Assay values in ppm unless otherwise stated

F by Method G006

Abbreviations

Bk = Black

Pkm = Marino Slate

Pks = Staveley Formation

Alt'd = altered

Table 5.16 Downhole minor and trace element geochemistry for hole GDH -03

Sample No.	Brief description of Interval	From-To (m)	Interval (m)	Au	Cu	Pb	Zn	Ag	As	V	Co	P	Ba	F	U	Bi	Mo	W	Sn
51209	Pkm with qtz veins	10-12	2.0	0.04	561	5	7	0.6	54	111	52.2	444	462	1050	10.0	1.8	2.4	12	<5
51214	Pks Breccia	20-22	2.0	<0.01	<2	<5	6	<0.2	13	151	108.0	242	90	240	2.2	0.4	1.0	<1	<5
51219	"	30-32	2.0	<0.01	262	<5	7	0.3	70	59	255.0	541	2144	190	8.3	0.7	3.5	16	<5
51225	"	40-42	2.0	<0.01	7	<5	7	0.2	16	191	33.1	273	260	200	1.9	0.4	1.0	<1	11
51231	"	50-52	2.0	0.01	616	6	13	0.5	182	22	346.0	1095	1685	370	53.9	1.8	13.9	3	<5
51236	Bk Pkm with Py & veins	60-62	2.0	<0.01	88	5	<5	0.5	112	13	70.2	368	802	500	15.7	1.4	9.5	2	<5
51241	"	70-72	2.0	<0.01	257	5	<5	0.6	126	27	79.8	237	554	980	18.7	1.4	10.0	3	<5
51246	Pkm	80-82	2.0	<0.01	129	<5	<5	0.4	209	53	95.5	459	687	1340	11.9	1.3	8.7	3	<5
51251	"	90-92	2.0	<0.01	110	<5	7	0.3	110	87	37.3	469	737	830	8.9	1.0	5.0	5	<5
51256	Bk Pkm with Py & veins	100-102	2.0	<0.01	280	<5	5	0.4	212	81	83.9	442	713	1140	12.0	1.5	6.7	6	<5
51261	"	110-112	2.0	<0.01	217	5	7	0.3	101	68	40.5	487	746	830	9.6	1.2	7.2	4	<5
51266	"	120-122	2.0	0.01	614	<5	8	0.4	136	55	61.1	445	716	1220	14.4	1.1	7.2	3	<5
51272	Bk Pkm with Py & veins	30.0-131.4	1.45	0.39	1.37%	14	18	0.9	1050	41	690.0	561	524	270	43.0	1.5	10.3	2	<5
16302	Pkm - pervasively alt'd	31.45-132.	0.75	1.64	1.16%	25	27	1.4	1550	19	1350.0	473	413	180	78.1	5.2	19.7	3	<5
16305	with veins & sulphides	134.2-135.3	1.10	1.20	2.01%	20	25	1.5	610	50	720.0	590	447	190	52.5	4.5	62.2	8	<5
16308	"	137.2-137.5	0.30	0.48	0.74%	49	14	0.9	420	15	540.0	352	366	190	119.0	2.0	22.0	3	<5
16319	"	144.7-148.1	3.40	0.22	0.56%	16	16	1.0	330	39	330.0	421	574	300	39.5	3.9	19.1	4	<5
16327	Bk Pkm with veins	54.25-155.	1.35	0.02	386	9	6	0.7	1400	53	940.0	453	341	520	89.2	3.1	22.9	4	<5
16337	Microdiorite	163.9-164.9	1.00	0.02	49	<5	22	0.5	65	215	720.0	506	531	470	35.1	2.3	37.0	3	9
16346	Pervasively alt'd Pkm	72.0-172.9	0.95	0.12	123	12	80	0.8	481	48	504.0	435	542	1080	105.0	1.7	18.5	162	<5

* Assay values in ppm unless otherwise stated

Interval 130.0 - 137.7 metres (7.7 metres) average 0.45 g/t Au and 0.85% Cu

Analytical results by ALS (Townsville and Brisbane)

Au by Meth (Fire Assay)

Cu by Method G001 and A101 (A.A.S.) for samples >5000 ppm

Pb Zn V P by IC587 (I.C.P.)

Ag As Bi Mo Co W U by MS532

Sn B by XRF1

F by Method G006

Abbreviations

Bk = Black

Pkm = Marimo Slate

Pks = Staveley Formation

Alt'd = altered

chalcopyrite which were observed when microprobing i.e. chalcopyrite and microcline \pm sericite were coprecipitating.

There also appears to be a negative Au - Co and possibly Au - As. This may suggest that cobaltite and erythrite were being replaced (possibly by Fe, S and Cu) during gold mineralisation. Figure 5.3 also shows that Au increased independently of Fe, K and W while Cu increased largely independently of Co and As, however the possible weak negative correlation between Cu - As and Cu - Co may confirm that cobaltite and erythrite was being progressively replaced by Fe, Cu and S.

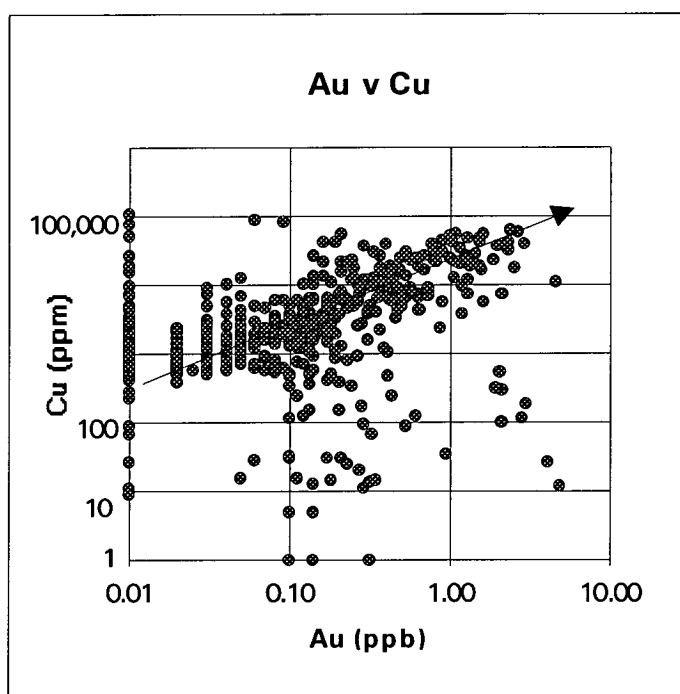


Figure 5.9 Plot of Au v Cu for all core holes where Au > 0.1ppb or Cu > 500ppm. Only samples below base of oxidation plotted. (n = 588).

Ch 5.3 The Geochemistry of Felsic Intrusives of the Marimo Basin

The Marimo Basin is located within a very long regional gravity low which immediately to the south, can be correlated with the Williams Batholith, and to the north, the Naraku Batholith. The Marimo Basin contains very few felsic intrusives and may in fact be underlain by the Williams or Naraku Batholith at depth.

Wyborn and Heinrich (1993) suggests that the Williams and Naraku Batholiths may have mineralising potential, and there appears to be a progression in alteration from an early high - K, low - Na, magnetite bearing alteration through a high - Na, low - K, hematite alteration to a late K - rich, low - Na, hematite rich phase. They note that the intrusives post date regional deformation and peak metamorphism, and consequently primary porosity and permeability in the surrounding country rock are likely to be low, with the exception of breccia bodies surrounding some of the plutons particularly south of and around the southern Marimo Basin, and fracture induced permeability through the breccias and fault zones is likely to be the main means of fluid migration. They suggest that the granites need not be intermediate in composition and the highly fractionated ($>60\%$ SiO_2) portions of the Williams Batholith may be metallogenically important. Wyborn et al. (1987) and Wyborn (1992) geochemically characterised and noted the chemical similarity between the Williams Batholith and granites of the central Gawler Craton and the Stuart Shelf, South Australia. Wyborn et al. (1987) demonstrate that these granites are highly fractionated I-types characterised by high Na_2O values compared with older Proterozoic felsic granites and that the K_2O values are lower and the Na_2O and Ba values are relatively higher with elevated Th, U, La and Ce values.

A direct relationship between felsic intrusives and mineralisation has not been proved but is the subject of recent research. This study aims to geochemically characterise the relatively few felsic intrusives in the vicinity of the Southern Marimo Basin so that the mineralising potential may eventually be evaluated should a causal link to mineralisation be established one day. Table 5.17 shows the chemical composition of various intrusives in the immediate vicinity of the Greenmount deposit (within 3 km) and Table 5.18 shows the chemical composition of other felsic intrusives in or near the Marimo Basin. The freshest possible sample was selected and the most weathered surfaces were sawn off, however all samples were partially altered or weathered. The data indicates that the intrusives near the Greenmount deposit have relatively uniform major element geochemistry with SiO_2 values above 72% and Na_2O greater than 7%. The distal intrusives have a generally lower SiO_2 content (61 - 78% SiO_2) and lower Na_2O content (4.9 to 6.4% Na_2O) with the exception of the Lady Karen granite (sample 94206525) which is geochemically more similar to the granites near Greenmount. The Lady Karen Granite is also near the next major mineralising centre as suggested by the concentrations of historical metal prospects. It is located within the Copper Canyon - Lady Karen area, which includes similar styles of mineralisation as seen at Greenmount, and is near a similar lithostructural and stratigraphic setting.

The intrusives near Greenmount have a relatively higher Nb and Th content and appear to have a higher average W, Zr, U, F, Cr and Ba content than the more distal intrusives.

Table 5.17 Geochemical Whole Rock Analyses of Intrusives Near Greenmount

					Sample Number:	94206524
Major Elements %	**94206524	**J2	**D1	*94206523	Location:	Jasmin Granite. Granitic outcrop several hundred metres south of the Greenmount Deposit.
SiO2	72.01	74.10	76.80	77.39	Description:	Albitised Leucogranite
TiO2	1.30	1.09	0.05	0.03		
Al2O3	14.32	13.70	13.40	13.60	Sample Number:	J2
Fe2O3 (total)	0.71	1.24	0.83	0.41		
Fe2O3	0.31	n.a.	n.a.	0.18	Location:	Greenmount approx. 9100N 5000E. Dyke which is almost parallel to Pkm/Pks contact.
FeO	0.36	n.a.	n.a.	0.21		
MgO	0.66	0.13	0.14	0.09	Description:	Partly weathered intrusive. Mafic silicates selectively sericitised then removed by weathering. Now comprises ser/plag(58%)-qtz(28%)-Musc(2%)-rut(2%)-ap(< 1%) & 8% limonite & pores.
CaO	0.89	0.71	0.18	0.14		
Na2O	7.88	7.39	7.36	7.35	Sample Number:	D1
K2O	0.38	0.33	0.55	0.33		
P2O5	0.55	0.48	<.01	0.01	Location:	Desolation Prospect approx. 3Km South of Greenmount.
H2O+	0.00	n.a.	n.a.	0.00		
H2O-	0.00	n.a.	n.a.	0.00	Description:	Similar to sample J2 but lacking rutile & apatite and has granophyric texture.
LOI	1.03	0.86	0.56	0.78		
<u>TOTAL</u>	<u>100.4</u>	<u>100.03</u>	<u>99.87</u>	<u>100.18</u>	Sample Number:	94206523
Trace Elements (ppm)					Location:	Desolation Prospect approx. 3Km South of Greenmount and 400m west of sample D1.
Au	n.a.	0	<5	n.a.	Description:	Similar to sample J2 but lacking rutile & apatite and has granophyric texture.
Ar	30	n.a.	n.a.	0		
Cu	8	25	29	10	Sample Number:	94206523
Co	24	7.85	23.2	4		
As	n.a.	0	2.7	n.a.	Location:	Desolation Prospect approx. 3Km South of Greenmount and 400m west of sample D1.
Sb	n.a.	<2	<.2	n.a.		
Ba	68	348	163	57	Description:	Similar to sample J2 but lacking rutile & apatite and has granophyric texture.
Bi	-2	n.a.	n.a.	<2		
Br	n.a.	<2	<2	n.a.	Sample Number:	94206523
Ce	139	267	42.2	15		
Cs	n.a.	<1	<1	n.a.	Location:	Desolation Prospect approx. 3Km South of Greenmount and 400m west of sample D1.
Cr	2	161	154	1		
Eu	n.a.	1.94	0.69	n.a.	Description:	Similar to sample J2 but lacking rutile & apatite and has granophyric texture.
F	0	260	70	0		
Ga	24	n.a.	n.a.	26	Sample Number:	94206523
Hf	n.a.	24.7	6.33	n.a.		
Ir	n.a.	<20	<20	n.a.	Location:	Desolation Prospect approx. 3Km South of Greenmount and 400m west of sample D1.
La	70	176	21.6	11		
Li	24	n.a.	n.a.	1	Description:	Similar to sample J2 but lacking rutile & apatite and has granophyric texture.
Lu	n.a.	1.29	0.49	n.a.		
Mn	351	100	300	48	Sample Number:	94206523
Mo	-2	<5	<27	<2		
Nd	63	n.a.	n.a.	4	Location:	Desolation Prospect approx. 3Km South of Greenmount and 400m west of sample D1.
Ni	16	n.a.	n.a.	1		
Nb	51	n.a.	n.a.	56	Description:	Similar to sample J2 but lacking rutile & apatite and has granophyric texture.
Pb	9	n.a.	n.a.	4		
Rb	49	<20	<20	17	Sample Number:	94206523
Sm	n.a.	17	3.22	n.a.		
Sc	11	10.1	2.03	1	Location:	Desolation Prospect approx. 3Km South of Greenmount and 400m west of sample D1.
Se	n.a.	<10	<5	n.a.		
Ag	1	<5	<5	<1	Description:	Similar to sample J2 but lacking rutile & apatite and has granophyric texture.
Sr	24	<100	<100	25		
S	30	n.a.	n.a.	60	Sample Number:	94206523
Ta	n.a.	11.1	9.51	n.a.		
Th	87	93.8	23	32	Location:	Desolation Prospect approx. 3Km South of Greenmount and 400m west of sample D1.
Sn	9	n.a.	n.a.	<2		
W	73	61.5	3.61	6	Description:	Similar to sample J2 but lacking rutile & apatite and has granophyric texture.
U	13	10.8	14.6	14		
V	60	n.a.	n.a.	5	Sample Number:	94206523
Y	108	n.a.	n.a.	17		
Yb	n.a.	9.25	3.08	n.a.	Location:	Desolation Prospect approx. 3Km South of Greenmount and 400m west of sample D1.
Zn	3	<100	136	2		
Zr	635	1100	200	93	Description:	Similar to sample J2 but lacking rutile & apatite and has granophyric texture.

NOTES

* Samples collected by R. Krcmarov and submitted to AGSO for analyses and entry into Rockchem database.

** Samples analysed for major elements by ALS (commercial laboratory) in Townsville and for trace elements by Neutron Activation Analyses at Bequerel Laboratories.

Freshest possible sample selected and the most weathered surfaces were sawn off.

NOTES

* Samples collected by R. Krcmarov and submitted to AGSO for analyses and entry into Rockchem database.

** Samples analysed for major elements by ALS (commercial laboratory) in Townsville and for trace elements by Neutron Activation Analyses at Bequerel Laboratories.

Freshest possible sample selected and the most weathered surfaces were sawn off.

Table 5.18 Geochemical whole rock analyses of felsic intrusives of the Marimo Basin Environs

Major Elements (Wt%)	94206522	94206525	94206526	Sample Number: 94206522
SiO2	61.44	78.32	69.82	Location: Mt Michael - A granite outcrop approx. 4Km E of Greenmount AMG 7677620N 456822E
TiO2	1.13	0.26	0.42	
Al2O3	11.73	12.22	14.27	Description: Partially weathered and altered fine grained granite
Fe2O3 (total)	16.60	0.70	2.54	
Fe2O3	15.48	0.46	1.38	
FeO	1.01	0.22	1.04	
MgO	0.41	0.07	1.53	Sample Number: 94206525
CaO	0.50	0.16	1.54	
Na2O	4.92	6.39	6.22	Location: Northern part of Lady Karen prospect - approx. 11km north of the Greenmount Deposit at AMG 7688215N & 448535E.
K2O	0.84	0.16	1.35	
P2O5	0.28	0.02	0.11	
H2O+	0.00	0.00	0.00	
H2O-	0.00	0.00	0.00	Description: Partially weathered fine grained albitised granite.
LOI	1.87	1.09	2.18	
TOTAL	100.04	99.55	100.06	Sample Number: 94206526
Trace Elements (ppm)				
Au	n.a.	n.a.	n.a.	Location: 308 granite located approx. 14km NNE of the Greenmount Deposit at AMG 7691424N & 451872.
Ar	4	8	0	
Cu	2137	100	1	Description: Partially weathered fine grained albitised granite.
Co	97	13	11	
As	n.a.	n.a.	n.a.	Sample Number: 94206526
Sb	n.a.	n.a.	n.a.	
Ba	84	54	236	Location: 308 granite located approx. 14km NNE of the Greenmount Deposit at AMG 7691424N & 451872.
Bi	<2	<2	<2	
Br	n.a.	n.a.	n.a.	Description: Partially weathered fine grained red granite.
Ce	90	104	136	
Cs	n.a.	n.a.	n.a.	Sample Number: 94206526
Cr	2	<1	36	
Eu	n.a.	n.a.	n.a.	Location: 308 granite located approx. 14km NNE of the Greenmount Deposit at AMG 7691424N & 451872.
F	0	0	0	
Ga	26	23	20	Description: Partially weathered fine grained red granite.
Hf	n.a.	n.a.	n.a.	
Ir	n.a.	n.a.	n.a.	Sample Number: 94206526
La	45	49	74	
Li	5	1	5	Location: 308 granite located approx. 14km NNE of the Greenmount Deposit at AMG 7691424N & 451872.
Lu	n.a.	n.a.	n.a.	
Mn	158	178	189	Description: Partially weathered fine grained red granite.
Mo	<2	<2	<2	
Nd	48	59	45	Sample Number: 94206526
Ni	14	2	31	
Nb	17	17	14	Location: 308 granite located approx. 14km NNE of the Greenmount Deposit at AMG 7691424N & 451872.
Pb	<2	<2	4	
Rb	42	4	87	Description: Partially weathered fine grained red granite.
Sm	n.a.	n.a.	n.a.	
Sc	27	5	6	Sample Number: 94206526
Se	n.a.	n.a.	n.a.	
Ag	1	1	<1	Location: 308 granite located approx. 14km NNE of the Greenmount Deposit at AMG 7691424N & 451872.
Sr	27	58	48	
S	40	20	10	Description: Partially weathered fine grained red granite.
Ta	n.a.	n.a.	n.a.	
Th	<2	5	37	Sample Number: 94206526
Sn	<2	2	3	
W	7	9	5	Location: 308 granite located approx. 14km NNE of the Greenmount Deposit at AMG 7691424N & 451872.
U	3	1	17	
V	5	6	53	Description: Partially weathered fine grained red granite.
Y	95	96	25	
Yb	n.a.	n.a.	n.a.	Sample Number: 94206526
Zn	9	5	6	
Zr	206	507	225	Location: 308 granite located approx. 14km NNE of the Greenmount Deposit at AMG 7691424N & 451872.

NOTES
Samples collected by R. Krcmarov and submitted to AGSO for analyses and entry into Rockchem database.

Freshest possible sample selected and the most weathered surfaces were sawn off.

Samples 94206524 and J2 are closest to the Greenmount deposit. They have a distinctly higher Ti, Na, P, Ar, Ce, La, Li, Nd, Nb, Th, Sn, W, V, Y and Zr content than all other intrusives. The Cu, Au and Co values however are very low and hence may indicate that the felsic intrusives do not constitute a likely source for these metals. They may however, be petrogenetically related to other, as yet unidentified mineralising intrusives.

CHAPTER 6 *Stable Isotopes*

Ch 6.1 Sulphur Isotopes

A sulphur isotope study was carried out to determine the possible sulphur source (or sources), and to possibly gain an insight into mineralisation processes, particularly since the source of metals remains equivocal.

6.1.1 Procedures

Doubly polished 150 μm acetone soluble thin sections were made. The sample was then described and detailed drawings of the areas for analysis were made to aid in spot location as well as sulphide type or style of occurrence.

A laser ablation extraction system for laser ablation extraction of SO_2 gas from sulphide minerals for sulphur isotope analyses was used, from the Central Science Laboratory at the University of Tasmania. This system can determine $\delta^{34}\text{S}$ with a 1σ precision of 0.4 to 0.5‰ from 100 - 300 μm spots. The sulphur isotopes are extracted by various heating and freezing operations, before analysis by a VG Micromass mass spectrometer as described by Huston et al. (1992). Each day the mass spectrometer was calibrated with a Broken Hill ($\delta^{34}\text{S}_{\text{CDT}} = 3.4\text{‰}$) or a Rosebery ($\delta^{34}\text{S}_{\text{CDT}} = 12.4\text{‰}$) reference gas. The $\delta^{34}\text{S}_{\text{CDT}}$ of the sample gas was estimated by linear interpolation and extrapolation from analyses of the reference gases. The $\delta^{34}\text{S}_{\text{CDT}}$ of the analysed mineral was determined by adding the appropriate fractionation factor (below) to $\delta^{34}\text{S}_{\text{CDT}}$ of the produced gas.

Mineral	Fractionation Factor (‰)	Uncertainty (1σ) (‰)
pyrite/marcasite	5.75	0.41
chalcopyrite	4.45	0.44

During the analyses, several samples were checked for consistency and reproducibility by analysing adjacent spots.

6.1.2 Isotopic Variation

All Greenmount sulphides range between $\delta^{34}\text{S} = -10.3$ and 24.9‰ , average 8.66‰ and have a Normal distribution (Figure 6.1, Table 6.1 and Table 6.2). The mean of all $\delta^{34}\text{S}$ chalcopyrite (8.44‰) is less than the mean of all $\delta^{34}\text{S}$ pyrite (8.70‰) which is the correct fractionation order expected if the two minerals were deposited in equilibrium, however many mineral pairs in detail display isotopic disequilibrium since sulphur isotopes may not completely respond to

MARIMO SHALE HOSTED SULPHIDES							STAVELEY FORMATION SULPHIDES						
n = 63 Samples							n = 10						
Sample No.	Hole	Depth (m)	Approx. Distance From Staveley Formation	Mineral	Sulphide Style	S34S Value o/oo	Sample No.	Hole	Depth (m)	Mineral	Sulphide Style	S34S Value o/oo	
85009	GDH-01	119.8	67m	pyrite	disseminated	17.30	85027	GDH-02	199.7	cpy	vein	9.86	
					disseminated	19.70					vein	11.32	
					disseminated	16.00	85054	GDH-05	95.9	pyrite	disseminated	8.4	
85017	GDH-02	127.4	74m	pyrite	vein	7.89					disseminated	1	
					vein	5.74					disseminated	5	
					vein	8.07	85604	GDH-02	183.3	pyrite	disseminated	3.1	
					vein	5.68					disseminated	2.8	
					vein	5.68					disseminated	8.2	
					vein	7.12	85614	GDH-02	203.1	pyrite	disseminated	-0.1	
					vein	6.44					disseminated	-1.4	
85019	GDH-02	135	65 m	pyrite	vein	15.31							
					vein	15.76							
					vein	3.74							
					vein	10.00							
					vein	12.32							
85020	GDH-02	139.5	60 m	*cpy	vein	9.07							
				*pyrite	vein	7.98							
85021	GDH-02	141	58 m	*cpy	vein	7.64							
				*pyrite	vein	9.36							
				*pyrite	vein	6.93							
				*cpy	vein	8.18							
				pyrite	vein	2.69							
85023	GDH-02	149.8	50 m	pyrite	vein	2.10	85037	GDH-03	161.2	pyrite	disseminated	4.6	
				pyrite	vein	0.60							
				cpy	vein	2.96							
				*pyrite	vein	8.41	85059	GDH-05	208.7	pyrite	disseminated	-5.28	
				*cpy	vein	10.63					disseminated	-3.1	
				pyrite	vein	15.36					disseminated	-5	
				pyrite	vein	5.05					disseminated	-10.3	
				*pyrite	vein	6.97							
				*cpy	vein	8.30							
				cpy	vein	10.96							
				cpy	vein	8.20							
				pyrite	vein	6.57							
				cpy	vein	7.40							
				cpy	vein	6.76							
85025	GDH-02	177.7	20 m	pyrite	vein	10.16							
85030	GDH-03	131.65	50 m	pyrite	disseminated	23.09							
85033	GDH-03	140.9	+ 10 m	pyrite	vein	5.62							
					vein	10.70							
					vein	6.93							
					vein	7.17							
					vein	5.87							
					vein	4.77							
					vein	6.08							
					vein	6.09							
					vein	5.28							
85034	GDH-03	141.7	9 m	pyrite	vein-massive	5.72							
					vein-massive	4.75							
					vein-massive	6.05							
85064	GERC42	68	+ 5 m	pyrite	disseminated	-0.60							
85065	GERC42	169	260 m	pyrite	stringer	15.30							
					stringer	18.20							
85066	GERC44	164	350 m	pyrite	disseminated	24.90							
					stringer	23.80							
					stringer	21.60							
					stringer	21.00							
85067	GERC44	134	370 m	pyrite	stringer	24.10							
					stringer	20.30							
85068	GRC45	86		pyrite	disseminated	17.50							
					disseminated	24.20							
85611-V	GDH-02	170.2	30 m	pyrite	vein	9.50							
					vein	9.20							

* Denotes mineral pairs

Table 6.1 Sulphur isotope analyses for samples from Greenmount

the changes in the chemical environment during mineral deposition; processes such as boiling, mixing of fluids and/or redox reactions may result in isotopic disequilibrium (Rye and Ohmoto, 1974). The notoriously inaccurate isotopic thermometer for pyrite - chalcopyrite pairs (Ohmoto and Rye, 1979) was not used. Fluid inclusions (Chapter 7) are used to estimate the temperature of sulphide deposition.

TABLE 6.2 - A summary of the statistical variation of $\delta^{34}\text{S}\text{‰}$ for all samples as a function of rock-type and occurrence.

Category	n =	mean	S.D.	Min	Max
All sulphides	78	8.66	7.10	-10.3	24.9
All pyrite	66	8.70	7.67	-10.3	24.9
All chalcopyrite	12	8.44	2.17	2.96	11.32
Pkm vein pyrite	38	7.52	3.40	0.60	15.76
Pkm disseminated and stringer pyrite	15	19.09	6.07	-0.60	24.9
Pkm vein chalcopyrite	10	7.10	3.15	2.96	10.96
Pks pyrite	8	3.38	3.39	-1.40	8.40
Pks chalcopyrite	2	10.59	0.73	9.86	11.32
Diorite pyrite	5	-3.82	2.66	-10.3	4.60
All sulphides related to main vein array	47	7.62	3.11	0.60	15.76

Figure 6.2 shows a plot of $\delta^{34}\text{S}\text{‰}$ values for main vein array sulphides. These immediately preceded (and possibly included the main stage of mineralisation) and comprise chalcopyrite from veins in the Staveley Formation and the Marimo Slate, as well as pyrite in veins hosted by the Marimo Slate. These sulphides have a mean of 7.62‰ and range from 0.60‰ to 15.76‰ (Table 6.2). This mean approximates to the mean of all chalcopyrite values (8.44‰) and hence the isotopic composition of sulphides during main stage mineralisation averaged around 7-9‰.

Disseminated and stringer pyrite in unaltered black shale is interpreted to represent "background" diagenetic - metamorphic pyrite. With the exception of a single sample (-0.60‰) all other values range from 15.3‰ to 24.9‰ with a total mean of 19.09‰. This approximates to, but is slightly heavier than the average $\delta^{34}\text{S}$ value of marine sulphate during the Proterozoic which was 17‰ (Claypool et al., 1980). Muir et al. (1987) suggest that Australian Mid-Proterozoic seawater sulphate averaged 20 - 25‰. The crystallisation of sedimentary sulphate from seawater (evaporite formation) produces a relatively small $\delta^{34}\text{S}$ enrichment of $1.65 \pm 0.12\text{‰}$ (Thode and Monster, 1965) and hence other processes may have fractionated the sulphur at Greenmount to greater than 20‰. Gautier (1982) reported that

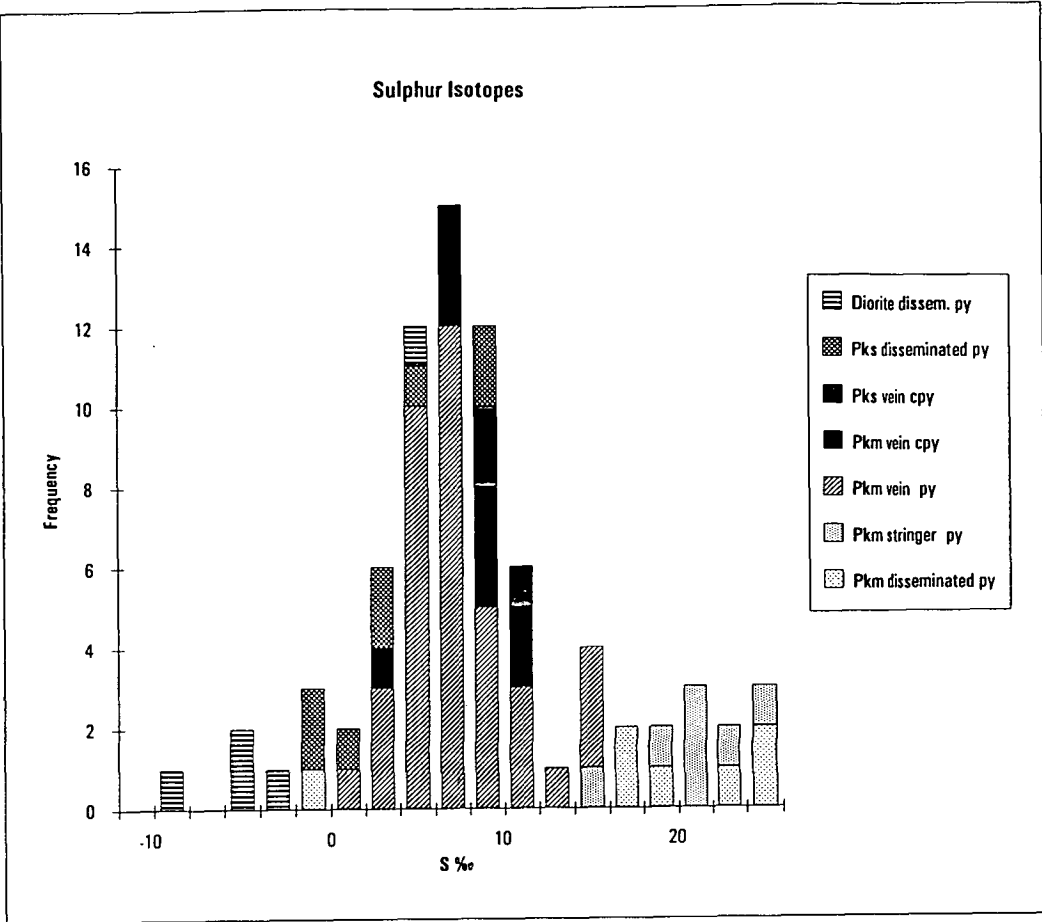


Figure 6.1 Histogram of all Greenmount sulphur isotope values.

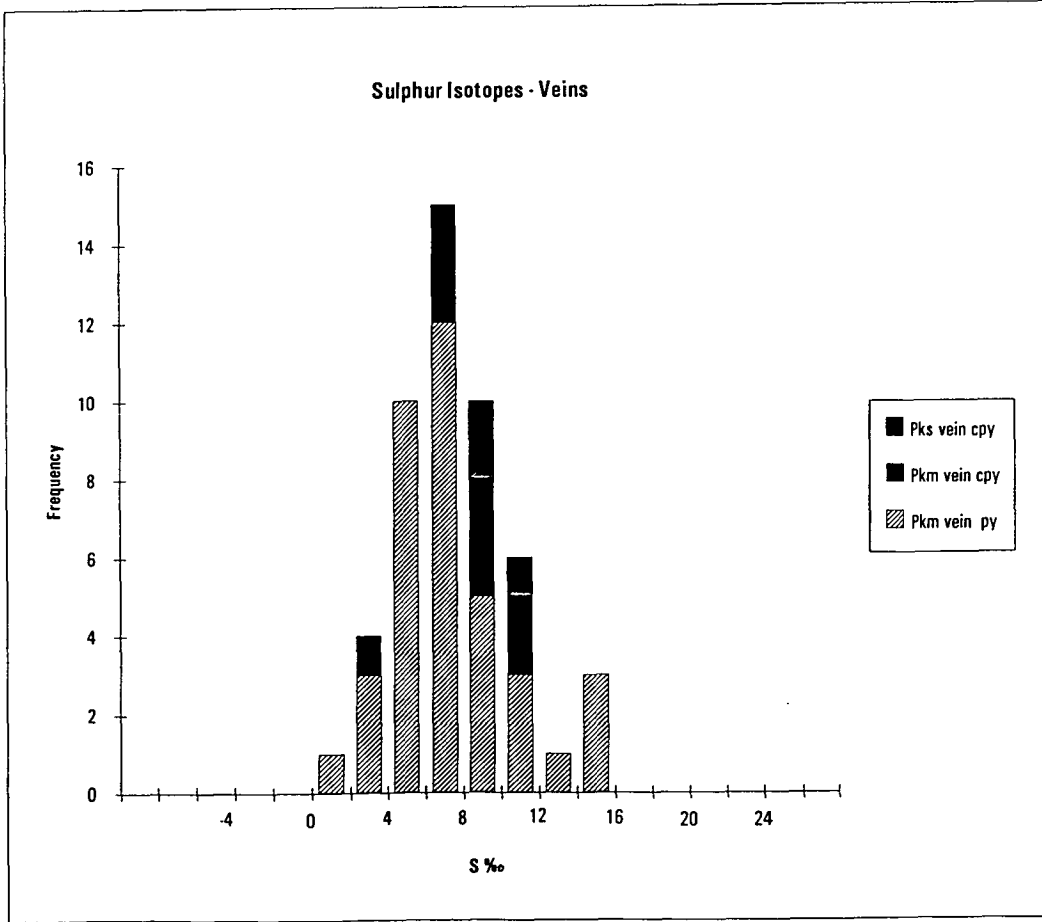


Figure 6.2 Histogram of sulphur isotope values from veins at Greenmount.

many sediments with high organic carbon content ($> 4\%$) have very low and tightly clustered $\delta^{34}\text{S}$ pyrite values. This is clearly not the case for the Marimo Slate at Greenmount. Anderson et al. (1987) reported diagenetic pyrite $\delta^{34}\text{S}$ values for organic rich shales of the Upper Devonian - Lower Carboniferous New Albany Shale Group (Illinois Basin) that increase with increasing organic carbon content. In a closed system in which sulphide is removed by either the loss of H_2S gas or the precipitation of sulphide minerals the isotopic fractionation of sulphur is controlled by Rayleigh fractionation (Ohmoto, 1986). In this case the isotopic composition of the sulphate also changes with decreasing sulphate concentration and the residual sulphate may have very high $\delta^{34}\text{S}$ values (eg. Richardson et al., 1988). The bacterial oxidation of sulphide to sulphate as documented by Hattori (1989) for the Archean, may have been an important process at Greenmount.

Disseminated pyrites in the diorite have a mean of -3.8‰ and range from -10.3‰ to 4.6‰ and hence form a distinct population (Figure 6.1, Table 6.2). They are isotopically lighter than the average mafic intrusive (Figure 6.3) and hence appear to have undergone isotopic fractionation. Many workers have documented non-zero $\delta^{34}\text{S}$ values for mafic igneous rocks eg the Muskox intrusion (0 to 17‰ : Sasaki, 1969), the Duluth Complex (0 to 17‰ : Ripley, 1981) and the Bushveld Complex (-9 to -6‰ : Liebenberg, 1970). Ohmoto (1986) questions whether this is due to mantle heterogeneity in S isotopic composition or to assimilation of crustal sulphur during emplacement of mafic magmas. Ohmoto (op. cit.) further argues that it is highly unlikely that magmas generated by partial melting of the mantle produced igneous rocks with $\delta^{34}\text{S}$ values outside the range of -3 to 3‰ without assimilation of crustal sulphur. Figure 6.4 shows sulphur isotope values from other hydrothermal systems.

This implies that the diorite was either not the source of sulphur, and the diorite underwent sulphidation from an external source during alteration, or that the diorite assimilated substantially isotopically depleted sulphur from another source. The values for the diorite at Greenmount are similar to those for chalcocite and pyrite veins from the Swan Prospect (-6.5 to -4.9‰) some 55 km to the south, as documented by Davidson and Dixon (1992). As for the Greenmount Diorite, the Swan calcilutite breccias also contain abundant magnetite and hence have a high oxidation state. Davidson and Dixon (op. cit.) suggest that this might explain the light isotopic character because sulphides in oxidised systems can display substantial negative fractionation from the $\delta^{34}\text{S}$ value of the fluid. Large (1975) and Phillips et al. (1986) suggest that these oxidised systems commonly show a wide isotopic range, which is seen for the Greenmount diorite. In the case for the narrow negative range for the SWAN prospect, Davidson and Dixon propose that there was a thermally-degraded organic sulphur source or dissolution of "open system" biogenic pyrite.

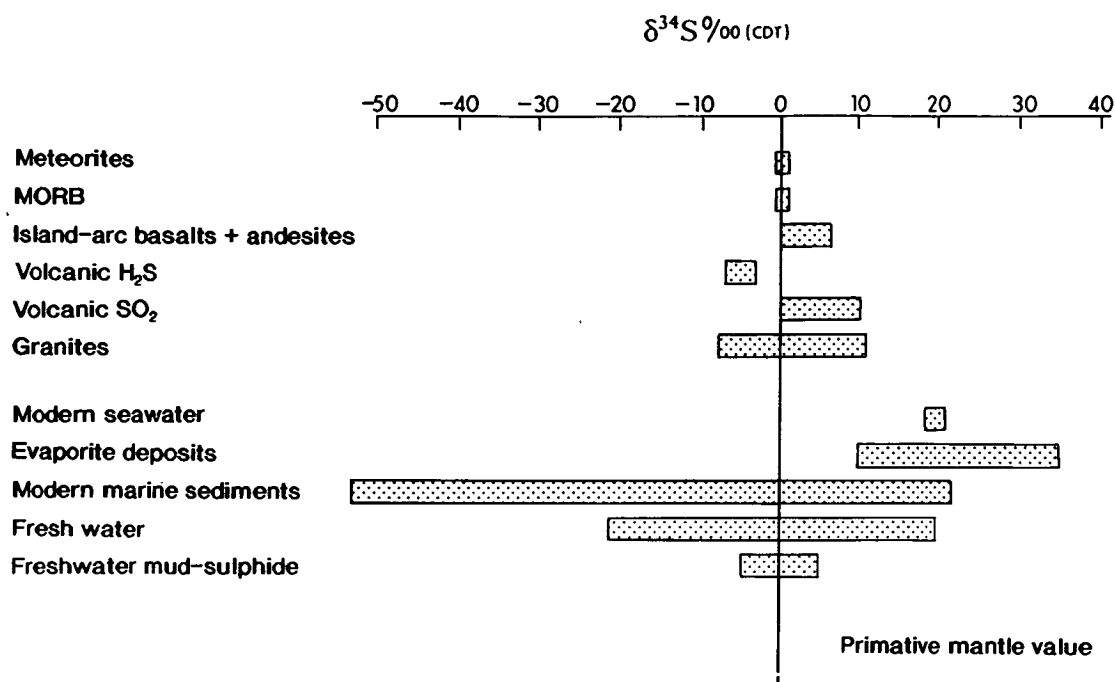


Figure 6.3

Natural sulphur isotope reservoirs. Data from: Sakai et al. 1982; Ueda and Sakai, 1984; Claypool et al. Kerridge et al. 1983; Chambers, 1982; Coleman, 1977; Chaussidon et al. 1989.

A similar diagram for hydrothermal sulphur-bearing minerals is given in Figure 6.4

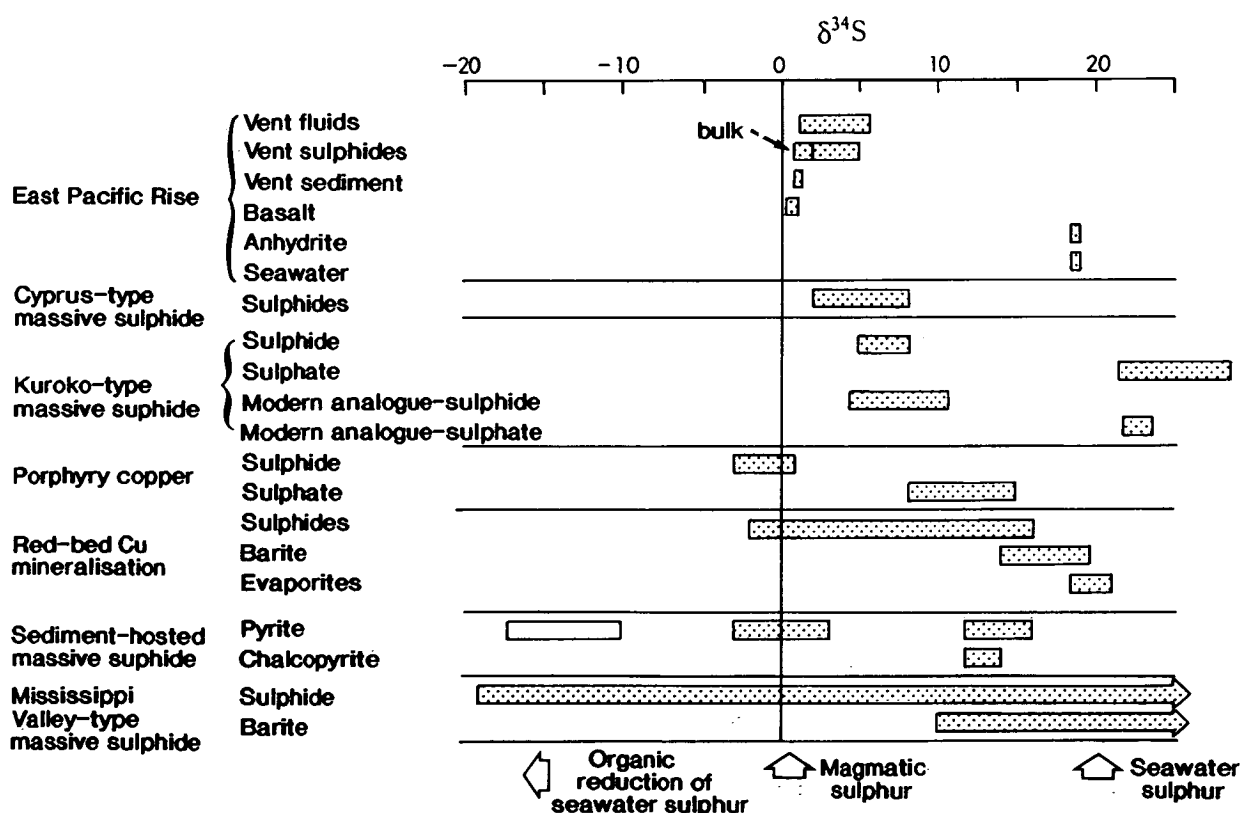


Figure 6.4

The $\delta^{34}\text{S}$ values for sulphur-bearing minerals in hydrothermal deposits. Data from Kerridge et al. (1988), Ohmoto and Rye (1979), Halbach et al. (1989), Naylor et al. (1989) and Eldridge et al. (1988)

The $\delta^{34}\text{S}$ ‰ values for pyrite disseminated in the Staveley Formation have a mean of 3.38‰ and range from -1.4 to 8.4‰, and hence form a distinct population (Table 6.2). They are substantially isotopically lighter than disseminated pyrite in the Marimo Slate (mean 19.09‰). These values do not approach the mean value for mid-Proterozoic seawater sulphate (17‰) which would be expected given the evaporitic nature of the Staveley Formation approximately 10 km to the north, as documented by Stewart (1991). K. Scott (pers. comm. 1995) found that at Mt Dore, deep within the footwall Staveley Formation, pyrite had markedly variable values of 0.7, 4.4 and 12.0‰ in three samples, which is similar to values obtained for the Staveley Formation at Greenmount.

The disseminated pyrite in the Staveley Formation at Greenmount is not interpreted to be diagenetic in origin, but is probably a product of hydrothermal activity related to the veining event. This interpretation explains the lack of overlap between Staveley Formation sulphides and the diagenetic Marimo Slate hosted pyrite as well as the closer similarity to vein hosted sulphides (Figure 6.1).

When compared to sulphur isotope values for other deposits in the Mt Isa Inlier, the vein stage sulphides at Greenmount are most similar in range and mean to those from the epigenetic copper ore and the stratiform Pb-Zn ore from the Mt Isa deposit of the Western Succession as well as the Dugald River pyrite and the Cu-Au Answer mines of the Eastern Succession (Figure 6.5). Mineralisation at the Answer mine comprises pyrite and chalcopyrite in quartz veins hosted by a shear zone within the Answer Slate member of the Mary Kathleen Group. Davidson and Dixon (1992), suggested that the small range in values (8.4 to 9.1‰) indicated a single sulphur source, with mineral precipitation under reduced conditions over a narrow temperature range. They suggested that the most likely source was local sediment sulphur extracted from the Answer Slate. At the Mount Isa mine, Andrew et al. (1989) formulated a model of distal leaching of evaporitic sulphate to produce a circulating oxidised brine, from which sulphate was subsequently reduced by interaction with the footwall basalt while simultaneously leaching copper, below the Mount Isa Pb-Zn ores. Copper ores then precipitated because of an interaction between this reduced fluid and the pre-existing Pb-Zn ore.

Table 6.3 and figure 6.6 show a progressive increase in $\delta^{34}\text{S}$ values away from the diorite and the Staveley Formation. This could imply that for the Staveley Formation, the veining and main mineralisation there was a mixed sulphur source between the isotopically depleted diorite and the isotopically heavy diagenetic pyrite. Alternatively the values from sulphides in the vicinity of the orebody were derived from a distal blind granitic intrusive (around 0‰) which

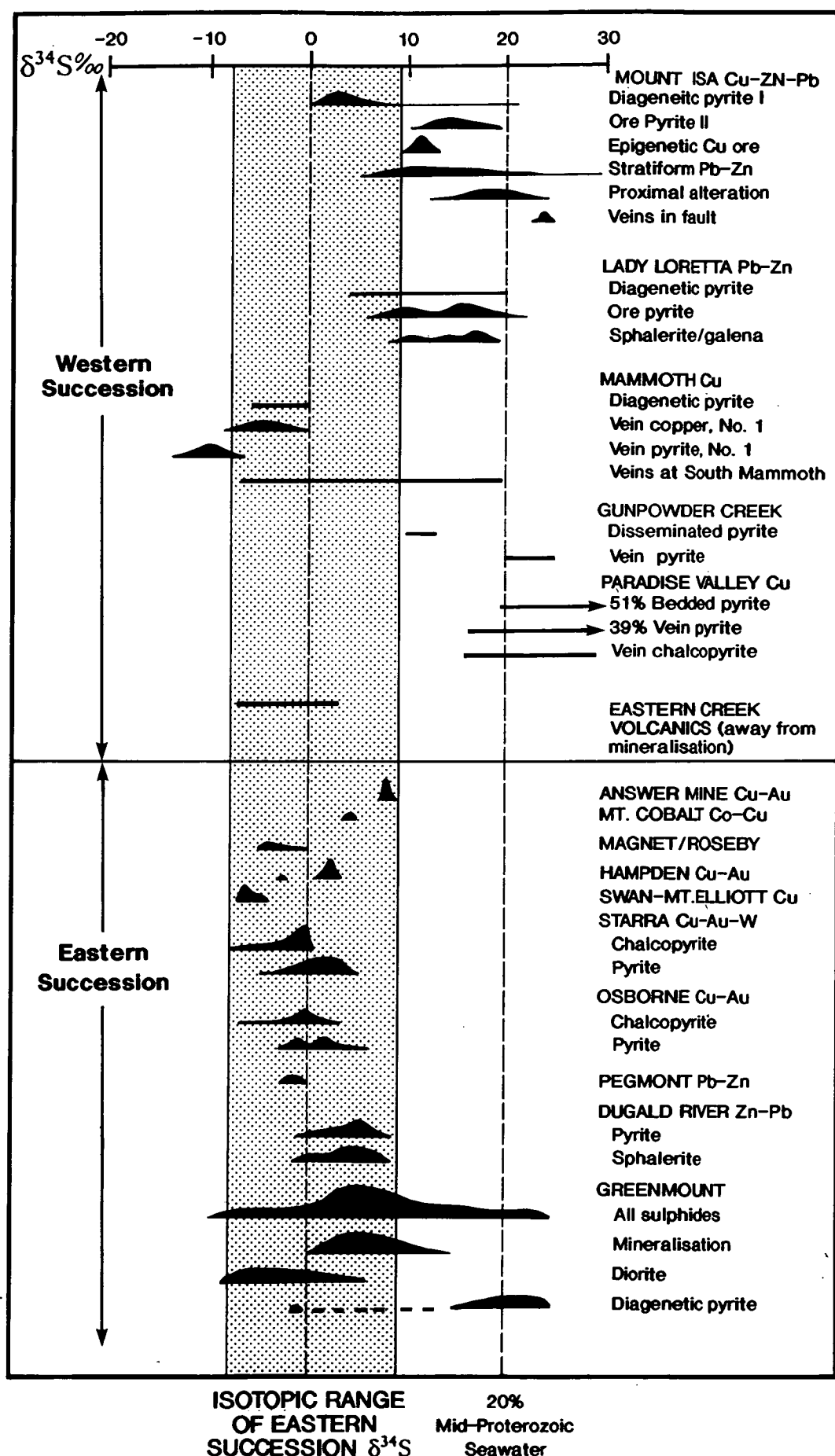


Figure 6.5

A comparison of the sulphur isotopic ranges of deposits within the Western Succession from previous studies, and those of the Eastern Succession from this study and Davidson and Dixon (1992). Most Eastern Succession deposits occur in the range -8 to 9‰ , whereas Western Succession deposits display a huge isotopic variation. Western Succession data was obtained from Scott et al. (1985), Carr and Smith (1977), Taylor and Scott (1976) and Andrew et al. (1989). Figure adapted from Davidson and Dixon (1992).

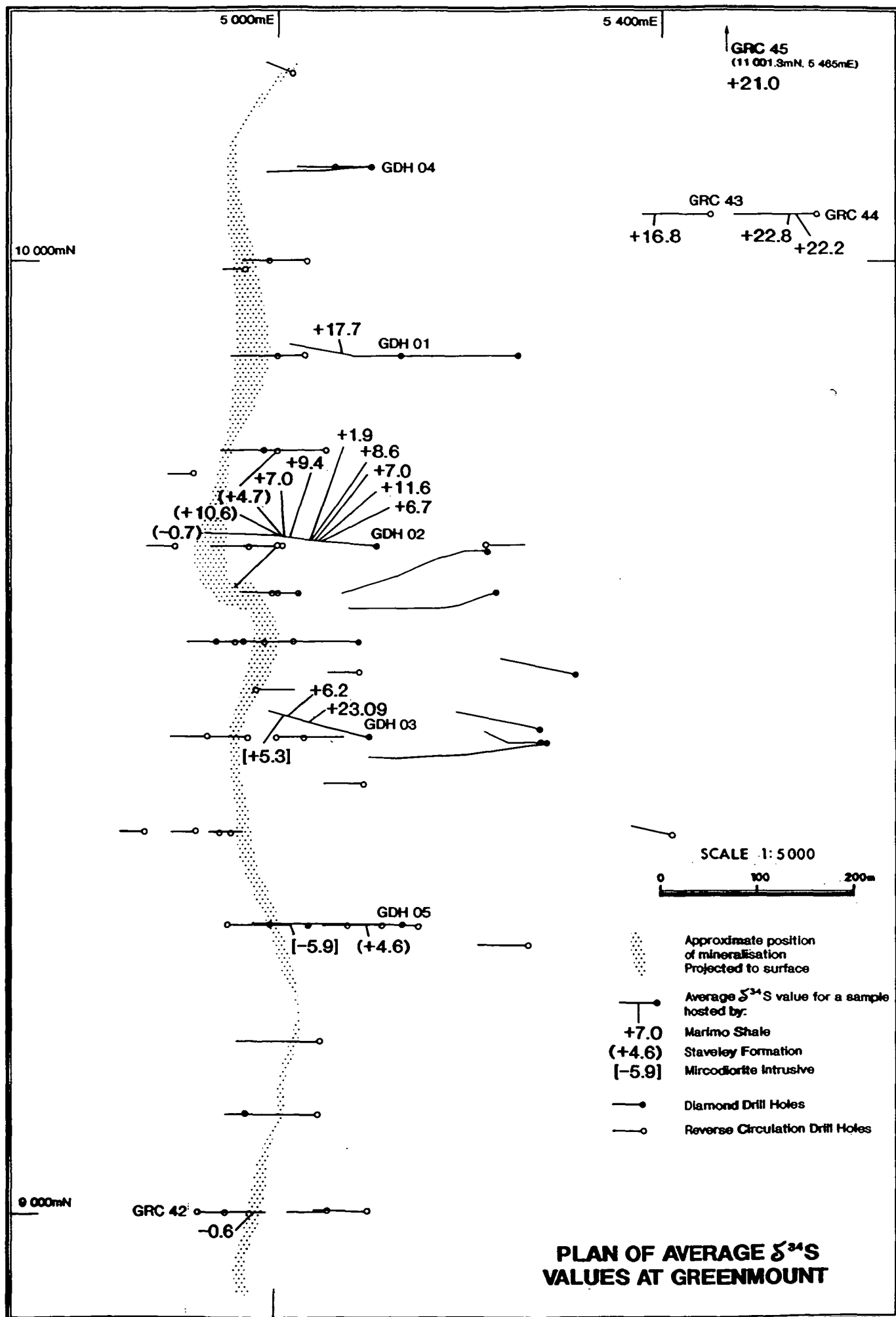


Figure 6.6

assimilated isotopically heavy sulphides from crustal sediments (eg. Marimo Slate or evaporites) to produce a relatively homogenised average value, of around 2 - 15‰.

TABLE 6.3 - Mean $\delta^{34}\text{S}\text{‰}$ for all sulphides as a function of rock type and distance from the Pkm - Pks lithostructural contact.

	all diorite hosted sulphides	all Pks hosted sulphides	all Pkm hosted - distance from Pks contact		
			0 - 50 m	50 - 100 m	> 100 m
mean	-3.82‰	4.82‰	7.31‰	9.81‰	21.09‰

TABLE 6.4 - $\delta^{34}\text{S}\text{‰}$ values for Marimo Slate hosted pyrites as a function of pyrite morphology.

Pyrite morphology	n =	mean
euheedral	14	3.04
euheedral and pitted (earlier)	3	22.2
fractured	3	22.1
fine grained aggregates (porphyroblastic/diagenetic)	3	17.67

Davidson and Dixon (1992) suggested that large isotopic variations absent in the Eastern Succession may suggest that primary evaporite sequences were halite dominated but sulphate poor, and/or contained only limited volumes of organic-sulphur-rich sediment and were therefore less likely hosts for giant stratiform Pb-Zn deposits, because of their paucity of sulphur. This study suggest that this may not be the case in the Marimo Basin. Stewart described evaporitic sulphate textures for the Staveley Formation at Just Found, and this study confirms the presence of organic rich shales with Proterozoic seawater derived sulphur which could possibly be of evaporitic origin, and therefore may deem the Marimo Basin prospective for giant stratiform Pb-Zn deposits.

Ch 6.2 *Carbon and Oxygen Isotopes*

An isotopic study was carried out to determine the origin and affinities of the carbonates in various vein types and hosted by various lithologies.

The main carbonate types are:

1. Sulphidic ferroan dolomite in veins hosted by the Staveley Formation;

2. Late barren carbonates;
3. Carbonate matrix to the brecciated Staveley Formation;
4. Carbonate veins in the diorite.

A plot of the analyses does not reveal any systematic trends (Figure 6.7).

6.2.1 Method

Calcite (25 mg) was drilled from vein samples and reacted with H_3PO_4 (phosphoric acid) at 25°C for a 24 hour period, using the method of McCrea (1950). The isotopic composition of C and O in the extracted CO_2 was obtained from a Micromass 602D stable-isotope mass spectrometer. Weights of matrix sample were obtained in proportion to the modal abundance of calcite. A review of previous analyses of the international standard Biggenden calcite gave a standard error for $\delta^{13}\text{C}$ of $\pm 0.06\text{‰}$, and $\pm 0.1\text{‰}$ for $\delta^{18}\text{O}$ for this machine; standards analysed with the samples were well within this precision. Oxygen and carbon isotope values are quoted with respect to SMOW and PDB respectively.

6.2.2 Other Carbon and Oxygen Isotope studies

The ranges of C-O isotopic data from relatively unmetamorphosed Proterozoic Northern Australian and Canadian Hypersaline dolomite sequences are shown in Table 6.5. The Staveley Formation estimate corroborates the Proterozoic marine $\delta^{18}\text{O}$ value was about 18‰ and Budai et al. (1987) showed that evaporitic dolomite is about 4‰ heavier than marine carbonate.

Source	Age	Stratigraphic Unit	Isotopic composition	
			$\delta^{13}\text{C}\text{‰}$ (PDB)	$\delta^{18}\text{O}\text{‰}$ (SMOW)
(1)	1700-1600 Ma	McArthur Group, McArthur Basin, N.T.	-2.0 to 0 av. -1.0	+17.2 - +25.6 av. +21.2
(2)			-4.9 - 0	+19.9 - +22.9
(3)			-2.2 - 0	+18.2 - +26.1
(4)	~1700 Ma	Reward Dolomite, McArthur Basin, N.T.	-3.0 - 0.2 av. -0.9	+19.8 - +24.7 av. +22.3
(5)	~1700 Ma	Lady Loretta Fm., N.W. Qld.	-2.4 - -1.6 av. -2.0	
(6)	~1600 Ma	Bungle Bungle Dolomite, W.A.	-1.0 - -0.25	+19.85 - +24.78
	~1800 Ma	Earaheedy Gp., Canada	-2.41 - +1.0	+17.90 - +23.39
	~2000 Ma	Pethei Gp., associated with BIF, Canada	+1.25 - +1.62	+15.7 - +18.35
	~2000 Ma	Wyloo Gp., associated with BIF, W. Australia	+0.35 - +0.99	+15.13 - +18.36
(7)	~1720 Ma	STAVELEY FM. ESTIMATE	-0.99 - -0.36	+18.78 - +23.50
	1780-1750 Ma	CORELLA FM. ESTIMATE	-0.32 - +1.54	+20.80 - +22.60

Table 6.5 Ranges of C-O isotopic data from relatively unmetamorphosed Proterozoic northern Australian and Canadian hypersaline dolomite sequences. (1) Smith and Croxford (1975); (2) Veizer and Hoefs (1976); (3) Rye and Williams (1981); (4) Walker et al. (1983); (5) Carr and Smith (1977); (6) Schidlowski et al. (1983); (7) Davidson (1989).

Davidson (1989) reported C and O isotope values from the Starra and Trough Tank (Osborne) deposits and Beardsmore (1992) conducted eight analyses on dolomite, ferroan dolomite and calcite from the Mt Dore deposit. Cannell (1994) analysed six carbonate samples from the Great Australia Mine.

Davidson (op. cit.) analysed five regional samples from dolomites and calcareous sandstones in the Staveley Formation from outside the potential circulation of Starra hydrothermal fluids and was able to calculate the premetamorphic isotopic character of the Staveley Formation. The results varied between $\delta^{13}\text{C} = -5.26$ to -0.38‰ and $\delta^{18}\text{O} = 14.50$ to $+22.42\text{‰}$, a spread suggesting that the original carbonate was heterogeneous or exchanged light oxygen and carbon during diagenesis (Figure 6.8). Davidson also extensively analysed carbonates from the hangingwall (Staveley Formation) matrix, hangingwall veins, hangingwall shears, ironstone matrix and veins as well as veins associated with dolerite at Starra. A summary of his data together with the range of values obtained at Greenmount by this study are presented in Figure 6.8. Davidson proposed a model involving the introduction of saline metamorphic fluids along the Starra Shear, which mixed with low - $\delta^{18}\text{O}$ meteoric water in fractures away from the shear. He demonstrated that veins showed little isotopic relationship to ore, and were generally barren, and that equilibration between vein-fluids and matrix had destroyed pre-existing carbonate isotopic signatures in the hangingwall metasediments. Davidson concluded that the distinctive negative character of the O-C trend in ironstone resulted from the mixing between leached components of $\delta^{18}\text{O}$ - rich limestone and organic carbon, with deposition of the carbonate during exhalation.

At Mt Dore, Beardsmore (1992) observed no apparent difference between ferroan and non-ferroan dolomite. He obtained a range of $\delta^{13}\text{C} = -5.5$ to -8.1‰ (median -6.25‰) and $\delta^{18}\text{O} = 10.1$ to 24.5‰ (median 17.85) from replacement style and vein carbonates. Beardsmore demonstrated that carbonate alteration equilibrated with a later, salt-undersaturated, CO_2 -poor, aqueous fluid believed to be the descendent of the salt-saturated aqueous immiscible phase from which quartz precipitated. He showed that the source of oxygen was that of a metamorphic or magmatic fluid, and that the calculated fluid $\delta^{13}\text{C}$ was slightly depleted in ^{13}C relative to PDB, suggesting a deep-seated or average crustal origin for the carbon.

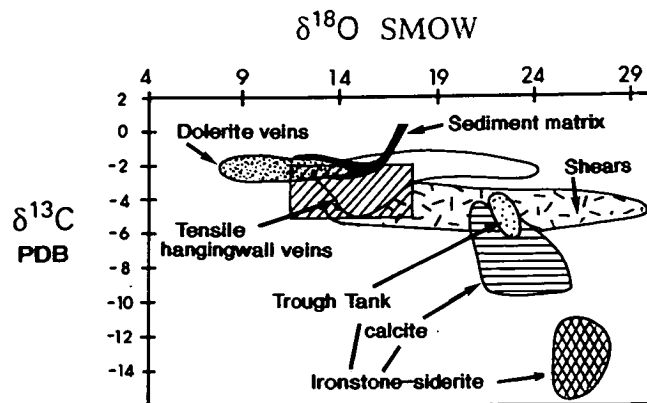


Figure 6.8a

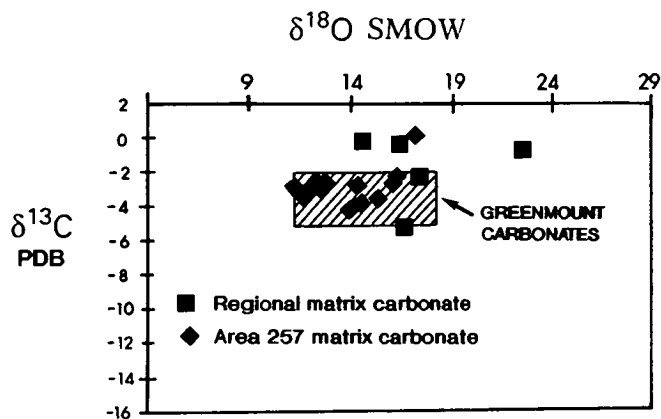


Figure 6.8b

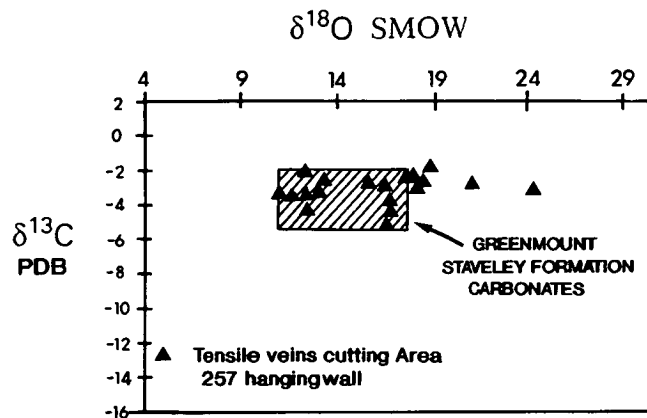


Figure 6.8c

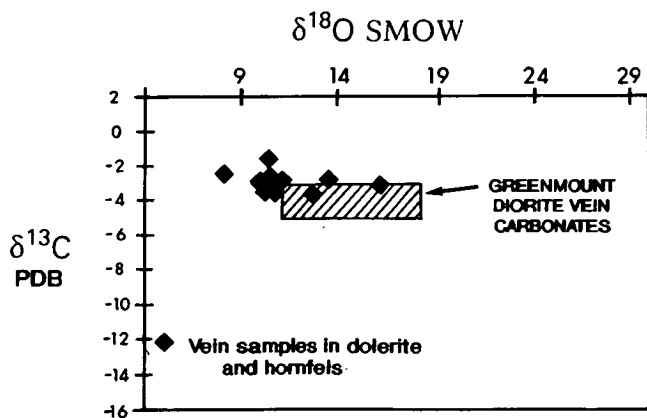


Figure 6.8d

Figures 6.8a-d Adopted from Davidson (1989).

Figure 6.8a Carbon - Oxygen isotope fields of all Starra sample groups.

6.8b Regional carbonate, compared to Area 257 matrix carbonate.

6.8c Veins in the Starra hangingwall metasediments.

6.8d Veins in hornfels and dolerite, generally >70m from the main Starra Shear.

Cannell (1994) obtained a range of $\delta^{13}\text{C} = -3.1$ to -6.1‰ and $\delta^{18}\text{O} = +10.0$ to $+18.4\text{‰}$ from carbonates at the Great Australia Mine. He suggested that the isotopic signature of quartz indicated a magmatic to transitional metamorphic source for the fluid, but could not interpret the isotopic sources of carbon due to poorly constrained temperature estimates.

6.2.3 Results

The results are summarised in Figure 6.7 and do not show a systematic trend. The individual analyses are shown but these have been divided into four groups (denoted by colour):

- (1) Staveley Formation Matrix carbonate;
- (2) Sulphide - carbonate veins in the Staveley Formation;
- (3) Late barren carbonate veins;
- (4) Carbonate veins in diorite.

These categories do not form clustered groups and it would appear that the source of C and O was not the diorite.

Some natural oxygen isotope reservoirs are shown in Figure 6.9, and the values from Greenmount are within the ranges for metamorphic rocks or detrital sediments, however a pre-metamorphic Staveley Formation precursor which was subsequently fractionated, is considered possible.

Compared to Mt Dore, all Greenmount carbonate analyses have similar $\delta^{18}\text{O}$ values but are isotopically depleted in carbon. Hoefs (1980) and Faure (1986) cite the primary sources of carbon in hydrothermal fluids as marine carbonates ($\delta^{13}\text{C}_{\text{PBD}} \sim 0\text{‰}$), deep seated or average crustal sources ($\delta^{13}\text{C}_{\text{PBD}} \sim -7\text{‰}$), and biogenic organic compounds ($\delta^{13}\text{C}_{\text{PBD}} \sim -25\text{‰}$) and some of these are summarised in Figure 6.10. Rye and Ohmoto (1974) showed that the isotopic composition of CO_2 in solution was also a function of pH, $f\text{O}_2$, temperature, ionic strength of fluid and total concentration of carbon so that the variation of these factors may produce CO_2 with a $\delta^{13}\text{C}$ significantly different from that of the bulk fluid.

Thus the possible sources of carbon are either deep seated, from the Marimo Slate or from isotopically fractionated (depleted) pre-metamorphic Staveley Formation. There are no data

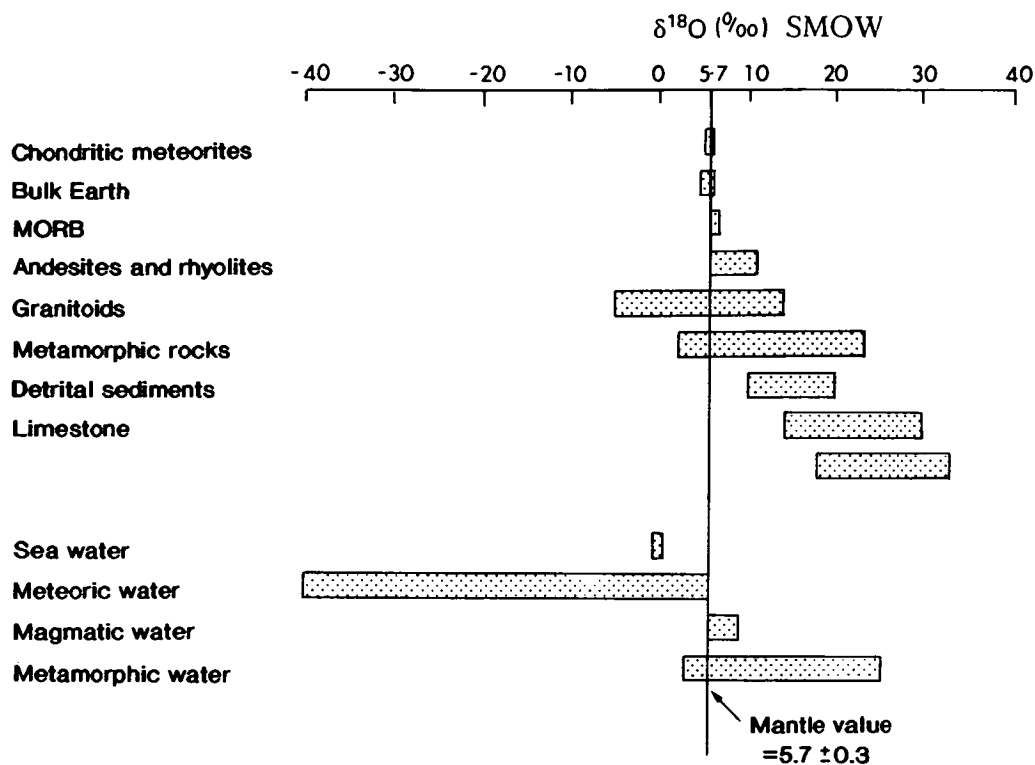


FIGURE 6.9

Natural oxygen isotope reservoirs. Data from: Taylor (1974), Onuma et al. (1972), Sheppard (1977), Graham and Harmon (1983) and Hoefs (1987).

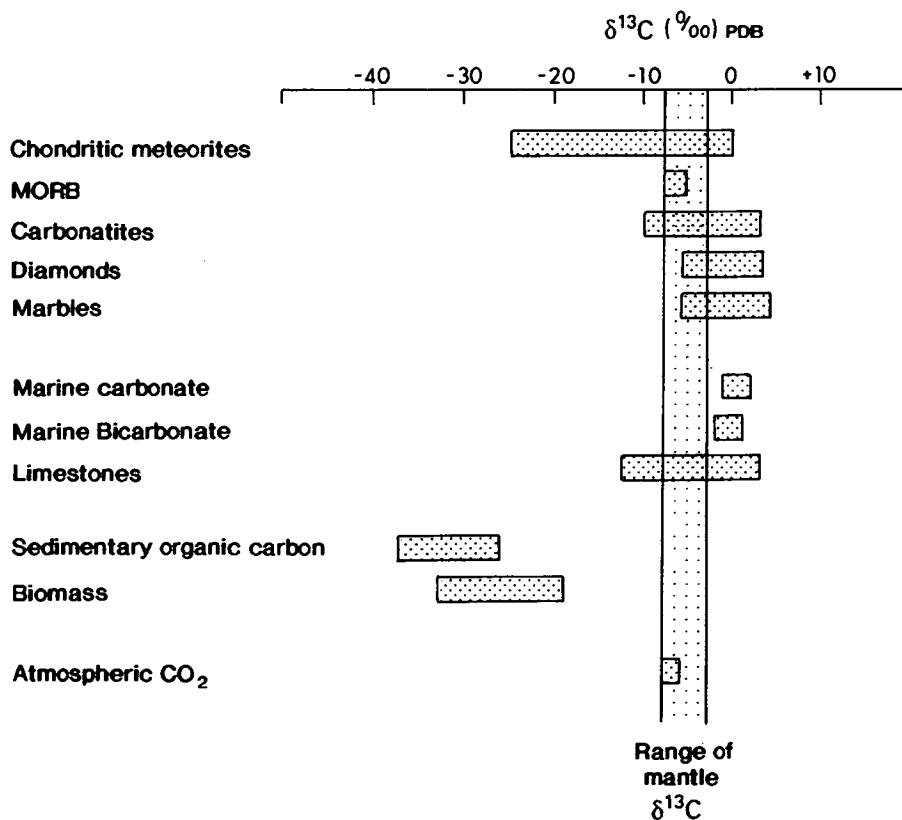


FIGURE 6.10

Natural $\delta^{13}\text{C}$ reservoirs. The ranges of $\delta^{13}\text{C}$ values in natural, carbon-bearing samples. Data from Kerridge (1985), Exley et al. (1986), Field and Fifarek (1986), Hoefs (1987) and Schidlowski (1987).

on $\delta^{13}\text{C}$ values from the Marimo Slate but a line of best fit through the Greenmount data indicates that the Staveley Formation may be a carbon and oxygen source. Compared to values from Starra, the Greenmount analyses plot mainly within the fields for tensile hangingwall veins and sediment matrix (from the Staveley Formation; Figure 6.8).

CHAPTER 7 Fluid Inclusion Study

7.0 Introduction

Primary and pseudosecondary types of fluid inclusions can provide a means of estimating the temperature and composition of fluids at the time of mineral deposition as long as the inclusions have not undergone leakage or stretching since their time of formation. At Greenmount, much of the mineralisation continued after the deposition of vein gangue minerals and hence this study also examines secondary inclusions which may or may not be related to post veining mineralisation.

A total of 18 doubly polished thin sections were prepared and examined for this study. Only twelve of these yielded workable inclusions. No workable inclusions were found from the early pervasive alteration and all of the data presented herein is from veins which cut both pervasively altered and relatively unaltered lithologies.

Samples were collected from core holes GDH-01 (36 analyses), GDH-02 (32 analyses), GDH-03 (25 analyses) and GDH-05 (33 analyses) and thus there is very little geographic bias. Workable inclusions were common in quartz and carbonate, less common in albite and absent in all other minerals.

7.1 Method of Study

Prior to heating and freezing experiments, the doubly polished plates were examined in detail under the petrographic microscope for several days. The inclusions were located under low to medium magnification to record their distribution and inclusion type, and to determine their spatial and temporal relationships. Phase relations were studied and photographed under high magnification (40x).

A USGS heating/freezing stage was used and the stage was calibrated by means of synthetic fluid inclusion sets. The temperature uncertainty was believed to be $\pm 0.2^{\circ}\text{C}$. Freezing experiments were done first to minimize stretching, leakage and decrepitation. The super cooling rate varied from 10-20 $^{\circ}\text{C}$ /minute. During heating runs a heating rate of about 5 $^{\circ}\text{C}$ /minute was maintained until the vapour bubble nearly homogenised into the liquid, at

which point the heating rate was reduced to about 2°C/minute. The heating and freezing experiments were done at least twice (and up to four times) and reproducibility is believed to be better than $\pm 2.3^{\circ}\text{C}$. The results which are reported herein are the average of multiple heating and freezing runs. Inclusions which showed evidence of necking or leakage were rejected. A general tendency for slightly higher homogenisation temperatures during repeat runs was observed, which indicates that some stretching had occurred.

7.2 *Classification of Inclusion Types*

Fluid inclusions were classified based on phases observable in the inclusions at room temperature, as suggested by Shepherd et al. (1985). The paragenesis is determined by interpretation of individual inclusions as primary, pseudosecondary or secondary, following the criteria of Roedder (1984). The primary and pseudosecondary inclusions used in this study are only those which are greater than at least several primary inclusion diameters from the nearest obvious secondary inclusion planes and which show no other evidence of modification by secondary fluids. Table 7.1 summarizes the characteristics of the different classes. The complete thermometric data is presented in Table 7.3.

7.3 *Inclusion Types*

7.3.1 *Type I liquid - vapour inclusions*

These inclusions are typically 6-8 μm in size, often have good negative shapes and frequently display vapour bubble motion (B/M) approaching total homogenisation (Plates 7.6 and 7.8). Although no daughter salts are present, final melting temperatures of ice indicate variable but typically low salinities.

7.3.2 *Type II liquid - CO₂ vapour inclusions*

These inclusions are similar to Type I inclusions but they have a higher degree of fill and the vapour phase is dominated by CO₂ which has a darker and thicker wall (Plates 7.1, 7.3 and 7.10). They also frequently display vapour bubble motion approaching total homogenisation (T_L) and final ice melting temperatures indicate variable low to moderately high salinities. Some clathrates may have formed, but these were difficult to detect.

Plate 7.1 (A) Primary Type II fluid inclusions in carbonate.

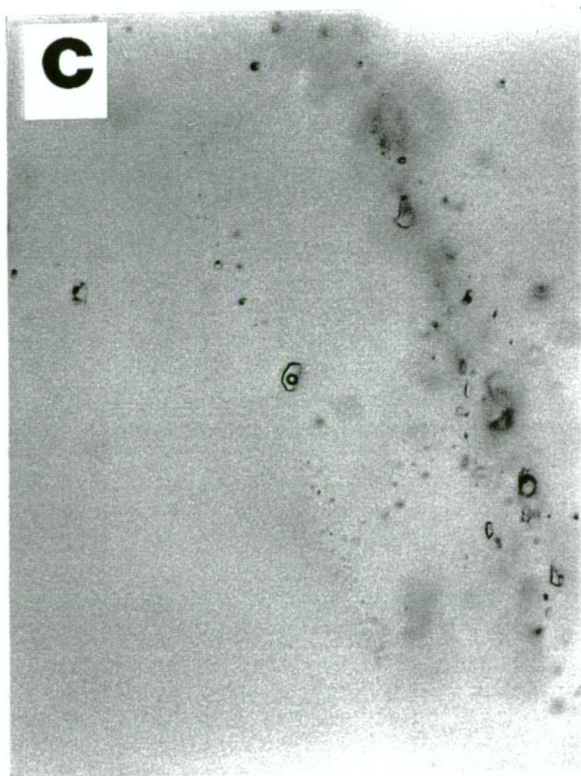
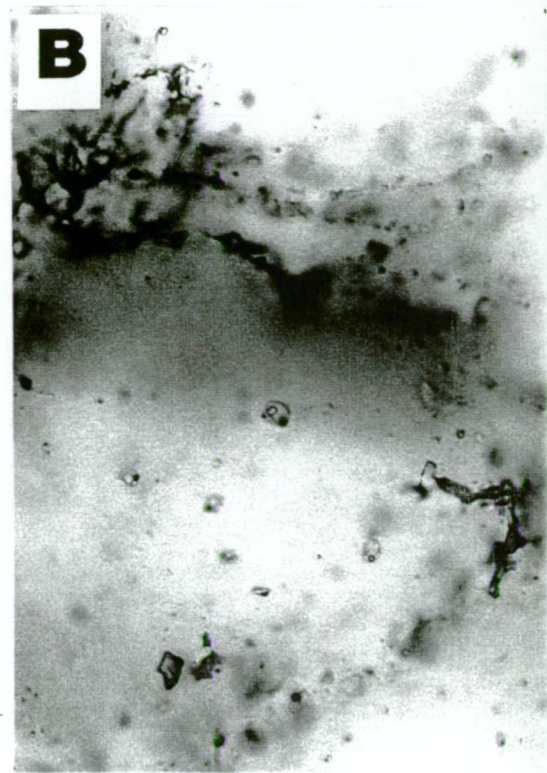
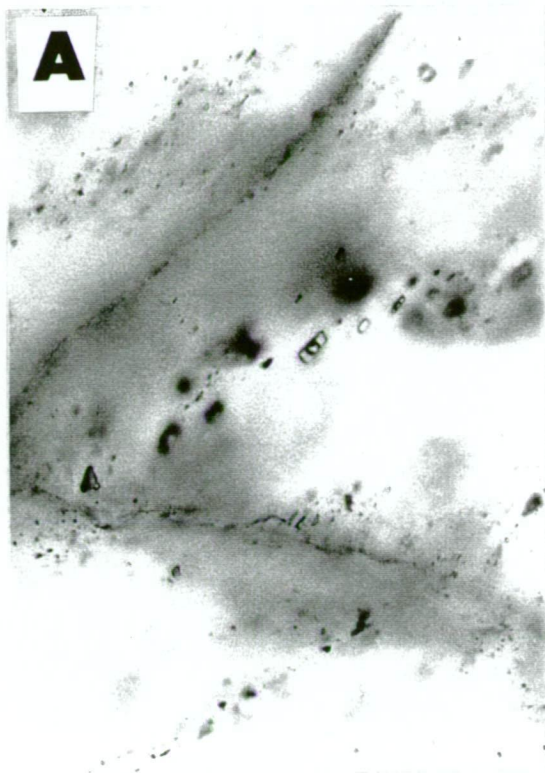
Plate 7.2 (B) Coexisting Type III A (centre and lower right field of view) and Type III B (centre left field of view) fluid inclusions in quartz.

Plate 7.3 (C) Coexisting Type II (centre) and Type III A (left) inclusions in carbonate.

**Plate 7.4 (D) Type III C liquid - CO₂ vapour - multisolid inclusion in quartz.
This particular inclusion included a hematite solid.**

Plate 7.5 (E) Halite - hydrocarbon ? inclusion in centre of field of view with smaller Type II inclusion above it.

*** *Refer to Table 7.1 for fluid inclusion type characteristics.***



0 50
Microns

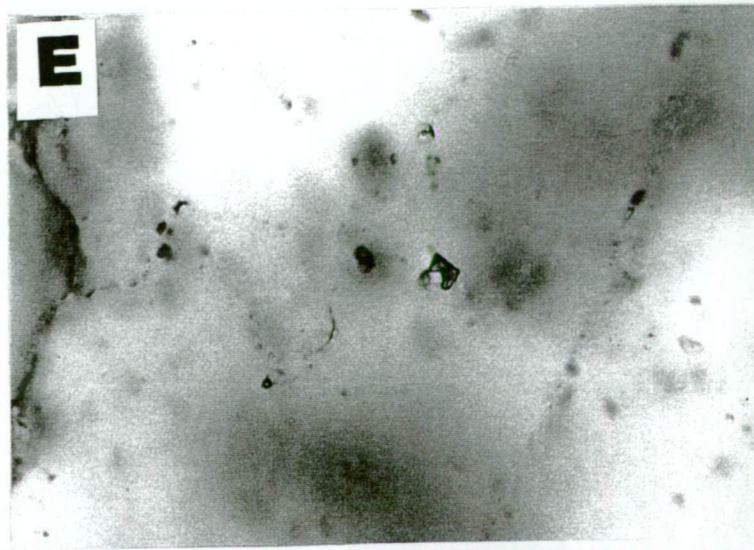


Plate 7.6 (A) Large primary Type I liquid - vapour inclusions.

Plate 7.7 (B) Secondary Type IV liquid - vapour inclusions in carbonate.

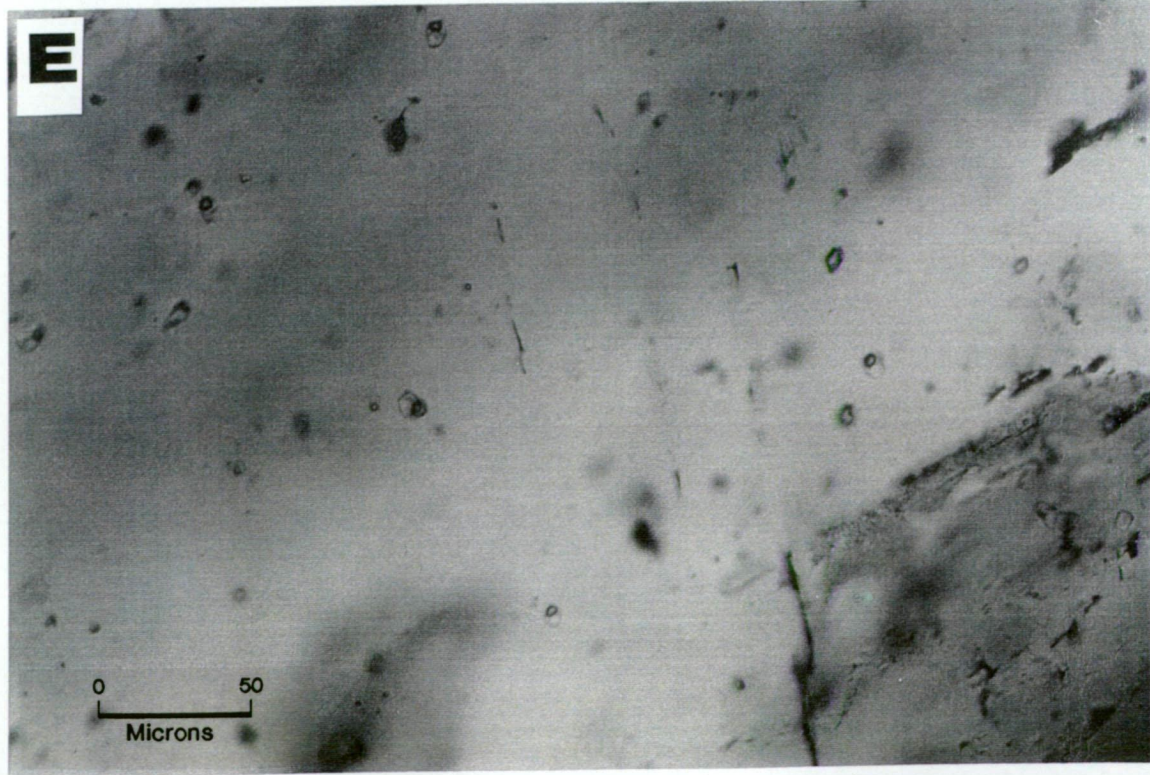
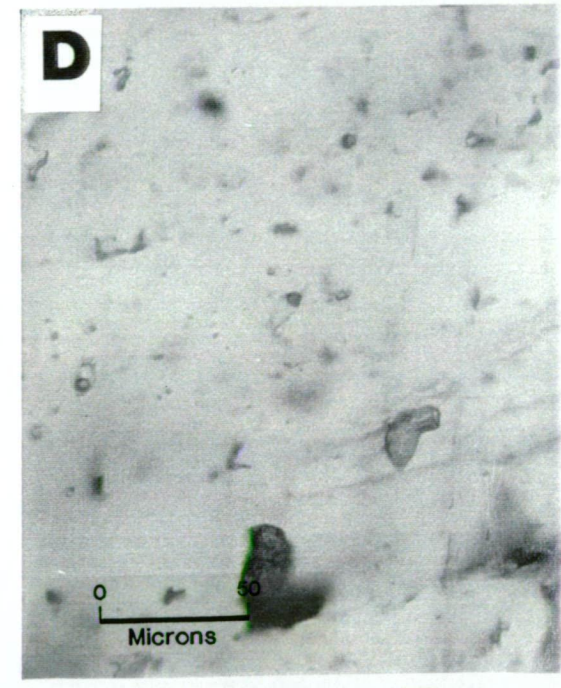
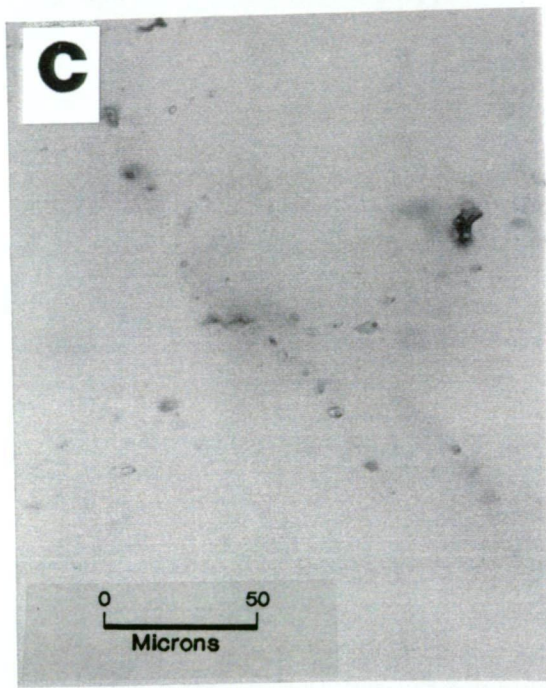
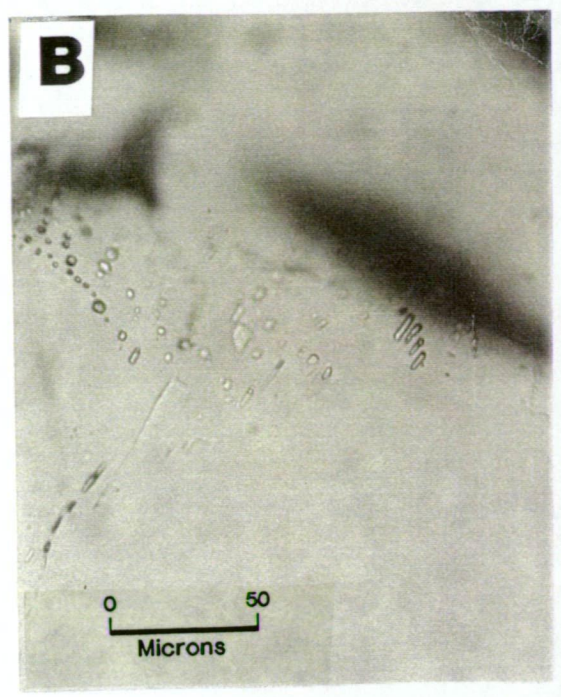
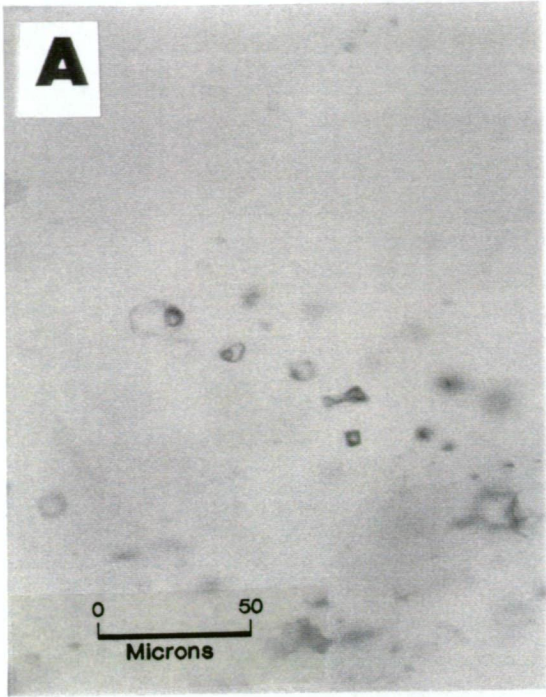
Plate 7.8 (C) Pseudosecondary Type I inclusions in carbonate.

**Plate 7.9 (D) Type III (c) liquid - CO₂ vapour - unidentified solid - halite
(halite almost invisible in this photograph) in quartz.**

The inclusion is in the middle-right of the field of view.

Plate 7.10 (E) Coexisting Type II and Type III A inclusions in quartz.

*** *Refer to Table 7.1 for inclusion type characteristics.***



7.3.3 Type IIIA liquid - vapour - solid inclusions

The solid inclusion is always halite and hence they are saturated with respect to halite (Plates 7.2, 7.3 and 7.10). The halite is typically large, cubic, colourless and isotropic. It commonly occupies about half of the inclusion. Heating experiments show that vapour always homogenises to liquid before halite, and hence at time of trapping, the fluid may have been undersaturated with respect to vapour.

TABLE 7.1 Summary of the main characteristics of different populations of fluid inclusions in various minerals from Greenmount.

Inclusion Type	Essential Phases	Typical Degree of Fill	Generation	Typical Size	Style of Occurrence
Type I	liquid + vapour	85-95	primary - pseudosecondary	6-8 μm (<12 μm)	isolated; discontinuous irregular planes; irregular aggregates.
Type II	liquid + CO ₂ vapour	75-85	primary - pseudosecondary	7-9 μm (<12 μm)	isolated; discontinuous irregular planes; irregular aggregates.
Type IIIA	liquid - vapour - I solid	80-95	primary	7-9 μm (<10 μm)	isolated; irregular aggregates.
Type IIIB	liquid - vapour - multisolid (up to 4 daughter salts)	90-95	primary	9-11 μm (<14 μm)	isolated; irregular aggregates.
Type IIIC	liquid - CO ₂ vapour - multisolid	80-85	primary	8-12 μm (<13 μm)	isolated; irregular aggregates.
Type IV	liquid + vapour	90-97	secondary	5-7 μm (<9 μm)	As swarms in densely packed planes. Often exhibit bubble motion (B/M).
Type V	solid only	-	-	5-7 μm	isolated.

7.3.4 Type IIIB liquid - vapour - multisolid inclusions

These hypersaline inclusions are similar to Type IIIA inclusions except they contain more than one daughter salt, and are slightly larger but contain a lower degree of fill (Plate 7.2). Up to four daughter salts are present but only halite is consistently positively identified, and present in every inclusion. Carbonate, hematite and possibly iron chloride have occasionally been

positively identified and the optical properties of these and other possible daughter phases are described in Table 7.2.

It should be noted that hematite, although uncommon, is not rare, and may be a foreign inclusion or “accidental”, transported as a suspended phase in the fluid. Alternatively, these hematite flakes could represent irreversible precipitation through oxidation of Fe^{2+} in the fluid by diffusion of H_2 from the inclusion, as suggested by Roedder and Skinner (1968). Hematite was however being precipitated in association with microcline veining as part of the alteration paragenesis possibly at the time of fluid inclusion formation, indicating that the fluid was relatively oxidised (above the hematite - magnetite buffer) and hence H_2 diffusion may not be required. The CaCl_2 - bearing fluid (inferred from cooling experiments) is likely to have been very viscous (Potter and Clynne, 1978) and capable of entraining solid phases. Two Type IIIB samples were submitted to the Australian Geological Survey Organisation in Canberra for RAMAN analyses. Spectra from one of these samples containing vapour, halite and a 3 μm rectangular solid in a 12 μm inclusion indicated that the rectangular solid was calcite. The other sample contained a 12 μm inclusion which contained vapour, calcite and halite. Spectra from this inclusion revealed that the vapour in this instance was methane (Appendix 5).

TABLE 7.2 Optical properties of the identified daughter phases in Type IIIA,B and C multiphase solid inclusions.

Name	Composition	Habit	Relief	Colour	Birefringence
Halite	NaCl	cubic	high	colourless	isotropic
Carbonate (probably calcite)	CaCO_3 or $\text{CaMgFe}(\text{CO}_3)_2$	rhombohedral or cubic	medium	colourless to pale green	high
Hematite	Fe_2O_3	platy	medium	red-orange	-
Sylvite	KCl	cubic	low	colourless	isotropic
Iron Chloride	$\text{FeCl}_2 \cdot 2\text{H}_2\text{O}$	tabular (often hexagonal)	medium	pale yellow- green	moderate
Antarcticite?	$\text{CaCl}_2 \cdot 6\text{H}_2\text{O}$	acicular	medium	colourless	moderate
Anhydrite?	Ca SO_3	needle-like	medium	colourless	high

SAMPLE NO	HOST ROCK	VEIN MINERALOGY & VEIN TYPE	MINERAL STUDIED	SIZE	INCLUSION SHAPE	TYPE	Degree Of Fill %	Th-l °C	Th H-s °C	Te °C	Tm °C	SALINITY NaCl Equiv wt%	REMARKS
85022 Hole GDH-02 at 142.0 m	Carbonaceous slate (Marimo Shale)	Mic-(phl-py-cpy-qtz) veined by late cpy	Ca	2x5 µm		IV	95	116.2					} Secondary inclusion swarms in very late } clear calcite. } Could not obtain primary workable } inclusions.
			Ca	2x5 µm		IV	95	115.8					
			Ca	2x5 µm		IV	95	116.8					
			Ca	2x5 µm		IV	95	116.7					
85011 Hole GDH - 01 at 156.5 m	Carbonaceous slate (Marimo Shale)	Mic-qtz-phl-ch-py-ca	Qtz	7 µm		III C	90	>508	233.1				NaCl - KCl solutes in system Opaque hematite inclusion; B/M B/M from 183 °C
			Qtz	5x8 µm		I	80			-23.1	-9.4	13.29	
			Qtz	8 µm		I	85	237.1			-14.3	18.04	
			Qtz	7x10 µm		III B	95		197.5			>23.3	
			Qtz	7x9 µm		IV	95	198			-8.4	12.16	
			Qtz	5x9 µm		I	97	238.9					
			Ca	9x11 µm		III B	92	445.5	353			50.51	
			Ca	8x12 µm		III B	90	410.6					
			Ca	9x13 µm		III C	85	>500	229.1			>56.37	
85004 Hole GDH-01 at 124.5 m	Black shale (Marimo Shale)	qtz-ab-(mic-phlog-rut-ap-py-ca)	Ca	4x6 µm		III A	97		346.2		-21.1	23.11	Heated to 346 °C but halite still not homogenised. Other inclusions begin decrepitating from 320 °C; B/M B/M
			Qtz	4x6 µm		I	85	275.3					
			Qtz	4 µm		I	85	273.4					
			Ca	3x6 µm		III A	85		394.9				
			Ca	4x7 µm		II	85	344.7					
85002 Hole GDH-01 at 123.9 m	Sericitised slate (Marimo Shale)	Mic-Ab-phl-qtz-py-cpy Now mostly ser.	Qtz	9 µm		II	92	243.3		-31.8	-0.6	1.05	MgCl ₂ in system. Clathrate formed? Bubble expands on freezing ~ -75°C. Thick inclusion walls Salt did not homogenise. Heated to 350 °C.
			Qtz	4x6 µm		II	80	327.8					
			Ab	9x14 µm		III B	90	>350	224.4			>41.77	
			Qtz	5x7 µm		II	70	289.2					
85031 GDH-03 at 131.8 m	Albitised shale (Marimo Shale)	Mic-Ab-cpy-ca (Late ser-cpy)	Ca	8x8 µm		I	95	267.8					Wallrock Qtz alteration
			Ca	5 µm		I	95	224.8					
			Qtz	6x10 µm		I	90	334					
			Ca	4 µm		I	85	340.9					
			Ca	5 µm		IV	95	160.2					
			Ca	3x5 µm		I	80	329.6					
85007Ab	Tourmalinized Albitised sericitic slate (Marimo Shale)	Ab-qtz-ap-rut-phlog and later Mic-qtz-phlog-py-cpy											No workable inclusions
													No workable inclusions

KEY: chl=chlorite; Ca=carbonate; Qtz=quartz; bi=biotite; mt=magnetite; ap=apatite; phlog=phlogopite; mi=microcline; ab=albite; ser=sericite; tour=tourmaline; Rut=rutile; py=pyrite; cpy=chalcopyrite; B/M=Vapour bubble motion.

TABLE 7.3 Details of fluid inclusion heating and freezing experiments (continues)

SAMPLE NO	HOST ROCK	VEIN MINERALOGY & VEIN TYPE	MINERAL STUDIED	SIZE	INCLUSION SHAPE	TYPE	Degree Of Fill %	Th-I °C	Th I+s °C	Te °C	Tm °C	SALINITY NaCl Equiv wt%	REMARKS		
85018	Argillized Pelite (Marimo Shale)	Mic-phlog-ab-cpy-rutile-py-qtz MATRIX (Marimo Shale)											No workable inclusions		
85016B	Feldspathised Pelite (Marimo Shale)												No workable inclusions		
85008Ab GDH-01 at 130.3 m	Feldspathised sericitic and phlogopitic slate (Marimo Shale)	Ab-qtz-Mic-phlog-rut-py-ca	Ca	6x12 µm		IIIC	90	160.1					>23.3	B/M	
			Ca	6x8 µm		IIIA	95	180					>23.3		
			Qtz	9x10 µm		IIIA	90	355.5							
			Qtz	6x12 µm		II	70	335.2							
			Qtz	3x8 µm		II	80	297.8							
			Qtz	4x10 µm		I	90	357.9			-8.8	12.62			
			Qtz	7x8 µm		I	85	352.7							
			Qtz	4x8 µm		IIIA	95	408.5	293.2			46.90	Vapour homogenises at 293.2°C		
			Qtz	4x8 µm		IIIA	100	398.6				45.98	Salt + Liquid only ie. no vapour bubble		
Qtz	5x10 µm		IIIA	80	486.8	458.9				54.89	Vapour homogenises at 458.9°C				
85052 Hole GDH-05 at 92.7 m	Py-ca-ab Pelite (Staveley Formation)	Mic-ca-qtz-py -musc which itself is veined by late Ca-py	Ca	4x6 µm		IIIA	80	>440	330.3				49.96	Heated up to 440 °C	
			Qtz	8 µm		I	90	284.3			-47.7	-1.5	2.57	A metastable salt formed at -21.3 °C and -20.1°C.	
			Qtz	6x10 µm		IIIC	80	>335			-60.9		>23.3	Brown colour ice. Bubble expands slightly on freezing ~ -80°C CaCl2 NaCl MgCl2	
			Qtz	5x8 µm		II	75	>336			-55.4	-16.3	19.68	Other inclusions (2) decrepitated at + 335 °C . Homogenisation Temp not reached.	
			Qtz	7 µm		IV	75	184.3						Decrepitated instantly at 335.7 °C - High V pressure	
			Qtz	4x9 µm		IIIC	80	>359					>23.3	NaCl - CaCl2 in system. Brown colour ice.	
			Qtz	4x7 µm		II	75	385.6						One salt dissolves at 340.1 °C. Other inclusions begin to decrepitate from 342 °C.	
			Qtz	5 µm		II	75	438.9						B/M approaching Th	
85051 Hole GDH-05 at 90.3 m	Carbonated & Feldspathised Pelite (Staveley Fm)	Mic-(Ca-Ab-ru) which itself is veined by Ca-qtz-(mic-Ab)-py. Py dominantly as vein selvage. All inclusions measured from late vein.	Ca	7 µm		I	92	190.2				-2.3	3.87	B/M	
			Ca	8x10 µm		I	95	169.9						B/M	
			Qtz	6x10 µm		I	90	271			-50.2	-1.8	3.06	CaCl2 - KCl solutes in system	
			Qtz	6 µm		I	92	220.2						B/M	
			Qtz	5x12 µm		I	90	254.4						B/M	
			Qtz	4x6 µm		I	90	294.1						B/M	
			Qtz	5x8 µm		IIIC	80		389.3			>23.3	Halite inclusion?		
			Qtz	6x8 µm		II	80	320.2			-1.5	2.57			
			Ab	3x7 µm		II	90	280.2				>23.3			
			Ca	4x8 µm		II	80	239.6							
			Ab	12 µm		IIIC	80	>420	377.5			>47.99	} Heated up to 420 °C. Good 1° inclusions.		
			Ab	5x7 µm		IIIC	85	>420	378.4			>47.99	} Salt still not dissolved		

TABLE 7.3 Details of fluid inclusion heating and freezing experiments (continues)

SAMPLE NO	HOST ROCK	VEIN MINERALOGY & VEIN TYPE	MINERAL STUDIED	SIZE	INCLUSION SHAPE	TYPE	Degree Of Fill %	Th-I °C	Th I+s °C	Te °C	Tm °C	SALINITY NaCl Equiv wt%	REMARKS
85056	Feldspathised Calci lutite (Staveley Formation)	Ca-Ab-mic-bi-qtz-py-mt	Ca	4x7 µm		IV	95	154.7		-39.7	-0.3	0.53	Vapour bubble disappears at - 39.7 °C. Mg Cl ₂ - KCl Checked by multiple runs.
			Ca	5 µm		IV	95	177.4					
				3x4 µm		IV	95	169.5					
				6 µm		IV	95	116.7					
			Ca	8x10 µm		II	85	209.6					Very late, clear calcite. Appears different compared to other calcite crystals. Could be zeolite?
			Ca	7 µm		II	85	240.2					Good primary inclusion
			Ca	3x7 µm		II	80	355.6		-30.2	-1.2	2.07	Te indicates Mg Cl ₂ in system; B/M
			Ca	3x5 µm		II	80	335.3		-31.6	-1.5	2.57	Te indicates Mg Cl ₂ in system
			Ca	4x6 µm		IV	97	167.2			-1.4	2.41	Bubble disappears on freezing down but re-appears at -1.4 °C ; B/M
			Ca	6 µm		IV	95	209.6			-0.4	0.70	Bubble disappears on freezing down but re-appears at -0.4 °C ; B/M
			Qtz	4x6 µm		IV	95	189.8			-0.2	0.35	Bubble almost disappears at - 40 °C on freezing down but pops after getting larger around -0.2 °C.
			Ca	3x7 µm		IV	95	152.9					
			Ca	3x7 µm		IV	95	167.7					
			Ca	3x7 µm		IV	95	189.2					
85037 Hole GDH-03 at 161.2 m	Micro-Diorite	Pervasive chl - ca-py (-cpy) Minor veins of mic-ca-qtz-py No inclusions observed in veins	Qtz	3x8 µm		I	75	455.4					B/M
			Qtz	7x3 µm		I	90	206.8					B/M
			Qtz	5x6 µm		II	75	444.4					B/M
			Ca	5x7 µm		II	75	360.6					B/M Bubble expands slightly ~ -80°C
			Qtz	7x8 µm		II	75	361.9		-43	-0.5	0.88	B/M
			Qtz	3x5 µm		IV/I ?	90	323.6			-0.2	0.35	B/M
			Ca	4x6 µm		IV	92	208.2					}
			Ca	2x6 µm		IV	92	206.4					} Part of secondary inclusion swarm
			Ca	4x6 µm		IV/II ?	80	282.3			-1.5	2.57	}
			Ca	3x5 µm		IV	95	160.2					B/M
			Ca	3x5 µm		IV	95	189.9			-1.7	2.90	B/M
			Ca	3x5 µm		IV	95	188.4					B/M
			Ca	3x5 µm		IV	95	188.4					B/M
			Ca	3x5 µm		IV	95	190.1					B/M
			Ca	5x6 µm		I	85	224.5					B/M
			Ca	8x10 µm		IV	95	154.6					B/M
			Ca	6x10 µm		IV	95	150.2					B/M
			Ca	6x12 µm		II	85	248.9		-42.1	-0.6	1.05	B/M
85059	Diorite	Pervasive alteration											No workable inclusions

TABLE 7.3 Details of fluid inclusion heating and freezing experiments (continues)

SAMPLE NO	HOST ROCK	VEIN MINERALOGY & VEIN TYPE	MINERAL STUDIED	SIZE	INCLUSION SHAPE	TYPE	Degree Of Fill %	Th-l °C	Th l+s °C	Te °C	Tm °C	SALINITY NaCl Equiv wt%	REMARKS
85011-V	Tourmalinized Micaeous sericitic graphitic shale (Marimo Shale)	Mic-qtz-phlog-chl-py-Ca											No workable inclusions
85011	Ser. graphitic shale (Marimo Shale)	Mic-qtz-phlog-chl-py-ca-ap-ab	Qtz	5x9 µm		IIIB	100		>500.0			>23.3	Neither salt homogenized to 500°C Vapour bubble disappeared at 335.2°C Anhydrite? + halite + vapour + liquid CO vapour ? + salt + liquid FeCl ₂ - NaCl in System Total homogenisation achieved.
			Qtz	7x11 µm		IIIB	90	439.4		335.2		49.90	
			Qtz	4x8 µm		IIIB	100	482.9				54.46	
			Qtz	5x8 µm		IIIA	70	485		-42.2	-7.9	11.58	
			Qtz	4x10 µm		IIIC	100	480.6				>23.3	
			Qtz	6x10 µm		IIIA	95	474.4		323.9			
85019 Hole GDH-02 at 135.0 m	Grey slate (Marimo Shale)	Mic-qtz-py-ap	Qtz	3x5 µm		I	85	350.6	167.3		-0.8	1.40	? Clathrate formed?
			Qtz	3x5 µm		I	80	356.1		-16.2	-0.7	1.22	NaCl - KCl solutes in system
			Qtz	3x5 µm		II	80	358.9		-10.2	-1.3	2.24	KCl in system
			Qtz	3x5 µm		II	80	335.9			-0.4	0.70?	Clathrate formed?
			Qtz	5x9 µm		I	90	285.4		-23.1	0		NaCl - KCl solutes in system
			Qtz	5x9 µm		I	90	287.6					
			Ab	6x12 µm		I	90	386.5		-22.1	-10.8	14.77	NaCl - KCl solutes in system
			Ab	5x10 µm		I	90	387.5					
			Ab	3x6 µm		I	95	281.4					
			Qtz	5x8 µm		IIIB	97	277.7			-28.6	27.78	Vapour homogenised at 167.3 °C ; Hematite inclusion.
												27.78	Salt homogenised at 277.7 °C
			Qtz	4x7 µm		II	80	327			-13.6	17.43	
			Qtz	2x5 µm		IV	95	278.2					
			Qtz	3x7 µm		I	80	340.5			-16.9	20.15	
			Qtz	3x7 µm		I	85	342.1					
			Qtz	5x8 µm		I	85	236.4		-37	-0.9	1.57	NaCl - FeCl ₂ solutes in system
			Qtz	9 µm		II	70	317.3			-1.7	2.90	
			Qtz	5x6 µm		I	90	? sample moved		-36.2	-1.5	2.57	Greenish ice FeCl ₃ ?
										-16.8	-1.5	2.57	NaCl - KCl solutes in system
			Qtz	4x6 µm		II	90	276.6		-37	-2.3	3.87	Greenish ice FeCl ₂
			Qtz	4x6 µm		IV	90	228.6					} Intra quartz inclusion swarm; Type A
			Qtz	4x6 µm		I	90	350.6					} Intra quartz inclusion swarm
			Qtz	4x6 µm		I	90	356.1					} Type B - (thicker - inclusion walls and slightly smaller than Type A
			Qtz	3x4 µm		IV	90	228.6			-0.2	0.35	} Intra quartz inclusion swarm Type A
			Qtz	4x8 µm		II	70	347.2			0.6		Clathrate formed?
			Qtz	4x8 µm		II	70	?			0.3		Clathrate formed?
			Qtz	3x5 µm		II	80	322.4		-22.8	-1.3	2.24	NaCl - KCl solutes in system
			Qtz	4x6 µm		IV	90	232.2			-1.2	2.07	} Intra quartz inclusion swarm Type A
			Qtz	3x6 µm		IV	90	233.5					}

TABLE 7.3 Details of fluid inclusion heating and freezing experiments

7.3.5 Type IIIC liquid - CO₂ vapour - multisolid inclusions

These inclusions are almost identical to Type IIIB inclusions but the dominant vapour phase appears to be CO₂ and the inclusions have a slightly higher degree of fill (Plates 7.4 and 7.9).

7.3.6 Type IV secondary liquid vapour inclusions

These inclusions are generally smaller and occur as swarms along secondary inclusion planes. They often exhibit bubble motion at room temperature and have a comparatively low vapour content (Plate 7.7).

7.3.7 Type V solid inclusions

Solid inclusions of halite up to 7 µm were observed in rare instances, spatially associated with Type IIIA, B and C inclusions. Their contact with the quartz host rims are nearly invisible indicating a similar refractive index.

The absence of related liquid or vapour rich “co-necked” inclusions suggest that they may have originally been present as solids supported in the highly saline primary fluid, rather than due to post entrapment necking of ordinary primary fluid inclusions.

7.4 Thermometry

Pressure Corrections

The mineralisation at Greenmount is hosted by sediments which barely attained lower to mid-greenschist facies during peak metamorphism. The mineral assemblage of the least altered pelite comprises microcline - quartz ± muscovite, dolomite, phlogopite or biotite and thus according to Spear (1993) the temperature range would be between about 420 - 570°C and the pressure is essentially unconstrained. However, Derrick et al. (1971) note the presence of andalusite in the Marimo Slate on the Marraba sheet, and the author has observed andalusite in the Marimo Slate 15 kilometres north of Copper Canyon. These areas are of similar metamorphic grade to the Greenmount area and therefore Spear's (1993) P-T grid for pelites constrains the pressure to a maximum of about 3 kilobars. Using the isochores of Crawford (1983) at pressure conditions of 3 kbars, and a geometric mean of 333.7°C for all primary and pseudosecondary fluid inclusions measured in this study, the temperature of trapping is

indicated to be about 650°C. This is geologically unreasonable and hence the pressure correction for the estimated lithostatic pressure is not correct. This suggests that mineralisation took place closer to hydrostatic pressures, and this is supported in part, by some open growth textures. Also the mineralisation post-dated peak metamorphism and was associated with a dominantly brittle to brittle-ductile vein array and extensive fracturing, and it was likely that the interconnected vein and fracture system would have provided the bulk rock with a high permeability even though open growth textures are not common. Under these conditions the fluid pressure gradient required to drive fluid flow would not have deviated significantly from hydrostatic pressure, therefore pressure corrections to the measured homogenisation temperatures are expected to be small regardless of fluid density (Roedder and Bodnar, 1980).

Effects of CO₂ vapour in inclusions

As some of the fluid inclusions in this study (Type II and Type IIIC) show evidence of CO₂, the apparent salinity obtained by the freezing of aqueous solutions for the inclusions will be higher than the actual salinity, as CO₂ acts as a solute and directly depresses the freezing point of the solution (Hedenquist and Henley, 1985; Oreskes and Einaudi, 1992). Freezing experiments show that some of the final ice melting temperatures are greater than 0°C in CO₂ bearing inclusions. This may indicate that clathrate formation took place. CO₂ clathrates entrap H₂O at a ratio of approximately 6:1 thereby increasing the actual salinity of the residual fluid in the inclusion (Collins, 1979). The large range in freezing point depressions of fluid inclusions at Greenmount could reflect variable CO₂ content, variable salinity or spurious readings due to undetected clathrate formation. As clathrate formation in this study remains equivocal, the salinities were not determined by the equation of Bozzo et al., (1973).

Behaviour of high salinity inclusions on heating

Highly saline inclusions usually decrepitated before homogenisation into a single fluid phase. In rare instances of total homogenisation of highly saline inclusions, the vapour bubble disappeared first, and the halite disappeared last and hence at the trapping temperature the fluid was undersaturated with respect to vapour and non-halite-salts. Leakage and decrepitation were common from temperatures of about 330°C upwards, but many inclusions which did not decrepitate even up to 500°C, still contained at least one undissolved solid phase. This limited the ability to obtain accurate salinity measurements.

Solute character of fluid inclusions

Table 7.2 describes some observed solid phases, however even the freezing behaviour of Type I and Type II inclusions is consistent with the presence of solutes in addition to NaCl. Freezing measurements were often not obtained because the small volume and high viscosity of liquid often obscured phase changes. However, where observed, the high degree of super cooling required to induce cooling (-60 to -120° C) and the occurrence of a variety of first melting temperatures (as low as -60.9° C) requires the presence of divalent solutes.

The presence of brown coloured, granular ice in some Staveley Formation hosted inclusions at temperatures between -49.5 and -58.0° C are characteristic of aqueous solutions rich in CaCl₂ (Borisenko, 1977).

Pale green coloured ice at -37° C observed in one inclusion may indicate the presence of FeCl₂. First melting temperatures for a variety of solutes are shown in Table 7.4. Thus the eutectic temperatures recorded in this study indicate a system dominated by CaCl₂ - NaCl - KCl - MgCl₂ - FeCl₂ - FeCl₃ - H₂O - CO₂. This is geologically feasible as alteration and vein minerals include ferroan dolomite, chlorapatite, sericite, phlogopite and hematite dusted microcline. The presence of fluorite salts is possible but was not detected, and is poorly described in the literature.

TABLE 7.4 First melting temperatures for various aqueous multiphase solid systems.

System	First Melting Temperature of Ice (°C)	Reference
KCl - H ₂ O	-10.8	Borisenko, 1977
NaCl - H ₂ O	-20.8	Potter et al., 1978
KCl - NaCl - H ₂ O	-23.5	Borisenko, 1977
MgCl ₂ - H ₂ O	-33.6	Borisenko, 1977
FeCl ₂ - H ₂ O	-35.0	Borisenko, 1977
MgCl ₂ - NaCl - H ₂ O	-35.0	Crawford, 1981
FeCl ₃ - H ₂ O	-36.5	Borisenko, 1977
FeCl ₂ - NaCl - H ₂ O	-37.0	Borisenko, 1977
MgCl ₂ - KCl - H ₂ O	-37.8	Borisenko, 1977
CaCl ₂ - H ₂ O	-49.5	Borisenko, 1977
CaCl ₂ - KCl - H ₂ O	-50.5	Borisenko, 1977
CaCl ₂ - MgCl ₂ - H ₂ O	-52.2	Borisenko, 1977
CaCl ₂ - KCl - NaCl - H ₂ O	-55.0	Yanatueva, 1946
CaCl ₂ - NaCl - H ₂ O	-55.0	Borisenko, 1977
FeCl ₃ - H ₂ O	-55.0	Linke, 1965
CaCl ₂ - MgCl ₂ - NaCl - H ₂ O	-58.0	Luzhnaja and Vereshtchetina, 1946

The effects of CH₄ vapour in inclusions

Although RAMAN spectroscopy revealed the presence of methane in a single inclusion from quartz hosted by the graphitic and carbonaceous Marimo Slate, its abundance is not known, but is thought to be low due to the prevalence of CO₂ in many inclusions, the possibility of anhydrite as rare daughter salt as well as the relatively oxidised mineral assemblage (hematite dusted microcline), and the graphite elimination selvage present around some veins. However, its presence does affect fluid behaviour and thus warrants some discussion.

Calcite is a common alteration product of many Archean greenstone hosted lode gold deposits. Most of these deposits are dominated by CO₂ - rich fluid inclusions (Ho et al., 1990) but many also contain CO₂ and CH₄ rich inclusions (eg. Wiluna, Hagemann et al., 1992; Golden Mile and Mt Charlotte, Ho et al., 1990; Marvel Loch, Hagemann and Ridley, 1993; Sand King and Missouri, Mernagh and Witt, 1994). Mernagh and Witt (1994) described mixed CO₂ and CH₄ inclusions from the Sand King and Missouri deposits and noted that the final melting temperature of their Type III inclusions averaged -65.2° C, which indicated the presence of significant amounts of CH₄. RAMAN Microprobe analyses indicated that the depression in melting point of CO₂ was caused by the presence of CH₄. They interpreted that the CH₄ rich fluid was locally generated in mafic or ultramafic units which may have been carbonated at their margins during interaction with the CO₂ - rich fluid, but have retained a very low fO₂ at the serpentinisation front.

Larsen et al., (1992) described methane bearing, aqueous saline inclusions from the Skaergaard intrusion.

Rumble and Hoering (1986) proposed that CH₄ - rich fluids may form during greenschist to amphibolite facies grade metamorphism of graphitic pelites at “low fO₂”.

Ettner et al. (1993) describe CH₄ - rich inclusions from the gold-rich ore zones at the Bidjovagge copper-gold deposit in Norway. Within deeper parts of the footwall veins, fluid inclusions are dominated by H₂O + CO₂ + salt, with salinities between 27 and 43 wt% NaCl

equiv., dominated by NaCl and CaCl₂. Fluid inclusions related to copper-rich mineralisation and syenodiorite intrusions comprise lower salinity aqueous solutions, up to 25 wt% NaCl equiv., dominated by NaCl and CaCl₂. Some of these inclusions also contain minor amounts of CH₄.

The veining at Greenmount was post peak metamorphic, however if some CH₄ is present, it may have formed from graphitic pelites during the same thermal event as hydrothermal activity or alternatively may have been sourced from the diorite as described by Larsen et al., (1992). Thus it is not clear whether the CH₄ is a reaction product ($2C + 2H_2O = CO_2 + CH_4$) or a component of the fluid. The former is considered more likely.

The mixing of CO₂ - rich and CH₄ - rich fluids may result in large changes in the oxidation potential of the (mineralising) fluid. Mernagh and Witt (1994) suggest that methane enrichment of fluids greatly increases the P-T range of fluid immiscibility, and H₂S, CH₄ and CO₂ would all be strongly partitioned into the vapour phase during unmixing of the ore fluid, leading to a decrease in the sulphur content of the residual fluid and, ultimately, gold precipitation. These mechanisms may operate over a wider range of pressures and temperatures than for the corresponding CO₂ - H₂O system.

Homogenisation temperatures

Inclusion details and homogenisation temperatures are presented in Table 7.3. The average of minimum homogenisation temperatures based on fluid inclusion type is summarised in Table 7.5 and the range of minimum homogenisation temperatures is shown in Figure 7.1.

From these data it is evident that in almost all cases Type III hypersaline inclusions have higher minimum homogenisation temperatures compared to Type I and II liquid and vapour inclusions regardless of host rock or mineral (albite in Marimo Slate hosted veins is the exception). The comparative difference in minimum Th between Type I and II, and Type III inclusions ranged from around 40 to 110°C. It should be noted that no Type III inclusions were recorded for the diorite.

TEMPERATURE OF HOMOGENISATION OF VAPOUR INTO LIQUID °C

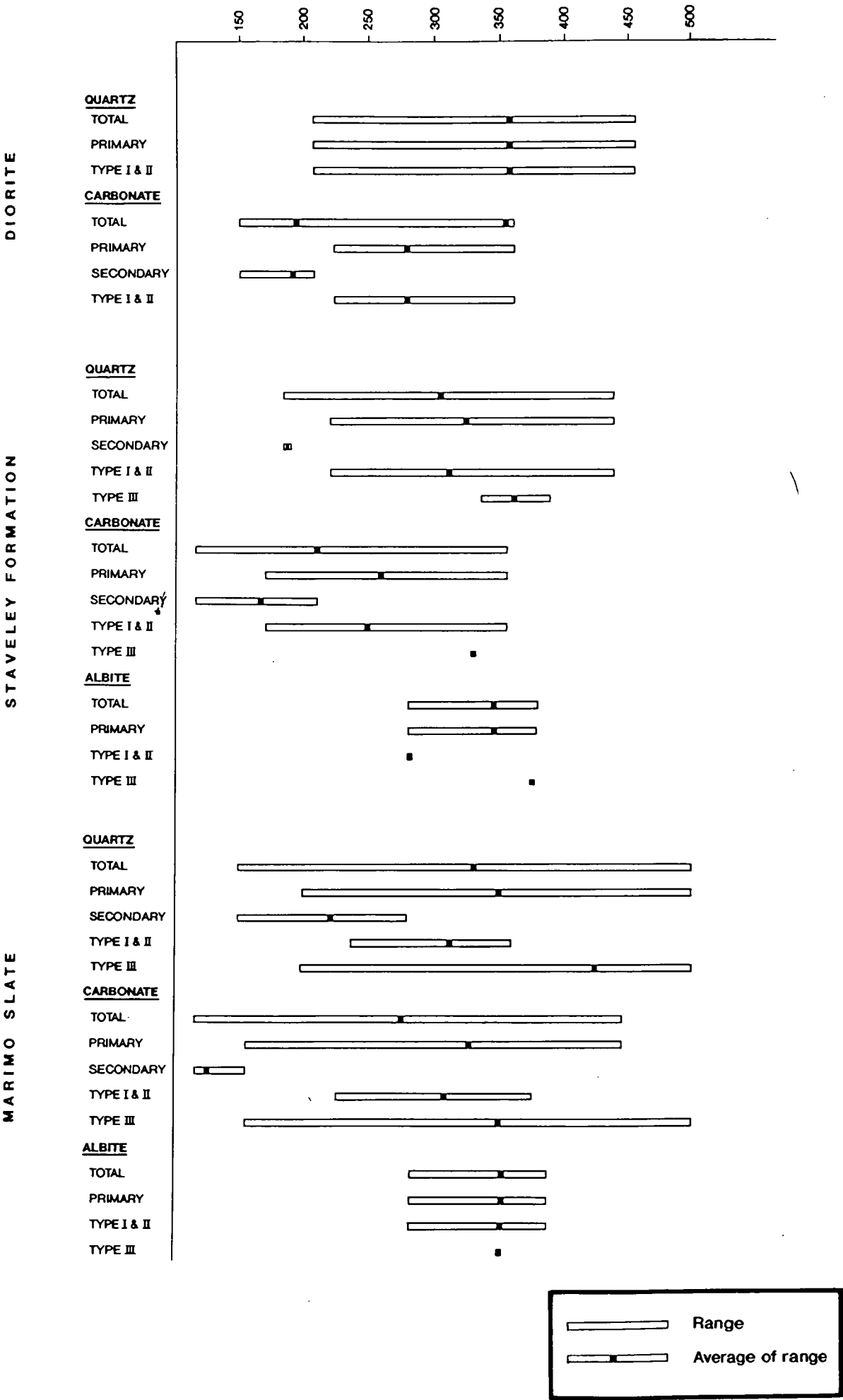


Figure 7.1 Temperature ranges of minimum homogenisation temperatures based on inclusion type, mineral and host rock.

In addition, all types of inclusions record higher homogenisation temperatures when hosted by quartz compared to the corresponding inclusion types when hosted by carbonate (Tables 7.5 and 7.6).

Histograms of the data, presented in Figures 7.2 (A, B and C) indicate a wide range of minimum homogenisation temperatures for any inclusion type in any mineral.

A plot of salinity against minimum homogenisation temperature reveals that there appears to be two distinct populations (Figure 7.3). Very few inclusions have salinities in the range of 5 to 15 wt% NaCl equivalent. The hypersaline inclusions generally have a higher minimum homogenisation temperature while inclusions less than 5 wt% NaCl equivalent generally cluster between 150-360° C.

TABLE 7.5 Average of minimum homogenisation temperatures based on fluid inclusion type, host mineral and host rock.

Vein Host	Mineral	Fluid Inclusion Type				
		Total	Primary	Secondary	Type I&II	Type III
Diorite	Qtz	358.4	358.4	-	358.4	-
Diorite	Ca	194.4	279.0	191.8	279.0	-
Pks	Qtz	304.4	324	187.0	311.6	361.1
Pks	Ca	210.3	258.8	167.2	248.6	330.3
Pks	Ab	345.3	345.3	-	280.2	377.9
Pkm	Qtz	329.1	347.5	221.2	312.6	422.6
Pkm	Ca	274.4	327.7	125.1	307.3	348.1
Pkm	Ab	351.3	351.3	-	351.8	350

TABLE 7.6 Minimum homogenisation temperature based on host mineral and inclusion generation.

Mineral	Inclusion Generation	Minimum Th	
All Quartz	Primary	326.6	n=61
	Secondary	213.6	n=9
All Carbonate	Primary	170.6	n=26
	Secondary	163.7	n=23
All Albite	Primary	348.7	n=7

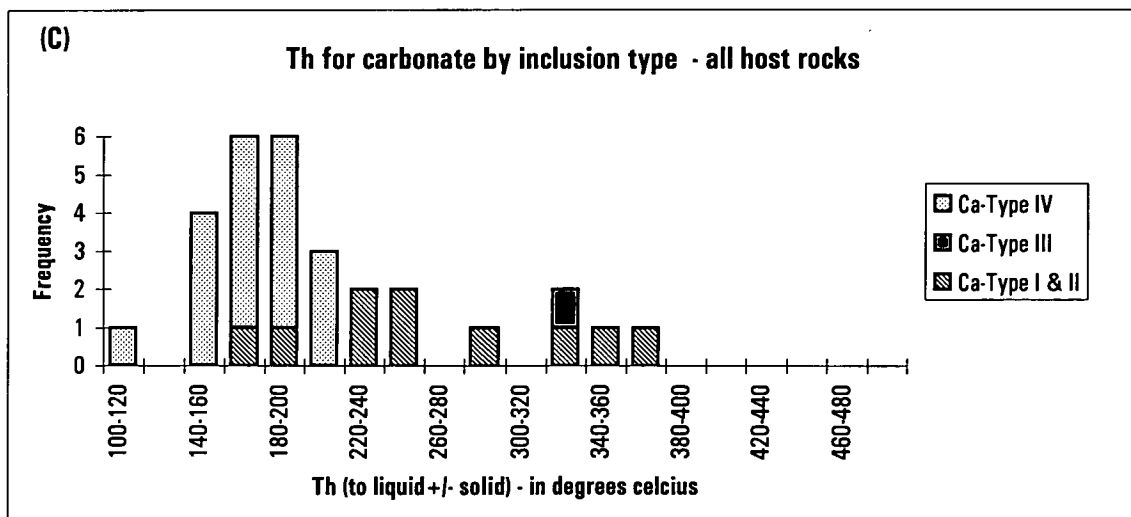
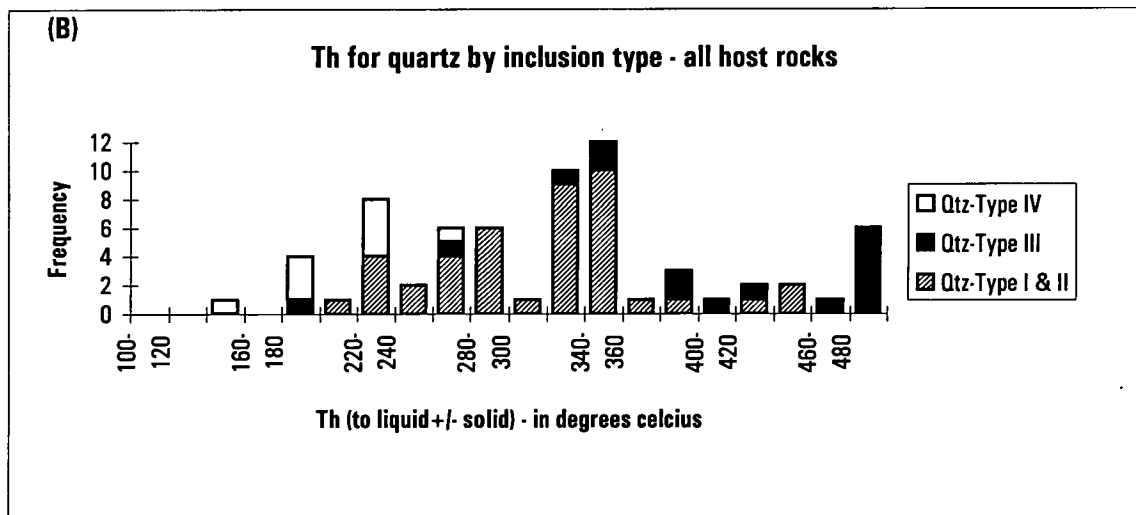
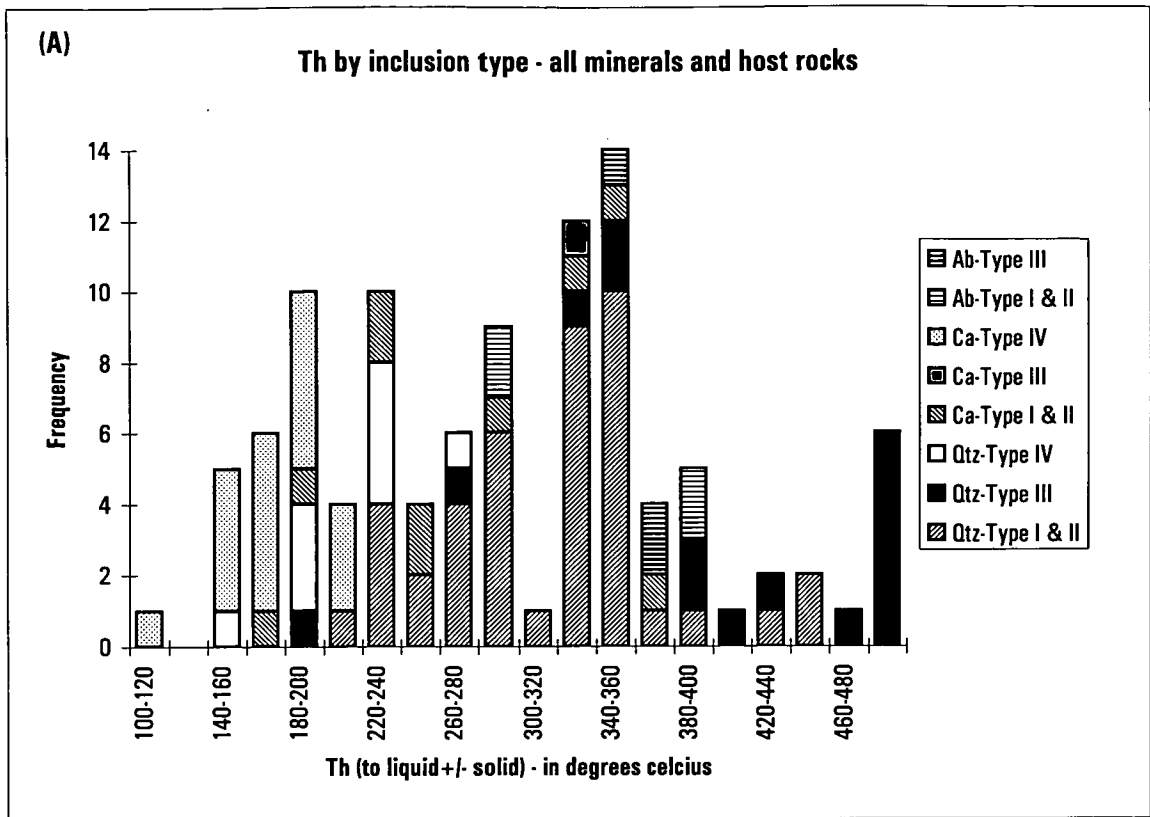


Figure 7.2 (A,B,C) Histograms of minimum homogenisation temperatures (vapour bubble disappearance) for various minerals, regardless of host rock.

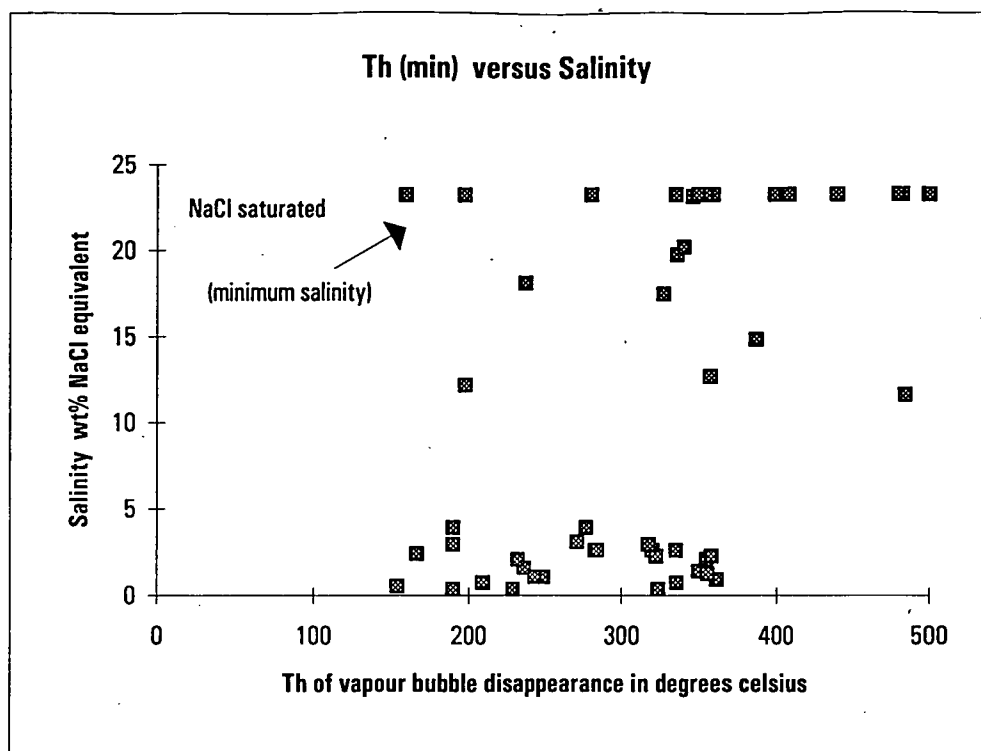


FIGURE 7.3 Th (min.) versus salinity plot for Type I, II and IV inclusions.

Discussion

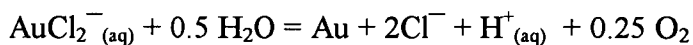
Fluid inclusions for the earlier pervasive style of alteration were not found but other workers in the district (eg. Williams and Blake, 1993) suggest that this style may be characterised by high salinity CaCl_2 - NaCl rich complex fluids typically 400-500°C and 20-40 wt% NaCl equivalent.

In this study almost all primary and pseudosecondary inclusion types from vein minerals may be present in the same crystal. Combined with the wide range of minimum homogenisation temperatures, lack of phase separation evidence and two salinity populations, it would appear that fluid mixing of two different fluids occurred. One would have been a hotter (~320-500°C) hypersaline fluid and the other was a cooler (220-360°C) lower salinity fluid. The overall trend appears to be one of decreasing temperature and salinity, with increasing carbonate deposition later in the paragenesis.

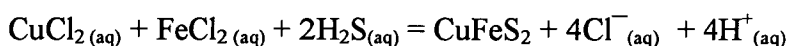
Observation of solid phases as well as eutectic temperatures indicate that both fluids contained a variety of solute species (Na^+ , K^+ , Fe^{2+} , Mg^{2+} , Ca^{2+} , Cl^- , CO_3^{2-} , CO_2 and possibly Fe^{3+} , SO_4^{2-} , F^-).

The presence of CO_2 and hematite (and possibly anhydrite) indicates that the fluid was relatively oxidised and therefore any sulphur present would have been predominantly as an oxidised species. Vein Microcline is usually not retrogressed to sericite and hence the pH would have been near neutral, however early fine grained pervasive feldspathic alteration commonly retrogressed to sericite indicating an even earlier lower pH fluid existed for that style of alteration.

Transport of base and precious metals at elevated temperatures is conventionally regarded to be by chloride or sulphide complexes. The primary fluid at Greenmount was a moderately to hypersaline oxidised chloride brine between about 250 to 500°C and probably poor in reduced sulphur. Chloride complexes were likely to have been dominant. Deposition of gold from chlorocomplexes may be described by the following equation



and deposition of chalcopyrite may be represented by:



Precipitation may be induced by (i) cooling the fluid; (ii) removal of oxygen by interaction with reduced species (eg. graphite, methane); (iii) reducing the activities of complexing ligands (ie. dilution); (iv) increasing the fluid pH (ie. boiling or carbonate buffering), or (v) increasing the activity of S^{2-} (Barnes, 1979).

Thus mechanisms (i), (ii), (iii) and (iv) may have played a part in chalcopyrite-gold deposition. The controlling factor appears to have been the availability of reduced sulphur which had to be scavenged from earlier (diagenetic) sulphide (as described for Mt Dore by Beardsmore, 1993) and fO_2 control by the reduced carbonaceous and graphitic shale. This is supported by sulphur isotope-evidence (Chapter 6) as well as

by the location of most economic mineralisation occurring in the carbonaceous Marimo Slate, although oxidised and porous Staveley Formation is also altered and veined.

CHAPTER 8 *Discussion and Summary*

8.0 *Introduction*

Diagenetic copper mineralisation was documented at the Just Found prospect by Stewart 1991, and hydrothermal mineralisation and fluids at Greenmount are discussed by this study, however the source of metals, particularly gold remains enigmatic. The following section reviews other carbonaceous sediment hosted deposits as well as similar Proterozoic Cu \pm Au \pm Co deposits, and compares the similarities and differences to the characteristics observed at Greenmount. Metal sources and genesis of similar deposits may provide an insight into the possible metal source or sources at Greenmount and may help to elucidate the fundamental controls on mineralisation.

8.1 *Ballarat-style slate belt gold deposits*

Most deposits occur in the Palaeozoic rocks of central Victoria which comprise Cambrian basalts and sediments overlain by extensive Ordovician to Middle Devonian shale, siltstone, sandstone and turbidite (Gray, 1988). These rocks were strongly deformed and metamorphosed to greenschist facies by the Middle Devonian Tabberabberan Orogeny (Ramsay and VandenBerg, 1990). Subsequent Silurian to Lower Carboniferous sedimentation was "molasse style", and includes sandstones, red beds, and acid and lesser mafic volcanics which Cas (1983) has compared to Cainozoic rocks in the Basin and Range Province of Western USA.

Most gold production shows a strong preference for carbonaceous metasedimentary and/or Fe-rich, mafic igneous host rocks (commonly diorites) with a bulk chemical composition favourable for gold deposition (Phillips and Hughes, 1995).

All significant primary gold occurrences in Victoria appear to be structurally controlled, and the bulk of these deposits are auriferous quartz veins emplaced along faults, within tension gashes or along fold crests as saddle and trough reefs. Ladder veins and veins in reverse faults (e.g. "leather jackets") are common. Many goldfields appear to occur near to, but offset major faults that are now inferred to flatten at depth (Cox et al., 1991; Gray and Wilman, 1991), and they exhibit a spatial relationship to antiformal axes. Most of the gold appears to be

introduced during or immediately after major deformational episodes (Ramsay and VandenBerg, 1990). The source of gold remains uncertain.

Phillips and Hughes (1995) describe the alteration around these deposit and suggest that wallrock alteration has been underestimated in the past. In mafic dykes alteration is moderately pervasive and intense, and includes a weak chlorite-carbonate halo and a more intense and local bleached margin (centimetres to metres in width) of albite, carbonate, and white mica adjacent to veins. In slates, intense alteration adjacent to veins is restricted to thin margins (centimetres in width) of chlorite, carbonate, and white mica. Haloes of disseminated pyrite and arsenopyrite, and widespread areas of carbonate spotting (over widths of metres to hundreds of metres) are now recognised as gold-related alteration in metasedimentary rocks (Phillips and Powell, 1993).

Arsenic is enriched in the majority of deposits, and trace stibnite is common. Elevated Mo, W, Ag, B, Bi and Te, and significant amounts of Cu, Pb and Zn are restricted to a few specific districts or in proximity to granites.

Fluid inclusion studies have demonstrated a preponderance of H₂O-CO₂-H₂S fluid inclusions without daughter products (Phillips and Powell, 1993). Trapping temperatures are inferred to be near 300°C. Methane appears to be common near carbonaceous slates and the sulphur appears to be reduced.

Greenmount-style mineralisation differs from slate belt gold deposits in that the fluids at Greenmount were more saline and oxidised. In addition, Greenmount contains more intense alkali dominated veins and pervasive alteration, as well as a slightly different metal assemblage. Also, the veining and mineralisation at Greenmount is post-folding.

8.2 Global examples of carbonaceous sediment hosted mineralisation

The Ashanti Gold Belt - Ghana

Numerous economic mesothermal gold deposits are hosted by Early Proterozoic greenschist facies carbonaceous and carbonate bearing turbidites and greywackes as well as carbonate altered mafic dykes, in both brittle and brittle-ductile regimes (Mumin et al., 1994). The

structurally deeper ores are dominated by large crack-seal quartz veins with sheared margins and disseminated sulphides comprising Au-bearing arsenopyrite, arsenian pyrite, chalcopyrite, sphalerite, minor cobaltite, silicate gangue and inclusions of wallrock, whereas the structurally higher ores are dominated by Au-bearing arsenian pyrite and arsenopyrite.

Mumin et al. (1994) describe the country rocks as being metamorphosed to a chlorite - epidote - carbonate - quartz - sericite - rutile greenschist facies assemblage. Significant bleached zones of ankerite - siderite - sericite - quartz alteration occur in the mafic dykes, however distinct zones of hydrothermal wall rock alteration do not occur in the host sediments. The gangue mineralogy of veins includes quartz, ankerite, sericite, albite, siderite and rutile. These workers suggest that the generation of ore fluid occurred at depth below the gold deposits as a result of metamorphic decarbonation dehydration reactions, and gold deposition occurred over a temperature of approximately 340° to 140°C. This ore deposit is similar to other “slate-belt style” mesothermal lode gold deposits such as the Ballarat Slate Belt (Sandiford and Keays, 1986; Phillips and Powell, 1993; Phillips and Hughes, 1995) and the Alaska - Juneau deposits (Goldfarb et al., 1989, 1991).

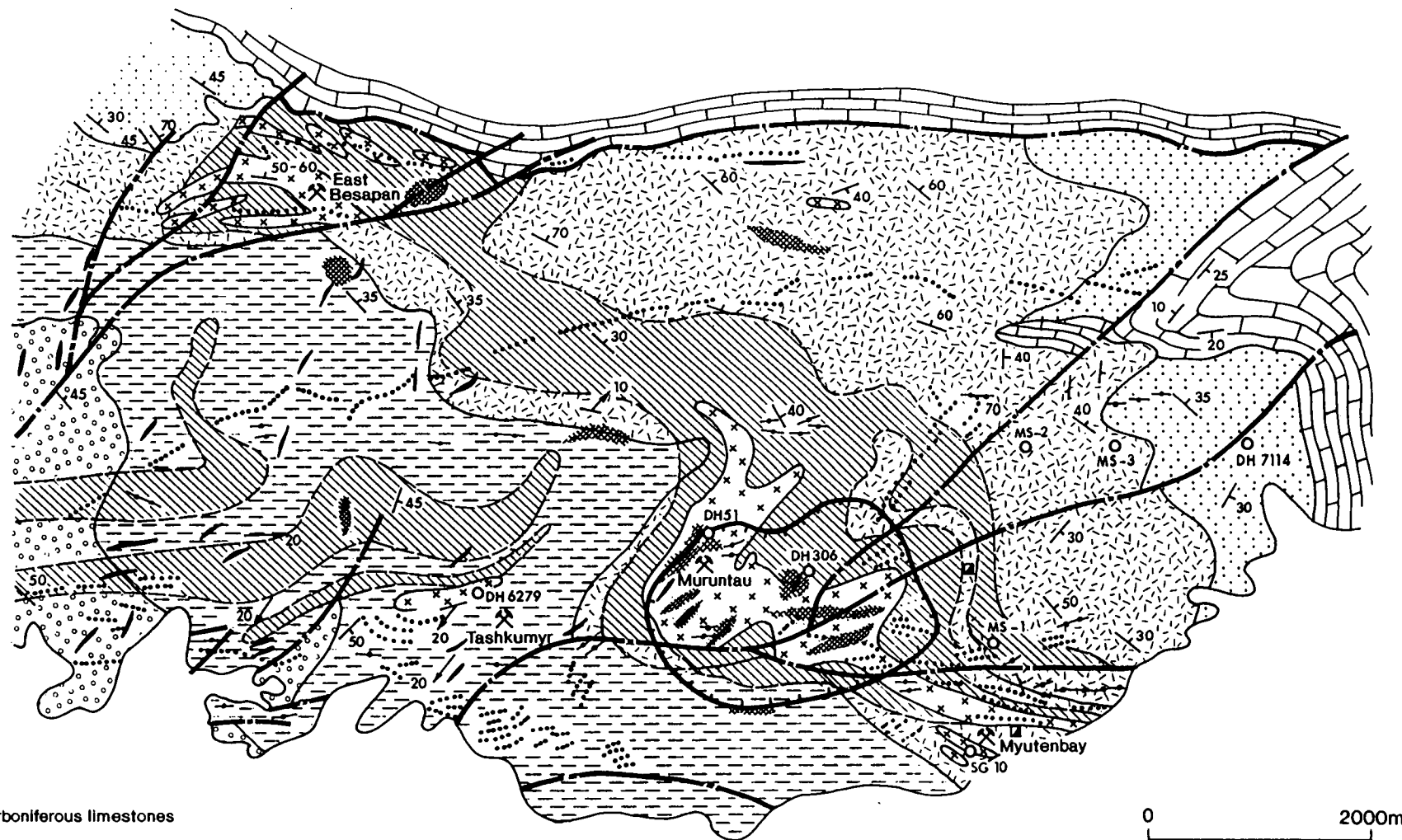
Thus while sharing some characteristics with Greenmount, such as age, metamorphic grade, temperature of vein deposition, carbonaceous character of host rock, spatial association with altered mafic dykes and some similar ore and gangue minerals, there are notable differences such as absence of microcline, albite, apatite, evaporitic lithologies, substantial copper and cobalt enrichment as well as lack of pervasive alteration of wallrocks associated with veining and mineralisation. It should be noted that some veins at Greenmount display brittle and brittle-ductile characteristics without pervasive alteration selvages, but the main ore zone is intimately associated with (spatially and genetically) intense wallrock alteration, and thus Greenmount is not a typical mesothermal mineral deposit.

The Muruntau Deposit - Uzbekistan

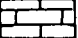

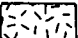
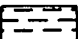
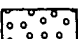

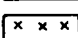
Another carbonaceous shale hosted deposit which shares some similarities to Greenmount is the giant Muruntau deposit in Uzbekistan. Past production plus mineable reserves total in excess of 100 million ounces of gold. Muruntau is hosted by the Ordovician to Silurian Besapan unit which was deposited on an eroded basement of Proterozoic schists, gneisses and









migmatites and metamorphosed to greenschist facies (Berger, 1992). A map of the geology of the district is presented in figure 8.1. Regionally, the Besapan contains 1 - 3% organic carbon and 11.2 to 25.8 ppb Au which is enriched to 483 ppb Au in the mine district (Marakushev and Khokhlov, 1992) and thus a synsedimentary protore may be implicated. The main intrusive in the district is the Sardarin Pluton which is a two Mica, S-type “granosyenite”, however a range of dykes including quartz diorite, syenite, diorite and granosyenite are also common (Kotov and Poritskaya, 1992). Post - gold deposition alkalic and dioritic dykes contain quartz - pyrite - tourmaline veinlets with K-feldspar - sericite - quartz selvages. The host rock has been altered to a distinctive auriferous “metasomatite”. Alteration comprises albite - quartz - apatite prior to gold deposition and quartz - K-feldspar - ankerite - biotite - chlorite - monazite \pm apatite accompany the gold mineralisation (Lehrman, 1993; Berger, 1992). Calcite and pyrite is the last stage of alteration. There are two styles of mineralisation: “stockwork and banded” and “central” veins. The stockwork mineralisation is the earliest stage of gold deposition, and veins were emplaced in a brittle - ductile regime after the main period of folding. The central veins cross cut the stockwork ore and are related to brittle deformation. The bulk of the ore is stockwork and averages 2.5 to 3 g/t Au. The central veins average 5 g/t Au. The gold is associated with pyrite, arsenopyrite and ankerite in milky white quartz with minor amounts of galena, sphalerite, chalcopyrite pyrrhotite, scheelite, telluride bismuthinite and molybdenite. Salinity data is not reported, however homogenisation temperatures of fluid inclusions from the various stages of veining (from early to late) are 420 - 450°C, 310 - 390°C and 230 - 185°C with pressures of formation in the range of 200 - 300 Mpa which equates to about 10 km depth (Zairi and Kurbanov, 1992). Zairi and Kurbanov (*op cit.*) characterise the fluid characteristics and describe the fluid inclusions as CO₂ dominated with subordinate CH₄. A summary of their findings is presented in Table 8.1.

These workers suggest that the most important controlling features of the physical - chemical regime of fluid evolution are an increase in the content C_{org} in the country rock adjacent to the ore-controlling Southern fault zone which underwent strong post ore displacement, and a pressure change within the fluid system from 100 Mpa (during gold - sulphide mineralisation) to 200 Mpa (quartz - gold - sulphide mineralisation). They further suggest that their results cast doubt on the involvement of granitic magmatism in the mineralisation. In contrast, Marakushev and Khokhlov (1992) offer a hypothesis of “fluid - magmatic replacement” of



LEGEND

-  Devonian and carboniferous limestones and dolomites
-  Silurian sandstone with quartz-chlorite cement (green Besapan)
-  Lower Palaeozoic metasilts (variegated Besapan)
-  Chlorite-muscovite phyllites with relicts of metasilts (grey Besapan)
-  Biotite-muscovite phyllites
-  Zones of higher metamorphic grade, disseminated mineralisation. Biotite alteration and carbon metasomatism.
-  Auriferous biotite-two feldspar-quartz rocks and ores.

-  Auriferous quartz veins
-  Wallrock diaphthorite
-  Tourmaline rich veins
-  Diorite and lamprophyre dykes
-  Faults
-  Faults with displacement
-  Faults with strike-slip
-  Mines and deposits






-  Dip of foliation or bedding
-  Plunge of fold axis
-  Shafts
-  Drillholes
-  Open pit

Figure 8.1

Geology of the Muruntau district
(figure adapted from Marakushev
and Khokholov, 1992)

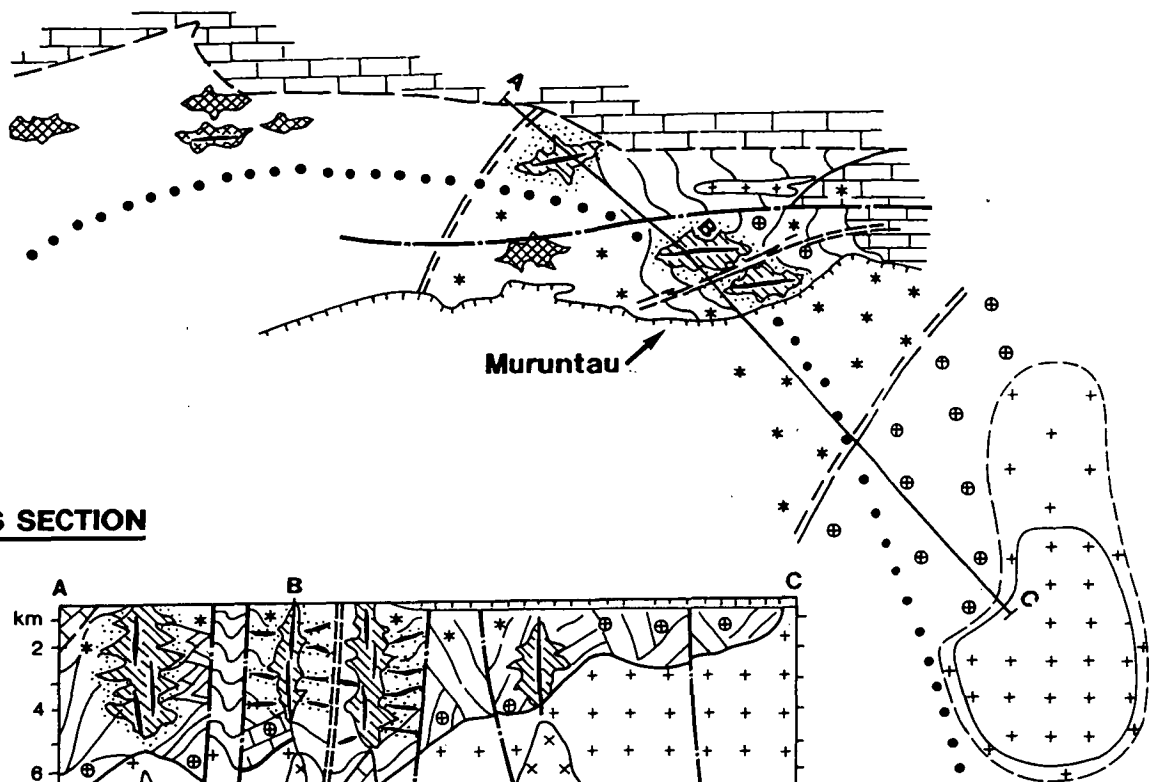
initially gold-rich carbonaceous shales by infiltration of a lamprophyric magma. Kotov and Poritskaya (1992) emphasize the multistage nature of the mineralisation and suggest that hydrothermal activity occurred in the aureole of a late collisional granite pluton (Figure 8.2). These workers suggest that mineralisation proceeded under reduced conditions and cited the presence of carbonaceous micro-inclusions in auriferous quartz as well as the formation of carbonaceous sericitolites along the Southern fault as evidence for this. The carbonaceous matter in the black slates maintained a reducing hydrothermal environment which facilitated transport of gold by the fluid. Hydrothermal mineralisation is suggested to have occurred in stages during successive drops in temperature from 450°C to 230°C at a pressure of 200 - 300 Mpa.

Isotopic - geochemical associations (IGA)				
	Core Zone		⇒	Frontal Zone
	Za ₁	Za ₂	Za ₃	Za ₄
δ ³⁴ S‰	7.5 - 5	5 - 3	3 - 0	0 to -4
T°C (average)	350	300	250 - 200	150
pH	6 - 6.6	6.5 - 7.3	7.4 - 8.3	8.3 - 9.2
log fO ₂	-31.94	-34.8	-40.82	-48.47
P, Mpa	200	200	200	200

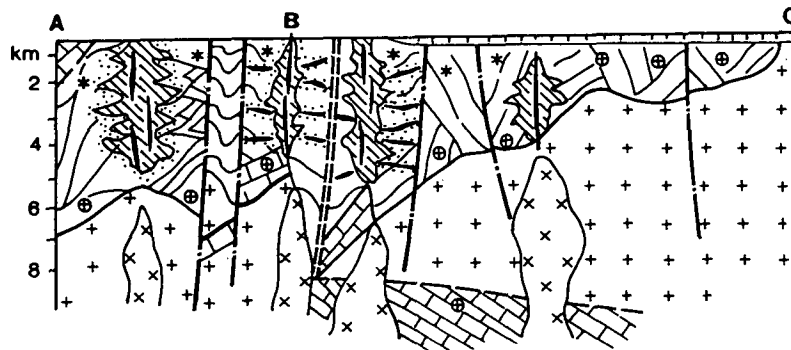
TABLE 8.1 Isotopic - Geochemical and physicochemical parameters of Muruntau mineralisation. (Data from Zairi and Kurbanov, 1992).

Greenmount shares some similar characteristics to Muruntau including host lithology, temperature, metamorphic grade, proximity to alkalic intrusive activity, similar sulphur isotopic signatures, vein style, vein timing with respect to folding, temperature of vein formation as well as similar pervasive alkali dominated alteration (“metasomatite”) assemblages and vein gangue minerals. Notable exceptions though are age, gold grade, cobalt and copper content and salinity of fluids. In addition limited geochemical evidence from this study does not suggest that the least altered Marimo Slate is particularly enriched in gold, so as to form a protore source as at Muruntau.

PLAN



CROSS SECTION



LEGEND

- | | | | |
|--|---|--|--|
| | Carbonate country rocks | | Quartz - chlorite - sericite alteration |
| | Black slate - metamorphosed to greenschist facies | | Quartz - chlorite - sericite - albite alteration |
| | Intra-ore dykes | | Quartz - biotite - two feldspar rock |
| | Leucocratic granite | | Auriferous quartz veins |
| | Granodiorite - adamellite of the sadarin pluton | | Carbonaceous sericitolite |
| | Hornfels | | Subconcordant faults |
| | Knotted and spotted schists | | Approximate axis of Dzhambulak anticlinoid |
| | | | Boundary of Mesozoic - Cainozoic sediments |

Figure 8.2
Plan and cross section of the regional geology of the Muruntau district.
(figure adapted from Kotov and Poritskaya, 1992)

Synsedimentary to Diagenetic mineral deposits and Metalliferous black shales

Muruntau and several other nearby deposits appear unique in that levels of anomalous background gold content of all other carbonaceous shales of the world do not approach the levels at Muruntau. Fan Delian (1983) and Coveney and Nansheng (1989) report thin centimetre scale bands of “polyelement” sulphide mineralisation with up to 7% Mo, 4% Ni, 2% Zn and nearly 1 g/t Au from Chinese Lower Cambrian black shales. Fan Delian (1983) suggested that submarine hot springs related to basement faulting contributed metals to the water column during sediment deposition. Coveney and Nansheng (1989), however, suggested a non-syngenetic component to the mineralisation based on sulphur isotope values being heavier in the more metal-rich portion of the samples.

The Polish and German Kupferschiefer deposits occur in evaporites of the Permian Zechstein sequence. Host lithologies comprise dolomite, dolomitic limestones and shales, aurenites and Kerogen shales (Haynes, 1986), and occur in a similar tectonostratigraphic position as deposits of the Marimo Basin (Hodgson et al., 1988). The Lubin deposits in Poland contain appreciable precious metal contents eg. 2600 m t at 2% Cu, 30 - 80 ppm Ag and 0.1 ppm Au, with locally enriched Au (up to 3000 ppm), Pt - Pd - Bi (up to 1000 ppm), Cobalt (up to 1.92%), Ni (up to 0.51%) and elevated Pb, Zn, As, Hg, Mo, P, and vanadium (Kirkham, 1989; Kucha and Pawlikowski, 1986; Kucha and Pocheć, 1983). The Rote Fäule described by Kucha and Pawlikowski (1986) is analagous to the “red rock” (hematite dusted feldspar) alteration observed in the Cloncurry district. These workers favour a diagenetic origin for mineralisation, and interpret the Rote Fäule as a result of oxidation of iron bearing minerals at paleosol, aquifer, regolith and near shoreline (emergent) positions. Stewart (1991) documents early hematite alteration at the Just Found prospect north of Greenmount, occurring as minor inclusions in chert nodule pseudomorphs after sulphate. In contrast to the synsedimentary or early diagenetic models proposed by many workers, Maynard (1992), Jowett (1986, 1989) and Jowett et al. (1987) prefer a late diagenetic model. Jowett (1986) articulates a model in which elevated heat flow from basement highs associated with Triassic rifting initiated fluid flow. The fluid was a chloride-rich brine which flowed convectively through the Rote Fäule areas, depositing metals on contact with biogenic sulphides in the Zechstein strata. Maynard (1992) suggests that essential factors are rifting accompanied by mafic volcanism; deposition of coarse grained volcanic derived clastics in an arid environment; early diagenetic reddening of the

clastics with transfer of copper and other metals to grain surfaces; deposition of an impermeable caprock; and, finally, renewed rifting with convective overturn of brines within the sedimentary pile, a circulation that leaches metals from the redbeds as described by Zielinski et al. (1983), and deposits them in the overlying black shale interval. There is general disagreement as to the source of metals in the Kupferscheifer.

A similar controversy exists for the Cu - Co mineralisation on the Zambian Copper belt, which formed within a rift basin in a marginal marine setting. Redbeds and typical evaporitic basin stratigraphy are present. Garlick (1981, 1989) is the main syngenetic proponent but Maynard (1992) suggests that this model runs into serious difficulties in explaining numerous crucial aspects of the Zambian deposits. Such difficulties reviewed along with several other aspects by Sweeney et al. (1991), are avoided in a genetic model which includes the subsurface circulation of chloride brines transporting metals as soluble metal-chloride complexes. The sulphide zoning apparent at some of these deposits may be explained by a prominent flow of ore solutions both across and along bedding. Annels (1989) proposed that ore solutions rose, at basin scale, along permeable clastic rocks overlying the basement/Roan contact, and then at mine scale, migrated laterally along bedding.

Schultz (1991) globally reviewed some particularly metalliferous black shale units and noted that their U, V, Mo, Pb, Zn, Ni and Cu contents were generally highly anomalous but the gold content was low.

Therefore, it would appear that globally, with the exception of Muruntau, there is very little unequivocal evidence for black shales as a significant source of gold. The Besapan in Uzbekistan and some Chinese black shales are the only known examples where there is general agreement for elevated gold contents which may possibly constitute a protore source of gold. Stewart (1991) documents unequivocal evidence of diagenetic chalcopyrite-tourmaline-cobaltite-apatite mineralisation from the Staveley Formation at the Just Found prospect (Chapter 3.3.2), and hence a diagenetic and/or a hydrothermally remobilised diagenetic source of Cu - Co - P and several other elements, remains a contender for a component of mineralisation at Greenmount. However any evidence for these early processes have been obliterated by subsequent hydrothermal and metamorphic events, and in addition, Stewart

(1991) did not find anomalous background gold. Another source of gold is required. Anatexis or assimilation of metalliferous black shales and carbonates by ascending granites and subsequent magmatic - hydrothermal reworking is not considered likely, as the mineralising fluids at Greenmount were demonstrably oxidised.

Stratiform Cu - Co - Au deposits of the Idaho Cobalt belt

These deposits are temporally and metallogenically similar to the Greenmount deposit and warrant some discussion. The deposits are hosted by the Middle Proterozoic Yellowjacket Formation comprising argillite, siltstone, fine grained quartzite and other metasediments. The Yellowjacket Formation is also characterised by distinctive chemical and mineralogical compositions including halogen rich biotite dominated strata and magnetite rich units (Nash and Connor, 1993). Copper - cobalt - gold mineralisation extends for more than 40 km, with widespread enrichment of Fe, K, Li, Mg, P, Ti, Cu, Sb, V, Y and Yb, as well as local enrichments of Ba, Pb and Zn.

Nash and Hahn (1989) describe ore minerals at the Blackbird Mine which chiefly comprise cobaltite, chalcopyrite and pyrite. The non-metallic minerals present include biotite, quartz, garnet, tourmaline, muscovite, chloritoid, apatite and siderite, however, evidence of ore associated alteration around the lodes is described as subtle to virtually non-existent greater than 1 m from ore. These workers also note the abundance of hypersaline fluid inclusions in quartz containing as many as six daughter minerals including halite, sylvite and several unidentified birefringent varieties. Halite solution temperatures of 250 - 350°C and filling temperatures of 275 - 375°C are reported with the suggestion that these hot, saline fluids may have caused potassic metasomatism and formation of biotite and white mica. Nash and Hahn (*op cit.*) conclude that mafic rocks are a likely source of most metals.

Nash and Connor (1993), argue that the Fe-rich strata are probably exhalative units related to mafic volcanism and submarine hot springs, and that chlorine enrichment occurred during diagenesis. They suggest that lack of evidence of evaporitic strata in the Yellowjacket Formation could indicate that the Cl reflects a submarine brine that carried Fe, K and base metals. It should be noted though that the potential for preservation of evaporites under mid greenschist metamorphism (defined by the presence of garnet and biotite) is considered low.

In the Cloncurry district, Davidson (1989, 1992) documents copper \pm gold bearing oxide ores from the Staveley Formation at the Starra mine, and proposed the term “volcanogenic copper-bearing oxide” to describe exhaled seafloor sediments, which are dominated by magnetite, quartz and hematite, with subordinate chalcopyrite, pyrite and in some cases gold. Ore formation is attributed to precipitation from the oxidised and H₂S deficient version of a volcanic-hosted massive sulphide fluid in an oxidised water column. He also suggests that a second possible source of oxidised metal-bearing fluids is highly fractionated magnetite series granites. Laing (1993) however, suggests that a large component of the iron was introduced during deformation.

The numerous hematitic ironstones hosted by the Staveley Formation immediately west of (and stratigraphically below) the Greenmount deposit are notably barren with respect to ore metals. In addition, petrography suggests that most of the hematite present is detrital, and there is only a very minor intermediate volcanic component to the sediments (Joyce, 1993). There is no evidence of proximal volcanic activity to Greenmount, nor is there evidence for any mafic related exhalative brines as suggested by Nash and Connor (1993).

The Bidjovagge Copper - gold deposit

This deposit has been described by Bjorlykke et al. (1987) and is located in the Lower Proterozoic Kautokeino greenstone belt of northern Norway. It shares some similar characteristics with Greenmount including the Cu - Au association, carbonaceous and graphitic slate host, spatial association to mafic dykes (dolerites) and extensive pervasive feldspathisation of host rocks (dominated by albite at Bidjovagge and microcline at Greenmount).

The deposit is hosted by the Cas'Kejas Formation which comprises (from base to top) dolomitic carbonates, variably carbonaceous and altered argillites, “tuffites” and amphibolites. This sequence has been intruded by diabase sills. Structurally, the deposit is located on the limb of an 8.5 km long anticline. All lithologies have been altered to varying degrees. The main alteration product is albite and the most intensely altered lithology is the argillic units which are termed “albitic or graphitic felsite”, which is associated with the diabase sills.

Albitisation is often accompanied by carbonatisation with subordinate quartz, mica, amphibole and scapolite. The orebodies are generally tabular, strike for 100 to 200 m and are between 5 to 35 m thick. Grades are typically 1.8% Cu, 0.5 ppm Au, 3 ppm Ag, 0.05 ppm Ni, 80 - 300 ppm Co with low Pb and Zn contents.

The main ore mineral is chalcopyrite which occurs in aggregates and veins. Pyrite and pyrrhotite commonly occur with the chalcopyrite. Other accessory sulphides include marcasite, cobalt and nickel-rich pyrite, sphalerite, galena, pentlandite, violarite, mackinawite and molybdenite. Magnetite hematite, illmenite and rutile are all common accessory minerals. Magnetite often occurs as euhedral inclusions in sulphides and rutile is often disseminated in the felsites.

Bjorlykke et al. (1987) suggest that the main mineralisation is restricted to the oxidised part of the albitic felsite, where hematite deposition has occurred in footwall rocks, implying ore-forming solutions within the stability field for hematite.

Copper in mineralisation appears to be associated with brecciation, formation of ankerite - actinolite veins and oxidation of graphitic felsite. Some disseminated chalcopyrite occurs in albitite dykes (which themselves are cut by late carbonate veins), but the association with these dyke is uncertain. Bjorlykke et al. (1987) suggests that boiling and temperature decrease could have been an important factor in copper ore genesis. Between the different orebodies, gold may or may not be correlated with copper and is sometimes elevated near the oxidation front of the graphitic felsite. These workers tentatively suggest an fO_2 and pH control on gold deposition.

While this deposit shares many similarities with Greenmount, the mafic intrusive (diorite) at Greenmount is geochemically barren in gold and may not represent a suitable source of gold, however, as at other deposits (eg. Mufulira, White Pine) they may constitute a suitable source of copper or cobalt. The absence of brittle and brittle-ductile veining at Bidjovagge is a notable difference.

Cloncurry District analogues

Beardsmore (1992) documents mineralisation at Mount Dore, which is located approximately 55 km south of Greenmount within quartz-muscovite schists and carbonaceous slates of the Kuridala Formation which is structurally overlying meta-calcarenes, calcilutites, marbles and metabasalts of the Staveley Formation, and immediately adjacent to the Mt Dore Granite. Brecciation, alteration and hydrothermal activity is associated with movement along the Mount Dore Fault Zone.

Early alteration produced K-feldspar (or biotite), tourmaline, sericite and quartz with later alteration dominated by dolomite, calcite, apatite and chlorite. Thus the deposit sequence lithologies and the alteration products are similar to those found at Greenmount.

Sulphide mineralisation is associated temporally with carbonate alteration. Primary sulphide minerals are pyrite and chalcopyrite with minor sphalerite and galena. Fluid inclusion data from Mount Dore are similar to results from Greenmount with hot ($>500^{\circ}\text{C}$), oxidised, hypersaline, CO_2 bearing inclusions, possibly of metamorphic or magmatic origin.

Beardsmore (1992) interprets that after initial separation and loss of a CO_2 -rich phase, the residual aqueous fluid became more dilute with time, probably by mixing with cooler, less saline, low CO_2 fluids possibly also of metamorphic origin. Early potassic and silicic alteration released Cu, Pb, Zn, Ag, Co, U, Au to the fluid from host rocks during dilation and hydraulic brecciation associated with movements on the Mount Dore Fault Zone. Sulphide precipitation was controlled by sulphate reduction with carbon released from host. Pyrite scavenged most of this and later Cu - Pb - and Zn - sulphides formed by scavenging of sulphur from pyrite.

Beardsmore (1993) concludes that epigenetic mineralisation across the Cloncurry Fold Belt appears to be the result of large-scale devolatilisation of the crust during waning stages of regional deformation and metamorphism, and that the characteristics of individual deposits depends on the combination of local factors such as structure and rock-types available adjacent to these structures for leaching of metals.

The Hampden group of deposits are located approximately 20 km south of Greenmount within a series of interlayered black shale, siltstone and concordant amphibolite sills of the Kuridala

Formation which are less than 100 m from a package of quartzites and schists. Mineralisation is focused along a complex zone of dilation and brecciation controlled by strike slip fault movements.

The main 1 - 20 m thick massive sulphide zone is enclosed by brecciated, tourmalinised and potassified (mainly biotite) shale and silicified and quartz-carbonate-sulphide veined shales with an outer halo of weakly silicified shale containing stockworks of quartz-microcline-pyrite (Derrick, 1994). Derrick (1994) suggests that the strong potassic alteration, tourmalinisation and some minor fluorite may indicate some granitic fluid input into the mineralisation. This deposit shares some similar alteration and veining characteristics as well as proximity to mafic intrusives, to Greenmount, but does not appear to be located near the Staveley Formation, however the protolith to the hangingwall quartzites and schists, is not known and may have possibly once been evaporitic in character.

Several other Greenmount type deposits, showing similar alteration and veining parageneses are the Notlor and Victory deposits. Both are located within altered carbonaceous shales of the Soldiers Cap Group. Notlor is significantly enriched in fluorite, and footwall and hangingwall lithologies to the slate comprise monotonous laminated carbonates of the Corella Formation, intruded in parts by dolerites.

Kuridala, Notlor and Victory deposits, illustrate that it is not specifically the Marimo Slate which is unique in hosting this deposit-style and that any carbonaceous slate may be prospective.

Similarly the role of the Staveley Formation as a source of metals (particularly gold) becomes questionable, as it is not present at some of these deposits. At Greenmount, the Staveley Formation may have acted as a relatively porous fluid conduit for metamorphic, metasomatic and mineralising fluids, and supplied some of the major elements (and possibly some remobilised copper and cobalt). It also served to act as a redox contrast compared to the carbonaceous slates and the abundant carbonates present would have buffered any low pH fluids. The reddened and oxidised nature of the Staveley Formation possibly explains why it is apparently not mineralised in the Greenmount system and confirms the importance of a

reducing host required for mineral deposition of the high log fO_2 fluids, which were probably in the hematite stability field. Similarly, the mafic intrusives may supply a source of Cu - Co \pm Au (cf Blackbird deposit and Bidjovagge deposit) or may be incidental (cf Kuridala, Notlor, Muruntau) and simply a product of larger tectonostratigraphic processes.

In conclusion, the source of gold and possibly some of the other metals is interpreted to be from an as yet unidentified granitic intrusive which is related to a late, post-peak metamorphic, highly fractionated phase of the Williams Batholith, and is probably non-magnetic. It may or may not be petrogenetically related to the Greenmount diorite. In a waning metamorphic regime, and under high salinity conditions, such a fluid may travel a substantial distance from its source, particularly through an oxidised porous host such as the Staveley Formation which underwent diagenetic alteration and oxidation. The most fundamental controls on metal deposition were redox contrasts, availability of pre-existing wallrock sulphur, fluid mixing with a lower salinity and lower temperature fluid, thereby achieving a drop in temperature and salinity, as well as structural dilation.

BIBLIOGRAPHY

- ANDERSON, T.F., KRUGER, J. AND RAISWELL, R., 1987. C-S-Fe relationships and the isotopic composition of pyrite in the New Albany Shale of the Illinios Basin, USA *Geochimica Acta* 51, 2795-2805.
- ANDREW, A.S., HEINRICH, C.A., WILKINS, R.W.T., PATTERSON, D.J., 1989. Sulfur isotope systematics of copper ore formation at Mount Isa, Australia. *Econ. Geol.* 84: 1614-1627.
- ANNELS, A.E., 1989. Ore genesis in the Zambian Copper Belt, with particular reference to the northern sector of the Chambishi Basin. In: Sediment hosted copper deposits. Ed. by R.W. Boyle, A.C. Brown, C.W. Jefferson, E.C. Jowett and R.V. Kirkham. *Geol. Assoc. of Canada. GAC Special Paper* 36.
- BARNES, H.L., 1979. Solubilities of ore minerals. In Barnes, H.L. (ed.), *Geochemistry of hydrothermal ore deposits*. Wiley Interscience: 404-460.
- BEARDSMORE, T.J., 1992. Petrogenesis of the Mount Dore-style breccia-hosted copper \pm gold mineralisation in the Kuridala-Selwyn region of north-western Queensland; *Unpublished PhD thesis, James Cook University of north Queensland*.
- BEARDSMORE, T.J., NEWBERRY, S.P., & LAING, W.P., 1988. The Maronan Supergroup - an inferred early volcanosedimentary rift sequence in the Mount Isa Inlier, and its implications for ensialic rifting in the Middle Proterozoic of northwest Queensland. *Precambrian Research* 40/41, 487-507.
- BELL, T.H., 1983. Thrusting and duplex formation at Mount Isa, Queensland, Australia. *Nature* 304, 493-497.
- BERGER, B., 1992. Mining the mystery at Muruntau. *USGS Mineral Resources Newsletter*; Vol 3, No 2.
- BLAINEY, G., 1970. Mines in the Spinifex. *Angus and Robertson, Sydney*.
- BLAKE, D.H., & STEWART, A.J., 1992. Stratigraphic and tectonic framework, Mount Isa Inlier. In: STEWART, A.J., & BLAKE, D.H. (Editors), Detailed Studies of the Mount Isa Inlier. *Bureau of Mineral Resources, Australia, Bulletin* 243.
- BLAKE, D.H., 1982. A review of the Corella Formation, Mount Isa Inlier, Queensland. *BMR Journal of Australian Geology & Geophysics*, 7, 113-118.
- BLAKE, D.H., 1987. Geology of the Mount Isa Inlier and environs, Queensland and Northern Territory - 1:500 000 scale.

- BLAKE, D.H., 1987. Geology of the Mount Isa Inlier and environs, Queensland and Northern Territory. *BMR geology and geophysics, Bulletin 225*, pp. 83.
- BLAKE, D.H., 1992. Documentation and significance of a major unconformity in the Wonga Belt of the Mount Isa Inlier, northwest Queensland. *Australian Journal of Earth Sciences*.
- BLAKE, D.H., AND PAGE, R.W., 1988. Early Proterozoic migmatitic basement in the Kalkadoon-Leichhardt Belt of the Mount Isa Inlier, northwestern Queensland. *BMR. Journal of Australian Geology and Geophysics*, v.10: 323-328.
- BLAKE, D.H., BULTITUDE, R.J., DONCHAK, P.J.T., WYBORN, L.A.I., & HONE, I.G., 1984. Geology of the Duchess-Urandangi region Mount Isa Inlier, Queensland: *Australian Bureau of Mineral Resources Bulletin 219*, 96p.
- BLAKE, D.H., JAQUES, A.L., & DONCHAK, P.J.T., 1983. 1:100 000 geological map commentary Selwyn Region Queensland: *Australian Bureau of Mineral Resources, Canberra*, 29p.
- BORISENKO, A.S., 1977. Cryometric technique applied to studies of the saline composition of solution in gaseous fluid inclusions in minerals. *Akad. Nauk SSSB Sib. Otdel., Geol. I. Geofiz*, V8: 16-27 (in Russian; English abstract).
- BORTKIKOV, N.S., GENKIN, A.D., DOBROVOL'SKAYA, M.G., MURAVITSKAYA, G.N. AND FILIMONOVA, A.A., 1991. The nature of chalcopyrite inclusions in sphalerite: Exsolution, coprecipitation, or "disease"? *Economic Geology*, v.86: 1070-1082.
- BOZZO, A.T., R. CHEN AND A.J. BARDUHN, 1973. The properties of hydrates of chlorine and carbon dioxide in *Fourth international Symposium on Fresh Water from the Sea*, A. Delyannis and E. Delyannis, Eds., v. 3, p. 437-451.
- BRESCIANINI, R.F., ASTEN, M.W., and McLEAN, N., 1992. Geophysical characteristics of the Eloise Cu-Au deposits, NW Queensland: *Exploration Geophysics*, v. 23, p. 33-42.
- BUDAI, J., LOHMANN, K., WILSON., 1987. Dolomitisation of the Madison Group, Wyoming and Utah Overthrust Belt. *AAPG Bull.*; 71:909-924.
- BULTITUDE, R.J., GARDNER, C.M. AND NOON, T.A., 1977. A recently discovered unconformity near the base of the Proterozoic Cloncurry Complex south of Mount Isa, northwestern Queensland. *BMR. Journal of Australian Gology and Geophysics*, v. 2: 311-314.
- CANNELL, J., 1994. Geology and genesis of the Great Australia Deposit, North Queensland. *Unpublished Bsc. (Hons) Thesis, University of Tasmania*.
- CARR, G. AND SMITH, J., 1975. A comparative isotopic study of the Lady Loretta zinc-lead-silver deposit. *Mineral. Dep.*;10: 269-276.

- CARR, G., SMITH, J., 1977. A comparative isotopic study of the Lady Loretta zinc-lead silver deposit. *Mineral. Deposita* 12: 105-110.
- CARTER, E.K., BROOKS, J.H., & WALKER, K.R., 1961. The Precambrian mineral belt of north-western Queensland. *Bureau of Mineral Resources, Australia, Bulletin* 61.
- CAS, R.A.F., 1983. Palaeogeographic and tectonic development of the Lachlan fold belt of southeastern Australia: *Geological Society of Australia, Special publication*, 10.
- CHAMBERS, L.A., 1982. Sulfur isotope study of modern intertidal environment and the interpretation of ancient studies. *Geochim. Cosmochim. Acta*, 46, 721-728.
- CHAUSSIDON, M., ALBAREDE, F. AND SHEPPARD, S.M.F., 1989. Sulphur isotope variations in the mantle from ion microprobe analyses of micro-sulphide inclusions. *Earth Planet. Sci. Lett.*, 92, 144-156.
- CLAYPOOL, G.E., HOLSER, W.T., KAPLAN, I.R., SAKAI, H. AND ZAK, I., 1980. The age curves of sulfur and oxygen isotopes in marine sulfate and their mutual interpretation. *Chemical Geol.*, 28, 199-260.
- COLEMAN, M.L., 1977. Sulphur isotopes in petrology. *f. Geol. Soc. Lond.*, 133, 593-608.
- COLLINS, P.L.F., 1979. Gas hydrates in fluid inclusions and the use of freezing for estimation salinity. *Econ Geol.*, v. 74, p. 1435-1444.
- COX, K.G., BELL, J.D. AND PANKHURST, R.J., 1979. The interpretation of igneous rocks. *George, Allen and Unwin, London*.
- COX, S.F., ETHERIDGE, M.A., CAS, R.A.F. AND CLIFFORD, B.A., 1991. Deformational style of the Castlemaine area, Bendigo - Ballarat Zone: implications for evolution of the crustal structure across southeast Australia: *Australian Journal of Earth Sciences*, v.38, p.151-170.
- CRAWFORD, M.L., 1983. Phase equilibria in aqueous fluid inclusions. In Hollister, L.S. and Crawford, M.L. (editors), *Fluid inclusions: Applications to Petrology. Mineralogical Association of Canada Short Course Handbook*, v.6: 75-100.
- CROOKES, R.A., 1993. The gology of the host lithologies to the enigmatic gold mineralisation at the Tick Hill deposit, N.W. Queensland: Symposium on Recent Advances in the Mount Isa Block. *Australian Institute of Geoscientists Bulletin*. 13, p. 43-45.
- DAVIDSON, G.J., 1988. Types of tourmaline and expoloration applications in the Selwyn District. University of Tasmania: *Proterozoic gold-copper project - Workshop Manual No. 2*, December, 1988: 143-159.

- DAVIDSON, G.J., LARGE, R., KARY, G., and OSBORNE, R., 1989. The BIF-hosted Starra and Trough Tank Au-Cu mineralization: a new stratiform association from the Proterozoic eastern succession of Mt. Isa, Australia: *Econ. Geol. Monograph*, 6, p. 135-150.
- DAVIDSON, G.J., 1989. Starra and Trough Tank : Iron - Formation - Hosted Gold - Copper Deposits of North - West Queensland, Australia. *Unpublished PhD Thesis, University of Tasmania*.
- DAVIDSON, G.J., AND DIXON, G.H., 1992. Two sulphur isotope provinces deduced from ores in the Mount Isa Eastern Succession. *Mineral Deposita* 27, 30-41.
- DEER, W.A., HOWIE, R.A. AND ZUSSMAN, J., 1966. An introduction to the rock-forming minerals. *Longman*: 528 pp.
- DERRICK, G.M., WILSON, I.H. AND HILL, R.M., 1976a. Revision of stratigraphic nomenclature in the Precambrian of northwestern Queensland. I. Tewinga Group. *Queensland Government Mining Journal*, v.77: 97-102.
- DERRICK, G.M., WILSON, I.H. AND HILL, R.M., 1976b. Revision of stratigraphic nomenclature in the Precambrian of northwestern Queensland. II. Haslingden Group. *Queensland Government Mining Journal*, v.77: 300-306.
- DERRICK, G.M., WILSON, I.H. AND HILL, R.M., 1976c. Revision of stratigraphic nomenclature in the Precambrian of northwestern Queensland. III. Mount Isa Group. *Queensland Government Mining Journal*, v77: 403-405.
- DERRICK, G.M., WILSON, I.H. AND HILL, R.M., 1976d. Revision of stratigraphic nomenclature in the Precambrian of northwestern Queensland. IV. Malbon Group. *Queensland Government Mining Journal*, v77: 515-517.
- DERRICK, G.M., WILSON, I.H. AND HILL, R.M., 1976e. Revision of stratigraphic nomenclature in the Precambrian of northwestern Queensland. V. Soldiers Cap Group. *Queensland Government Mining Journal*, v77: 601-604.
- DERRICK, G.M., WILSON, I.H. AND HILL, R.M., 1977a. Revision of stratigraphic nomenclature in the Precambrian of northwestern Queensland. VI. Mary Kathleen Group. *Queensland Government Mining Journal*, v78: 15-23.
- DERRICK, G.M., WILSON, I.H. AND HILL, R.M., 1977b. Revision of stratigraphic nomenclature in the Precambrian of northwestern Queensland. VII. Mount Albert Group. *Queensland Government Mining Journal*, v78: 113-116.
- DERRICK, G.M., 1980. Marraba, Qld 1:100,000 scale, *BMR Canberra*.

- DERRICK, G.M., 1976. Some insights into old and new zinc mineralization at Dugald River and Squirrel Hills, and uranium at Mary Kathleen, Queensland. *BMR Journal of Australian Geology & Geophysics*, 1, 251.
- DERRICK, G.M., WILSON, I.H., & HILL, R.M., 1977. Revision of stratigraphic nomenclature in the Precambrian of northwestern Queensland. VII: Mount Albert Group. *Queensland Government Mining Journal*, 78, 113-116.
- DERRICK, G.M., 1994. Summary Report on mineral deposits of the Mt Isa Inlier. *Unpublished compilation by G.M. Derrick*.
- DONCHAK, P.J.T., BLAKE, D.H., JAQUES, A.L., and NOON, T.A. 1983. The geology of the Kuridala Region 1:100,000 scale, *BMR Canberra*.
- ELDRIDGE, C.S., COMPSTON, W., WILLIAMS, I.S., BOTH, R.A., WALSHE, J.L. AND OHMOTO, H., 1988. Sulfur isotope variability in sediment-hosted massive sulfide deposits as determined using the ion-microprobe, SHRIMP: I. An example from the Rammelsberg orebody. *Econ. Geol.*, 83, 443-449.
- ELLIS, D.J., & WYBORN, L.A.I., 1984. Petrology and geochemistry of Proterozoic dolerites from the Mount Isa Inlier. *BMR Journal of Australian Geology & Geophysics*, 9, 19-32.
- ERA - MAPTEC, 1994a. Structural Interpretation of the Marimo Basin, Cloncurry Mapping Project, North Queensland. *Unpublished report completed for Homestake Gold of Australia Ltd*.
- ERA - MAPTEC, 1994b. Structural analysis of the Greenmount Au-Cu-Co orebody, Marimo Basin, Queensland. *Unpublished report completed for Homestake Gold of Australia Ltd*.
- EXLEY, R.A., MATTEY, D.P., CLAGUE, D.A. AND PILLINGER, C.T., 1986. Carbon isotope systematics of a mantle 'hot-spot': a comparison of Loihi seamount and MORB glasses. *Earth Planet. Sci. Lett.*, 78, 189-199.
- FAURE, G., 1986. Principles of isotope geology. 2nd edition, Wiley, New York.
- FIELD, C.W. AND FIFAREK, R.H., 1986. Light stable isotope systematics in the epithermal environment. In: Berger, B.R. and Bethke, P.M. (eds.), *Geology and geochemistry of epithermal systems*. Society of Economic Geologists, Rev. Econ. Geol., 2, 99-128.
- FORCE, E.R., EIDEL, J.J., and MAYNARD, J.B. Sedimentary and Diagenetic Mineral Deposits: A basin Analysis approach to Exploration. *Reviews in Geology*, Volume 5.
- GARLICK, W.G., 1981, Sabkhas, skumping, and compaction at Mufulira, Zambia: *Economic Geology*, v. 76, pp. 1817-1832.

- GARLICK, W.G., 1989. Genetic Interpretation from Ore Relations to Algal Reefs in Zambia and Zaire in Sediment-hosted Stratiform Copper Deposits Ed. by R.W. Boyle, A.C. Brown, C.W. Jefferson, E.C. Jowett and R.V. Kirkham. *Geol. Assoc. of Canada. GAC Special Paper* 36.
- GAUTIER, D.L., 1985. Interpretation of early diagenesis in ancient marine sediments. In: Relationship of Organic Matter and Mineral Diagenesis. Society of Economic Palcontologists and Mineralogists Short Course 17, 6-78.
- GOLDFARB, R.J., LEACH D.L., Rose, S.C., Landis, G.P., 1989. Fluid inclusion geochemistry of gold-bearing quartz veins of the Juneau gold belt, Southwestern Alaska. *Econ. Geol. Monogr.* 6:363-375.
- GOLDFARB, R.J., NEWBERRY, R.J., PICKTHORN, W.J., GENT, C.A., 1991. Oxygen, hydrogen, and sulfur isotope studies in the Juneau Gold Belt, south-eastern Alaska: constraints on the origin of hydrothermal fluids. *Econ. Geol.* 86: 66-80.
- GRAHAM, C.M. AND HARMON, R.S., 1983. Stable isotope evidence on the nature of crust-mantle interactions. In: Hawkesworth, C.J. and Norry M.J. (eds.), *Continental basalts and mantle xenoliths*. Shiva, Nantwich, pp. 20-45.
- GRAY, D.R., 1988. Structure and tectonics, In: Geology of Victoria: *Geological Society of Australia*, Melbourne, p.1-36.
- GRAY, D.R. AND WILLMAN, C.E., 1991. Deformation in the Ballarat Slate Belt, central Victoria, and implications for the crustal structure across southeast Australia: *Australian Journal of Earth Sciences*, v.38, p.171-201.
- HAGEMANN, S.G., GROVES, D.I., RIDLEY, J.R. AND VEARNCOMBE, J.R., 1992. The Archaean lode-gold deposits at Wiluna, Western Australia: high level brittle-style mineralisation in a strike-slip regime. *Economic Geology*, 87, 1022-1053.
- HAGEMANN, S.G., AND RIDLEY, J.R., 1993. Hydrothermal fluids in epi- and katazonal crustal levels in the Archaean: implications for P-T-X-t evolution of lode-gold mineralisation. In: Williams, P.R. and Haldane, J.A. (compilers). An international conference on crustal evolution, metallogeny and exploration of the Eastern Goldfields, Extended Abstracts, *Australian Geological Survey Organisation, Record*, 1993/54, 123-130.
- HALBACH, P. AND 17 OTHER AUTHORS, 1989. Probable modern analogue of Kuroko-type massive sulphide deposits in the Okinawa Trough back-arc basin. *Nature*, 338, 496-499.
- HATTORI, K., 1989. Barite-celestine intergrowths in Archaean plutons: the product of oxidising hydrothermal activity related to alkaline intrusions. *Amer. Mineral.*, 74, 1270-1277.

- HEDENQUIST, J.W., AND HENLEY, R.W., 1985. The importance of CO₂ on freezing point measurements of fluid inclusions: Evidence from active geothermal systems and implications for epithermal ore deposition: *Econ. Geol.* v: 80, p. 1379-1406.
- HILL, E.J., LOOSVELD, R.J.H. AND PAGE, R.W., 1992. Structure and geochronology of the Tommy Creek Block, Mount Isa Inlier. In: Stewart, A.J. and Blake, D.H. (Editors). Detailed studies of the Mount Isa Inlier. *Bureau of Mineral Resources, Australia, Bulletin* 243.
- HO, S.E., BENNETT, J.M., CASSIDY, K.F., HRONSKY, J.M.A., MIKUCKI, E.J. AND SANG, J.H., 1990. Nature of ore fluid, and transportational and depositional conditions in sub-amphibolite facies deposits. In Ho, S.E., Groves, D.I. and Bennett, J.M., (Editors). Gold deposits of the Archaean Yilgarn block, Western Australia: nature, genesis and exploration guides. The *University of Western Australia, Geology Department and University Extension, Publication*, 20, 198-211.
- HOEFS, J., 1987. *Stable isotope geochemistry*. 3rd edition, Springer-Verlag, Berlin.
- HOLCOMBE, R.J., PEARSON, P.J., & OLIVER, N.H.S., 1992. Structure of the Mary Kathleen Fold Belt. In: STEWART, A.J., & BLAKE, D.H. (Editors), Detailed Studies of the Mount Isa Inlier. *Bureau of Mineral Resources, Australia, Bulletin* 243, p257-288.
- HOMESTAKE, 1989. Report on research of Mining Wardens' Reports for the period 1867 to 1940.
- HOMESTAKE, 1988-1994. *Various unpublished internal Monthly Reports*.
- HURST, R.W., 1989. Geochemical and isotopic constraints on silica and carbonate diagenesis in the Miocene Monterey Formation, Santa Maria and Venture basins, California. In: *Developments in sedimentology* 47. *Diagenesis III* (Editors K.H. Wolf and G.V. Chilgarian). P 387-434.
- HUSTON, D.L., POWER, M. AND LARGE, R.R., 1992. Laser ablation sulphur isotope analysis at the University of Tasmania - preliminary results from a new technique with research and exploration applications. *Bull. Geol. Surv. Tasmania*. 70:93-95.
- JOYCE, A.S., 1993. Petrological report on a suite of samples from the Cloncurry District. *Unpublished report prepared for Homestake Australia Limited*.
- KARY, G.L., and HARLEY, R.A., 1990. Selwyn gold-copper deposits. In, Hughes F.E., ed., *Mineral Deposits of Australia and Papua New Guinea*. AusIMM, Melbourne. p. 955-960.

- KERRIDGE, J.F., HAYMON, R.M. AND KASTNER, M., 1983. Sulfur isotope systematics at the 21°N site, East Pacific Rise. *Earth Planet. Sci. Lett.*, 66, p91-100.
- KERRIDGE, J.F., 1985. Carbon, hydrogen and nitrogen in carbonaceous chondrites: abundances and isotopic compositions in bulk samples. *Geochim. Cosmochim. Acta*, 49, 1707-1714.
- KORZHINSKIY, M.A., 1981. Apatite solid solutions as indicators of the fugacity of HCl° and HF° in hydrothermal fluids. *Geochemistry International*, v. 18(3): p44-60.
- KOTOV, N.V., and PORITSKAYA, L.G., The Muruntau Gold Deposit: Its Geologic Structure, Metasomatic Mineral Associations and Origin. *International Geology Reviews*, 1992, 34, No 1, pp. 77-87.
- KRUGER, J. and RAISWELL, R., 1987. C-S-Fe relationships and the isotopic composition of pyrite in the New Albany Shale of the Illinois Basin, USA. *Geochimica et Cosmochimica Acta* 51, p2795-2805.
- LAING, W.P., and BEARDSMORE, T.J., 1986. Stratigraphic rationalisation of the eastern Mount Isa block, recognition of key correlations with Georgetown and Broken Hill blocks in an eastern Australian Proterozoic terrain, and their metallogenic implications. *Eighth Australian Geological Convention, Geological Society of Australia, Adelaide, Abstracts* 15, 163-164.
- LARGE, R.R., 1975. Zonation of hydrothermal minerals at the Juno Mine, Tennant Creek goldfield, Central Australia. *Econ. Geol.* 70: 1387-1413.
- LARSEN, R.B., BROOKS, C.K. AND BIRD, D.K., 1992. Methane-bearing, aqueous, saline solutions in the Skaergaard intrusion, east Greenland. *Contributions to Mineralogy and Petrology*, 112, 428-437.
- LIEBENBERG, L., 1970. The sulfides in the layered sequence of the Bushveld Complex. *Geol. Soc. South Africa, Spec. Pub.* 1, 108-207.
- LIGHT, M.P.R., AND POSEY, H.H., 1989. Diagenesis and its relation to mineralisation and hydrocarbon reservoir development: Gulf Coast and North Sea basins. In: *Developments in Sedimentology* 47. Diagenesis III p 435-510 (Editors K.H. Wolf and G.V. Chilgarian).
- LINKE, W.G., 1965. *Solubilities of inorganic and metal compounds*, 4th edition: American Chemical Society, v.1 and 2: 1050p.
- LOOSVELD, R.J.H., 1988 - Structure and tecton-thermal history of the eastern Mount Isa Inlier, Australia. *Unpublished Ph.D. thesis, Australian National University*.
- LOOSVELD, R.J.H., 1989. The intra-cratonic evolution of the central eastern Mount Isa Inlier, northwest Queensland, Australia. *Precambrian Research* 44, 243-276.

- LOOSVELD, R.J.H., 1992. Structural geology of the central Soldiers Cap Belt, Mount Isa Inlier, Australia. In: Stewart, A.J. and Blake, D.H., eds. Detailed Studies of the Mount Isa Inlier, *AGSO Bulletin* 243, p.349-359.
- LUZHNAYA, N.P. AND VERESHTCHETINA, I.P., 1946. Sodium, calcium, magnesium chlorides in aqueous solutions at -57 to +25° (polythermic solubility). *Zhurnl. Prikl. Khimii*, v.19: 723-733.
- MARAKUSHEV, A.A., and KHOKHLOV, V.A., 1992. A Petrological Model for the Genesis of the Muruntau Gold Deposit. *International Geology Review*, 1992, 34, No 1. pp. 59-76.
- MASON, D.R., 1994. Petrographic and mineralogical studies on a suite of eight samples, Northwestern Queensland. *Unpublished report to Homestake Gold of Australia Limited*.
- McKINLAY, J., ca. 1863. McKinlay's Journal of Exploration in the interior of Australia. *Melbourne, Bailliere*.
- McLEAN, G. and BENJAMIN, P., 1993. The geology and development of the Mount Elliot copper-gold deposit: *Symposium on Recent Advances in the Mount Isa Block. Australian Institute of Geoscientists Bulletin no. 13*, p. 47-54.
- MERNAGH, T.P. AND WITT, W.K., 1994. Early, methane-rich fluids and their role in Archean gold mineralisation at the Sand King and Missouri deposits, Eastern Goldfields Province, Western Australia. *AGSO Journal of Aust. Geol. and Geophy.* v.15: 297-312.
- MILNER, S., 1993. The Paddock Lode - Great Australia Cu-Au prospect: In Derrick, G., ed. Core Shack Explanatory Notes, AMF Course 832/93, *Australian Mineral Foundation*, Glenside, SA. p. 46-48.
- MUIR, M.D., 1979. A sabkha model for the deposition of part of the Proterozoic McArthur Group of the Northern Territory, and its implication for mineralisation. *BMR Journal of Australia Geol. and Geophys.*; 4: 149-162.
- MUIR, M.D., 1981. Depositional environments of host rocks to northern Australian lead-zinc deposits, with special reference to McArthur River. *Min. Assoc. Canada, Short Course Notes*; Sediment-hosted stratiform Pb-Zn deposits.; 9: 141-174.
- MUIR, M., DONNELLY, T., WILKINS, R. AND ARMSTRONG, K., 1987. Stable isotope, petrological and fluid inclusion studies of minor mineral deposits from the McArthur Basin, implications for the genesis of some sediment-hosted base-metal mineralisation from the N.T. *Aust. J. of Earth Sci.*; 32: 239-260.
- MUMIN, A.H., FLEET, M.E., and CHRYSOULIS, S.L., 1994. Gold mineralisation in As-rich mesothermal gold ores of the Bogoso-Prestea mining district of the Ashanti Gold Belt, Ghana: remobilisation of "invisible" gold. *Mineral Deposita* 29, 445-460.

- NAYLOR, H., TURNER, P., VAUGHAN, D.J., BOYCE, A.J. AND FALLICK, A.E., 1989. Genetic studies of redbed mineralisation in the Triassic of the Cheshire basin, northwest England. *f, Geol. Soc. Lond.*, 146, 685-699.
- NEWBERRY, S., 1991. Iron formation hosted base metal mineralisation in the Cloncurry Terrane, Mount Isa Inlier: *James Cook University Economic Geology Research Unit Contribution* n. 38, p. 89-99.
- OHMOTO, H. AND RYE, R.O., 1979. Isotopes of sulphur and carbon. In: Barnes, H.L. (Editors), *Geochemistry of hydrothermal ore deposits*. Wiley Interscience: 509-567.
- OHMOTO, H., 1986. Stable isotope geochemistry of ore deposits. In: Valley, J.W., Taylor, H.P. and O'Neil, J.R. (eds.), *Stable isotopes and high temperature geological processes. Reviews in Mineralogy* 16, *Mineral. Soc. Amer.*, pp. 460-491.
- OLIVER, N.H.S., HOLCOMBE, R.J., HILL, E.J., & PEARSON, P.J., 1991. Tectono-metamorphic evolution of the Mary Kathleen Fold Belt, northwest Queensland: a reflection of mantle plume processes? *Australian Journal of Earth Sciences* v. 38, p. 425-455.
- ONUMA, N., CLAYTON, R.N. AND MAYEDA, T.K., 1972. Oxygen isotope cosmo-thermometer. *Geochim, Cosmochim. Acta*, 36, 169-188.
- ORESKE, N. AND EINAUDI, M.T., 1992. Origin of Hydrothermal and fluids at Olympic Dam. Preliminary results from fluid inclusions and stable isotopes. *Econ. Geol.* v.87, 64-90.
- PAGE, R.W., 1983. Timing of superposed volcanism in the Proterozoic Mount Isa inlier, Australia. *Precambrian Research*, v.21: 223-245.
- PAGE, R.W. and LAING, W.P., 1992. Felsic metavolcanic rocks related to the Broken Hill Pb-Zn-Ag orebody, Australia: geology, depositional age and timing of high grade metamorphism. *Econ. Geol.* v. 87, p. 2138-2168.
- PAGE, R.W., & BELL, T.H., 1986. Isotopic and structural response of granite to successive deformation and metamorphism. *Journal Geol.*, v. 94, p.365-379.
- PAGE, R.W., 1978. Response of U-Pb zircon and Rb-Sr total rock and mineral systems to low-grade regional metamorphism in Proterozoic igneous rocks, Mount Isa, Australia. *Journal of the Geological Society of Australia* 25, 141-164.
- PAGE, R.W., 1988. Geochronology of Early to Middle Proterozoic fold belts in northern Australia: a review. *Precambrian Research* 40/41, 1-19.
- PAGE, R.W., 1993. Geological constraints given by U-Pb zircon geochronology in the Mount Isa Inlier. Symposium on Recent Advances in the Mount Isa Block. *Australian Institute of Geoscientists Bulletin* 13, p.13-15.

- PASSCHIER, C.W., 1986. Evidence for early extensional tectonics in the Proterozoic Mount Isa Inlier, Australia. *Geology* 14, 1008-1011.
- PEARSON, P.J., HOLCOMBE, R.J., & PAGE, R.W., 1992 - Synkinematic emplacement of the Middle Proterozoic Wonga Batholith into a mid-crustal extensional shear zone, Mount Isa Inlier, Queensland, Australia. In: STEWART, A.J., & BLAKE, D.H. (Editors), Detailed Studies of the Mount Isa Inlier. *Bureau of Mineral Resources, Australia, Bulletin* 243, p289-328.
- PHILLIPS, G.N., GROVES, D.I., NEALL, F.B., DONNELLY, T.H., LAMBERT, I.B., 1986. Anomalous sulfur isotope compositions in the Golden Mile, Kalgoorlie. *Econ. Geol. (Sci. Comm.)* 81:2008-2015.
- PHILLIPS, G.N. AND HUGHES, M.J., 1995. Victorian Gold: A sleeping giant. *SEG Newsletter No. 21*, p. 1-9.
- PHILLIPS, G.N. AND POWELL, R., 1993. Link between gold provinces: *Economic Geology*, v.88, p.1084-1098.
- POTTER, R.W., II and CLYNNE, M.A., 1978. Solubility of highly soluble salts in aqueous media - Part I: NaCl, KCl, CaCl₂, Na₂SO₄ and K₂SO₄. *United States Geological Survey Journal of Research*, v.6(6): 701-705.
- POTTER, R.W., II. AND CLYNNE, M.A., 1978. Solubility of highly soluble salts in aqueous media - Part I: NaCl, KCl, CaCl₂, Na₂SO₄ and K₂SO₄. *United States Geological Survey Journal of Research*, v.6(6): 701-705.
- RAMSAY, W.R.H. AND VANDENBERG, A.H.M., 1990. Lachlan Fold Belt in Victoria - regional geology and mineralisation, In: *Geology of the Mineral Deposits of Australia and Papua New Guinea* (Ed. F.E. Hughes), pp. 1269-1273 (The Australasian Institute of Mining and Metallurgy: Melbourne).
- RIPLEY, E.M., 1981. Sulfur isotopic studies of the Dunka Road Cu-Ni deposit, Duluth Complex, Minnesota. *Econ. Geol.* 76, 610-620.
- RICHARDSON, G.K., RYE, R.O. AND WASSERMAN, M.D., 1988. The chemical and thermal evolution of the fluids in the Cave-in-rock fluorspar district, Illinois: stable isotope systematics at the Deardorff mine. *Econ. Geol.*, 83, 765-783.
- ROCHE, M.T., 1994. The Cannington silver-lead-zinc deposit - at feasibility: In, *Proceedings of the Australasian Institute of Mining Metallurgy Annual Conference, Darwin, 5-9 August 1994*, Melbourne, Australasian. Institute of Mining and Metallurgy, p. 193-197.
- ROEDDER, E. AND SKINNER, B.J., 1968. Experimental evidence that fluid inclusions do not leak. *Economic Geology*, v.63: 715-730.

- ROEDDER, E., 1979. Fluid inclusions as samples of ore fluids. In Barnes, H.L. (editor), *Geochemistry of hydrothermal ore deposits*. Wiley Interscience: 684-737.
- ROEDDER, E., AND BODNAR, R.J., 1980. Geologic pressure determinations from fluid inclusion studies: *Ann. Rev. Earth Planet. Sci.*, v. 8, p. 363-301.
- ROEDDER, E., 1984. *Fluid inclusions*. Mineralogical Society of America, *Reviews in Mineralogy*, v.12: 644p.
- RUMBLE, D., III AND HOERING, T.C., 1986. Carbon isotope geochemistry of graphite vein deposits from New Hampshire, USA. *Geochimica et Cosmochimica Acta*, 50, 1239-1247.
- RYBURN, R.J., WILSON, I.H., GRIMES, K.G., & HILL, R.M., 1988. Cloncurry, Queensland 1:100 000 Geological Map Commentary. *Australian Bureau of Mineral Resources, Canberra*, p. 32.
- RYE, R.O. AND OHMOTO, H., 1974. Sulphur and carbon isotopes and ore genesis. *Economic Geology*, v.69: 826-842.
- RYE, D.M. and WILLIAMS, N., 1981. Studies of base metal sulphide deposits at McArthur River, NT, Australia #3: The stable isotope geochemistry of the HYC, Ridge and Cooley deposits. *Econ. Geol.*; 76: 1-26.
- SAKAI, H., CASADEVALL, T.J. AND MOORE, J.G., 1982. Chemistry and isotope ratios of sulfur in basalts and volcanic gases at Kilauea volcano, Hawaii. *Geochim. Cosmochim. Acta*, 46, 729-738.
- SASAKI, A., 1969. Sulfur isotope study intrusion, District of Mackenzie. *Geol. Survey. Can. Paper* 68.
- SANDIFORD, M., KEAYS, R.R., 1986 Structural and tectonic constraints on the origin of gold deposits in the Ballarat Slate Belt, Victoria. In: Keppie, J.D., Boyle, R.W. Haynes, S.J. (eds) Turbidite-hosted Gold deposits. *GAC Special Paper* 32: 15-24.
- SCHIDLOWSKI, M., HAYES, J. AND KAPLAN, I., 1983. Isotopic inferences of ancient biochemistries: carbon, sulphur, hydrogen and nitrogen. In: Schopf J.W. (ed.), *Earths Earliest Biosphere: its origin and evolution.*; ch 7: 149-186.
- SCHIDLOWSKI, M., 1987. Application of stable isotopes to early biochemical evolution on earth, *Ann. Rev. Earth Planet. Sci.*, 15, 47-72.
- SCHREIBER, B.C., 1988 - Evaporites and Hydrocarbons. *Columbia Uni. Press. New York*.
- SCOTT, K.M., SMITH, J.W., SUN, S.-S., TAYLOR, G.F., 1985. Proterozoic copper deposits in NW Queensland, Australia. *Mineral. Deposita* 20: 116-126.

- SCHULTZ, R.B., 1991. Metalliferous Black Shales: Accumulation of Carbon and Metals in Cratonic Basins. *Reviews in Economic Geology*, Volume 5.
- SHEPHERD, T.J., RANKIN, A.H. AND ALDERTON, D.H.M., 1985. A practical guide to fluid inclusion studies. *Blackie (Glasgow)*: 239p.
- SHEPPARD, S.M.F., 1977. The Cornubian batholith, SW England: D/H and $^{18}\text{O}/^{16}\text{O}$ studies of kaolinite and other alteration minerals. *f. Geol. Soc.*, 133, 573-591.
- SISSON, V.B., 1987. Halogen chemistry as an indicator of metamorphic fluid interaction with the Ponder Pluton, Coast Plutonic Complex, British Columbia, Canada. *Contributions to Mineralogy and Petrology*, v.95: 123-131.
- SKRZECYNSKI, R., 1993. From concept to Cannington: a decade of exploration in the eastern succession: Symposium on Recent Advances in the Mount Isa Block. *Australian Institute of Geoscientists Bulletin* n.13, p. 35-37.
- SMITH, J.W. AND CROXFORD, N.J.W., 1975. An isotopic investigation of the environment of deposition of the McArthur mineralisation. *Mineral. Dep.*, 10: 269-276.
- SPEAR, F., 1993. Metamorphic phase equilibria and pressure - temperature - time paths. *Min. Soc. Am. monograph*, p. 799.
- STEWART, J.I., 1991. Proterozoic Geology and Gold Geochemistry of the Marimo Basin area. Cloncurry, NW Queensland. *Unpublished M.Sc. Thesis, James Cook University*.
- STEWART, J.I., 1994. The Role of Evaporitic-Shale Sediment Packages in the Localisation of Copper-Gold Deposits: Copper Canyon Area, Cloncurry. *The AusIMM Annual Conference, Darwin, 5-9 August 1994*.
- STRECKEISEN, A. AND LE MAITRE, R.W., 1979. A chemical approximation to the modal QAPF classification of igneous rocks. *Neues Jahrb, Mineral. Abh.*, 136, 169-206.
- SWEENEY, M.A., BINDA, P.L. and VAUGHAN, D.J., 1991. Genesis of the Ores of the Zambian Copperbelt. *Ore Geology Reviews*, 6, pp. 51-76.
- TAYLOR, H.P., 1974. The application of oxygen and hydrogen isotope studies to problems of hydrothermal alteration and ore deposition. *Econ. Geol.*, 843-883.
- TAYLOR, G.F., SCOTT, K.M., 1976. The geochemistry of ironstones and core samples from the Mount Kelly area, northwest Queensland. *Unpubl. report, CSIRO Mineral Research Laboratories*.
- THODE, H.G. AND MONSTER J., 1965. Sulphur isotope geochemistry of petroleum, evaporites and ancient seas. *Amer. Assoc. Pet. Geol. Mem.*, 4, 367-377.

- UEDA, A. AND SAKAI, H., 1984. Sulphur isotope study of Quaternary volcanic rocks from the Japanese islands arc. *Geochim. Cosmochim. Acta*, **48**, 1837-1848.
- VEIZER, J. AND HOEFS, J., 1976. The nature of O^{18}/O^{16} and C^{13}/C^{12} secular trends in sedimentary carbonate rocks. *Geochim. Cosmochim. Acta*, **40**: 1387-1395.
- WILLIAMS, P.J., AND BLAKE, K.L., 1993. Alteration in the Cloncurry District. Roles of Recognition and Interpretation in Exploration for Cu-Au and Pb-Zn-Ag deposits. *EGRU Contribution* 49.
- WILLIAMS, P.J., AND HEINEMANN, M., 1993. Maramungee: a Proterozoic Zn skarn in the Cloncurry district, Mount Isa Inlier, Queensland, Australia: *Economic Geology*, v. 88, p. 1114-1134.
- WYBORN, L.A.I., 1988. Petrology, geochemistry and origin of a major Australian 1880-1840 Ma felsic volcano-plutonic suite: a model for intracontinental felsic magma generation. *Precambrian Research* 40/41, p 37-60.
- WYBORN, L.A.I., 1992. The Williams and Naraku batholiths, Mount Isa Inlier: an analogue of the Olympic Dam granites? *BMR Research Newsletter*, n.16, p.13-16.
- WYBORN, L.A.I., PAGE, R.W., & McCULLOCH, M.T., 1988. Petrology, geochronology and isotope geochemistry of the post-1830 Ma granites of the Mount Isa Inlier: mechanisms for the generation of Proterozoic anorogenic granites. *Precambrian Research* 40/41, 509-541.
- WYBORN, L.A.I., PAGE, R.W., & PARKER, A.J., 1987. Geochemical and geochronological signatures in Australian Proterozoic igneous rocks. *Geological Society Special Publication* 33, 377-394.
- WYBORN, L.A.I., and HENRICH, C.A., 1993. The relationship between late-tectonic felsic intrusives and Cu-Au mineralisation in the eastern fold belt. Mount Isa Inlier: Symposium on recent advances in the Mount Isa Block. *AIG Bulletin* No. 13, pp. 27-30.
- YANATIEVA, O.K., 1946. Solubility polytherms in the system $CaCl_2$ - $NaCl$ - H_2O and $CaCl_2$ - $MgCl_2$ - H_2O . *Zhur. Prikladnoi Khimii*, v.19: 707-722.
- ZAIRI, N.M., and KURBANOV, N.K., 1992. Isotopic-Geochemical Model of Ore Genesis in the Muruntau Ore Field. *International Geology Review*, 1992, 34, No. 1, pp. 88-94.
- ZIELINSKI, R.A., BLOCH, S., and WALKER, T.R., 1983. The mobility and distribution of heavy metals during the formation of first cycle red beds: *Economic Geology*, v. 78, pp. 1574-1589.

APPENDIX 1

INDEX OF SAMPLES

APPENDIX 2

DRILL HOLE LOGS

HOLE NUMBER GDH-01

DESCRIPTION

MARIMO SHALE

102 - 121 m	Carbonaceous black shale, fissile up to 108 m. 1 - 2% spotting - scapolite (?) pseudomorphed by pyrite (possibly diagenetic pyrite). Rare pyritic fractures <2 mm at 0 - 10° CAA eg. 118.10 m.
121.40 m	Parallel to foliation, see concretionary pyrite after scapolite and 4 mm quartz-feldspar anastomosing network vein with fine grained pyrite selvage (within vein margin). Also trace sericite and chalcocite, accompanied by concentric pyrite to 2 mm.
122 m	Increasing pervasive silicification more quartz-albite veins with pyrite and chalcocite with later thin <1 mm hematite dusted microcline
123.7 to 131.9 m	Moderate to intense pervasive sericite and vein type feldspar alteration. Intense from 123.73 - 124.92 m.
123.2 m	Interval commences with 0° CAA pink microcline-quartz vein with traces of very fine chalcocite, then foliation parallel creamy green pervasive feldspar - sericite with 2% disseminated fine chalcocite. Note the later cross cutting pink microcline with coarser chalcocite.
123.9 m	Intense pervasive creamy white sericite with some pervasive but sometimes crudely banded pink microcline. Brittle fracturing filled by very fine grained massive chalcocite veinlets is dominantly parallel to foliation and chiefly in the creamy sericite alteration. It becomes broken up and chalcocite becomes coarser when in or near the pink microcline vein. Blebs of disseminated chalcopyrite being replaced by chalcocite occur in the creamy alteration and are sometimes streaked out parallel to foliation.
124.50 m	Quartz-albite vein hosts up to 35% chalcocite and 10% pyrite. Chalcopyrite occurs as small disseminated blebs as a halo around the vein. No visible fractures occur near the chalcopyrite.
125.80 m	Occurrence of pink microcline vein subparallel to foliation not associated with creamy alteration but is partly sericitised. Sericitisation occurs as a selvage to fractures in the microcline and commonly contain disseminated chalcocite. Some chalcopyrite blebs occur disseminated in the pink microcline vein.
126.10 m	Note the late barren quartz vein cross-cutting but also incorporating pink microcline and creamy white alteration. It also cross cuts a chalcocite filled fracture.
125.4 m	Note the 3 cm wide (30° CAA) quartz-microcline veinlet. Microcline is mostly on the margins. A bleb of chalcopyrite occurs near the quartz-microcline transition interface. A weakly sericitized selvage forms around the vein. Similar vein at 126.9 m but this appears brecciated and chalcocite fills open space fractures almost exclusively in microcline.
128.4 m	Note early creamy-green albite vein with sharp contact, contains 1% fine disseminated chalcopyrite and some very fine chalcocite in fine fractures at 80° CAA. This has been brecciated/fractured and filled by pink microcline which contains no chalcopyrite but does contain coarser chalcocite. Microcline fractures at low CAA. Note the chalcopyrite/chalcocite adjacent to the zone of bleaching and the microcline fracture. Minor quartz in middle of microcline vein.
130.3 m	Mottled quartz-phlogopite-sericite alteration post-dates foliation parallel bleaching which has been fractured, and contains rare chalcocite, but is itself cut by late quartz-albite vein.

HOLE NUMBER GDH-01

DESCRIPTION

MARIMO SHALE

131.9 to 154.7 m	Moderately silicified black shale which is weakly fissile from 135.0 to 155.5m. Rare epidote, chlorite, pyrite, hematite on foliation surface. CAA foliation 45° - Note the late 3 cm wide massive pyrite-hematite-chalcocite vein at 139.0 m. This 0.6 m interval assays 1.62 g/t Au, 5750 ppm Cu. Hosted by very mildly pyritic black shales. Similarly for interval 141.7 m - 144.7 m (70% core loss) 0.63 g/t Au, 7450 ppm Cu hosted by pyrite/hematite in pyrite black shale.
154.7 to 158.55 m	Patchy late brittle open spaced fracturing, filled with microcline-quartz-phlogopite and chalcocite ± pyrite occasionally with bleached selvage. Minor pyrite trace chalcocite.
158.55 to 161.9 m	Commences with moderate to intense pervasive and vein style sericite-feldspar alteration comprising microcline-quartz-phlogopite-sericite.
(155.55 to 162.0 m)	Note the dominantly pervasive greenish-white sericite - feldspar alteration with blebs of disseminated pyrite-chalcocite-trace chalcopyrite which has subsequently been fractured and veined by chalcocite and pyrite at 158.9 m. This interval assays 0.17 g/t Au and 3450 ppm Cu.
161.9 to 168.8 m	Commences with mostly intense pervasive dominantly albite alteration which has been subsequently fractured and open space filled by chalcocite-pyrite-trace chalcopyrite. This has been re-fractured and filled by late microcline-silica which has a chalcocite selvage eg. 163.9 m. Strongly hematite dusted, brecciated and sericitised with chalcocite-microcline vein at 167.0 m.
168.8 to 175.05 m	Moderately silicified open space fractured black shale with trace disseminated pyrite. Fractures filled by late quartz-microcline ± muscovite veins with trace pyrite. Similar to 154.7 to 158.55 m interval.
175.05 to 179.0 m	Zone of intense Kaolinite-microcline alteration (pervasive). Some disseminated chalcocite and possibly fracture filled chalcocite - arsenopyrite-cobaltite.
179.0 to 180.5 m	Core Loss.

STAVELEY FORMATION

180.5 to 209.95 m (END OF HOLE)	Conspicuously porous, vughy and moderately weathered micaceous metasediment. Possibly originally an evaporitic dololutite/dolosandstone. Strongly brecciated microcline which has been sericitised and Kaolinised from 180.5 to 183 m. Abundant fine grained pyrite blebs and pyrite-chalcocite.
(185.0 to 189.0 m)	Note bedding preserved at 70° CAA load casts and graded bedding younging up hole. Barren quartz vein from 188.14 to 188.4 m then 40 cm gossan.
(188.8 to 189.1 m)	Brecciated metasediment with hematite coated fractures and vughs and rare late cross cutting pyrite veinlets.
(189.1 to 204.0 m)	Abundant dissolution (of carbonate ± halite ?) channels and vughs, sometimes brecciated. Plastic flow and displacement of bedding is common. Opaline silica matrix 200.2 to 201.0 m.
204.0 m	(END OF HOLE) Strongly brecciated metasediment with argyllic matrix. Clast supported. Clasts are often redrock altered or silicified with some open space fracturing filled by feldspar. Also clasts of brecciated quartz.

HOLE NUMBER GDH-02

DESCRIPTION

MARIMO SHALE

108.0 to 109.2 m	Moderately silicified black shale. Open spaced fracturing filled by quartz (with disseminated pyrite and chalcopyrite) and quartz-microcline. Veins and host rock are brecciated.
109.2 - 119.5 m	Intense pervasive and vein type feldspathisation. From 109.2 to 110.45 m note the brecciation of veins and shale and pervasive phyllic alteration.
(110.45 to 113.3 m)	Intense creamy-greenish pervasive feldspar alteration which has been finely fractured. Disseminated pyrite-chalcocite and trace chalcopyrite. Coarser pyrite-chalcocite-chalcopyrite in hairline network of fractures. Note the hematite dusted microcline veining postdates pervasive bleaching and hairline fracturing. These veins are often vuggy, probably from dissolution of calcite and contain veins and local enrichments of (massive) pyrite.
(113.3 to 116.0 m)	Massive (redrock) hematite dusted microcline locally brecciated and filled by pyrite eg. 113.7 - 113.9 m. From 115.0 to 116.0 m hole drilled down a massive pyrite 95% - clay vein with jagged sharp margins. Redrock is vuggy. Vein is barren.
(116.0 to 119.5 m)	Mostly intensely bleached greenish cream plagioclase and sericite alteration. Some vuggy redrock and massive pyrite. Zone is brecciated 118.3 - 119.0 m and contains a clast of "redrock". Matrix is pyrite. Pyrite here is very late (last).
119.5 to 125.80 m	119.5 - 119.6 m Black shale - feldspathic vein breccia. 119.6 - 125.8 m Fractured, moderately silicified black siltstone with open space vein filling increasing in density towards 125.8 m. Minor patchy pervasive bleached greenish sericite-cream-feldspar-silica-disseminated pyrite alteration with hairline fractures filled with pyrite, is veined by late pink microcline-quartz-phlogopite veins which contain rare disseminated pyrite. These veins can be sharp and straight (probably along remnant bedding/foliation) or pygmatic and as open space fracture filling eg. 125.80 m.
125.8 to 128.2 m	Zone of intense brecciation, alteration and mineralisation. Early greenish-yellow ?sericitic clasts with very fine grained disseminated but bedding/foliation parallel ? pyrite with minor hematite staining, brecciated then microcline-phlogopite (minor) veins were emplaced and re-brecciated. Late pyrite-chalcocite forms as matrix, veins and fracture fill-rare chalcopyrite is being replaced by chalcocite.
128.2 to 133.5 m	Dominantly earlier silica-plagioclase pervasive alteration with very fine disseminated pyrite-chalcocite, incipient fracturing filled by pyrite-chalcocite. Some zones are hematite dusted. Zones of pink microcline-quartz postdate pervasive alteration and when brecciated commonly host abundant pyrite and minor chalcocite as stringers and matrix eg. 129.7 m.
(133.1 to 135.5 m)	Moderate to strong pervasive silicification and feldspathisation of shale with abundant hairline fractures. Some disseminated chalcopyrite-bornite-chalcocite but mostly copper sulphides in fine fractures. A late quartz-microcline-phlogopite vein is itself fractured and contains chalcopyrite-chalcocite at 133.45 m.
133.5 to 144.3 m	Weakly to moderately silicified black shale. CAA cleavage ~45°. Very fine disseminated pyrite and cobaltite throughout <<1%. Occasional discontinuous microfractures filled with chalcopyrite, pyrite and ?cobaltite. Occasional quartz-microcline ± pyrite ± chalcopyrite and cobaltite veinlets and open spaced fracture fill occur occasionally. Where these are brecciated or fractured eg. 139.0, 144.9 and 142.1 m chalcopyrite-cobaltite-pyrite content (and grade increases).
144.3 to 149.5 m	Weakly to moderately silicified black shale with increasing brecciated and fractured quartz and quartz-microcline veins with chalcopyrite-pyrite in fractures eg. 145.3, 146.4, 147.4, 147.5, 147.7, 149.3 m note cobaltite at 147.7 m. Muscovite or phlogopite occurs in some of these veins.

HOLE NUMBER GDH-02

DESCRIPTION

MARIMO SHALE

149.5 to 150.5 m	Vein of strongly fractured and brecciated pink microcline with occasional clasts of silicified less fractured siltstone. Fractures and veins and open spaces filled by pyrite-chalcopryrite-(bornite)-chalcocite and rare cobaltite. Some pervasive silicification.
150.5 to 150.7 m	As for 144.3 to 149.5 m interval.
150.7 to 151.2 m	As for 149.5 to 150.5 m interval.
151.2 to 195.0 m	Black shale with pink microcline-quartz ± sulphide veinlets and veins. Moderately silicified throughout. Trace very fine grained pyrite throughout.
(156.0 to 157 m)	Zone of more intense veining comprising brecciated pink microcline and lesser quartz with late pyrite in fractures and matrix. Lesser chalcopryrite-bornite-chalcocite. This is accompanied by an increase in grade i.e. 0.36 g/t Au 0.89% Cu. Relict bedding 65° CAA at 160 m. Note the weakly fractured pink orange microcline vein at 162.30 m cut by a late quartz-pyrite-(chalcopryrite) vein.
(163.0 to 172.0 m)	Zone characterised by more frequent irregular (ghost) veining and open space fracturing. Veins comprise pink-orange microcline-quartz occasionally very weakly fractured. Some phlogopite in veins. Arsenopyrite/cobaltite?, pyrite and trace chalcopryrite occur in the veins. Host black shale is distinctly foliated and weakly sheared, which predates veining.
(180.2 to 181.0 m)	Brecciated and fractured orangey-pink microcline-quartz vein cut by pyrite veinlets and muscovite/phlogopite and massive pyrite matrix and void fill. Pyrite and mica are intergrown.
(181.0 to 195.0 m)	More veining but dominated by quartz-pyrite ± microcline ± chalcopryrite.
195.0 to 199.4 m	Similar to above but silica flooding of flaser bedding (80° CAA) which is sometimes fractured. Some oxidation of sulphides occurs from 194.0 m. Very fine grained pyrite throughout. Note at 198.6 m the late quartz-chalcopryrite-arsenopyrite/cobaltite?-pyrite vein cross cutting earlier silica flooding.

STAVELEY FORMATION

199.4 m to END OF HOLE.	Conformable (?) transition into Staveley Formation. Commences with pervasive silica-feldspar-sericite flooding of weakly bedded ex-dololite? which becomes fractured and filled by pinky-orange microcline-quartz-chalcopryrite-pyrite from 199.5 - 200.0 m. Pyrite gradually disappears around 204 m. Calcite in open spaces and as matrix commences at 202.50 m and becomes matrix to what appears to be a solution collapse breccia of an intensely feldspathised and silicified ex-carbonate rock. Some late calcite fractures are unmineralised. Note the presence of occasional late quartz-tourmaline in thin <2 mm irregular fractures. Light pink manganoan (?) calcite with pyritic stylolite occurs at 213.0m. Relict disturbed bedding 80° CAA near end of hole. Fluorite with pyrite and trace chalcopryrite in vugh 212.9 m.
-------------------------	--

HOLE NUMBER GDH-03

DESCRIPTION

MARIMO SHALE

131.45 to 136.2 m	Moderately silicified and albitised black siltstone with <<1% fine disseminated pyrite and (diagenetic?) chalcopyrite. Weak incipient (hairline) fracturing. Some pyrite-chalcopyrite in fractures. Disseminated rare arsenopyrite/cobaltite usually in or adjacent to late 1-3 mm quartz veins eg. 131.50 m. Chalcopyrite more abundant (1%) in or near zones of pervasive and vein type alteration. Bedding foliation CAA 35°. Note chalcopyrite-pyrite-arsenopyrite/cobaltite in a fine fracture, cross-cutting a vein and pervasive type alteration at 132.15 m. Arsenopyrite/cobaltite also occurs within quartz-microcline-phlogopite veins eg. 132.25 m.
(134.2 to 135.3 m)	Zone of more intense mottled pink-creamy microcline-feldspar-silica-albite-sericite alteration with very fine disseminated pyrite-chalcocite-(chalcopyrite) which has been fractured incipiently and cavity filled by pyrite-chalcopyrite-chalcocite.
136.2 to 137.7 m	Similar to 134.2 - 135.3 m but more fractured with wider pyrite-(chalcopyrite) veins and cavity fill. Chalcopyrite often replaced by chalcocite. Rare cobaltite. Early pervasive plagioclase with vein type albite-microcline-quartz ± sulphides.
137.7 to 140.1 m	Black shale ± early pervasive ? plagioclase with very fine <<1% disseminated pyrite, ± later brick red ? microcline-albite with <1% pyrite (trace chalcopyrite). All weakly fractured with late <1% pyrite (chalcopyrite) cavity and fracture fill eg. 139.30 m.
140.1 to 143.0 m	Mottled pervasive creamy pink plagioclase with very fine grained disseminated pyrite-chalcocite fractured and veined by later microcline-albite? -quartz-phlogopite ± pyrite-chalcopyrite-chalcocite. All fractured with pyrite-chalcopyrite-rare arsenopyrite ± silica in fractures and cavities.
(141.6 to 141.7 m)	Massive pyrite vein. Pyrite is fine grained, anhedral but in spheroidal blebs to 4 mm with quartz filling open spaces and rare fragments of microcline-quartz. Possibly a breccia. Some pale blue oxidation of pyrite? has occurred since exposure to atmosphere possibly an oxide of cobalt or covellite?
143.0 to 145.6 m	Zone of broken core. Similar to previous interval but less sulphide and more clay alteration. Occasional visible arsenopyrite/cobaltite? in fractured late microcline veins eg. 144 m. Probably a fault zone.
145.6 to 150.0 m	Commences with black shale hosting irregular vein 5° CAA. Vein is anastomosing, crudely banded and possibly colloform textured? Feldspar-quartz which itself hosts minor disseminated and late veinlet pyrite-chalcopyrite-cobaltite-chalcocite. This is followed by pervasive creamy green ? plagioclase-sericite alteration with disseminated fine pyrite and trace chalcocite. This has been fractured and veined by pyrite-chalcopyrite-arsenopyrite/cobaltite? often veined by quartz-microcline ± arsenopyrite-chalcopyrite (microcline near margins of vein) and rebrecciated with chalcopyrite-pyrite-cobaltite-chalcocite in fractures and as cavity fill. This last fracturing in the quartz-microcline veinset (minor sulphides) hosts the strongest mineralisation.
150.0 to 152.4 m	Zone of broken core. Similar to 143 - 145.6 m. Note disseminated euhedral cobaltite (early) in a quartz-albite-microcline vein at 150.9 m. This vein is folded and cut by later quartz-rich quartz-microcline veinlet. The vein has a chloritised selvage.
152.4 to 155.6 m	Dominantly black shale with frequent ghosted quartz-microcline veins and veinlets ± pyrite, disseminated cobaltite in veins. Rare disseminated cobaltite near veins in black shale eg. 155.5 m. Note late quartz-pyrite-cobaltite vein 4 mm cross cutting quartz-microcline at 152.5 m.
155.6 to 157.4 m	Similar to 140.1 - 143.0 m interval, but less chalcopyrite.

MARIMO SHALE

158.4 to 160.45 m	As above but strong pervasive chlorite-sericite alteration and intense brecciation of early stage alteration.
160.45 to 167.95m	Speckled, mottled chlorite-plagioclase-biotite-(sericite, quartz) rock-possibly microdiorite. Contains <1% disseminated pyrite. Frequently veined by indistinct quartz-microcline \pm pyrite and later quartz-albite veins \pm pyrite eg. 160.95 m and quartz-calcite \pm pyrite veins eg. 164.90 m. No visible chalcopyrite-arsenopyrite/cobaltite?
167.95 to 168.8 m	Zone of argyllic broken core.
168.8 to 169.0 m	Brecciated fractured quartz-microcline filled with pyrite and brecciated pyrite filled with microcline-quartz 40% pyrite.
169.0 to 169.4 m	Partly oxidised, poorly unconsolidated medium grained sandy quartz-feldspar-biotite?-magnetite with 10% pyrite. Probably intrusive?
169.4 to 172.95 m (END OF HOLE)	Black shale, sericite veined black shale and pervasively argyllised black shale - Broken Core.

HOLE NUMBER GDH-04

DESCRIPTION

MARIMO SHALE

189.8 to 142.4 m	Carbonaceous, often graphitic, black shale. Bedding foliation 65° CAA. Rare thin pyrite coatings on fractures. Rare traces of disseminated pyrite. Occasional bedding parallel quartz ± pyrite veins to 3 cm. Occasional irregular cross-cutting quartz-pyrite veins to 1 cm - sometimes brecciated. - rare S1 foliation eg. 98.5 m which is post pyrite-quartz veining - some minor bleached white clay on fracture coatings - increasing strained quartz-pyrite veining toward end of interval.
142.4 to 147.50 m	Commencement of first quartz-microcline-pyrite-phlogopite veining and quartz-pyrite veining. Note the barren weakly fractured quartz-microcline-phlogopite vein. Quartz generally occurs in the middle of the vein. Appears to have filled open spaces in fractured black shale but has been coarsely brecciated itself.
147.5 to 148.4 m	Large brecciated and fractured dominantly quartz-(microcline) vein with pyrite in fractures and as matrix in open spaces. Some pyrite is oxidised to hematite.
148.4 to 150.7 m	Brecciated and partly oxidised pervasive feldspar-quartz-sericite ± disseminated and vein pyrite.
150.7 to 152.0 m	Intense pervasive sericite-argyllite. Note the late microcline-pyrite vein at 151.1m.
152.0 to 154.0 m	Sheared weak to intensely argyllic black shale with some quartz-microcline with disseminated pyrite, veins.
154.0 to 158.0 m	Black shale with thin cross cutting (foliation 45° CAA) strained and sometimes brecciated quartz vein with hematite-goethite in fractures and limonite along foliation adjacent to quartz vein. Occasional quartz-mica-feldspar-(rare pyrite) breccia. Becoming increasingly pervasively silicified toward 158 m. Coarse hematite cubes after pyrite and pyrite, as well as late pyrite in fractures within a weathered quartz-feldspar rock at 157.8 m.
158.0 to 164.3 m	Quartz-microcline-goethite/limonite breccia with pyrite pseudomorphs and intervals of sheared (eg. 162.7 m) or tightly folded (eg. 163.5 m) silicified shale. Major fault.

STAVELEY FORMATION

164.3 to 181.3 m	Probable commencement of STAVELEY FORMATION. Bedded but sheared, weathered, potassified orange-brown, sometimes finely interbedded siltstone-metasandstone. Bedding 10-30° CAA. Note flaser bedding at 170.10 m. Numerous quartz-hematite breccias transect bedding. Probably in the influence of the fault zone.
181.3 to 184.5 m	Mostly a vuggy quartz-lesser microcline ± disseminated pyrite aggregates, vein in metasediment.
184.5 to 199.3 m (END OF HOLE)	Weathered bedded (35-40° CAA) metasediment. Some plastic disruption of beds and preferential weathering. Rare late strained quartz veins. Relatively unfractured and brecciated.

HOLE NUMBER GDH-05

DESCRIPTION

MARIMO SHALE

89.65 to 90.0 m Black shale with thin microcline-pyrite veins.

STAVELEY FORMATION

90.0 to 94.4 m Strong pervasive microcline-albite alteration cut by later calcite-microcline \pm albite \pm rare disseminated pyrite eg. 90.2 m. This in turn is fractured/brecciated and veined by quartz-pyrite (eg. 90.2 m), pyrite stringers (eg. 92.0 m) quartz-calcite and quartz-albite \pm disseminated euhedral pyrite (eg. 94.1 m).

94.4 to 98.0 m Mottled, partly oxidised, silicified sediment (Black Shale?) breccia with indistinct clast margins and silica (\pm calcite) matrix. Note the microcline altered host is cut by a calcite-microcline vein which itself hosts later infill textured calcite at 95.9 m. Pyrite appears in the feldspathised host as well as in the veins within quartz-sometimes adjacent to calcite but never as inclusions in calcite. Hematite dusting occurs throughout this interval.

98.0 to 207.5 m Calcilutite breccia. Probably after calcilutite. Dominantly 60 - 80% clasts but some zones less than 2 m wide can be matrix rich. Matrix comprises calcite and quartz-calcite \pm pyrite. Relict bedding in clasts typically 45° CAA, but there are some disrupted zones. Clasts almost never contain disseminated pyrite. Some clasts have a hematite dusted rim while some zones are pervasively hematite dusted. Clasts appear dismembered. Darker clasts probably contain more biotite. Note the quartz-calcite-magnetite vein at 115.9 m. Note the rare disseminated $<<1\%$ chalcopyrite in wallrock and calcite around the calcite open space fill.

(163.35 m) Note the fluorite on cleavage.

(168.4 m) Quartz-calcite-microcline veining hematite dusted, fractured siltstone.

(183.6 m) Note CAA 5° also quartz-calcite cutting earlier quartz-microcline vein . Hematite dusting becoming more prominent from about 170 m.

(187.90 m) Fluorite in calcite vugh at 187.90 m in quartz-albite-calcite vein. Also at 206.6 m.

207.5 to 213.9 m Diorite intrusive? Dark green-grey-black. Variable weak patchy hematite dusting. Strongly magnetic. Chlorite-Biotite-hornblende-feldspar and disseminated calcite throughout as well as late irregular calcite veins. Calcite veining postdates hematite dusting. About 1% disseminated pyrite. Minor sericite \pm chlorite \pm epidote alteration of intrusive.

213.9 to 217.35 m Mosaic of spotty pervasive pale pink-brown feldspar quartz with spotty hematite and chlorite blebs veined by quartz-hematite dusted microcline-calcite. Trace disseminated pyrite.

217.35 to 248.95m Intrusive as above. Note hematite dusting/redrock selvedge to veins of quartz-calcite \pm microcline eg. 220-228 m. Some zones of rock as for 213.9 - 217.35 m interval.

248.95 to 319.25m
(END OF HOLE) Calcite-silica breccia as for 98-207.5 m.

APPENDIX 3

THIN SECTION DESCRIPTIONS

APPENDIX 3 - THIN AND POLISHED THIN SECTION DESCRIPTIONS

SAMPLE NUMBER: 85002

HOLE NUMBER: GDH-01

DEPTH: 123.9 m

OTHER ANALYSES

DESCRIPTION:

Host rock comprises mildly sericitic siltstone (Pkm) with disseminated rutile, pyrite, tourmaline.

Veins comprise microcline (65%)-albite (15%) - quartz (15%) - Phlogopite (3%) - chlorite - pyrite - chalcopyrite (cc).

This vein is cut by chlorite, sericite, chalcocite stringers.

SAMPLE NUMBER: 85003

HOLE NUMBER: GDH-01

DEPTH: 125.8 m

OTHER ANALYSES

DESCRIPTION:

Host rock comprises tourmalinised sericitic slate (rare rutile).

Veins comprise mildly strained coarse microcline with marginal patches of fine rutile and central patches of quartz (<1%) - apatite (3%) - phlogopite - chalcopyrite.

The apatite is commonly cut by sericitic replacement veins.

SAMPLE NUMBER: 85004

HOLE NUMBER: GDH-01

DEPTH: 124.5 m

OTHER ANALYSES

DESCRIPTION:

Contact between grey slate and pervasively bleached slate.

Grey slate comprises weakly pyritic, slightly carbonaceous siltstone with disseminated aggregates of fine rutile. Slate grains composed dominantly of quartz - albite.

Bleached equivalent is depleted in pyrite and carbonaceous matter but carries trace chalcocite (after cpy) along with small muscovite porphyroblasts.

Veins within bleached zone are of fracture style. Veins contain quartz (67%) - albite (30%) - Microcline (2%) early rutile - calcite - pyrite and late phlogopite and apatite.

SAMPLE NUMBER: 85009

HOLE NUMBER: GDH-01

DEPTH: 119.8 m

OTHER ANALYSES

DESCRIPTION:

Host rock comprises pyritic (possibly diagenetic or syngenetic), graphitic slate with incipient potassium feldspathisation and tourmalinisation.

Pyrite occurs as disseminated small lenses of porphyroblastic grains. Slate is mostly muscovite or sericite.

SAMPLE NUMBER: 85006
HOLE NUMBER: GDH-01
DEPTH: 128.4 m

OTHER ANALYSES

DESCRIPTION:

Hosted by pervasively feldspathised shale, with disseminated rutile and trace tourmaline which has been aligned with schistosity (Pkm). Disseminated small ragged chalcopyrite grains display incipient replacement by very fine pyrite and covellite.

An earlier microcline vein is cut by a microcline - quartz - apatite - sulphide vein. Most chalcopyrite occurs as aggregates (to 2 mm) which often enclose pyrite euhedra. The chalcopyrite also occupies interstices between microcline crystals.

Most pyrite occurs as euhedral small crystals (10 microns to 200 microns) enclosed within chalcopyrite. In places small pyrite crystals are peppered through chalcopyrite and microcline. Very fine grained pyrite can occasionally be seen to replace chalcopyrite near grain margins and along thin, irregular microfractures. This type of pyrite is also associated with traces of very fine replacement pyrrhotite.

Marcasite may occur within the massive, elongate pyrite aggregates.

Rare anhedral sphalerite (to 300 microns) occurs enclosed within chalcopyrite.

Covellite replaces pyrite and chalcopyrite.

Rutile occurs as subhedral crystals and granular aggregates, irregularly and sparsely distributed through the veins.

An approximate composition of the vein would be microcline (55%) - quartz (20%) - apatite (2%) - phlogopite (2%) - calcite (1%) - chalcopyrite (10%) - pyrite (9%) - marcasite (1%) - sphalerite (trace) - Rutile (trace) and traces of supergene covellite - pyrite - pyrrhotite.

SAMPLE NUMBER: 85008
HOLE NUMBER: GDH-01
DEPTH: 130.3 m

OTHER ANALYSES

DESCRIPTION:

Host rock comprises pale grey sericitic slate comprising sericite - quartz (79%) ± feldspar (20%) - rare rutile and tourmaline

Host is in sharp folded contact with spotty finely sandy textured rock, with phlogopitic (30%) and spotted feldspathic [(Kspar + Ab) (67%)] composition.

Veins comprise albite (65%) - quartz (30%) microcline (5%) with trace carbonate - phlogopite - rutile.

SAMPLE NUMBER: 85007
HOLE NUMBER: GDH-01
DEPTH: 128.45 m

OTHER ANALYSES

DESCRIPTION:

Host rock comprises sericitic slate composed of sericite (75%) - quartz/albite (15%) - brown tourmaline (8%) and rutile (2%).

Next to albite veins and tight fractures, sericite becomes albitised. Tourmaline and rutile remain unchanged.

Early albitic veins contain albite (96%) - quartz (3%) - phlogopite 1% and traces of rutile and apatite.

These veins are cut by Microcline (92%) - quartz (5%) - phlogopite (2%) - chlorite - pyrite - chalcopyrite. Later very thin fracture veins comprise sericite and chlorite.

Quartz in veins contain some salt bearing fluid inclusions.

SAMPLE NUMBER: 85016B
HOLE NUMBER: GDH-02
DEPTH: 127.5 m

OTHER ANALYSES

DESCRIPTION:

Tourmalinised, sulphide impregnated pelite was argyllised, then brecciated and cemented by coarse vein minerals e.g. microcline (56%) - phlogopite (25%) - albite (10%) - chalcocite (5%) - pyrite (2%) - quartz (2%) - rutile.

Late sericite - chalcopyrite veinlets cut all other minerals veins and alteration styles.

SAMPLE NUMBER: 85011
HOLE NUMBER: GDH-01
DEPTH: 156.5 m

OTHER ANALYSES

DESCRIPTION:
Host rock comprises pyritic (possibly diagenetic or syngenetic), graphitic slate with incipient potassium feldspathisation and tourmalinisation (Pkm).

Veins are irregular fracture filling style, generally coarse grained. They comprise microcline (52%) - quartz (25%) - phlogopite 20% and minor chlorite - carbonate - pyrite.

Quartz poor parts are associated with phlogopite
Quartz rich parts of the vein are associated with carbonate.

Alteration selvages to veins involve elimination of carbonaceous matter, substitution of feldspar for muscovite - sericite and impregnation with disseminated pyrite.

SAMPLE NUMBER: 85017
HOLE NUMBER: GDH-02
DEPTH: 127.4 m

OTHER ANALYSES

DESCRIPTION:
Tourmalinised then argillised and mildly sulphide impregnated and brecciated fine grained sediment cemented by a network of microcline (60%) - phlogopite (20%) - albite (10%) - covellite (5%) - chalcocite (1%) - chalcopyrite (trace) - pyrite (2%) - quartz (2%) - trace rutile (Pkm). Late thin sericite - illite veins with some chalcocite occur.

Pyrite is generally restricted to the coarse grained veins and matrix and is present as small ragged disseminations in the argillised host rock. In veins it occurs as (1-2 mm) ragged aggregates with some smaller subhedral (0.2 - 0.4 mm) discrete crystals.

Chalcopyrite was present in significant amount, occurring near pyrite as ragged grains in veins as well as peppered through microcline and phlogopite, but has almost been completely replaced by the supergene copper minerals. Sparsely disseminated chalcopyrite in the host rock is also being replaced by covellite.

SAMPLE NUMBER: 85013
HOLE NUMBER: GDH-01
DEPTH: 185.55 m

OTHER ANALYSES

DESCRIPTION:
Banded, laminated, finely micaceous slate comprising sericite/muscovite/biotite 78% - potassic feldspars 15% - quartz 5% and minor tourmaline, rutile, hematite (Pks).

Interbedded with more porous, weathered, ironstained coarser quartzofeldspathic siltstone comprising microcline (50%) - sericite (37%) quartz (10%) and possible traces of chalcocite.

i.e. Rock was slightly tourmalinised pervasively potassium feldspathised and lightly sericitised prior to weathering

SAMPLE NUMBER: 85018
HOLE NUMBER: GDH-02
DEPTH: 127.4 m

OTHER ANALYSES

DESCRIPTION:
Tourmalinised pelite was impregnated with sulphide (py-cpy) and intensely feldspathised (Pkm). This was brecciated and cemented by microcline (53%) - albite (15%) - pyrite (15%) - phlogopite (15%) - chalcopyrite (2%) trace quartz - rutile.

This was then veined by thin sericite -quartz veins.

SAMPLE NUMBER: 85017
HOLE NUMBER: GDH-02
DEPTH: 127.4 m

OTHER ANALYSES

DESCRIPTION:

Tourmalinised then argillised and mildly sulphide impregnated and brecciated fine grained sediment cemented by a network of microcline (60%) - phlogopite (20%) - albite (10%) - covellite (5%) - chalcocite (1%) - chalcopyrite (trace) - pyrite (2%) - quartz (2%) - trace rutile (Pkm). Late thin sericite - illite veins with some chalcocite occur.

Pyrite is generally restricted to the coarse grained veins and matrix and is present as small ragged disseminations in the argillised host rock. In veins it occurs as (1-2 mm) ragged aggregates with some smaller subhedral (0.2 - 0.4 mm) discrete crystals.

Chalcopyrite was present in significant amount, occurring near pyrite as ragged grains in veins as well as peppered through microcline and phlogopite, but has almost been completely replaced by the supergene copper minerals. Sparsely disseminated chalcopyrite in the host rock is also being replaced by covellite.

SAMPLE NUMBER: 85019
HOLE NUMBER: GDH-02
DEPTH: 135.0 m

OTHER ANALYSES

DESCRIPTION:

Host rock comprises a foliated graphitic slate with uniformly disseminated subhedral rutile crystals and occasional tourmaline needles which are aligned with the foliation (Pkm). This is cut by a vein comprising microcline (50%) - quartz (15%) - albite (2%) - apatite (1%) - phlogopite (2%) - pyrite (30%) - trace covellite and chalcopyrite.

In the host rock, pyrite occurs as rare small subhedral crystals with abundant minute gangue inclusions. Traces of chalcopyrite occur as ragged disseminated grains as well as micron sized inclusions in rutile.

In the vein, pyrite occurs as euhedral and subhedral crystals and aggregates, generally in the central portions of the vein. Chalcopyrite generally appears as inclusions in quartz, and is mostly replaced by covellite.

SAMPLE NUMBER: 85018
HOLE NUMBER: GDH-02
DEPTH: 127.4 m

OTHER ANALYSES

DESCRIPTION:

Tourmalinised pelite was impregnated with sulphide (py-cpy) and intensely feldspathised (Pkm). This was brecciated and cemented by microcline (53%) - albite (15%) - pyrite (15%) - phlogopite (15%) - chalcopyrite (2%) trace quartz - rutile.

This was then veined by thin sericite -quartz veins.

SAMPLE NUMBER: 85020
HOLE NUMBER: GDH-02
DEPTH: 139.5 m

OTHER ANALYSES

DESCRIPTION:

Weakly pervasively feldspathised and foliated carbonaceous shale with rutile and tourmaline aligned with foliation (Pkm). Pyrite cubes are sparsely disseminated through the host. Chalcopyrite is disseminated in the host, but mostly adjacent to veins.

Veins are composed of anhedral quartz (52%) - albite (25%) - microcline (15%) and traces of epidote. Chalcopyrite (5%) occurs as ragged grains within the vein but also extending into the wallrock. Pyrite forms subhedral crystals, but is also euhedral within chalcopyrite.

Lack of strain extinction in quartz, and lack of alignment of vein minerals suggests formation by open space filling processes. Late fractures introduced clays.

SAMPLE NUMBER: 85021
HOLE NUMBER: GDH-02
DEPTH:

OTHER ANALYSES

DESCRIPTION:

Graphitic black shale veined by microcline (40%) - quartz (8%) - phlogopite (1%) and filled by pyrite (30%) and chalcopyrite (20%) with rare covellite (1%) supergene enrichment (Pkm).

Pyrite occurs mostly as small euhedral and subhedral crystals and crystalline aggregates. It is commonly enclosed by ragged chalcopyrite. Some of the chalcopyrite is free from pyrite inclusions. Most of the sulphides occur in the interstices of the vein minerals and chalcopyrite can also be seen to form thin discontinuous veinlets which cut feldspar and quartz.

The vein is mildly strained and liberally finely fracture veined by chalcopyrite with associated minor sericite and quartz. The last thin veins are sericitic.

SAMPLE NUMBER: 85023
HOLE NUMBER: GDH-02
DEPTH: 149.8 m

OTHER ANALYSES

DESCRIPTION:

Similar to 85021. Graphitic shale veined by microcline (65%) - quartz (7%) - phlogopite (2%) - pyrite (15%) - chalcopyrite (10%) - supergene covellite (1%) with trace rutile and marcasite.

Rutile is sparsely scattered through the vein minerals as well as sulphides.

Pyrite is concentrated in massive aggregates, often massive but occasionally euhedral to subhedral. Gangue inclusions are common in the more massive areas. Elongated relict structures and rare relict elongated marcasite aggregates occur in the inclusion-rich pyrite. These features suggest that much of the massive and structured pyrite may have formed initially as marcasite.

Chalcopyrite mostly occurs in the interstices between gangue crystals but occasionally cross cuts them. It can also be seen to be replacing feldspar rims.

SAMPLE NUMBER: 85022
HOLE NUMBER: GDH-02
DEPTH: 142.0 m

OTHER ANALYSES

DESCRIPTION:

Carbonaceous, tourmalinised, feldspathised slate (minor rutile).

Vein comprises coarsely crystalline microcline with minor fine phlogopite (early) then pyrite then more abundant (2%) chalcopyrite and trace quartz.

The vein is mildly strained and liberally finely fracture veined by chalcopyrite with associated minor sericite and quartz. The last thin veins are sericitic.

SAMPLE NUMBER: 85025
HOLE NUMBER: GDH-02
DEPTH: 177.7 m

OTHER ANALYSES

DESCRIPTION:

Foliated and crenulated graphitic slate with disseminated aggregates of rutile, veined by microcline (85%) - quartz (10%) - phlogopite (3%) and pyrite (2%) (Pkm). Some rutile also occurs as disseminations in the vein. Pyrite occurs as small euhedral crystals and aggregates of crystals. It also occurs as more ragged and elongate aggregates which contain minute gangue inclusions, which was probably once marcasite (but has since inverted to pyrite). Pyrite and traces of muscovite appear to be incipiently replacing feldspar grains.

SAMPLE NUMBER: 85027
HOLE NUMBER: GDH-02
DEPTH: 199.7 m

OTHER ANALYSES

DESCRIPTION:
Hosted by Staveley Formation, muscovite schist with disseminated scattered euhedral tourmaline and small granular aggregates of rutile and microcline. Near veins, thin veinlets of microcline have invaded along foliation traces as well as discordant veinlets. A trace of chalcopyrite and pyrite occurs in these microveinlets, as well as in the schistose wall rock.

The schist is veined by polycrystalline mosaics of microcline (64%) - angular interstitial quartz (30%) - traces of anhedral apatite - irregularly scattered ragged chalcopyrite. Some of the quartz displays incipient recrystallisation to finer grained granoblastic mosaics. Much of the chalcopyrite (3%) has been replaced by chalcocite. Pyrite occurs as rare (1%) euhedral to subhedral grains.

SAMPLE NUMBER: 85035
HOLE NUMBER: GDH-03
DEPTH: 146.0 m

OTHER ANALYSES

DESCRIPTION:
Carbonaceous slate intensely tourmalinised and potassium feldspathised, then brecciated and veined by microcline (64%) - quartz (35%) - chalcopyrite - pyrite.

SAMPLE NUMBER: 85036
HOLE NUMBER: GDH-03
DEPTH: 160.95m

OTHER ANALYSES

DESCRIPTION:
Vein of slightly deformed, coarsely crystalline quartz - calcite - pyrite hosted by the Staveley Formation.

SAMPLE NUMBER: 85028
HOLE NUMBER: GDH-02
DEPTH: 211.2 m

OTHER ANALYSES

DESCRIPTION:
Calcareous pelite (feldspar - calcite - quartz - tourmaline - bi otite - rutile), finely tourmalinised, intensely feldspathised (dominantly K-spar with lesser albite), then brecciated and cemented by calcite - feldspar - quartz - minor phlogopite and rutile (Pks).

Very late cavity fillings in the clasts and cement are dominated by calcite with minor quartz and brown biotite.

SAMPLE NUMBER: 85037
HOLE NUMBER: GDH-0
DEPTH: 161.2 m

OTHER ANALYSES

DESCRIPTION:
Microdiorite has been heavily chloritised and carbonated. Sparsely disseminated sulphides comprise pyrite and chalcopyrite (these are impregnated).

Irregular veins comprise coarser calcite (33%) - quartz (30%) and finer pyrite (2%) - microcline (35%).

SAMPLE NUMBER: 85030
HOLE NUMBER: GDH-03
DEPTH: 131.65m

OTHER ANALYSES

DESCRIPTION:

Pervasively feldspathised and tourmalinised graphitic black shale (Pkm), veined by microcline (88%) - quartz (3%) - apatite (1%) - albite (2%) - phlogopite (3%) - chalcopyrite (3%). Carbonaceous slate, tourmalinised, intensely feldspathised [(dominantly albite (66%) lesser K-spar (15%)].

Sparsely disseminated through the wallrock are small subhedral crystals of pyrite (1%), small ragged grains of chalcopyrite (1%) and small granular aggregates of rutile. Contains early syn/diagenetic (?) pyrite.

Mason (1994) observed disseminated rhombic crystal sites up to 1 mm in size which have been filled by fine grained feldspar and quartz which he suggested that they may have been porphyroblasts of dolomite. Late thin fracture veins of quartz - sericite - pyrite cuts the earlier veins.

SAMPLE NUMBER: 85034
HOLE NUMBER: GDH-03
DEPTH: 141.7 m

OTHER ANALYSES

DESCRIPTION:

This is a sample of massive fractured sulphide vein rock (hosted by altered shale - Pkm). Pyrite occurs as subhedral euhedral crystals, up to 1 mm, and tends to be grouped into polycrystalline aggregates. Subparallel closely-spaced fractures cut most of the pyrite, and form a moderately well-defined network.

Chalcopyrite occurs as small inclusions within pyrite, and also as small discrete grains in interstitial quartz. Microcline (5%) and quartz (2%) fill the interstices between sulphides.

SAMPLE NUMBER: 85031
HOLE NUMBER: GDH-03
DEPTH: 131.8 m

OTHER ANALYSES

DESCRIPTION:

Finely albitized pelite with concordant bands and discordant fracture veins of microcline (92%) - albite (5%) - chalcopyrite (<1%) ± calcite (3%).

Late thin sericite - chalcopyrite cuts the earlier veins.

SAMPLE NUMBER: 85033
HOLE NUMBER: GDH-03
DEPTH: 140.9 m

OTHER ANALYSES

DESCRIPTION:

Pervasively albitised pelite with disseminated prismatic tourmaline crystals aligned within a faint foliation. Small rutile granules cluster into aggregates. Ragged chalcopyrite (0.5%) and euhedral pyrite grains occur disseminated through the rock.

This has been cut by non-planar quartz (65%) - albite (25%) - pyrite (10%). Pyrite forms subhedral euhedral crystals and granular aggregates. Some of the pyrite aggregates display a considerable degree of fracturing. Where pyrite abuts the wallrock, fine grained replacement pyrite has formed in the vein selvage. Some late thin planar clay filled and weakly pyritic (very fine grained) veins cut all earlier structures.

It is notable that albitic veins formed in albitic wallrock and Mason (1994) interprets that wallrock materials may have contributed to veins. Mason also suggests that the pyrite and chalcopyrite may have formed in the wallrock during the pervasive feldspathic alteration as observed by Krcmarov.

SAMPLE NUMBER: 85044
HOLE NUMBER: GDH-04
DEPTH: 155.0 m

OTHER ANALYSES

DESCRIPTION:
Carbonaceous slate (no tourmaline and rutile) which is finely foliated and lenticular and has been silicified. Some inferred pyrite occurs as tiny cubes within finely siliceous lenses (Pkm).

Discordant or concordant fracture veins comprise quartz (97%) with a fine selvage of microcline (1%) as well as some pyrite.

SAMPLE NUMBER: 85045
HOLE NUMBER: GDH-04
DEPTH: 159.1 m

OTHER ANALYSES

DESCRIPTION:
Fault breccia goethite/limonite (74%) - microcline (14%) - quartz (8%) - pores (4%) and rare muscovite.

SAMPLE NUMBER: 85047
HOLE NUMBER: GDH-04
DEPTH: 170.4 m

OTHER ANALYSES

DESCRIPTION:
Slightly tourmalinised, mildly micaceous intensely potassium feldspathised pelite (looks Staveley Formation) which was brecciated and veined by hydrothermal Microcline (72%) - biotite (3%) and possibly carbonate. There are no obvious sulphide textures, but the rock has been intensely weathered. The remaining composition of the rock is limonite/goethite (20%) and pores (5%).

SAMPLE NUMBER: 85048
HOLE NUMBER: GDH-04
DEPTH: 183.4 m

OTHER ANALYSES

DESCRIPTION:
Heavily tourmalinised, intensely potassium feldspathised (patchy retrogressive sericite alteration), formerly carbonaceous pelite.

The veins are dominated by moderately strained and partially recrystallised coarse quartz (77%) with fine microcline selvage (20%) and late subhedral pyrite (3%), traces of muscovite and rare calcite.

SAMPLE NUMBER: 85049
HOLE NUMBER: GDH-04
DEPTH: 193.15m

OTHER ANALYSES

DESCRIPTION:
Laminated siltstone and shale, was
tourmalinised, intensely feldspathised and
retrogressively sericitised (Pks).

Finest bands comprise foliated brown biotite,
clear grains of microcline, abundant plagioclase
(now sericitised) and minor fine tourmaline and
rutile.

Coarser bands comprise microcline and limonite
stained aggregates of sericite after plagioclase.
Some have goethite and minor chalcocite after
inferred patchily disseminated sulphides.

A crude estimate of the banded host rock is
microcline (46%) - sericite (45%) - biotite (3%) -
tourmaline (3%) - weathered sulphides (2%) -
rutile (1%).

Thin discordant fracture veins comprise quartz
(42%) - possible carbonate (now pores and iron
oxides) (5%) - biotite (20%) - and inferred
sulphides (4%) (now goethite).

SAMPLE NUMBER: 85052
HOLE NUMBER: GDH-05
DEPTH: 92.7 m

OTHER ANALYSES

DESCRIPTION:
Carbonated (47%) and albitised (47%) pelite
with disseminated fine rutile (1%) and
poikiloblastic faceted pyrite (5%) enriched along
vein contacts (Pks).

Early vein comprise microcline (60%) - calcite
(20%) - quartz (15%) - muscovite (1%) -
multifaceted pyrite (4%).

Late veins comprise calcite (65%) - pyrite (35%).

SAMPLE NUMBER: 85051
HOLE NUMBER: GDH-05
DEPTH: 90.3 m

OTHER ANALYSES

DESCRIPTION:
Carbonated and intensely feldspathised
(microcline and albite) pelite (? shale) with fine
aggregates of rutile, and euhedral faceted pyrite
adjacent to veins (Pks).

Early veins comprise microcline (80%) - calcite
(10%) - albite (10%) - trace rutile.

Later veins comprise calcite (65%) - quartz
(30%) microcline (2%) - albite (2%) - pyrite
(1%).

SAMPLE NUMBER: 85054
HOLE NUMBER: GDH-05
DEPTH: 95.9 m

OTHER ANALYSES

DESCRIPTION:
Early vein of microcline (49%) - calcite (49%) -
multifaceted pyrite (2%).

Late vein of coarser calcite with sparse
disseminated pyrite.

SAMPLE NUMBER: 85055
HOLE NUMBER: GDH-05
DEPTH: 102.2 m

OTHER ANALYSES

DESCRIPTION:

Well foliated sericite (68%) mingled with quartz and feldspar (25%), minor brown biotite (2%), tourmaline (1%) and rutile (trace). Numerous disseminated subhedral magnetite (but no sulphide) was impregnated (4%).

This was brecciated and hydrothermally cemented by calcite (88%) with a thin outer lining of earlier fine quartz (10%) - microcline (2%) with subhedral pyrite, lesser subhedral magnetite and anhedral, ragged chalcopyrite.

SAMPLE NUMBER: 85056
HOLE NUMBER: GDH-05
DEPTH: 116.0 m

OTHER ANALYSES

DESCRIPTION:

Clasts are platy dismembered segments of altered, laminated pelite (Pks).

Darker clasts comprise sericite (70%) - brown biotite (15%) - feldspars (15%) and tourmaline. Most common clasts comprise silt sized fine plagioclase and microcline (88%) - calcite (10%) - tourmaline (2%) - trace carbonaceous matter and biotite.

A hydrothermal cement between the clasts initially crystallised albite (15%) - microcline (10%) - biotite (5%) - quartz (3%) - faceted pyrite (2%) but progressed to coarser calcite with disseminated fine euhedral magnetite.

SAMPLE NUMBER: 85057
HOLE NUMBER: GDH-05
DEPTH: 134.15m

OTHER ANALYSES

DESCRIPTION:

Clasts comprise fine plagioclase and microcline (70%) - sericite (20%) - tourmaline (3%) and trace rutile. Some clasts are more sericitised. The clasts are essentially thoroughly disrupted, laminated pelite (Pks).

Clasts are cemented by a hydrothermal assemblage of early microcline (35%) - albite (3%) - faceted pyrite (1%) - later quartz (2%) and very late coarse calcite (59%)

SAMPLE NUMBER: 85058
HOLE NUMBER: GDH-05
DEPTH: 140.0 m

OTHER ANALYSES

DESCRIPTION:

Meta-calclutite comprising very fine grained calcite - albite - microcline - quartz and lesser biotite.

Disseminated tourmaline and rutile occurs throughout. Calcite and lesser quartz occur as coarser grained patches and as thin discontinuous veins. Ragged chalcopyrite is associated with these patches of coarser calcite. Pyrite occurs as small disseminated subhedral to euhedral cubic crystals. Larger pyrite crystals are closely associated with a larger magnetite grain which appears poikiloblastic and is also intergrown with chalcopyrite - feldspar - quartz. Magnetite mostly occurs as small disseminated grains and subhedral cubic crystals.

SAMPLE NUMBER: 85059
HOLE NUMBER: GDH-05
DEPTH: 208.7 m

OTHER ANALYSES

DESCRIPTION:

Zoned alteration assemblage. Probably outer margin of microdiorite.

Dark grey regime : slightly reddened albite (30%) - unstrained quartz (24%) - magnetite (22%) - biotite (20%) - minor calcite and rare pyrite.

Narrow yellowish-grey zone: finer calcite - albite - quartz and minor fine magnetite.

Narrow pyritic band: anhedral calcite with multifaceted annealed pyrite.

Pale red zone: calcite (25%) - slightly reddened albite (54%) - slightly reddened microcline (15%) - quartz (5%) - minor fine magnetite (1%).

SAMPLE NUMBER: 85061
HOLE NUMBER: GDH-05
DEPTH: 217.15 m

OTHER ANALYSES

DESCRIPTION:

Host rock is of uncertain origin (possibly a microdiorite) but comprises microcline (65%) - calcite (30%) - minor biotite (1%), muscovite (3%), rutile (1%).

Fracture veins comprise calcite (97%) - microcline (2%) - albite (1%) - biotite (<1%) - trace rutile.

SAMPLE NUMBER: 85062
HOLE NUMBER: GDH-05
DEPTH: 218.8 m

OTHER ANALYSES

DESCRIPTION:

Fine grained diorite originally carrying hornblende or pyroxene which has now been pseudomorphed by biotite. It has been hornfelsed to biotite grade and partly carbonated.

The altered diorite now comprises plagioclase (46%) - biotite (38%) - calcite (10%) - magnetite (4%) - rutile (2%).

SAMPLE NUMBER: 85063
HOLE NUMBER: GDH-05
DEPTH: 247.5 m

OTHER ANALYSES

DESCRIPTION:

Prismatic mafic silicates have been pseudo-morphed by biotite, calcite and fine euhedral grains of magnetite. Grains of inferred ilmenite have been replaced by aggregates of sphene and magnetite. The microdiorite was infilled (carbonated) with late calcite. Patches of fine chlorite, sericite and epidote can be found.

The present composition is plagioclase (48%) - biotite (35%) - calcite (8%) - magnetite (5%) - sphene (2%) - chlorite (1%) - sericite (1) - epidote (<1%).

A fracture vein contains outer zones of albite (10%) (retrogressively altered to sericite) - microcline (30%) and later calcite (58%) - biotite (2%) and trace rutile.

SAMPLE NUMBER: 85064
HOLE NUMBER: GERC42
DEPTH: 68-70 m

OTHER ANALYSES

DESCRIPTION:
Euhedral but rounded disseminated crystals hosted by fine grained pervasively sericitised and hematite dusted microcline altered graphitic shale.

Some of the graphitic shale has been weakly carbonated.

SAMPLE NUMBER: 85065
HOLE NUMBER: GERC43
DEPTH: 168-170

OTHER ANALYSES

DESCRIPTION:
Pyrite vein in carbonaceous and graphitic black shale. Pyrite is anhedral and displays a network of fine hairline fractures, and inclusions of host rock.

SAMPLE NUMBER: 85066
HOLE NUMBER: GERC44
DEPTH: 162-165 m

OTHER ANALYSES

DESCRIPTION:
Carbonaceous and graphitic black shale with disseminated pitted anhedral pyrite grains and vein of fractured pyrite with hostrock inclusions.

SAMPLE NUMBER: 85067
HOLE NUMBER: GERC
DEPTH: 134-13

OTHER ANALYSES

DESCRIPTION:
Veinlet of anhedral pyrite with inclusions of hostrock. Hostrock comprises carbonaceous and graphitic shale (Pkm).

SAMPLE NUMBER: 85068
HOLE NUMBER: GRC45
DEPTH: 86 m

OTHER ANALYSES

DESCRIPTION:
Sheared carbonaceous, graphitic and weakly dolomitic black shale with subhedral pitted pyrite crystals (Pkm).

SAMPLE NUMBER: 85604
HOLE NUMBER: GDH0
DEPTH: 183.3

OTHER ANALYSES

DESCRIPTION:
Clasts comprise fine microcline - quartz - calcite - dolomite - sericite - rutile and tourmaline (Pks). Matrix comprises calcite - quartz - pyrite.

SAMPLE NUMBER: 85611-V
HOLE NUMBER: GDH02
DEPTH: 170.2 m

OTHER ANALYSES

DESCRIPTION:
Irregular quartz (85%) - microcline (5%) and pyrite (10%) vein in black carbonaceous shale with disseminated pyrite crystals (Pkm). The hostrock shale has partly been incipiently altered to microcline near the vein selvage.

SAMPLE NUMBER: 85614
HOLE NUMBER: GDH0
DEPTH: 203.1

OTHER ANALYSES

DESCRIPTION:
Laminated calcareous and dolomitic pelite comprising microcline - quartz - albite - biotite - rutile - calcite - dolomite which contains bands of disseminated and aggregated (fine grained) anhedral, unpitted fractured pyrite and trace chalcopyrite which is approximately parallel to the compositional layering (bedding). The sulphides contain minor inclusions of hostrock.

APPENDIX 4

MICROPROBE ANALYSES

CHALCOPYRITE MICROPROBE ANALYSES
MARIMO SHALE VEIN / MATRIX HOSTED

TRACE ELEMENT	SAMPLE NUMBER (SPOT NUMBER)									
	85018 (R7KCP1)		85018 (R7KCP2)		85031 (R7CP1)		85031 (R5CP1)		85031 (R8CP1)	
	Wt %	Normalised atom. c	Wt %	Normalised atom. c	Wt %	Normalised atom. c	Wt %	Normalised atom. c	Wt %	Normalised atom. c
Fe	24.83	21.1	24.64	20.76	29.60	24.7	29.46	24.41	29.29	24.53
S	33.80	50.05	33.44	49.09	33.69	48.98	33.91	48.93	33.48	48.84
Co	0.00	0	0.00	0	0.00	0	0.00	0	0.00	0
Cu	38.39	28.68	40.61	30.08	35.85	26.3	36.62	26.66	36.12	26.6
Zn	0.00	0	0.04	0.02	0.01	0	0.00	0	0.00	0
Mn	0.02	0.01	0.00	0	0.01	0.01	0.01	0	0.04	0.03
Se	0.08	0.05	0.01	0	0.01	0	0.00	0	0.00	0
Cd	0.25	0.1	0.08	0.03	0.00	0	0.00	0	0.00	0
Hg	0.00	0	0.00	0	0.00	0	0.00	0	0.00	0
As	n.d.		n.d.		n.d.		n.d.		n.d.	
Ag	n.d.		n.d.		n.d.		n.d.		n.d.	
Sb	n.d.		n.d.		n.d.		n.d.		n.d.	
Ni	n.d.		n.d.		n.d.		n.d.		n.d.	
Pb	n.d.		n.d.		n.d.		n.d.		n.d.	
Bi	n.d.		n.d.		n.d.		n.d.		n.d.	
TOTAL	97.37	99.99	98.82	99.98	99.17	99.99	100.00	100	98.93	100

TRACE ELEMENT	SAMPLE NUMBER (SPOT NUMBER)							
	85031 (R1BCPY)		85031 (R1CPX)		85031 (R3ECP)		85031 (R3FCP)	
	Wt %	Normalised atom. c	Wt %	Normalised atom. c	Wt %	Normalised atom. c	Wt %	Normalised atom. c
Fe	26.94	24.2	27.45	24.97	29.46	24.59	9.07	22.47
S	31.26	48.9	30.48	48.3	33.71	49.01	11.05	47.71
Co	0.00	0	0.00	0	0.00	0	0.00	0
Cu	34.06	26.88	33.36	26.67	35.95	26.38	13.68	29.8
Zn	0.00	0	0.00	0	0.00	0	0.01	0.02
Mn	0.01	0	0.00	0	0.00	0	0.00	0
Se	0.00	0	0.00	0	0.00	0	0.00	0
Cd	0.02	0.01	0.12	0.06	0.04	0.02	0.00	0
Hg	0.03	0.01	0.00	0	0.00	0	0.00	0
As	n.d.		n.d.		n.d.		n.d.	
Ag	n.d.		n.d.		n.d.		n.d.	
Sb	n.d.		n.d.		n.d.		n.d.	
Ni	n.d.		n.d.		n.d.		n.d.	
Pb	n.d.		n.d.		n.d.		n.d.	
Bi	n.d.		n.d.		n.d.		n.d.	
TOTAL	92.32	100	91.41	100	99.16	100	33.81	100

CHALCOPYRITE MICROPROBE ANALYSES
MARIMO SHALE WALL ROCK HOSTED

TRACE ELEMENT	SAMPLE NUMBER (SPOT NUMBER)			
	85031 (R2DCP)		85031 (R1ACP)	
	Wt %	Normalised atom. c	Wt %	Normalised atom. c
Fe	29.42	24.43	29.47	24.45
S	33.68	48.71	33.86	48.92
Co	0.03	0.03	0.00	0
Cu	36.64	26.74	36.41	26.55
Zn	0.01	0	0.00	0
Mn	0.00	0	0.01	0
Se	0.00	0	0.06	0.03
Cd	0.00	0	0.00	0
Hg	0.40	0.09	0.23	0.05
As	n.d.		n.d.	
Ag	n.d.		n.d.	
Sb	n.d.		n.d.	
Ni	n.d.		n.d.	
Pb	n.d.		n.d.	
Bi	n.d.		n.d.	
TOTAL	100.18	100	100.04	100

PYRITE MICROPROBE ANALYSES
MARIMO SHALE VEIN / MATRIX HOSTED

TRACE ELEMENT	SAMPLE NUMBER (SPOT NUMBER)							
	85016B (R5PY1)		85016B (R5PY2)		85016B (R1PY2)		85016 (R1PY1)	
	Wt %	Normalised	Wt %	Normalised	Wt %	Normalised	Wt %	Normalised
	atom. c		atom. c		atom. c		atom. c	
Fe	45.74	35.56	45.65	34.89	43.71	33.06	44.39	33.4
S	47.42	64.21	48.38	64.4	48.88	65.87	50.80	66.49
Co	0.16	0.12	0.78	0.56	1.22	0.91	0.10	0.07
Cu	0.04	0	0.01	0.01	0.01		0.08	0.07
Zn	0.00	0	0.00	0	0.03		0.00	
Mn	0.00	0	0.00	0.01	0.00		0.00	
Se	0.02	0.01	0.10	0.06	0.00		0.10	0.06
Cd	0.00	0	0.20	0.07	0.00		0.00	
Hg	0.47	0.1	0.00	0	0.47	0.1	0.00	
As	n.d.		n.d.		1.77	1.01	0.00	
Ag	n.d.		n.d.		0.00		0.01	
Sb	n.d.		n.d.		0.00		0.00	
Ni	n.d.		n.d.		n.d.		n.d.	
Pb	n.d.		n.d.		n.d.		n.d.	
Bi	n.d.		n.d.		0.53	0.11	0.00	
TOTAL	93.85	100	95.12	100	96.62	101.06	95.48	100.09

	SAMPLE NUMBER (SPOT NUMBER)							
	85018 (R5PY)		85018 (R4EPY)		85018 (R4DPY)		85018 (R4FPY)	
	Wt %	Normalised	Wt %	Normalised	Wt %	Normalised	Wt %	Normalised
	atom. c		atom. c		atom. c		atom. c	
Fe	45.80	33.12	45.97	33.07	46.80	33.63	46.17	33.29
S	52.45	66.05	52.69	66.02	52.55	65.77	52.03	65.34
Co	0.94	0.64	0.21	0.14	0.73	0.5	0.32	0.22
Cu	n.d.		n.d.		n.d.		n.d.	
Zn	0.00		0.03		0.02		0.00	
Mn	n.d.		n.d.		n.d.		n.d.	
Se	0.03		0.01		0.05	0.03	0.01	
Cd	n.d.		n.d.		n.d.		n.d.	
Hg	n.d.		n.d.		n.d.		n.d.	
As	0.24	0.13	0.01		0.03		0.98	0.53
Ag	0.00		0.00		0.11	0.04	0.09	0.03
Sb	n.d.		n.d.		n.d.		n.d.	
Ni	0.02		1.03	0.7	0.02		0.84	0.57
Pb	0.16	0.03	0.17	0.03	0.03		0.03	
Bi	n.d.		n.d.		n.d.		n.d.	
TOTAL	99.64	99.97	100.12	99.96	100.34	99.97	100.47	99.98

PYRITE MICROPROBE ANALYSES
STAVELEY FORMATION WALL ROCK HOSTED

TRACE ELEMENT	SAMPLE NUMBER (SPOT NUMBER)					
	85056 (R3PY1)		85056 (R2PY1)		85052 (R8P1)	
	Wt %	Normalised	Wt %	Normalised	Wt %	Normalised
	atom. c		atom. c		atom. c	
Fe	43.81	32.85	43.71	32.97	43.74	32.95
S	50.81	66.29	50.44	66.17	50.56	66.26
Co	2.08	1.5	2.21	1.62	1.75	1.27
Cu	0.01		0.01		0.01	
Zn	0.03		0.01		0.01	
Mn	0.00		0.00		0.01	
Se	0.04		0.00		0.06	
Cd	0.00		0.00		0.11	0.04
Hg	0.65	0.14	0.00		0.00	
As	0.00		0.03		0.00	
Ag	0.02		0.03		0.01	
Sb	0.00		0.00		0.00	
Ni	n.d.		n.d.		n.d.	
Pb	n.d.		n.d.		n.d.	
Bi	0.00		0.34	0.07	1.05	0.21
TOTAL	97.45	100.78	96.78	100.83	97.31	100.73

PYRITE MICROPROBE ANALYSES
STAVELEY FORMATION VEIN / MATRIX HOSTED

TRACE ELEMENT	SAMPLE NUMBER (SPOT NUMBER)			
	85052 (R2PY1)		85052 (R5PY1)	
	Wt %	Normalised	Wt %	Normalised
		atom. c		atom. c
Fe	45.15	33.96	44.21	33.15
S	50.37	65.91	50.76	66.25
Co	0.00		1.37	0.98
Cu	0.03		0.00	
Zn	0.00		0.02	
Mn	0.00		0.00	
Se	0.04		0.03	
Cd	0.00		0.00	
Hg	0.00		0.50	0.11
As	0.00		0.00	
Ag	0.00		0.00	
Sb	0.00		0.00	
Ni	n.d.		n.d.	
Pb	n.d.		n.d.	
Bi	1.10	0.22	0.44	0.09
TOTAL	96.69	100.09	97.33	100.58

PYRITE MICROPROBE ANALYSES
MARIMO SHALE WALL ROCK HOSTED

TRACE ELEMENT	SAMPLE NUMBER (SPOT NUMBER)			
	85031 (R1APYINC)		85009 (R2PY1)	
	Wt %	Normalised	Wt %	Normalised
		atom. c		atom. c
Fe	46.91	33.93	45.09	32.81
S	52.54	66.01	52.75	66.84
Co	0.01	0.01	0.16	0.11
Cu	n.d.		n.d.	
Zn	0.00		0.07	0.05
Mn	n.d.		n.d.	
Se	0.00		0.00	0
Cd	n.d.		n.d.	
Hg	n.d.		n.d.	
As	0.04	0.02	0.20	0.11
Ag	0.00		0.00	0
Sb	n.d.		n.d.	
Ni	0.03	0.02	0.07	0.05
Pb	0.07	0.01	0.16	0.03
Bi	n.d.		n.d.	
TOTAL	99.60	100	98.51	100

ALBITE MICROPROBE ANALYSES
DIORITE HOSTED

% Cations based on 8 O

MAJOR ELEMENTS	SAMPLE NUMBER (SPOT NUMBER)			
	85063 (R3A1)		85063 (R2F1)	
	% Cations		% Cations	
SiO2	66.27	2.9216	68.13	2.9699
TiO2	0.00	0	0.00	0
Al2O3	20.91	1.0863	20.27	1.0417
K2O	0.15	0.0084	0.15	0.0085
Na2O	10.06	0.8602	10.97	0.9268
BaO	0.00	0	0.02	0.003
SrO	0.25	0.0064	0.21	0.0053
FeO	0.14	0.0052	0.00	0
MnO	0.00	0	0.00	0
CaO	1.69	0.0797	0.34	0.0157
MgO	0.00	0	0.01	0.0009
Cr2O3	0.03	0.0011	0.15	0.0052
TOTAL	99.50	4.9689	100.25	4.977
Albite	90.70		97.42	
Orthoclase	0.89		0.89	
Anorthite	8.41		1.65	
Ca	0.00		0.04	

MICA MICROPROBE ANALYSES
DIORITE HOSTED

% Cations on 24
(O, OH, F, Cl) basis

MAJOR ELEMENTS	SAMPLE NUMBER (SPOT NUMBER)					
	85063 (R5B1)		85063 (R3B1)		85063 (R5B2)	
	% Cations		% Cations		% Cations	
SiO2	36.93	5.7077	37.34	5.7611	36.94	5.6964
TiO2	1.43	0.1663	1.32	0.1536	1.41	0.1633
Al2O3	13.70	2.496	13.55	2.4644	13.57	2.4671
MgO	15.42	3.5513	15.69	3.6081	15.51	3.5645
CaO	0.00	0	0.00	0	0.03	0.0049
MnO	0.03	0.0041	0.00	0	0.05	0.0064
FeO	15.30	1.9779	14.46	1.8661	15.61	2.0136
Na2O	0.08	0.0233	0.15	0.0446	0.07	0.0201
K2O	9.77	1.926	9.93	1.9546	9.97	1.9612
H2O	3.29		3.50		3.52	
F	0.89		0.39		0.36	
Cl	0.68		0.79		0.75	
TOTAL	97.52	15.8526	97.14	15.8525	97.79	15.8975
O = F	-0.37		-0.16		-0.15	
O = Cl	-0.15		-0.18		-0.17	
TOTAL	96.99		96.80		97.47	

MAGNETITE MICROPROBE ANALYSES
DIORITE HOSTED

Cations on 4 O Basis

MAJOR ELEMENTS	SAMPLE NUMBER (SPOT NUMBER)					
	85063 (R4MT1)		85063 (R3MT1)		85063 (R2MT1)	
	% Cations		% Cations		% Cations	
TiO2	0.04	0.001	0.01	0.0002	0.03	0.0008
Al2O3	0.04	0.0017	0.05	0.0022	0.01	0.0006
V2O3	0.31	0.0094	0.32	0.0102	0.25	0.0078
Cr2O3	0.04	0.0011	0.01	0.0003	0.00	0
Fe2O3	69.07	1.988	66.51	1.9885	67.54	1.9918
MgO	0.03	0.0016	0.00	0	0.00	0
MnO	0.00	0	0.00	0	0.06	0.0019
FeO	31.13	0.9958	29.97	0.9958	30.39	0.996
ZnO	0.00	0	0.07	0.0021	0.00	0
TOTAL	100.66	2.9986	96.93	2.9993	98.28	2.9989

MICROCLINE MICROPROBE ANALYSES
STAVELEY FORMATION WALLROCK HOSTED

% Cations based on 8 O

MAJOR ELEMENTS	SAMPLE NUMBER (SPOT NUMBER)					
	85049 (WALFS2)		85049 (WALFS3)		85049 (WALFS4)	
	% Cations		% Cations		% Cations	
SiO2	63.82	2.9701	64.65	2.9841	63.98	2.9809
TiO2	0.01	0.0003	0.01	0	0.00	0
Al2O3	18.82	1.0324	18.73	0.0003	18.48	1.0146
K2O	16.36	0.9716	14.24	0.8384	16.38	0.9735
Na2O	0.31	0.0281	1.68	0.1502	0.32	0.0292
BaO	0.02	0.0003	0.08	0.0014	0.02	0.0004
SrO	0.14	0.0037	0.21	0.0057	0.20	0.0055
FeO	0.14	0.0055	0.07	0.0029	0.22	0.0088
MnO	0.02	0.0007	0.02	0.0007	0.00	0
CaO	0.00	0.0002	0.00	0	0.01	0.0003
MgO	0.00	0.0002	0.00	0	0.00	0
Cr2O3	0.00	0	0.00	0	0.00	0
TOTAL	99.65	5.0131	99.69	3.9837	99.62	5.0132
Albite	2.81		15.17		7.35	
Orthoclase	97.13		84.69		92.03	
Anorthite	0.02		0.00		0.00	
Ce	0.03		0.14		0.62	

ALBITE MICROPROBE ANALYSES
MARIMO SHALE HOSTED

% Cations based on 8 O

MAJOR ELEMENTS	SAMPLE NUMBER (SPOT NUMBER)			
	85018 (R7NAB)		85018 (R9OAB)	
	% Cations		% Cations	
SiO2	67.86	2.9769	67.29	2.9763
TiO2	0.00	0	0.00	0
Al2O3	19.96	1.0319	19.88	1.0363
K2O	0.11	0.0061	0.10	0.0057
Na2O	11.15	0.9488	10.96	0.9399
BaO	0.01	0.0002	0.01	0.0001
SrO	0.26	0.0066	0.26	0.066
FeO	0.08	0.0031	0.00	0
MnO	0.00	0	0.00	0
CaO	0.20	0.0093	0.26	0.0121
MgO	0.00	0	0.02	0.0013
Cr2O3	0.03	0.0011	0.00	0
TOTAL	99.66	4.984	98.78	5.0377
Albite	98.38		98.12	
Orthoclase	0.64		0.60	
Anorthite	0.96		1.27	
Ce	0.02		0.01	

MICROCLINE MICROPROBE ANALYSES
MARIMO SHALE HOSTED

% Cations based on 8 O

MAJOR ELEMENTS

SAMPLE NUMBER (SPOT NUMBER)

	85016B (R1F1)		85016B (R1F2)		85016B (R4F1)		85016B (R4F2)	
	% Cations		% Cations		% Cations		% Cations	
SiO2	63.99	2.9798	63.68	2.9881	63.17	2.9779	63.52	2.9693
TiO2	0.03	0.0009	0.02	0.0007	0.00	0	0.00	0
Al2O3	18.59	1.0203	18.28	1.0108	18.41	1.0229	18.69	1.0296
K2O	16.65	0.9891	16.59	0.9932	15.94	0.9584	16.33	0.9739
Na2O	0.07	0.0062	0.06	0.0053	0.43	0.0391	0.40	0.0363
BaO	0.03	0.0005	0.05	0.001	0.11	0.002	0.08	0.0014
SrO	0.18	0.0048	0.17	0.0047	0.17	0.0046	0.18	0.005
FeO	0.01	0.0003	0.03	0.0013	0.10	0.0038	0.04	0.0018
MnO	0.00	0	0.00	0	0.00	0	0.06	0.0025
CaO	0.00	0	0.00	0	0.01	0.0006	0.00	0
MgO	0.00	0	0.00	0	0.00	0	0.01	0.0006
Cr2O3	0.09	0.0032	0.00	0	0.00	0	0.01	0.0004
TOTAL	99.64	5.0051	98.88	5.0051	98.34	5.0093	99.32	5.0208
Albite	0.62		0.53		3.91		3.59	
Orthoclase	99.32		99.38		95.83		96.27	
Anorthite	0.00		0.00		0.06		0.00	
Ce	0.05		0.10		0.20		0.14	

85011 (R4FK4)		85018 (R3CF)		85018 (R2BM)	
% Cations		% Cations		% Cations	
63.57	2.9715	63.25	2.9743	63.16	2.9696
0.00	0	0.00	0	0.01	0.0003
18.75	1.033	18.61	1.0316	18.61	1.0315
15.71	0.9369	15.76	0.9457	15.81	0.9484
0.60	0.0542	0.39	0.0358	0.55	0.0503
0.16	0.0029	0.13	0.0025	0.12	0.0022
0.18	0.0049	0.23	0.0064	0.16	0.0044
0.03	0.0011	0.11	0.0042	0.09	0.0036
0.00	0	0.00	0	0.09	0.0035
0.00	0	0.00	0	0.00	0
0.00	0	0.00	0.0003	0.00	0
0.05	0.002	0.00	0	0.00	0
99.05	5.0065	98.48	5.0008	98.60	5.0138
5.45		3.63		5.03	
94.26		96.11		94.75	
0.00		0.00		0.00	
0.29		0.25		0.22	

APATITE MICROPROBE ANALYSES
MARIMO SHALE HOSTED

% Cations on 26

(O, OH, F, Cl) basis

MAJOR ELEMENTS

SAMPLE NUMBER (SPOT NUMBER)

	85016B (R2A1)		85018 (R6HAP1)		85018 (R6HAP2)	
	% Cations		% Cations		% Cations	
P2O5	41.02	5.8089	39.95	5.7586	40.02	5.7803
CaO	54.80	0.0053	55.97	0	55.22	0.0003
SiO2	0.03	0	0.00	0	0.00	0
MgO	0.00	9.8197	0.00	10.2109	0.00	10.0945
FeO	0.00	0	0.01	0.002	0.04	0.0052
SrO	0.00	0	0.00	0	0.00	0
BaO	0.01	0.0006	0.03	0.0018	0.00	0
H2O	0.00		0.00		0.00	
F	6.21		5.14		5.36	
Cl	0.03		0.03		0.02	
TOTAL	102.10	15.6345	101.13	15.9733	100.66	15.8803
O = F	-2.61		-2.17		-2.26	
O = Cl	-0.01		-0.01		-0.01	
TOTAL	99.48		98.95		98.39	

ALBITE MICROPROBE ANALYSES
STAVELEY FORMATION HOSTED

% Cations based on 8 O

MAJOR ELEMENTS	SAMPLE NUMBER (SPOT NUMBER)							
	85052 (R7F1)		85052 (R7F2)		85052 (R4F1)		85056 (R6A1)	
	% Cations		% Cations		% Cations		% Cations	
SiO2	67.51	2.9768	67.38	2.9738	68.15	2.999	67.83	2.9927
TiO2	0.02	0.0006	0.00	0	0.00	0.0001	0.00	0
Al2O3	19.99	1.0386	20.06	1.0434	19.66	1.0198	19.69	1.024
K2O	0.10	0.0054	0.13	0.0072	0.14	0.0078	0.13	0.0076
Na2O	10.73	0.9173	10.63	0.9092	10.64	0.9078	10.89	0.9319
BaO	0.00	0	0.00	0	0.00	0	0.01	0.0001
SrO	0.28	0.0072	0.31	0.0079	0.27	0.0069	0.25	0.0065
FeO	0.00	0	0.00	0	0.08	0.003	0.00	0
MnO	0.00	0	0.00	0	0.05	0.0019	0.00	0
CaO	0.35	0.0164	0.41	0.0192	0.05	0.0025	0.05	0.0022
MgO	0.01	0.0004	0.01	0.0009	0.00	0	0.00	0
Cr2O3	0.04	0.0013	0.02	0.0008	0.00	0	0.00	0
TOTAL	99.03	4.964	98.95	4.9624	99.04	4.9488	98.85	4.965
Albite	97.68		97.18		98.88		98.95	
Orthoclase	0.58		0.77		0.85		0.81	
Anorthite	0.17		2.05		0.27		0.23	
Ce	0.00		0.00		0.00		0.01	

MICA MICROPROBE ANALYSES
MARIMO SHALE HOSTED

% Cations on 24
(O, OH, F, Cl) basis

MAJOR ELEMENTS	SAMPLE NUMBER (SPOT NUMBER)							
	85016B (R2B1)		85016B (R2B2)		85016B (R3B1)		85011 (R3CB1)	
	% Cations		% Cations		% Cations		% Cations	
SiO2	43.07	6.1768	43.47	6.2631	42.63	6.1162	41.90	6.0606
TiO2	0.17	0.0188	0.36	0.0395	0.22	0.0236	0.30	0.0331
Al2O3	13.22	2.2346	10.79	1.8312	11.41	1.9285	11.65	1.9867
MgO	22.54	4.8186	24.09	5.1734	24.68	5.2782	25.69	5.5386
CaO	0.03	0.0043	0.01	0.0021	0.00	0	0.00	0
MnO	0.06	0.0068	0.06	0.0068	0.00	0	0.00	0
FeO	4.26	0.5108	4.10	0.4934	4.72	0.5664	2.85	0.3451
Na2O	0.01	0.0038	0.06	0.0167	0.02	0.0059	0.07	0.0203
K2O	10.00	1.829	10.49	1.9278	10.71	1.96	10.17	1.8773
H2O	1.97		1.75		1.17		1.89	
F	4.65		5.06		6.31		4.73	
Cl	0.03		0.06		0.06		0.05	
TOTAL	100.01	15.6035	100.30	15.754	101.93	15.8788	99.30	15.8617
O = F	-1.96		-2.13		-2.66		-1.99	
O = Cl	-0.01		-0.01		-0.01		-0.01	
TOTAL	98.04		98.16		99.26		97.30	

	SAMPLE NUMBER (SPOT NUMBER)							
	85018 (R6IB1)		85018 (R7LB1)		85018 (R9PPH)		85011 (R4EB1)	
	% Cations		% Cations		% Cations		% Cations	
SiO2	42.89	6.1976	56.47	7.451	42.47	6.1887	42.19	6.0972
TiO2	0.29	0.0314	0.00	0	0.28	0.0309	0.23	0.0251
Al2O3	11.90	2.0273	21.00	3.2655	10.66	1.8312	11.42	1.9444
MgO	23.15	4.9863	6.91	1.3594	23.97	5.2063	25.58	5.5105
CaO	0.02	0.0029	0.04	0.0053	0.00	0	0.00	0
MnO	0.00	0	0.02	0.002	0.00	0	0.00	0
FeO	4.66	0.563	0.86	0.0944	5.01	0.6111	2.69	0.3256
Na2O	0.03	0.0098	0.03	0.0073	0.01	0.0006	0.06	0.0165
K2O	10.24	1.8881	8.73	1.4702	10.72	1.9926	10.79	1.989
H2O	2.10		3.89		1.39		2.08	
F	4.30		1.36		5.72		4.33	
Cl	0.02		0.04		0.06		0.08	
TOTAL	99.60	15.7064	99.35	13.6551	100.29	15.8614	99.45	15.9083
O = F	-1.81		-0.57		-2.41		-1.82	
O = Cl	-0.01		-0.01		-0.01		-0.02	
TOTAL	97.78		98.77		97.87		97.61	

MICROCLINE MICROPROBE ANALYSES
STAVELEY FORMATION VEIN HOSTED

% Cations based on 80

MAJOR ELEMENTS

SAMPLE NUMBER (SPOT NUMBER)

	85052 (R6F1)		85052 (R6F2)		85049 (R2F1)		85049 (R2F2)		85049 (R3F1)	
	% Cations		% Cations		% Cations		% Cations		% Cations	
SiO2	63.39	2.9733	64.04	2.9769	63.82	2.9695	63.70	2.9638	64.17	2.9831
TiO2	0.00	0	0.00	0	0.00	0	0.00	0	0.00	0
Al2O3	18.64	1.0303	18.73	1.026	18.81	1.0317	19.00	1.0418	18.61	1.0194
K2O	15.98	0.9564	16.07	0.9529	15.49	0.9193	15.42	0.915	15.48	0.9181
Na2O	0.39	0.0355	0.49	0.0439	0.81	0.0734	0.79	0.0711	0.80	0.0718
BaO	0.24	0.0043	0.13	0.0024	0.34	0.0062	0.44	0.0081	0.20	0.0037
SrO	0.17	0.0046	0.18	0.0049	0.20	0.0055	0.17	0.0046	0.14	0.0038
FeO	0.00	0.0001	0.04	0.0015	0.01	0.0002	0.00	0	0.00	0
MnO	0.07	0.0029	0.00	0	0.02	0.001	0.00	0	0.05	0.0019
CaO	0.00	0	0.00	0	0.00	0	0.02	0.0008	0.00	0.0001
MgO	0.00	0	0.00	0	0.01	0.0008	0.00	0	0.01	0.0004
Cr2O3	0.00	0	0.00	0	0.06	0.0022	0.06	0.0022	0.00	0
TOTAL	98.88	5.0074	99.68	5.0085	99.58	5.0098	99.59	5.0074	99.45	5.0023
Albite	3.57		4.39		7.35		7.15		7.23	
Orthoclase	96.00		95.37		92.03		91.96		92.39	
Anorthite	0.00		0.00		0.00		0.08		0.01	
Ca	0.43		0.24		0.62		0.81		0.37	

CARBONATE MICROPROBE ANALYSES
STAVELEY FORMATION HOSTED

% Based on 60

MAJOR ELEMENTS

SAMPLE NUMBER (SPOT NUMBER)

	85052 (R4C1)		85052 (R4C2)		85052 (R3D)		85052 (R1AD1)		85052 (R1BD2)	
	% Cations		% Cations		% Cations		% Cations		% Cations	
Ca(CO3)	52.52	0.9946	52.43	0.9737	52.13	0.9681	52.43	0.9846	52.19	0.9984
Mg(CO3)	31.35	0.7046	39.49	0.8705	38.81	0.8553	36.65	0.8169	31.66	0.7188
Fe(CO3)	16.95	0.2774	8.71	0.1398	10.17	0.1632	11.25	0.1826	15.68	0.2592
Mn(CO3)	1.34	0.0221	0.73	0.0118	0.75	0.0122	0.87	0.0143	1.29	0.0215
Al2(CO3)3	0.01	0.0002	0.00	0	0.06	0.001	0.00	0	0.00	0
Ti(CO3)2	0.00	0	0.03	0.0004	0.00	0	0.07	0.0008	0.00	0
Si(CO3)2	0.00	0	0.02	0.0003	0.02	0.0003	0.05	0.0007	0.04	0.0005
Zn(CO3)	0.06	0.0009	0.11	0.0016	0.00	0	0.00	0	0.00	0
Na2(CO3)	0.00	0	0.06	0.002	0.00	0	0.00	0	0.03	0.001
K2(CO3)	0.01	0.0001	0.00	0	0.00	0	0.01	0.0002	0.01	0.0004
TOTAL	102.24	1.9999	101.58	2.0001	101.94	2.0001	101.33	2.0001	100.90	1.9998

MICA MICROPROBE ANALYSES
STAVELEY FORMATION HOSTED

% Cations on 24

(O, OH, F, Cl) basis

MAJOR ELEMENTS

SAMPLE NUMBER

	85056 R1MB		85056 R1AB		85056 R1A2B		85056 R4B1		85056 R5B1	
	% Cations		% Cations		% Cations		% Cations		% Cations	
SiO2	26.64	0.4395	39.40	5.868	40.42	5.975	40.26	5.9544	39.40	5.8857
TiO2	0.07	0.0084	1.01	0.1133	0.99	0.1097	0.94	0.1044	1.29	0.1454
Al2O3	19.34	3.7617	12.95	2.2726	12.38	2.1573	12.27	2.1394	12.99	2.2862
MgO	16.34	4.0205	17.91	3.9764	19.26	4.2446	18.70	4.1235	17.57	3.9108
CaO	0.13	0.0231	0.04	0.0058	0.00	0	0.06	0.0101	0.00	0
MnO	0.00	0	0.00	0	0.09	0.0107	0.08	0.0097	0.03	0.0032
FeO	25.39	3.5039	13.31	1.6583	11.09	1.3711	12.57	1.5543	12.91	1.6131
Na2O	0.00	0	0.10	0.0288	0.12	0.0357	0.08	0.023	0.11	0.0304
K2O	0.00	0	10.25	1.9472	10.08	1.9013	10.22	1.9282	10.14	1.9325
H2O	3.41		2.36		2.31		2.65		2.63	
F	0.45		3.40		3.59		2.86		2.77	
Cl	0.01		0.21		0.18		0.17		0.29	
TOTAL	91.78	15.7142	100.94	15.8704	100.51	15.8054	100.86	15.847	100.13	15.8073
O = F	-0.19		-1.43		-1.51		-1.21		-1.17	
O = Cl	0.00		-0.05		-0.04		-0.03		-0.06	
TOTAL	91.59		99.46		98.96		99.62		98.90	

APPENDIX 5

LASER RAMAN SPECTRA

AUSTRALIAN
GEOL. SURVEY
ORGANISATION

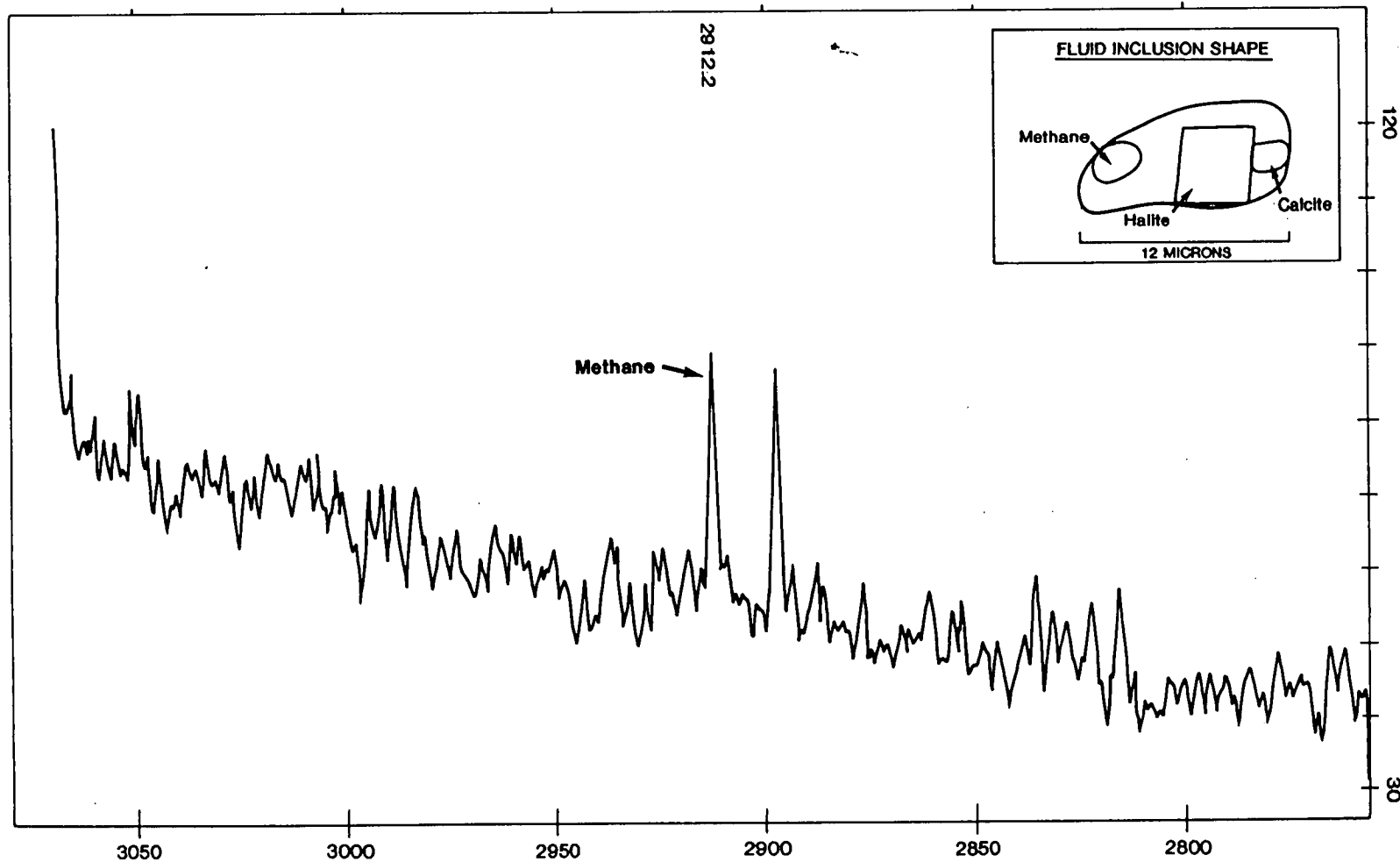
DILOR
MICRODIL 28

OPERATOR TPM
DATE 4/11/94
SAMPLE 85008 Ab
NUMBER 37-017
MODE MULTICHANNEL
REMARK: 6 μ m INCL + 2 SOLIDS

EXCIT: LINE (nm) 514.5319
LASER POW. (mW) 400
FOREMONO. (cm⁻¹) 16518
SPECTRO. (cm⁻¹) 16518
SLIT WIDTH (μ m) 100

SPECT. SLIT WIDTH (cm⁻¹) 2.43
DETECTOR (nbr of diodes) 512
FILTER NONE
INTEGRATION TIME (s) 5
NUMBER OF ACCUMULATIONS 10

LASER RAMAN SPECTRA



Sample 85008 Ab

37 - 017. TPM

AUSTRALIAN
GEOL. SURVEY
ORGANISATION

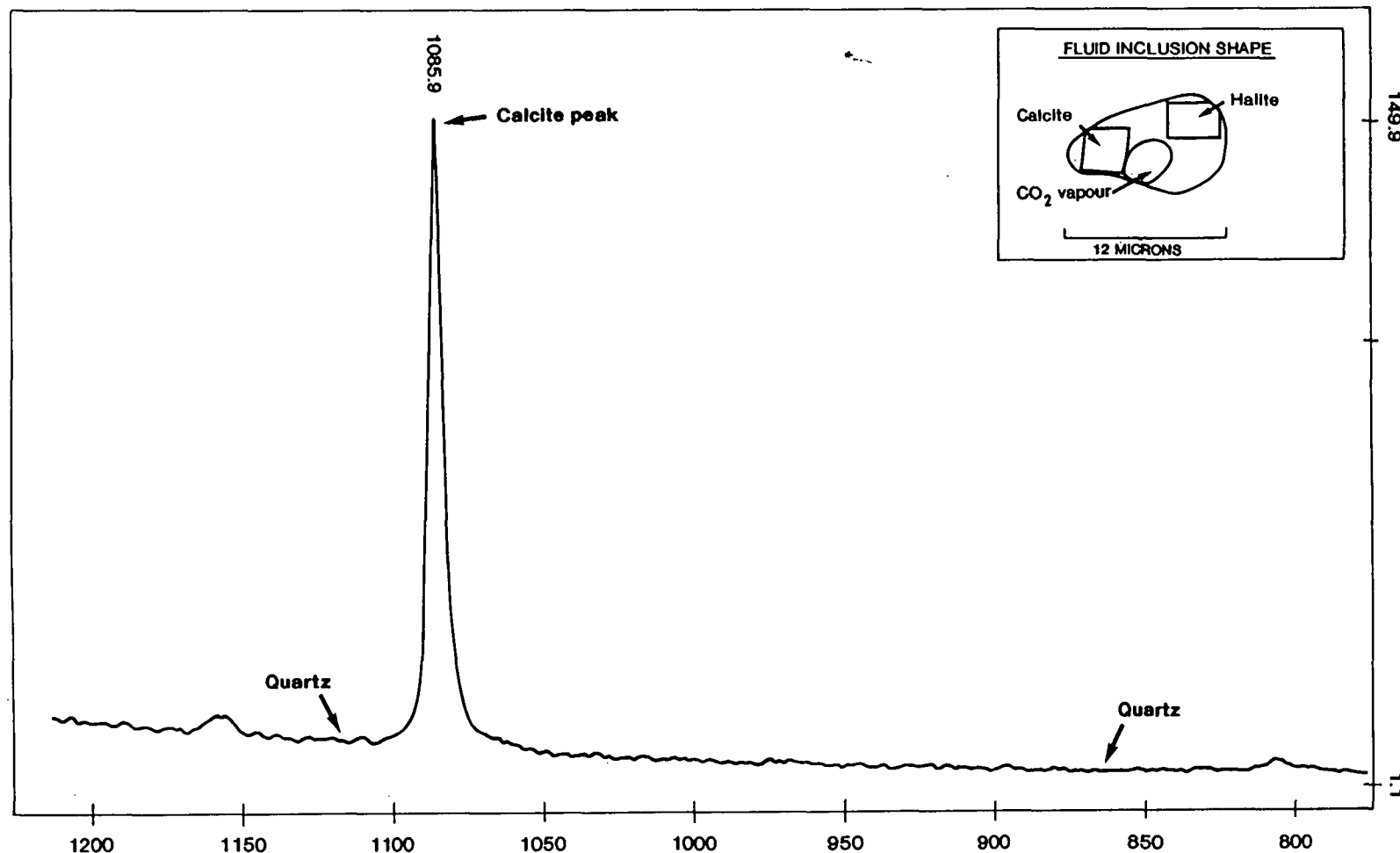
DILOR
MICRODIL 28

OPERATOR TPM
DATE 4/11/94
SAMPLE 85011
NUMBER 37-016
MODE MULTICHANNEL
REMARK: 3 μ m RECTANGULAR SOLID

EXCIT: LINE (nm) 514.5319
LASER POW. (nW) 200
FOREMONO. (cm⁻¹) 18435
SPECTRO. (cm⁻¹) 18435
SLIT WIDTH (μ m) 100

SPECT. SLIT WIDTH (cm⁻¹) 3.43
DETECTOR (nbr of diodes) 512
FILTER NONE
INTEGRATION TIME (s) 5
NUMBER OF ACCUMULATIONS 10

LASER RAMAN SPECTRA



Sample 85011

37 - 016.TPM